Predicting Performance Level of Reinforced Concrete Structures Subject to Corrosion as a Function of Time

Hakan Yalçıner

Submitted to the
Institute of Graduate Studies and Research
in partial fulfillment of the requirements for the Degree of

Doctor of Philosophy
in
Civil Engineering

Eastern Mediterranean University
January 2012
Gazimağusa, North Cyprus

Approval of the Institute of Graduate Studies and Research

Prof. Dr. Elvan Yılmaz
Director

I certify that this thesis satisfies the requirements as a thesis for the degree of Doctor of Philosophy in Civil Engineering.

Asst. Prof. Dr. Mürüde Çelikağ
Chair, Department of Civil Engineering

We certify that we have read this thesis and that in our opinion it is fully adequate in scope and quality as a thesis for the degree of Doctor of Philosophy in Civil Engineering.

Assist. Prof. Dr. Serhan Şensoy
Co-supervisor

Assoc. Prof. Dr. Özgür Eren
Supervisor

Examining Committee

1. Prof. Dr. Alemdar Bayraktar
2. Assoc. Prof. Dr. Khaled Marar
3. Assoc. Prof. Dr. Özgür Eren
4. Asst. Prof. Dr. Erdinç Soyer
5. Asst. Prof. Dr. Serhan Şensoy

ABSTRACT

Deterioration due to corrosion becomes a more serious problem when the exact time of expected earthquakes is unknown. Therefore, the prediction of performance levels of corroded reinforced concrete (RC) structures is important to prevent serious premature damage. Many models have been developed regarding the effects of corrosion as a function of time. It is possible to evaluate and identify the performance level of RC structures as immediate occupancy (IO), life safety (LS), collapse prevention (CP), and collapse (C). The first part of this study contributes to an understanding of time dependent effects of corrosion on seismic performance levels of corroded RC buildings that will be a guideline for the further studies for strengthening and assessing of RC buildings. The developed model in the first part of this thesis provide to predict the time dependent seismic performance levels of RC buildings by considering three major effects of corrosion (e.g., deformation due to bond-slip relationships, loss of cross sectional area of reinforcement bars and reduction in concrete compressive strength).

In second part of this thesis, the effect of corrosion on the bond strength between reinforcement bars and concrete was studied in a series of experiments. An accelerated corrosion method was used to corrode the reinforcement bars embedded in concrete specimens. Pullout tests were performed to develop an empirical model for the ultimate bond strength by evaluating bond strengths in two different concrete mixes, three concrete cover depths and different mass losses of reinforcement bars after corrosion. Bond-slip relationships for the different corrosion levels were compared for different concrete classes and concrete cover depths. In contrast to developed models found in the literature for the prediction of ultimate bond strength,

the newly developed bond strength models in this study provide to predict the bond strength as a function of corrosion level, concrete strength level, crack width and cover-to-diameter (c/D) ratios. It was found that previously developed bond strength models do not represent the actual corrosion behaviour where the bond strength decreases rapidly with increasing corrosion level in those models.

Keywords: Corrosion, time-history analysis, performance levels, pullout test, bond strength, bond-slip relationship.

ÖZ

Korozyondan dolayı meydana gelen kötüleşme ileride olması depremlerin kesin zamanın bilinmemesi ile daha çok ciddi bir problem haline gelir. Bundan dolayı korozyonlu betonarme yapıların performans seviyelerinin tahmin edilmesi erken hasarların önüne geçilmesi için önemlidir. Korozyonun zamana bağlı olarak etkileri hakkında birçok model geliştirilmiştir. Ayrıca betonarme yapıların performans seviyelerini hemen kullanılabilir, can güvenliği, göçme öncesi ve göçme olarak değerlendirmek ve tanımlamak mümkündür. Bu çalışmanın ilk bölümü zamana bağlı korozyon etkilerinin korozyonlu betonarme binalar üzerindeki sismik performans seviyelerin anlaşılmasına katkıda bulunmaktadır ki ileriki çalışmalara betonarme yapılarının güçlendirilmesi ve değerlendirilmesi için bir rehber olacaktır. Bu tezin birinci bölmünde geliştirilen model, korozyonun başlıca üç etkisini (örneğin, aderans-kayma ilişkisinden dolayı deformansyon, donatı alanındaki kayıp ve beton basınç mukavvemetindeki azalma) dikkate alarak betonarme yapıların zamana baglı olarak performans seviyelerini tahmin etmeyi sağlamaktadır.

Bu tezin ikinci bölmümde ise korozyonun donatı ve beton arasındaki aderans kuvveti üzerindeki etkisi bir takım seri deneyler ile çalışılmıştır. Beton numuneleri içerisine yerleştirilen donatılar hızlandırılmış korozyon metodu ile paslandırılmıştır. Aderans kuvvetini iki farklı beton karışımı, üç farklı paspayı ve farklı korozyon kütle kayıplarında değerlendirerek deneysel bir nihai aderans kuvvet modeli geliştirmek için çekme deneyi yapılmıştır. Farklı korozyon oranlarındakı aderans-kayma ilişkisi farklı beton sınıfları ve beton paspayları için karşılaştırılmıştır. Nihai aderans kuvvetini tahmin etmek için literatürde bulunan modellerden farklı olarak, bu tezin ikinci bölümünde yeni geliştirilen aderans modeli, aderans kuvvetini korozyon oranı,

beton mukavvemeti, çatlak genişliği ve paspayı donatı oranına bağlı bir fonksiyon olarak tahmin etmeyi sağlamaktadır. Daha önce geliştirilen aderans modellerinin gerçek korozyon davranışını sergilemediği bulunmuştur ki bu modellerde aderans kuvveti artan korozyon oranıyla ani azalım göstermektedir.

Anahtar Kelimeler: Korozyon, zaman-tanım analizi, performans seviyeleri, çekme deneyi, aderans kuvveti, aderans-kayma ilişkisi.

ACKNOWLEDGMENT

I am extremely grateful to my supervisor Assoc. Prof. Dr. Özgür Eren , who gave me the opportunity to study on this thesis. Without his guidance in our countless meetings and discussions, I would not have been able to complete my research. I should emphasize that the experimental work described in this thesis would not have been possible without the support by Assoc. Prof. Dr. Özgür Eren.

I would like to express my sincerest gratitude to my co supervisor, Assist. Prof. Dr. Serhan Şensoy who gave me the opportunity to be research assistant and begin my Ph.D education at EMU. I have learned many things from his graduate courses and helped me to focus on my research. His courses were good guide for me to develop models in this thesis. The experimental work described in this thesis would not have been possible without the support by Assist. Prof. Dr. Serhan Şensoy.

I would also like thank to Prof. Dr. Ghani Razaqpur for his excellent advises during as a visiting student at McMaster University in Canada.

Thanks to Mr. Ogün Kılıç for his help and technical guidance. It was not possible to complete experimental tests on time without the help of Mr. Ogün Kılıç. I can not forget the help of Nasim Mosavat and Temuçin Yardımcı for the heaviest job during the laboratory works. I am very happy to have a faithful friend Mazdak who has never left me alone in the darkness of laboratory during all my experimental works.

It is not easy to express my feelings towards to my parents. My father Gültekin Yalçıner who encouraged me to concentrate on my study especially when I encountered difficulties. My father believed and wanted for me to have this degree even more than me. My mother Yıldız Yalçıner who helped me to concentrate on completing my study and supporting mentally. My brother Kürşad Yalçıner who is

the one of the best civil engineer for me. I am very depth full to all of them. Without their help, this study would have not been completed.

To My Family

TABLE OF CONTENTS

LIST OF TABLES

LIST OF FIGURES

Chapter 1

INTRODUCTION

1.1 Objective of Thesis

Millions of dollars lost each year because of corrosion in construction industry. Since corrosion has time-dependent effects on both economical and structural safety issues, time-dependent corrosion models may be used to reduce its effects. Developed corrosion models in this thesis mainly provide;

- to predict time-dependent performance levels of corroded RC structures as a function of corrosion rate,
- to combine different corrosion models and illustrates how the integration of different parameters can be used in nonlinear analyses to predict the time-dependent performance level of corroded RC buildings as a function of corrosion rate,
- to have a better idea time decide on strengthening of corroded RC structures,
- to predict bond strength of uncorroded reinforcement bars as function of concrete compressive strengths and concrete cover depths,
- to predict bond strength of corroded reinforcement bars as function of corrosion rates, concrete compressive strengths, concrete cover depths and crack widths,
- to correlate design mass loss according to Faraday's law and actual mass loss as a result of accelerated corrosion method.

In order to achieve these goals, two important points were considered during this thesis as analytical model for the first part and experimental studies for the second part.

For the analytical model of this study, in contrast to previous developed corrosion models and assessment methods, three important combined effects of corrosion (loss in cross sectional area of reinforcement bars, reduction in concrete compressive strength and the bond-slip relationship) were used in structural analyses for both single-degree (SDOF) and multi-degree-of-freedom (MDOF) systems as a function of corrosion rate. Three different case studies were performed to represent the developed model in this study. In the literature it is possible to find similar and/or same formed sentences such that "corrosion affects on structural performance" [(Tuutti; 1980), (Ahmad; 2003), (Akgül et al. 2004), (Li and Melchers; 2006), (Vidal et al., 2007), (Chernin and Val; 2008), (Berto; 2009)]. On the other hand, to the knowledge of the author, up to date, none of the studies defined time-dependent performance levels of corroded RC buildings as a function of corrosion rate through nonlinear incremental dynamic analysis (IDA) procedure. Thus, with this thesis, an important gap in earthquake engineering has been tried to be filled. For the first part of this study, proved and developed corrosion models were used and they have been adapted into performance assessment of RC buildings. Therefore first part of this study addressed to two main issues; first, to find the answer of performance level for RC buildings which are subjected to corrosion as a function of time and secondly to develop a novel model for corroded RC buildings.

With the exception of design and construction faults of RC buildings, the main problem behind corrosion that causes deterioration and economical problems over time is defined as the threshold of corrosion rates (i_{corr}) in terms of the expected

damage using available assessment techniques. While thresholds of passive (negligible), low to moderate, moderate to high and high corrosion rates in some studies (e.g., (McCarter WJ and Vennesland; 2004, Song and Saraswathy; 2007)) have been defined as 0.1 $\mu A/cm^2$, 0.1-0.5 $\mu A/cm^2$, 0.5-1 $\mu A/cm^2$ and greater than 1 $\mu A/cm^2$, respectively. It is also possible to find huge differences in the defined thresholds of corrosion rates in other studies (e.g., Dhir et al.; 1994). Expected damage according to corrosion rates based on previously defined thresholds might be correct only if the loss of the cross sectional area of the reinforcement bars is considered while bond-slip relationships are neglected as a function of the corrosion rate. Moreover, since each structure is unique (i.e., the spacing of the reinforcement bars, the speed of corrosion, the permeability of the concrete, and environmental factors), the expected damage by corrosion rate causes different results in structural performance level when considering the factors above as a function of time. Among these factors, the spacing of reinforcement bars in particular requires major attention during time-dependent performance assessment of existing corroded structures since there are still important difficulties in both our understanding and the modelling of existing structures. The direction and amount of cracks are based on the spacing of reinforcement bars and the volume expansion of rust as a function of corrosion rate. The crack width model of Li et al. (2007) indicated that forming a fracture plane depends largely on the geometry and detailing of the concrete section, such as the concrete cover, location and diameter of the rebar. However, some of the well known and frequently used software programs are still not capable of modelling the exact location and spacing of reinforcement bars by taking into account the crack width due to corrosion during the assessment of existing structures. Therefore, the assumed location and required spacing between reinforcement bars in concrete sections of

corroded RC structures gives underestimated results due to the time-dependent behaviour of corrosion. In this thesis, by performing three different case studies for the following chapters, the importance of spacing of reinforcement bars during assessment of corroded RC structures were also defined. Thus, in this study effect of corrosion on the structural performance levels were examined as a function of time by combining different corrosion models (i.e., bond-slip and crack width) in order to integrate in structural performance assessment. Corrosion rate and its effects on structural performance analysis were studied as a function of time. Obtained time-dependent corrosion results were discussed on time-dependent performance level of the structure by using IDA under action of different scales of ground motion records.

In the second part of this thesis, series of experimental studies were performed to predict the ultimate bond strength of corroded and uncorroded specimens. Although considerable research has been conducted to predict concrete bond strengths, contradictions are found in the literature. In particular, the degradation of bond strength due to corrosion and in concrete mixtures of different strength levels, taking into account the effect of differences in the concrete cover depths used, requires further investigation. Moreover, the available models (e.g., (Cabrera; 1996, Auyeung et al.; 2000, Chung et al; 2008, Lee et al.; 2002) do not provide for the prediction of the ultimate bond strength as a function of a given concrete cover, crack width and concrete strength. Beside these, mainly the available models were developed by performing one concrete strength level and concrete cover depth where the reinforcement bars were only placed at the centres of the concrete samples. The present study further extends these studies to evaluate the influence of concrete covers of three different depths (i.e., c = 15 mm, 30 mm and 45 mm) and two concrete strength levels (i.e., f_c' = 23 MPa and f_c ' = 51 MPa) as upper and lower

bound on the bond strength and bond-slip relationships for different corrosion levels. The effects of different concrete covers and compressive strengths on corrosion rate were investigated. In this thesis, the developed new bond strength models provide to monitor the bond strength for different concrete strength levels, cracked or uncracked concrete conditions with different c/D ratios. As it is well known, theoretically mass losses due to corrosion can be predicted based on Faraday's law. However, Faraday developed his model as the reinforcement bars were directly immersed in the tank filled with water. In another word, Faraday's law assumed that corrosion starts as soon as electrical power was applied. In the case of reinforcement bars in concrete specimens, an amount of time and energy is needed to initiate the corrosion. Thus, it is inevitable to have differences between the measured actual and theoretically estimated corrosion mass losses based on Faraday's law. Therefore, another objective of this study is to determine a correlation between the actual and theoretically estimated mass losses that can be used for further studies.

1.2 Background

1.2.1 Corrosion

Corrosion is defined as the degradation of a metal by an electrochemical reaction with its environment (Uhlig, 1971). Once the passive layer has been broken down as a consequence of chloride ingress, the reinforcement can start to rust (corrode) if there is the right balance of moisture and oxygen. Corrosion of steel occurs because of the electro-chemical action which is usually encountered when two dissimilar metals are in electrical contact in the presence of moisture and oxygen. However, the same process takes place in steel alone because of differences in the electrochemical potential on the surface, which forms anodic and cathodic regions, connected by the

electrolyte in the form of the salt solution in the hydrated cement. The positively charged ferrous ions Fe^{2+} at the anode pass into solution while the negatively charged free electrons e^- pass along the steel into the cathode, where they are absorbed by the constituents of the electrolyte and combine with water and oxygen to form hydroxyl ions $(OH)^-$. These then combine with the ferrous ions to form ferric hydroxide and this is converted by further oxidation to rust (Ferreira, 2004). The chemical reaction of corrosion can be written as:

$$Fe \rightarrow Fe^{2+} + 2e^- \quad \text{(anodic reaction)}$$

$$4e^- + O_2 + 2H_2O \rightarrow 4(OH)^- \quad \text{(cathodic reaction)}$$

$$Fe^{2+} + 2(OH)^- \rightarrow Fe(OH)_2 \quad \text{(ferrous hydroxide)}$$

$$4Fe(OH)_2 + 2H_2O + O_2 \rightarrow 4Fe(OH)_3 \quad \text{(ferric hydroxide)}$$

As it is shown in these expressions, ferrous hydroxide forms as the $2Fe^{++}$ ions at the anode combine with the hydroxide $(4(OH)^-)$ ions flowing from the cathode. In the presence of oxygen and moisture, the ferrous hydroxide (2Fe (OH)2) converts to ferric oxide ($Fe_2O_3H_2O$) rust.

The background of corrosion needs to be defined by explaining the behaviour of corrosion. Two time periods namely called Initiation and Propagation periods plays an important role to define this behaviour.

- *Initiation period* can be defined as required time for chloride ion surrounding reinforcement bars to reach the critical level of corrosion.
- Once the protective layer around the reinforcement bars broken, moisture and oxygen take a place in the process of corrosion. With time, corrosion products start to occupy more space than the original reinforcement bars which cause expansive stresses. Due to volumetric expansion inside of concrete, cracking of concrete cover and spalling occur. The required time

which result in deterioration of concrete is known as the *Propagation period*. The concept of Initiation and Propagation periods can be illustrated by Tuutti's (1982) model shown in Figure 1.1.

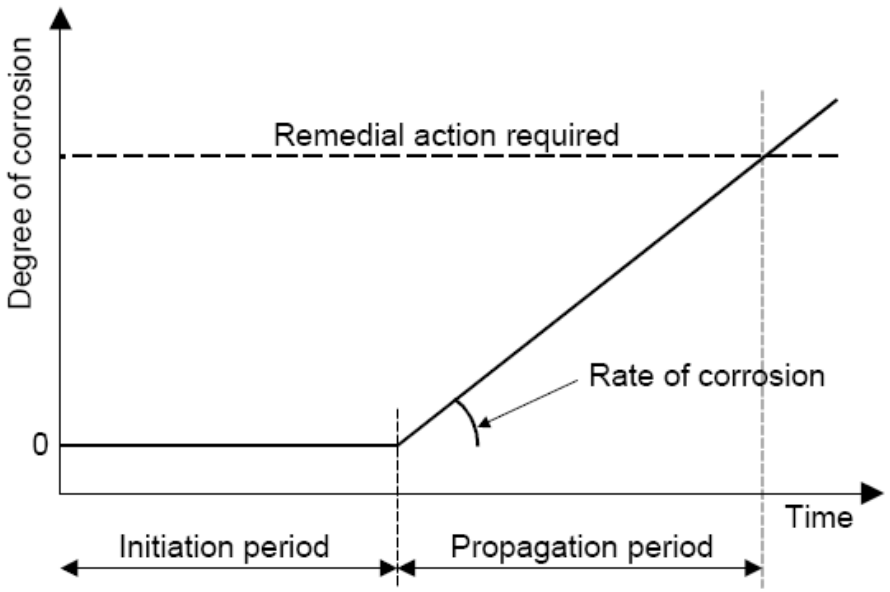

Figure 1.1: The corrosion process (Tuutti, 1982)

1.3. Effects of Corrosion

Two major effects of corrosion might be taken into account for construction industry. One of the major effects of corrosion is the economic impact on the construction industry. More important than the effect of corrosion on economy, structural safety plays an important role for RC buildings during earthquakes. Following subsections give brief information on the effect of corrosion.

1.3.1 Effect on Economy

Corrosion has significant economic effects on construction industry which might break the life cycle of a project. Different studies showed that the cost of damage due to corrosion took place in government reports. A study done by the Centre for Concrete Construction (BRE, 2001) noted that the predicted cost of corrosion damage to concrete was 750 million pounds in the UK, and the annual direct

estimated loss due to corrosion according to another study (Shibata; 2002) was 3937.69 billion yen for the year 1997 in Japan. Another study done by Brongers (2006) showed that the cost of corrosion in construction industry is $137.9 billion/year in U.S. Thus, the effects of corrosion on the construction industry require the development of different methods to analyze the cost of corrosion given the related maintenance and repairs, such as the well known model developed by Uhlig (1950).

1.3.2 Structural Safety

The cost of the corrosion is important for construction industry. However, cost is only one issue. Safety is the prime issue. A structure that is originally designed to meet code specifications may not have the same margin of safety once the structure has undergone significant corrosion (Choe et al., 2008). As the reinforcement corrodes, there is potential for cracking, spalling of concrete, reduction in reinforcement cross-section and bond strength between concrete and reinforcement bars. As it is well known, reinforced concrete structures have a limited service life. As much as reinforcement bars has been protected against to corrosion, the service life of the structure can be increased. From structural safety point of view corrosion, it is important to predict the service life of corroded RC structures to prevent premature damage during earthquakes or decide on correct time of repairing and strengthening of corroded structures. Next subsections describe the effects of three major parameters on structural safety that was considered in nonlinear seismic performance assessment of case studies in Chapter 3.

1.3.2.1 Loss in Cross Sectional Area of Reinforcement Bars

For corrosion to commence, the protective film on the steel-concrete interface must be broken or chemically dissolved (Hoar 1967). With time, effective cross-

sectional area of reinforcement decreases as a function of corrosion rate. Thus, the storage energy capacity of a section decreases by losing ductility of reinforcement bars with reduced energy dissipation through inelastic behaviour. As long as this energy is mostly dissipated by yielding of the reinforcement, the concrete is less loaded and thus the structure's integrity is ensured (Apostolopoulos and Pasialis, 2010). Due to loss in cross sectional area, reinforcement bars might buckle before reaching its yield capacity, thus load-carrying capacity of the structure reduces. Moreover, stiffness degradation due to premature yielding of reinforcement bars cause to sudden load transfer to the other structural members.

1.3.2.2 Bond-slip Relationships

Reduction in performance level of RC structures does not only depend on losing cross sectional area of reinforcement bars. For reliable structural analyses type of reinforcements such as ribbed or smooth bars need to be considered in nonlinear structural analyses. In macro level, dimensional loss of lugs of ribbed bars directly affects the friction and adhesion between reinforcement and concrete where the bond mechanism can be defined as interaction between reinforcement and concrete. Degradation of bond strength causes to increase global drift ratio of RC structures that calculation of associated roof drift ratios are determinative parameter on measurement of time-dependent performance level of RC structures. Developed bond-slip model by Alsiwat and Saatcioglu (1992) indicates that results in member end rotations due to slip must be considered in inelastic analyses, if reliable analytical predictions are sought. Another experimental study was done by Sezen (2002) to predict anchorage slip for four columns, and indicated that in some cases, the deformation due to reinforcement slip may be as large as column flexural deformations. Sezen and Moehle (2006) also in an other study investigated these four

columns and indicated that, slip deformations contributed 25 to 40 % of the total lateral displacement. Therefore, for present study slip deformation as a consequence of corrosion effect is also considered to be a matter of serious academic interest to predict time-dependent performance level of assessed RC building.

1.3.2.3 Reduction in Concrete Strength

While cross sectional area of reinforcement decreases, corrosion causes to increase the corrosion product form as a function of corrosion rate. As it is known, the volume of corrosion rust is generally 2 to 4 times larger than the volume of original reinforcement (Bažant 1979). The porous zone around the reinforcing bars is filled with this corrosion product which results in internal pressure on the surrounding concrete. As a consequence of volumetric expansion, concrete strength reduces as a function of crack width where loss of ductility of the columns is inevitable under seismic loading. Reduction in concrete compressive strength due to different parameters (i.e., sea water, different chloride content) experimentally studied by many authors. For instance, an experimental test was done by Liu et al. (2002) to examine reduction in concrete compressive strength by soaking specimens for 180 days into two different seawaters (live and dead). In that study recorded reduction in concrete compressive strength varied from 1.51% to 26.60% of sound sample. Another experimental study was done by Coronelli and Gambarova (2004) to investigate the ultimate bond strength and reduction in concrete compressive strength of corroded reinforcement bars with different depth of corrosion attacks. In that study reduction of concrete compressive strength varied from 38% to 45% due to corrosion. Due to the volumetric expansion in the steel bars causes cracking and spalling of concrete which would indicate the loss of performance level of RC structures. Figure 1.2 shows three corroded RC structures exposed to salt attack with

a distance from seaside are 50, 130 and 150 meters in North Cyprus, respectively. As shown in Figure 1.2, serious strength degradation occurred by volume expansion of corrosion rust after construction. Due to degradation of concrete members, energy absorption of damaged columns decrease as a function of corrosion rate that may result in brittle failure of columns.

(a)

(b)

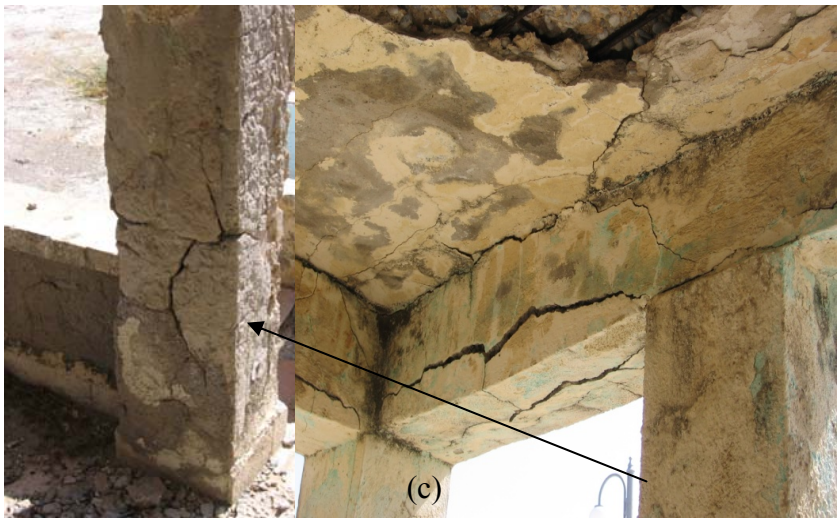

Figure 1. 2: Strength degradation due to corrosion: (a) Apostolo andreas monastery in Karpaz, 1985, (b) Corrosion rust in 35 years after construction, and (c) An old constructed RC building in Palmbeach.

The products of steel corrosion create volumetric expansion in the steel bars of the structure causing extremely high tensile forces within the concrete. Since the tensile strength of concrete is relatively low in comparison to its compressive strength, it is susceptible to the formation of cracks from the bar to the surface (inclined cracking) or between the bars. The cracks allow oxygen and moisture to travel directly to the bar at a faster rate which in turn increases the rate of corrosion. This eventually leads to spalling of the concrete from the surface of the structure (Capozucca; 1995).

Chapter 2

LITERATURE REVIEW

2.1 Introduction

When the column is subjected to a moment, the longitudinal reinforcement at the end of the column will extend, or slip. Therefore, it is important to examine the effect of slip on the performance levels of the structure either they are corroded or non-corroded. This chapter gives an overview of bond-slip models for both corroded and non-corroded structures. Then, three case studies in Chapter 3; a SDOF system, a MDOF system and a three dimensional single storey building model were performed to predict the time-dependent seismic performance levels of corroded reinforced concrete structures by modifying the developed bond-slip relationships of non-corroded structures by Sezen and Setzler (2008) in the following subsections. In those case studies, two different methods were also applied to ensure the effect of slippage of reinforcement bars (e.g., modifying plastic hinge properties and/or adding the displacement due to slippage of reinforcement bars directly to the top displacement of the structure obtained by lateral loading).

2.2 Slip Deformation Models of Non-Corroded Structures

Slippage of the reinforcing bars in the anchoring concrete causes rotation of the column. This increased rotation causes greater lateral drift of columns under lateral loads, and it is therefore important to account for reinforcement slip when determining the response of a RC structure to lateral loading. If the moment-slip

rotation relationship can be determined for a column, then the lateral displacement of the top of the column due to slip, Δ_s, can easily be calculated as using equation 1.1.

$$\Delta_s = \theta_s . L \tag{1.1}$$

where θ_s is the slip rotation at the column end (or the average slip rotation at the two ends for a cantilever column) and L is the height of the column. In the literature, it is possible to find different models for the calculation of slip. Descriptions of several models that were investigated in this study are examined below.

2.2.1 Method of Otani and Sozen (1972)

In 1972 a model for bar slip by Otani and Sozen (1972) was developed. Figure 2.1 shows the phases of developed model by Otani and Sozen (1972).

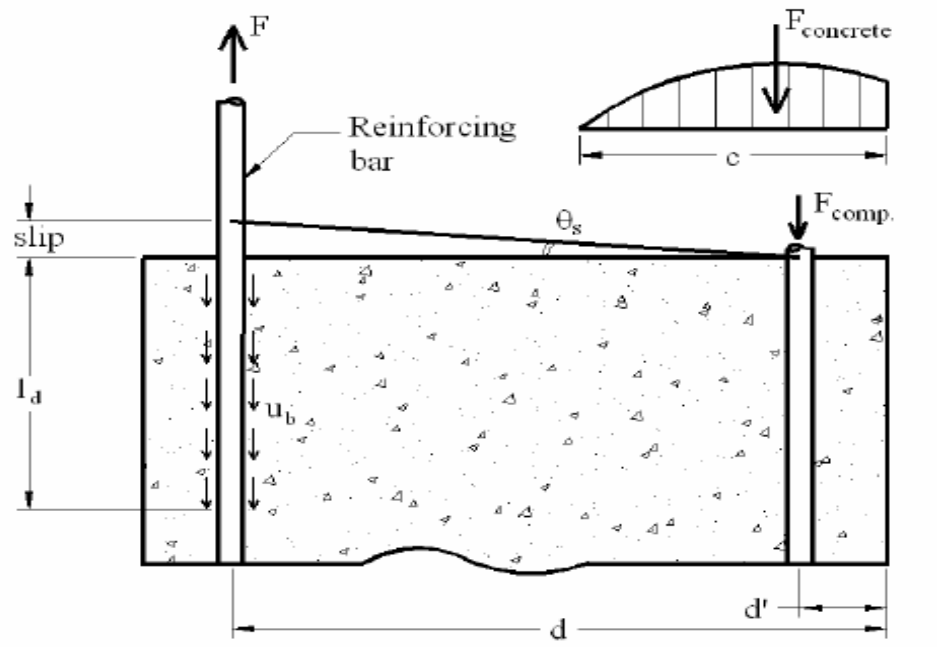

Figure 2.1: Developed slip model by Otani and Sozen (1972).

Otani and Sozen (1972) in their model proposed to calculate the slip rotation by assuming an average uniform bond stress by given equation 2.1:

$$u_b = 6.5\sqrt{f_c'} \tag{2.1}$$

where u_b *is the* uniform bond stress, f_c' is the concrete compressive strength. Otani and Sozen (1972) assumed a linear relationship between steel stress and bending moment at yield to determine the slip rotation as `` $\frac{f_S}{f_y} = \frac{M}{M_y}$ ``, where f_y and M_y are the steel stress and bending moment at yield. The rotation due to slip was defined by the given equation 2.2:

$$\theta_S = \frac{slip}{d - d`} \tag{2.2}$$

where "*slip"* is the slip in the tension bars, and *d* and *d'* are the distances to the centroid of the tension and compression steel from the extreme compression fiber, respectively.

2.2.2 Method of Alsiwat and Saatcioglu (1992)

Alsiwat and Saatcioglu (1992) proposed a model that uses a bi-uniform bond stress. In their model, the development length was divided into four regions, based on the state of the steel stress-strain relationship. Figure 2.2 indicates the proposed model by Alsiwat and Saatcioglu (1992) to predict slip deformation of reinforcing bars embedded in concrete using a stepped bond stress distribution. In Figure 2.2, an analytical model consists of four regions, an elastic region with length L_e, a yield plateau with length L_{yp}, a strain hardening region with length L_{sh} and pull-out cone region with length L_{pc}. In that model, elastic bond stress (u_e) was adopted from ACI Committee 408 (1979) and it can be calculated by the given equation 2.3:

$$u_e = u_{\text{ACI}} = \frac{f_y d_b}{4 l_d} \text{MPa} \tag{2.3}$$

where d_b is the bar diameter (mm).

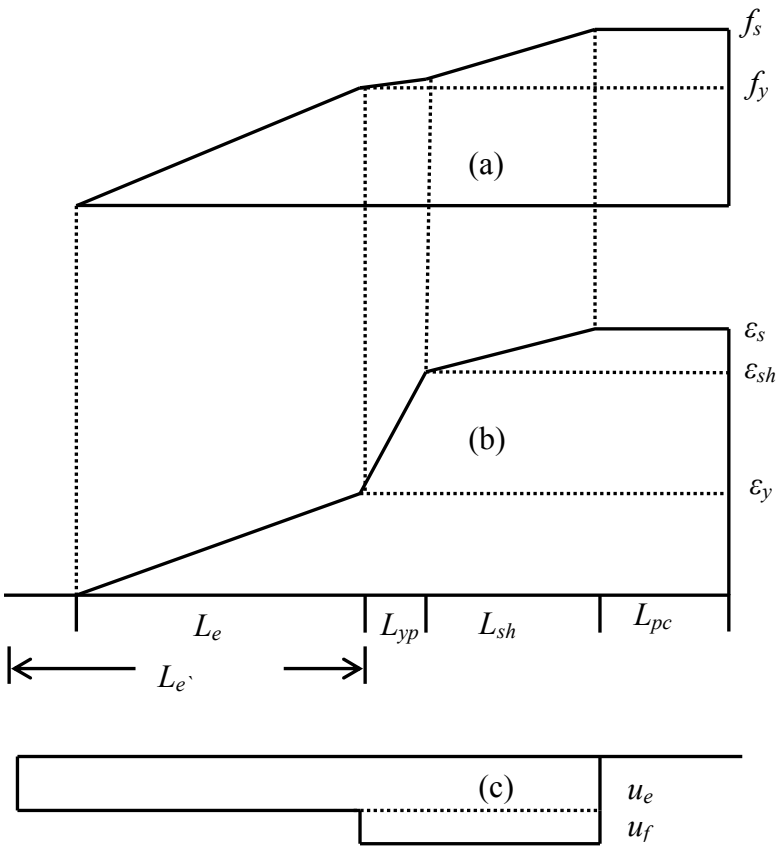

Figure 2. 2: (a) Stress Distribution; (b) Strain Distribution; (c) Bond Stress between concrete and steel.

Development length (l_d) was suggested to be calculated by using equation 2.4, where A_b is the bar area (mm^2), and it was suggested that coefficient K is equal to 3 times of the bar diameter for most practical applications.

$$l_d = \frac{440A_b}{K\sqrt{f_c'}}\frac{f_y}{400} \geq 300mm \tag{2.4}$$

However, if bar extension is limited to elastic range, Alsiwat and Saatcioglu (1992) suggested an analytical equation to calculate coefficient K for elastic bond stress. In that study, the length of the elastic region was determined from equilibrium of forces by the given equation 2.5:

$$L_e = \frac{f_s d_b}{4u_e} \tag{2.5}$$

The length of the yield plateau was obtained from equilibrium of forces by Alsiwat and Saatcioglu (1992) by the given equation 2.6:

$$L_{yp} = \frac{\Delta f_s d_b}{4u_f} \tag{2.6}$$

where Δf_s is the incremental stress. For strain hardening region, equation 2.6 was suggested by Alsiwat and Saatcioglu (1992)**.** Different then yield plateau, incremental stress is equal to difference in steel stress between the current load stage and the beginning of the strain-hardening range. In figure 2.2 (b), extension of reinforcement bar was suggested to be calculated by integrating the strains over the development length.

$$\delta_{ext} = \varepsilon_s L_{pc} + 0.5(\varepsilon_s + \varepsilon_{sh}) L_{sh} + 0.5(\varepsilon_{sh} + \varepsilon_y) L_{yp} + 0.5(\varepsilon_y) L_e \tag{2.7}$$

Alsiwat and Saatcioglu (1992) suggested that once extension of reinforcement is calculated, slip rotation can be calculated by using moment-curvature relationships by given equation 2.8:

$$\theta_s = \frac{\delta_{ext}}{d - c} \tag{2.8}$$

where d is the section depth, c is neutral axis of assessed section. Thus, lateral additional displacement due to slip (Δ_s) can be calculated by multiplying slip rotation along the height of the column by using equation 1.1. Developed model by Alsiwat and Saatcioglu (1992) has not been performed for corroded reinforced concrete structures. In inelastic behaviour of the structures, when the bond of the

reinforcement bars is considered as a function of corrosion rate instead of assumed uniform bond stress by Alsiwat and Saatcioglu (1992), developed model by Alsiwat and Saatcioglu (1992) can be also used for corroded reinforced concrete structures. For instance, frictional bond stress (u_f) of plain bars which was suggested by BS 110 (1985) can be easily adopted to calculate the length of the regions in Figure 2.2.

$$u_f = \beta\sqrt{f_c'} \tag{2.9}$$

where β is the bond coefficient.

2.2.3 Method of Lehman and Moehle (2000)

A bi-uniform bond stress was assumed by Lehman and Moehle (2000) to calculate the bar slips. Developed model by Lehman and Moehle (2000) mainly consisted of two regions. Figure 2.3 shows the developed model by Lehman and Moehle (2000).

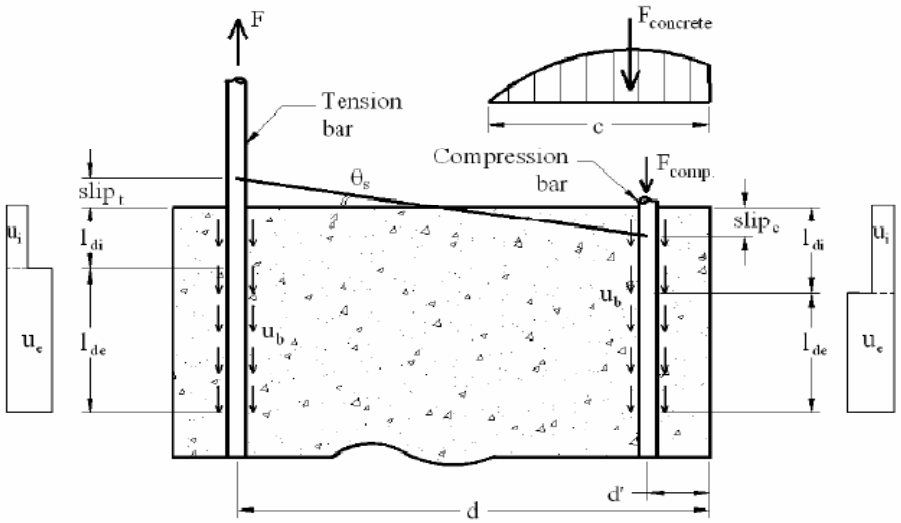

Figure 2. 3: Bond stress-slip relationships by Lehman and Moehle (2000).

For steel stresses less than f_y, a uniform elastic ($u_e = 12\sqrt{f_c`}$) bond stress was used. After yielding, $u_e = 6\sqrt{f_c`}$ was used for the inelastic bond stress. The elastic development length was suggested to be calculated from required development

length, where f_s was limited by the yield stress, and the slip was calculated by given equation 2.10:

$$slip = \frac{\varepsilon_s f_s d_b}{8u_e} \text{ for } \varepsilon_S \leq \varepsilon_y \tag{2.10}$$

Based on the equilibrium of forces, inelastic development length when the steel stress exceeds f_y was calculated by given equation 2.11:

$$l_{di} = \frac{(f_S - f_y)d_b}{4_{ui}} \tag{2.11}$$

As the integral of the strain distribution, slip was suggested to be calculated by given equation 2.12:

$$slip = \frac{\varepsilon_y l_{de}}{2} + \frac{(\varepsilon_S + \varepsilon_y)l_{di}}{2} = \frac{\varepsilon_y f_y d_b}{8u_e} + \frac{(\varepsilon_S + \varepsilon_y)(f_S - f_y)}{8_{ui}} \quad \text{for } \varepsilon_S > \varepsilon_y \tag{2.12}$$

Thus, the rotation of a section due to slip was defined by given equation 2.13:

$$\theta s = \frac{slip_t - slip_c}{d - d`} \tag{2.13}$$

where $slip_t$ and $slip_c$ are the values of bar slip in the tension and compression steel, respectively.

2.2.4 Method of Eligehausen et al. (1983)

One hundred twenty five pullout specimens were tested to determine a bond stress-slip relationship by Eligehausen et al. (1983). The developed model by Eligehausen et al. (1983) is shown in Figure 2.8.

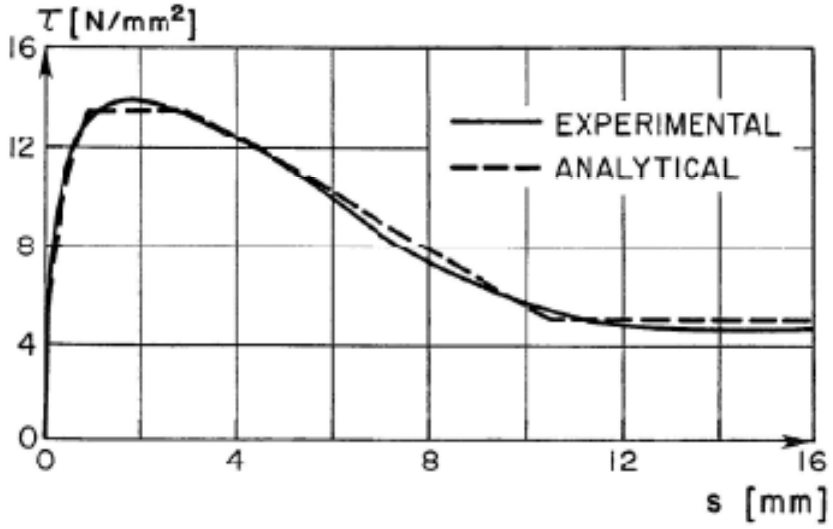

Figure 2.4: Bond stress-slip relationships by Eligehausen et al. (1983)

Developed model by Eligehausen et al. (1983) consisted of four regions and following equations were defined for those regions by Eligehausen et al. (1983).

for $S \le S_1$, $\lambda = \lambda_1 \left(\frac{S}{S_1} \right)^{\alpha}$ (2.14)

for $S_1 \le S \le S_2$, $\lambda = \lambda_1$ (2.15)

for $S_2 \le S \le S_3$, $\lambda = \lambda_1 - \frac{(S - S_2)}{(S_3 - S_2)} (\lambda_1 - \lambda_3)$ (2.16)

for $S \ge S_3$, $\lambda = \lambda_3$ (2.17)

where S is the slip and λ is the bond stress. For the bars tested by Eligehausen et al. (1983), the following values were chosen to define the bond stress-slip curve:

S_1=1.0 mm λ_1=13.5 MPa

S_2=3.0 mm λ_2=5.0 MPa

S_3=10.5 mm α=0.4

2.2.5 Method of Sezen and Setzler (2008)

In this study, recently developed bond-slip model by Sezen and Setzler (2008) was used to perform the case studies in Chapter 3. Additional lateral displacement due to slip as a consequence of corrosion effect was calculated to predict the time-dependent seismic performance levels. The model of Sezen and Setzler (2008) compared with five other analytical models proposed by other researchers (e.g., Otani and Sozen (1972); Eligehausen et al. (1983); Hawkins et al. (1987); Alsiwat and Saatcioglu (1992); Lehman and Moehle (2000)) and experimental results (e.g., Saatcioglu et al. (1992); Lehman and Moehle (2000)). Basically, Sezen and Setzler (2008) assumed a value of elastic uniform bond stress (u_b) for elastic steel stresses, and inelastic uniform bond stress (u'_b) for stresses greater than the yield stress. Model developed by Sezen and Setzler (2008) proposed to calculate slip rotation (θ_s) by using 2.18 and 2.19:

$$\theta_S = \frac{\varepsilon_S f_S d_b}{8u_b(d-c)} \quad \text{for } \varepsilon_S \le \varepsilon_y \tag{2.18}$$

$$\theta_S = \frac{d_b}{8u_b(d-c)}(\varepsilon_y f_y + 2(\varepsilon_S + \varepsilon_y)(f_S - f_y)) \quad \text{for } \varepsilon_S > \varepsilon_y \tag{2.19}$$

where d is the section depth and c is the neutral axis depth. As shown in equations 2.18 and 2.19, slip rotation is dependent on material properties. Since behaviour of reinforcing bars (i.e., strain and stress in reinforcing bars) and section capacity change as a function of time due to corrosion effect, additional displacement due to slip can be also calculated as a function of corrosion rate for different time periods. For present study, in order to predict the slip rotation as a consequence of corrosion effect, Stanish et al. (1999) bond stress model is adopted to calculate the bond stress

as a function of corrosion level and concrete compressive strength instead of assumming uniform bond stress by Sezen and Setzler (2008) in order to predict time-dependent slip rotation as a consequence of corrosion effect. The model developed by Stanish et al. (1999) to predict bond stress is expressed by given equation 2.20:

$$\frac{u_b}{\sqrt{f'_c}} = 0.63 - 0.041x \tag{2.20}$$

where x is the percent of mass loss of steel bar. By using time-dependent moment-curvature relationships as a consequence of corrosion effect, additional lateral displacement due to slip can be calculated by multiplying slip rotation along the height (L) of the column by using equation 1.1. If the distribution of curvatures along the height of the column for a given lateral load and corresponding linear moment diagram are known, first top displacement (Δ_1) of the structure can be obtained by integrating area under the curvature diagram to find rotation, and compute the moment of the area. By summing up additional displacement due to slip (Δ_s) and the first obtained top displacement (Δ_1) under lateral loading, time-dependent total lateral top displacement (Δ_t) of the structure can be obtained. Therefore, for present study, time-dependent total lateral top displacement of the SDOF frame (first case study) is expressed by equation 2.21 for two of the performed case studies in Chapter 3.

$$\Delta_t = \Delta_1 + \Delta_s \tag{2.21}$$

For other case studies in Chapter 3, different then the equation 2.21, the effect of slip displacement was ensured by modifying the plastic hinge properties.

2.3 Bond-slip Relationships of Corroded Members

2.3.1 Al-Sulaimani et al. (1990)

The pullout tests were performed on concrete cube specimens having 150 mm per side. Three different size of reinforcement bars (10, 14 and 20 mm) were centrally embedded in concrete specimens. 40 mm embedment length was chosen to ensure the bond failure. Concrete specimens were prepared from a concrete mixture with a *w/c* ratio of 0.55 having a 28 day average concrete compressive strength of 30 MPa. The corrosion percent was varied from 0% for control specimens to 7.8% for other specimens. The ultimate bond strengths have been reported for pre cracking, cracking and post cracking corrosion stages and as a function of percent corrosion.

2.3.2 Cabrera (1996)

The pullout tests were conducted on 150 mm concrete cube specimens having 12 mm diameter of reinforcement bars which were centrally embedded in the concrete specimens. 40 mm embedment length was chosen to ensure the bond-slip failure. Concrete specimens were prepared from a concrete mixture with a *w/c* ratio of 0.55. The 28-day concrete strength was not reported. In order to accelerate the corrosion process, sodium chloride was added to the concrete mixture. Before accelerated corrosion process, concrete specimens were partially immersed in a 5% sodium chloride solution. The corrosion percent was varied from 0% for control specimens to 12.6% for other specimens. The bond strengths have been reported as a function of percent corrosion. Cabrera (1996) proposed the bond strength for normal Portland cement concrete as a function of corrosion level as follows.

$$\tau = 23.478 - 1.313\, C_L \text{ (MPa).} \tag{2.23}$$

2.3.3 Auyeung et al. (2000)

Pullout tests were conducted on concrete prisms of size 175mm×175mm×350 mm having 19 mm diameter of reinforcement bars which were centrally embedded in the concrete specimen. The average compressive strength of concrete was 28 MPa. In order to accelerate the corrosion process, 3% chloride by weight of cement was added to the concrete mixture. Before accelerated corrosion process, concrete specimens were immersed in a 3% sodium chloride solution for three days. The corrosion percent was varied from 0% for control specimens to 5.91% for other specimens. Bond strengths and normalized bond strengths have been reported as a function of percent mass loss.

$$\tau = 8.0048 e^{(-0.3251 C_L)} \text{ (MPa)} \tag{2.24}$$

2.3.4 Lee et al. (2002)

Pullout tests were performed on cubic concrete specimens of 8D per side wherein 'D' is the diameter of reinforcing bar. Different than previous mentioned studies, Lee et al. (2002) used three different concrete mixture having *w/c* ratios of 0.45, 0.55 and 0.65. The reported 28 days concrete compressive strength levels were 42.1 MPa, 33.0 MPa and 24.7 MPa for used three *w/c* ratios, respectively. The single size of reinforcement bar was used where they centrally embedded in the concrete specimens for three different concrete cover depths. In that study it was assumed that at the time of cracking of concrete was occurred at 3% of corrosion level. The corrosion percent was varied from 0% for control specimens to 30% for other specimens. Maximum bond strengths have been reported as a function of percent

corrosion for different concrete strengths. Lee et al. (2002) proposed the bond strength as a function of corrosion level as follow:

$$\tau = 5.21e^{(-0.0561C_L)} \text{ MPa} \tag{2.25}$$

2.3.5 Fang et al. (2004)

Pullout tests were performed on concrete specimens of size 140mm×140mm×180 mm. 20 mm diameter of reinforcement bars were centrally placed in concrete specimens. The 28-day average compressive strength for concrete was 52.1 MPa. The corrosion percent was varied from 0% for control specimens to 9% for other specimens. The bond strengths have been reported as a function of percent corrosion for both smooth and deformed bars, with and without stirrups.

2.3.6 Chung et al. (2008)

Another novel equation for bond strength prediction was developed by Chung et al. (2008). Here, pullout tests were conducted on concrete prisms prepared from a concrete mixture with a *w*/*c* ratio of 0.58 having a 28 day average concrete compressive strength of 28.3 MPa. One concrete cover depth was considered, and the reinforcement bars were embedded in the centres of the concrete prisms. The corrosion percentage was varied from 0% to 10%. In contrast to previous studies, Chung et al. (2008) corroded the reinforcement bars before and after casting the concrete. The bond strength model has been reported as a function of percent corrosion where the bond strength assumed constant up to 2% of corrosion rate.

$$\tau = 24.7C_L^{-0.55} \text{ MPa for } C_L > 2.0\ \% \tag{2.27}$$

Chapter 3

DEVELOPED CORROSION MODEL TO PREDICT REDUCTION IN CONCRETE STRENGTH AS A FUNCTION OF CORROSION RATE AND MATERIAL MODELLING

3.1 Introduction

Previous chapters of this thesis (Chapter 1 and Chapter 2) presented the background information of Chapter 3. In this chapter, a new model to predict the reduction in concrete compressive strength as a function of corrosion rate was developed. Three combined corrosion parameters (i.e., loss of the cross sectional area of reinforcement bars, reduction of the concrete strength, and additional displacement due to slippage of reinfocement) as a consequence of corrosion effects were calculated as a function of the corrosion rate. A methodology was presented how combined corrosion models can be used in seismic analysis. For doing this, three case studies; a single-degree-of-freedom system, a multi-degree-of-freedom system and a three dimensional single storey building model were performed by using incremental dynamic analyses to predict time-dependent seismic performance levels of the assessed frames as a consequence of corrosion effects for five different time periods (existing, 25, 50, 75 and 100 years).

3.2 Effects of Corrosion on Global Behaviour of Structures

Corrosion is a long term process resulting in deterioration on global behaviour of RC structures. In order to investigate the effects of corrosion, different corrosion models are available for structural analyses. Developed models to predict corrosion rate (e.g., Morinaga 1988, Gulikers 2005, Ghods et al., 2007), time to cracking models (e.g., Liu and Weyers 1998, El Maaddawy and Soudki 2007), crack width models (e.g., Li et al., 2006, Li et al., 2005, Pantazopoulou and Papoulia 2001, Andrade et al., 1993), reliability-based failure models (e.g., Vu and Stewart 2000, Li et al., 2005 (b), Li and Melchers 2006, Thoft 1998), bond-slip relationships (e.g., Mangat and Elgarf 1999, Lundgren 2007, Vandewalle and Mortelmans 1988, Ouglova et al., 2008) are generally considered in studies of many authors. Firstly, these separately studied and developed models are needed to be used in structural analyses as a group model to achieve more accurate results on global structural behaviour.

Effects of corrosion start to damage from single structural member to global structural behaviour. Because of the complexities of the corrosion, it was preferred to perform single structural members rather than focusing on global structural behaviour. Stewart (2004) examined pitting corrosion on structural reliability for singly reinforced simply supported RC beam in flexure for different corrosion rate. A long term 17 years of RC beam under service loading is studied by Vidal et al. (2007) to define structural performance in terms of serviceability by cracking due to chloride attack of exposing salt to the beams. The relationship between corrosion rate and loss of structural serviceability from measurements of bond strength, cracking and deflection of concrete beams is studied by Cabrera (1996). It is not difficult to indicate that it is an overestimate to deduce the global behaviour of RC structures

from the single degradations of structural members. Moreover, proposed models were generally limited by RC beams whilst behaviour and effects of columns on global structure are more important during earthquakes since columns failure may lead to structural failures and result in total building collapses. Therefore, it would be more accurate to perform combined different corrosion models on the global structural behaviour of RC buildings instead of performing single structural members. Thus, in this thesis three combined major effects of corrosion was the interest to predict time-dependent performance level of a corroded RC building as a function of corrosion rate by using IDA for global structural behaviour.

3.2.1 Modifications to Model of Vecchio and Collins (1986) to Predict Reduction in Concrete Strength as a Function of Corrosion Rate

In order to predict the reduction in concrete strength as a function time, corrosion rate needs to be predicted. In this thesis, for the first case study corrosion rate was assumed while it was calculated from experimental study for the second and third case studies. Any available models in the literature can be used to predict corrosion rate and adopted for the proposed methodology here. For instance, one of the well known corrosion rate models was developed by Morinaga (1988). This model considers the rate of reinforcing steel due to carbonation for different environmental factors. Using Laplace's equation for electrical potential, a nonlinear finite element model was developed by Isgor and Razaqpur (2006). Ghods et al. (2007) improved the previously developed model by Isgor and Razaqpur (2006) by considering environmental factors that were or were not dependent on half-cell measurements. In order to demonstrate the integration of these models for the prediction of reduction in concrete strength, developed model Morinaga (1988) is used for the first case study. Developed model by Morinaga (1988) consider corrosion rate of reinforcing steel

due to carbonation by considering environmental factors. The developed expression to estimate corrosion rate is given by the following equation:

$$i_{corr,Cl} = 2.59 - 0.05.X_1 - 6.89.X_2 - 22.87X_3 - 0.99X_4 + 0.14X_5 + 0.51X_6 + 0.01X_7 + 60.18X_8 + 3.36X_9 + 7.32X_{10} \quad (3.1)$$

where i_{corr} is the rate of corrosion in term of 10^{-4}g/cm^2/year, X_1 is temperature (^{0}C); X_2 is corrected ambient relative humidity (X_2=(RH-45)/100); X_3 is percentage of relative atmospheric oxygen concentration, X_4 is salt content as percentage of NaCl by weight of mixing water; X_5 is interaction between X_1 and X_2; X_6 is interaction between X_1 and X_3; X_7 is interaction between X_1 and X_4; X_8 is interaction between X_2 and X_3; X_9 is interaction between X_2 and X_4; X_{10} is interaction between X_3 and X_4. The products of steel corrosion create volumetric expansion in the steel bars cause to cracks. The cracks let to absorb oxygen and moisture to the surface of reinforcement which increases the rate of corrosion as a function of time. The corrosion products occupy a larger volume and these induce stresses in the concrete cover concrete resulting in cracking, delamination and spalling [(Revathy et al. 2009)]. Thus, concrete elements begin to damage due to corrosion. Due to this damage, concrete strength may decrease and this factor is also needed to be considered in time-dependent performance assessment of RC buildings. A model developed by Vecchio and Collins (1986), predicts the reduction in concrete strength based on total crack width for a given corrosion level. According to this model, reduction in concrete strength can be calculated by following given equation 3.2:

$$f_c^* = \frac{f_c}{1 + K\varepsilon_1 / \varepsilon_{co}} \quad (3.2)$$

where f_c^* is the reduced concrete strength, K is the coefficient related to bar roughness and diameter (for medium-diameter ribbed bars a value K=0.1 has been proposed by Cape 1999); ε_{co} the represents strain at the peak compressive stress, and ε_1 the is average tensile strain in the cracked concrete at right angles to the direction of the applied compression that can be calculated by following given equation 3.3:

$$\varepsilon_1 = \frac{b_f - b_0}{b_0} \tag{3.3}$$

where b_f is the width increased by corrosion cracking, b_0 is the section width in the virgin state, and approximation of the increase of the width can be calculated as given equation 3.4:

$$b_f - b_0 = n_{bars} w_{cr} \tag{3.4}$$

where n_{bars} is the number of the bars in the top layer (compressed bars); and w_{cr} is total crack width for a given corrosion level. The proposed model by Vecchio and Collins (1986) is applicable in order to calculate the strength reduction in concrete due to corrosion. However, the proposed model has a disadvantage to predict the strength reduction in concrete as a function of time, in another world proposed model is not time dependent. The study done by Coronelli and Gambarova (2004) proposed to integrate crack width model of Molina et al. (1993) in to proposed model by Vecchio and Collins (1986) in order to calculate reduction in concrete strength, and it is assumed that ratio of volumetric expansion of the oxides with respect to the virgin material is equal to 2, thus diameter of each bar is assumed to increase two times of the depth of the corrosion attack, and w_{cr} is calculated from proposed model by Molina et al. (1993) as given equation 3.5:

$$w_{cr} = \sum u_{icorr} = 2\pi(\nu_{rs}-1)X \tag{3.5}$$

where v_{rs} is the ratio of volumetric expansion of the oxides with respect to the virgin material; X is the depth of the corrosion attack; and u_{icorr} is the opening of each single corrosion crack. The study done by Coronelli and Gambarova (2004) used crack width model of Molina et al. (1993) to calculate reduction in concrete strength. Developed model by Molina et al. (1993) provides to calculate length of the crack evolution in concrete. However, the proposed model is not time dependent; therefore reduction in concrete strength can be calculated only for that current time. Also other studies were done by Ohtsu and Yoshimura (1997), Kapilesh et al. (2006) in order to calculate crack width in concrete for a given current time. A large literature survey was done to decide for appropriate crack width model in order to integrate it into model of concrete strength reduction as a function of time. In this study crack width equation derived from proposed model by Li et al. (2007). Derived model by Li et al. (2007) also verified with both experimental and numerical data obtained from research literature. Like the previously proposed analytical models, the model is based on a thick-walled cylinder approach, in which the concrete surrounding a corroding reinforcing bar is considered as a thick-walled hollow cylinder with the wall thickness equal to that of the concrete cover. Proposed model by Li et al. (2007) used a well known Bažant's (1979) thick-walled model and it is almost used for many developed fundamental of corrosion models. Figure 3.1 presents a schematic diagram that is used for proposed crack width model by Li et al. (2007). In Figure 3.1, phase of no cracking, the concrete cylinder was considered to be isotropic so that the theory of elasticity was used to determine the radial stress $\sigma_r(r)$ and tangential stress $\sigma_\theta(r)$ at any point in the cylinder.

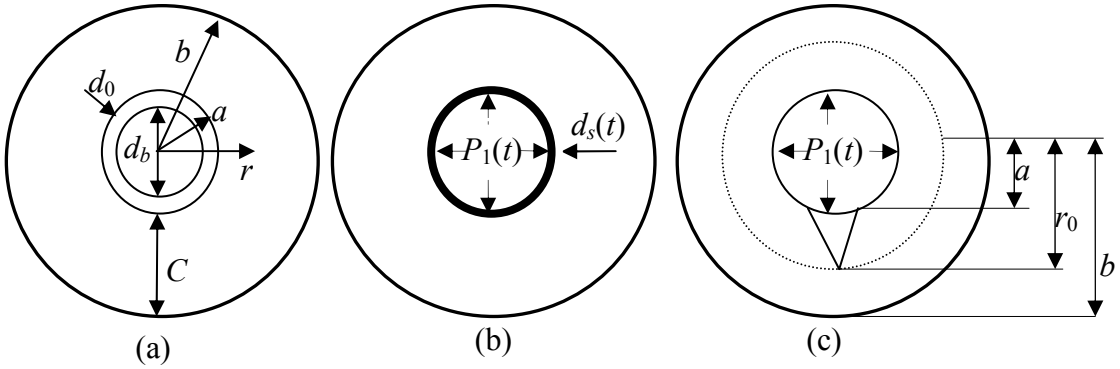

Figure 3.1: Phases of concrete damage: (a) Bažant's thick walled (1979), (b) Liu and Weyers (1998), (c) Li et al. (2007).

According to Li et al. (2007), the initial cracking time can be determined from tangential stress $\sigma_{\theta(r)}$ by satisfying the condition the tangential stress of a $\sigma_{\theta(a)}$ is equal to tensile strength of concrete f_t. As shown in Figure 3.1(c), after cracking initiation, the crack in the concrete cylinder propagates along a radial direction and stops arbitrarily at r_0 (which varies between the radii *a* and *b*) to reach a state of self-equilibrium Li et al. (2007). Developed model by Li et al. (2007), the corrosion induced concrete crack width model (w_{cr}) is expressed as following equation (3.6):

$$w_{cr} = 2\pi b\left[c_5 b^{(\sqrt{\alpha}-1)} + c_6 b^{(-\sqrt{\alpha}-1)} - \frac{f_t}{E_{ef}}\right] = \frac{4\pi d_s(t)}{(1-\nu_c)/(a/b)^{\sqrt{\alpha}} + (1+\nu_c)(b/a)^{\sqrt{\alpha}}} - \frac{2\pi b f_t}{E_{ef}} \tag{3.6}$$

where $d_s(t)$ is the thickness of corrosion product form; f_t is the tensile strength of concrete; E_{ef} is the effective elastic modulus of concrete ; ν_c is the Poisson's ratio of concrete; α is the tangential stiffness reduction factor ; a represents internal radius of the cylinder ($a=D+2d_0/2$) ; b is the exterior radius of the cylinder ($b=S/2$); S is the rebar spacing; c_5 and c_6 are boundary conditions as proposed by Li et al. (2007). Li et

al. (2007) developed an algorithm for computing tangential stiffness reduction factor. Detailed framework of algorithm is given in Figure 3.2.

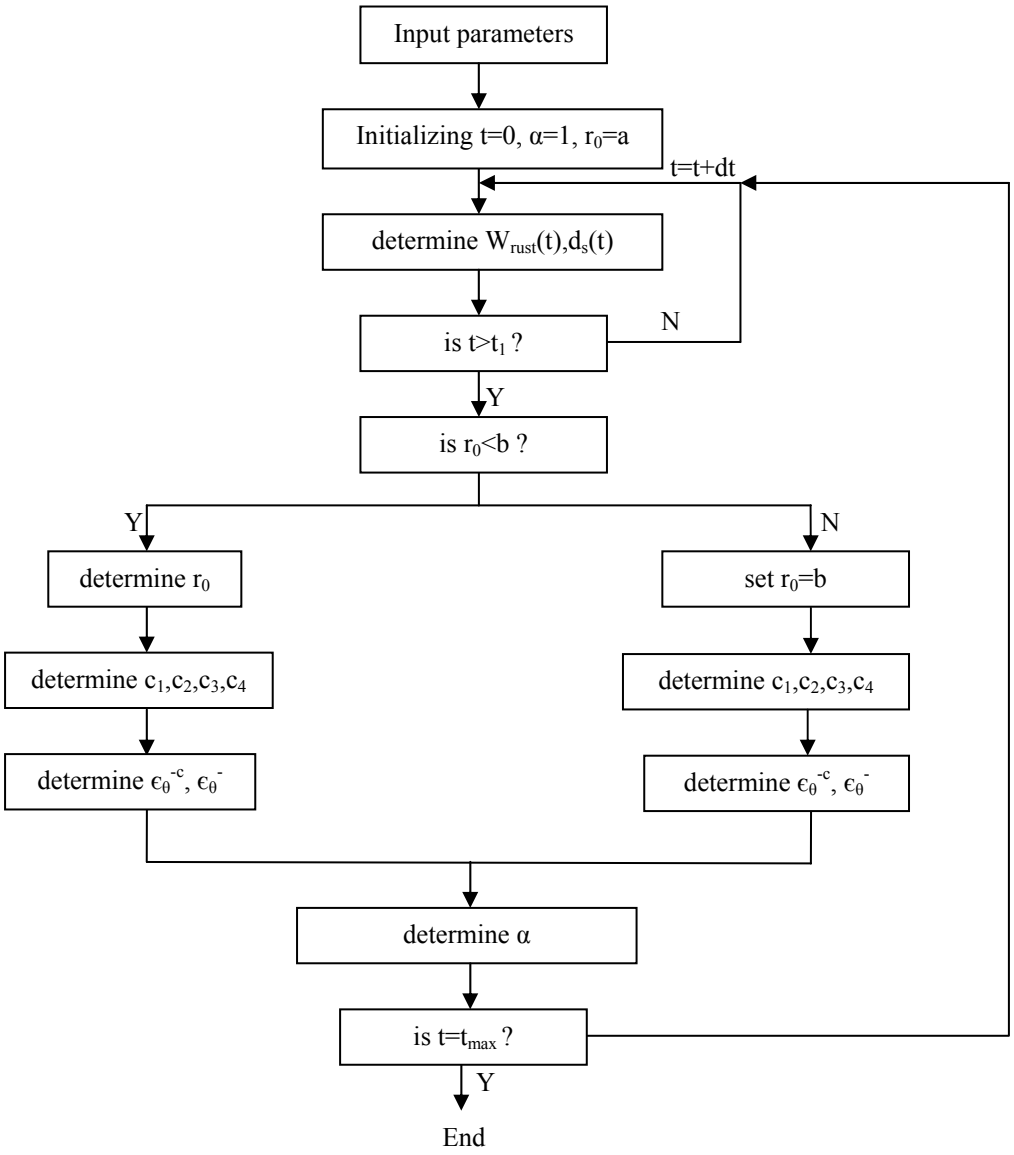

Figure 3. 2: Algorithm for computing tangential stiffness reduction factor α Li et al. (2007).

Proposed crack width model by Li et al. (2007), used developed model by Liu and Weyers (1998) in order to calculate thickness of corrosion product form $d_s(t)$ as given equation:

$$d_S(t) = \frac{W_{rust}(t)}{\pi(D + 2d_0)}\left(\frac{1}{\rho_{rust}} - \frac{\alpha_{rust}}{\rho_{st}}\right) \tag{3.7}$$

where W_{rust} is the mass of rust per unit length of rebar; D is the rebar diameter; α_{rust} is the coefficient related to the type of rust; ρ_{rust} is the density of rust; ρ_{st} is density of steel; d_0 is the thickness of the annular layer of concrete pores (i.e., a pore band). In order to calculate mass of rust per unit length of rebar (W_{rust}) following equation was proposed by Liu et al. (2007):

$$W_{rust}(t) = \left[2\int_0^t 0.105(1/\alpha_{rust})\pi D i_{corr}(t)dt\right]^{1/2} \tag{3.8}$$

As it is shown in these equations, reduction in concrete strength can be calculated as a time-dependent of corrosion rate in different years. Equation 3.6 above, concrete crack width (w_{cr}) model is a time-dependent of the thickness of corrosion product form $d_s(t)$. Moreover, thickness of corrosion product form $d_s(t)$ is a time-dependent of the mass of rust per unit length of rebar (W_{rust}). Thus, reduction in concrete strength can be obtained as a function of time according to different rate of corrosion. Once, corrosion rate is determined as a function of time, and then mass of rust per unit length of rebar (W_{rust}) can be calculated as a function of corrosion rate that provides to have thickness of corrosion product form $d_s(t)$ as a function of mass of rust per unit length of rebar which is going to provide to have a time-dependent reduction in concrete strength model. By substituting equation 3.1 into equation 3.8 the following equation for mass of rust per unit length of rebar (W_{rust}) as a function of corrosion rate in years can be calculated. The new obtained relation of mass of rust per unit length of rebar as a function of corrosion rate is given by following equation:

$$W_{rust}(t)=\left[2\int_0^t\left(\begin{array}{l}0.105(1/\alpha_{rust})\pi D(2.59-0.05.X_1-6.89.X_2-22.87X_3-0.99X_4+\\0.14X_5+0.51X_6+0.01X_7+60.18X_8+3.36X_9+7.32X_{10})(t)dt\end{array}\right)\right]^{1/2} \tag{3.9}$$

Thickness of corrosion product form $d_s(t)$ can be derived by substituting equation 3.9 into equation 3.7 in order to have time-dependent corrosion product form $d_s(t)$ as a function of corrosion rate for different years as given equation:

$$d_S(t)=\underbrace{\frac{\left[2\int_0^t\left(\begin{array}{l}0.105(1/\alpha_{rust})\pi D(2.59-0.05.X_1-6.89.X_2-\\22.87X_3-0.99X_4+0.14X_5+0.51X_6+0.01X_7+\\60.18X_8+3.36X_9+7.32X_{10})(t)dt\end{array}\right)\right]^{1/2}}{\pi(D+2d_0)}\left(\frac{1}{\rho_{rust}}-\frac{\alpha_{rust}}{\rho_{st}}\right)}_{X} \tag{3.10}$$

Let us call equation 3.10 ‘X’. By obtaining equation 3.10, thickness of corrosion product form $d_s(t)$ becomes as a function of corrosion rate and function of mass of rust per unit length of rebar for different years. Thus, concrete crack width can be calculated as a function of corrosion product form in a different corrosion rate for different years, and new developed time depended crack width model can be expressed by substituting equation 3.10 into equation 3.6 as given by following new proposed equation:

$$W_{cr}=X\left(\frac{1}{(1-\nu_c)/(a/b)^{\sqrt{\alpha}}+(1+\nu_c)(b/a)^{\sqrt{\alpha}}}\right)-\frac{2\pi b f_t}{E_{ef}} \tag{3.11}$$

These derived relations provide to have information between predictions of corrosion rate versus to reduction in concrete strength as a function of time. By obtaining equation 3.11, at the same time it is easy to take into account of corrosion effects on structural performance such as reduction in gross sectional area of steel bars, time effect, and reduction in concrete strength. In order to determine the reduced concrete strength as a function of time by using new proposed model the following steps need to be carried out. As a first step, mass of rust per unit length of rebar (see equation 3.9) can be calculated as a function of corrosion rate where corrosion rate is also can be calculated as a function of time by using equation 3.1. Then by following equations 3.10 and 3.11 concrete crack width can be calculated as a function of time for a given time-dependent corrosion rate. Thus, equation 3.4 will be calculated by using new proposed time-dependent crack width model (see equation 3.11) which is going to provide to have a numerical value of reduction in concrete strength as a function of time by substituting obtained value first into equation 3.2 then equation 3.2.

3.3 Non-linear Material Modelling

In order to understand the sectional behaviour of assessed SDOF and MDOF systems moment-curvature relations were constructed in three case studies by using new developed time-dependent corrosion model. Moment-curvature relations provide to predict the behaviour of the sections and here it was used to predict the behaviour of a section at any load. Actual material behaviour is non-linear, thus moment-curvature relations provide to determine accurately load-deformation behaviour of concrete section by using non-linear material stress-strain relationship. There are many models developed to indentify the stress-strain relation for both reinforced concrete and reinforcement steel. Hognestad (1951), Kent and Park

(1971), Mander et al. (1988), and Saatcioglu and Razvi (1992) are some of them. In this thesis, confined column of assessed section for both developed Kent and Park (1971), and Saatcioglu and Razvi (1992) models were performed for the stress-strain relation of RC section. Then, among them, for each case (existing, 25,50,75 and 100 years), those caused higher demands (lower elastic and inelastic stiffness and lower yield strength) were selected to be used in IDA for 20 different ground motion records. Descriptions of developed models by Kent and Park (1971) and Saatcioglu and Razvi (1992) that were investigated in this thesis were examined by following sub sections.

3.3.1 Stress-strain Relationships of Concrete by Kent and Park (1971)

The response of a structure under load depends to a large extent on the stress–strain relation of the constituent materials and the magnitude of stress. Since concrete is used mostly in compression, the stress–strain relation in compression is of primary interest (Kwak and Kim; 2002). The developed model of Kent and Park (1971) has been using more than 30 years. Basically, developed model by Kent and Park (1971), occurs with two branches. For the first branch (A-B), the curve reaches to maximum stress level which is equal to 0.002. After reaching maximum stress, two other different braches occurs (B-C, B-D) where two straight lines indicates different behaviour of concrete for confined and unconfined concrete. For the falling branch of the curve assumed to be linear and its slope specified by determining the strain when the concrete stress has fallen to 0.5 of maximum stress as suggested by Roy et al. (1982). Figure 3.3 shows the developed model by Kent and Park (1971). Kent and Park (1971) proposed a constitutive model for confined concrete using a parabolic stress–strain curve for the ascending branch and a linear stress– strain curve for the

descending branch. Equations below (3.12-3.18) defined by Kent and Park (1971) for modelling the stress-strain relationships of concrete.

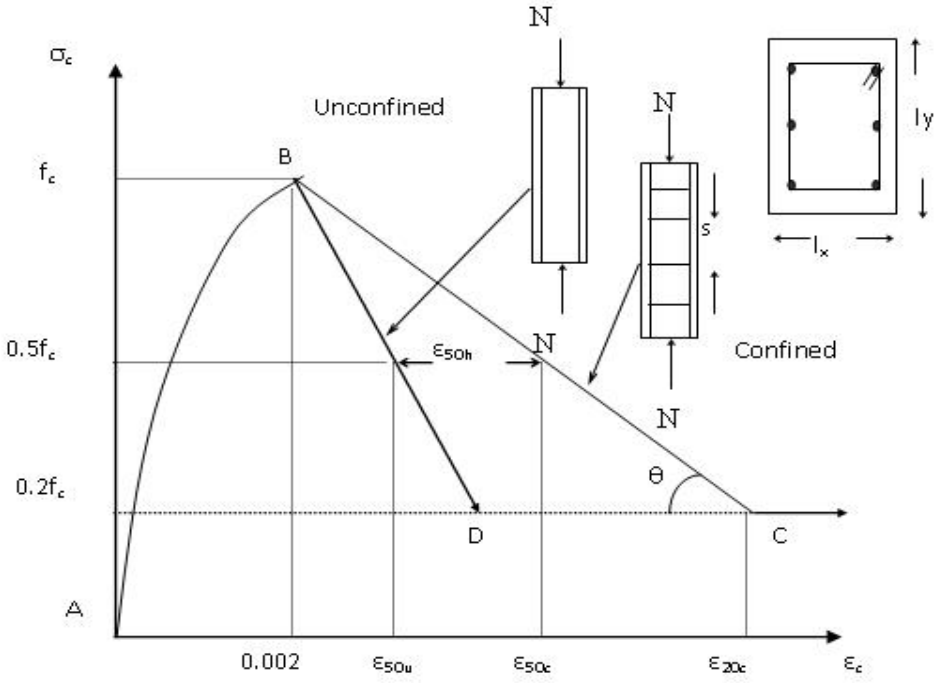

Figure 3.3: Stress-strain relationship of concrete by Kent and Park (1971).

$$\sigma_C = K.fc\left[\frac{2\varepsilon_C}{0.002K} - \left(\frac{\varepsilon_C}{0.002K}\right)^2\right] \qquad \varepsilon_C \le 0.002K \tag{3.12}$$

$$\sigma_C = K.fc\left[1 - Z\left(\varepsilon_C - 0.002K\right)\right] \ge 0.2K.f_C \quad \varepsilon_C > 0.002K \tag{3.13}$$

$$\sigma_C = 0.2K.fc \qquad \varepsilon_C > \varepsilon_{20c} \tag{3.14}$$

$$K = 1 + \frac{\rho_S f_{sy}}{f_C} \tag{3.15}$$

$$Z = \frac{0.5}{\varepsilon 50_u + \varepsilon 50_h - 0.002K} \tag{3.16}$$

$$\varepsilon 50_u = \frac{3 + 0.29 f_c}{145 f_c - 1000} \tag{3.17}$$

$$\varepsilon 50_h = \frac{3}{4} \rho_s \sqrt{\frac{h`}{s}} \tag{3.18}$$

where, ε_{c0} is the concrete strain at maximum stress, K is a factor which accounts for the strength increase due to confinement, Z is the strain softening slope, f_{sy} is the yield strength of stirrups, s is the center to center spacing of stirrups or hoop sets, ρ_s is the ratio of the volume of hoop reinforcement to the volume of concrete core measured to the outside of stirrups, $h`$ is the width of the concrete core measured to the outside of stirrups. In this study, developed model by Kent and Park (1971) was used for three case studies.

3.3.2 Stress-strain Relationships of Concrete by Saatcioglu and Razvi (1992)

Another model developed by Saatcioglu and Razvi (1992) proposed to construct a stress-strain relationship for confined and unconfined concrete. Saatcioglu and Razvi (1992) proposed to calculate lateral confinement pressure generated by circular and rectilinear reinforcement, and the resulting improvements in strength and ductility of confined concrete. The model consists of a parabolic ascending branch, followed by a linear descending segment. Figure 3.4 represents for the $\sigma - \varepsilon$ relation of RC sections proposed by Saatcioglu and Razvi (1992).

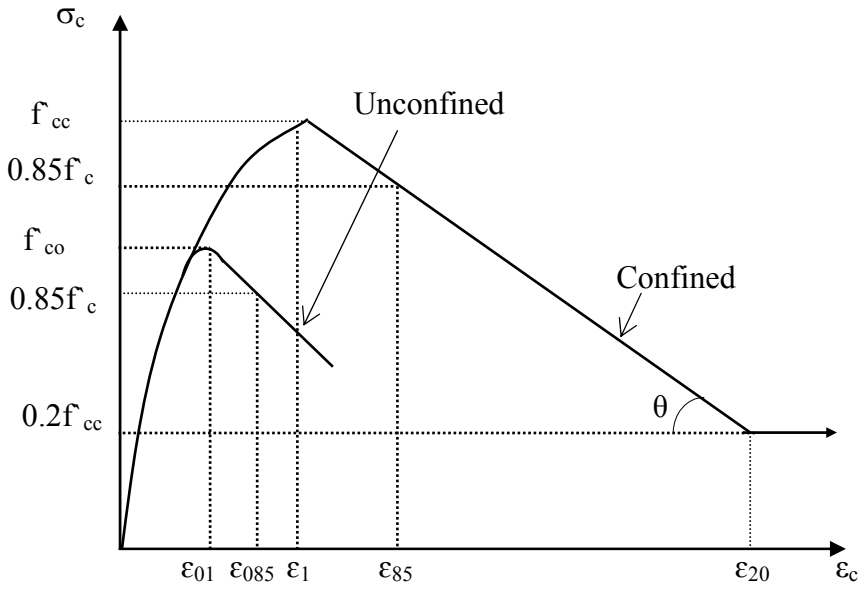

Figure 3.4: Stress-strain relationship of concrete by Saatcioglu and Razvi (1992).

An analytical model was proposed by Saatcioglu and Razvi (1992) to construct a stress-strain relationship for confined concrete. The proposed relationship by Saatcioglu and Razvi (1992) becomes identical to that proposed model by Hognestad (1951) for unconfined concrete, when confinement effects are negligible and the lateral confinement pressure is zero (Saatcioglu and Razvi; 1992). Equations below were defined by Saatcioglu and Razvi (1992) for modelling the stress-strain relationships of concrete.

$$\sigma_c = fcc\left[\frac{2\varepsilon c}{\varepsilon_{cc}} - \left(\frac{\varepsilon_c}{\varepsilon_{cc}}\right)^2\right]^{\frac{1}{1+2k}} \qquad \varepsilon_c \leq \varepsilon_{cc} \qquad (3.19)$$

$$\sigma_c = f_{cc}\left[1 - \frac{0.15(\varepsilon_c - \varepsilon_{cc})}{\varepsilon_{85} - \varepsilon_{cc}}\right] \qquad \varepsilon_{20} > \varepsilon_c > \varepsilon_{cc} \qquad (3.20)$$

$$\sigma_c = 0.2 f_{cc} \qquad \varepsilon_c > \varepsilon_{20} \qquad (3.21)$$

$$f_{cc} = k_3 f_c + k_1 f_{1e} \qquad (3.22)$$

$$\varepsilon_{cc} = \varepsilon_{c_0}(1 + 5\lambda) \tag{3.23}$$

$$\lambda = \frac{k_1 f_{1e}}{k_3 f_c} \tag{3.24}$$

$$k_1 = 6.7(f_{1e})^{-0.17} \tag{3.25}$$

$$\varepsilon_{85} = 260.\rho_s.\varepsilon_{cc} + \varepsilon_{085} \tag{3.26}$$

$$f_{1e} = \frac{f_{1ex}b_x + f_{1ey}b_y}{b_x + b_y} \tag{3.27}$$

$$f_{1ex} = \beta_x f_{1x} \tag{3.28}$$

$$f_{1ey} = \beta_y f_{1y} \tag{3.29}$$

$$f_{1ex} = \frac{\sum A_0.f_{sy}.Sin\alpha x}{sb_x} \tag{3.30}$$

$$f_{1ey} = \frac{\sum A_0.f_{sy}.Sin\alpha y}{sb_y} \tag{3.31}$$

$$\beta_x = 0.26\sqrt{\frac{b_x}{ax}.\frac{b_x}{s}.\frac{1}{f_{1x}}} \tag{3.32}$$

$$\beta_x = 0.26\sqrt{\frac{b_y}{a_y}.\frac{b_y}{s}.\frac{1}{f_{1y}}} \tag{3.33}$$

$$k = \frac{k_1 f_{1e}}{f_{c0}} \tag{3.34}$$

where f_{1e} is the equivalent uniform lateral pressure, f_{1x} is the pressure in x direction, f_{1y} is the pressure in y direction, f_{1ex} and f_{1ey} are the effective lateral pressures acting perpendicular to core dimensions b_x and b_y, respectively, k_1 is the coefficient of

related with the properties of concrete, A_0 is the area of transverse reinforcement, b_x is the core dimension measured center to center of perimeter hoop along the x-direction of a square or rectangular column, b_y is the core dimension measured center to center of perimeter hoop along the y-direction of a square or rectangular column, s is the spacing of transverse reinforcement in longitudinal direction, α is the angle to obtain concrete strip, f_{c0} is the unconfined concrete compressive strength in member, f_{cc} is the confined concrete compressive strength in member, ε_{01} is the strain corresponding to peak stress of unconfined concrete, ε_{85} is the strain corresponding to 85% of peak stress of confined concrete on the descending branch, ε_{085} is the strain corresponding to 85% of peak stress of unconfined concrete on the descending branch, ε_1 is the strain corresponding to peak stress of confined concrete. As shown equations above, developed model by Saatcioglu and Razvi (1992) provides to consider the spacing of reinforcement for both directions in concrete section. When the thickness of corrosion product form $d_s(t)$ is considered based on equation 3.7, developed model by Saatcioglu and Razvi (1992) provided an important approach for the modelling of corroded RC sections.

3.3.3 Stress-strain Relationships of Steel by Mander (1984)

Beside of concrete, σ−ε relation of steel is also needed to be model. Many models have been developed for strain-stress relation of steel, such as for hot rolled steel, Kent and Park (1973), Thompson and Park (1978) proposed different models. For cold work steel Kato (1979), Peterson and Popov (1977), Stanton and McNiven (1979) investigated other models. In this thesis, Mander's (1984) model was used for modelling stress-strain relationship of steel for performed three case studies. In 1984 Mander proposed a model which can be used either for both hot rolled steel and cold work steel. The model includes linear elastic region up to yield, elastic-perfect-

plastic region, and strain hardening region. The Mander's model (1984) has control on both strength and ductility where descending branch of the curve that first branch increases linearly until yield point then the curve continues as constant. Figure 3.5 shows the proposed model by Mander (1984) for $\sigma-\varepsilon$ relation of steel that was used for current study as a function of time.

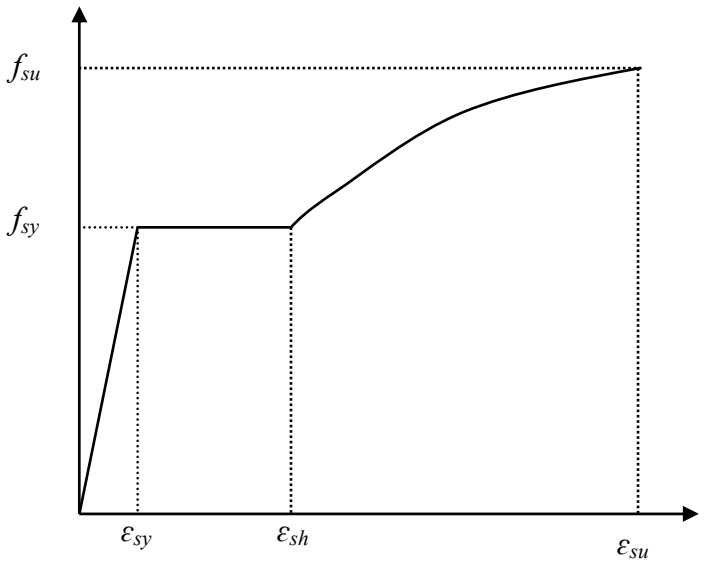

Figure 3.5: Stress-strain relationship of steel by Mander (1984).

Equations below were defined by Mander (1984) for modelling the stress-strain relationships of steel.

$$\sigma_S = E_S \varepsilon_S \qquad \varepsilon_s \le \varepsilon_{s\,y} \tag{3.35}$$

$$\sigma_s = f_{sy} \qquad \varepsilon_{sh} \ge \varepsilon_s > \varepsilon_{s\,y} \tag{3.36}$$

$$E_S = \frac{f_{sy}}{\varepsilon_{sy}} \tag{3.37}$$

$$\sigma_S = f_{su} + (f_{sy} - f_{su})\left[\frac{\varepsilon_{su} - \varepsilon s}{\varepsilon_{su} - \varepsilon_{sh}}\right]^h \qquad \varepsilon_{su} \ge \varepsilon_s > \varepsilon_{sh} \tag{3.38}$$

$$h = E_{sh}\left[\frac{\varepsilon_{su} - \varepsilon_{sh}}{f_{su} - f_{sy}}\right] \tag{3.39}$$

where σ_s is the stress in reinforcing steel, ε_s is the strain in reinforcing steel, ε_{sy} is the yield strain in reinforcing steel, ε_{sh} is the strain hardening in reinforcing steel, ε_{su} is the ultimate strain in reinforcing steel, f_{sy} is the yield strength in reinforcing steel, f_{su} is the ultimate strength in reinforcing bar corresponding to the ultimate strain in reinforcing bar,E_s is elastic modulus of steel, E_{sh} is the hardening elastic modulus of steel, h is the degree of hardening.

3.4 A Case Study of Time-dependent Seismic Performance Assessment of a SDOF System Subject to Corrosion by Using IDA

3.4.1 Description of the Analyzed Structure

In this case study, a SDOF frame was performed as a function of time by using new developed time-dependent corrosion model (equation 3.11). In order to analyse the frame required assumptions are mentioned below. It was assumed that assessed frame of the structure was located in a very close distance to seaside, soil class was classified as D (soft clay), building importance factor was taken 1 and effective ground acceleration coefficient (A_0) was equal to 0.3 g where calculated target pseudo acceleration was equal to 0.75 g according to Turkish earthquake code 2007 (TEQ, 2007). Used steel and concrete classes are selected as S420 (420 MPa) and C20 (20 MPa), respectively. Mechanical properties of used steel in the analyses were selected according to Turkish standard 500 (TS 500, 2000) that minimum rupture strength was 500 N/mm^2, and minimum rupture extension 0.12 % for diameter of the bars were less than 32 mm (ϕ<32 mm). The member names and sectional dimensions (in cm) of performed frame are shown in Figure 3.6. Performance level of assessed

frame has been performed for five different time periods as existing (*t*: 0), 25, 50, 75 and 100 years. For each scenario, firstly a corrosion rate which is defined as the loss of metal per unit of surface area was calculated for each year based on required assumptions. The corrosion rate was calculated by using Morinaga (Morinaga, 1988) model as shown in equation 3.1. In order to predict the corrosion rate as a function of time by using Morinaga model, required values of basic variables are represented in Table 3.1.

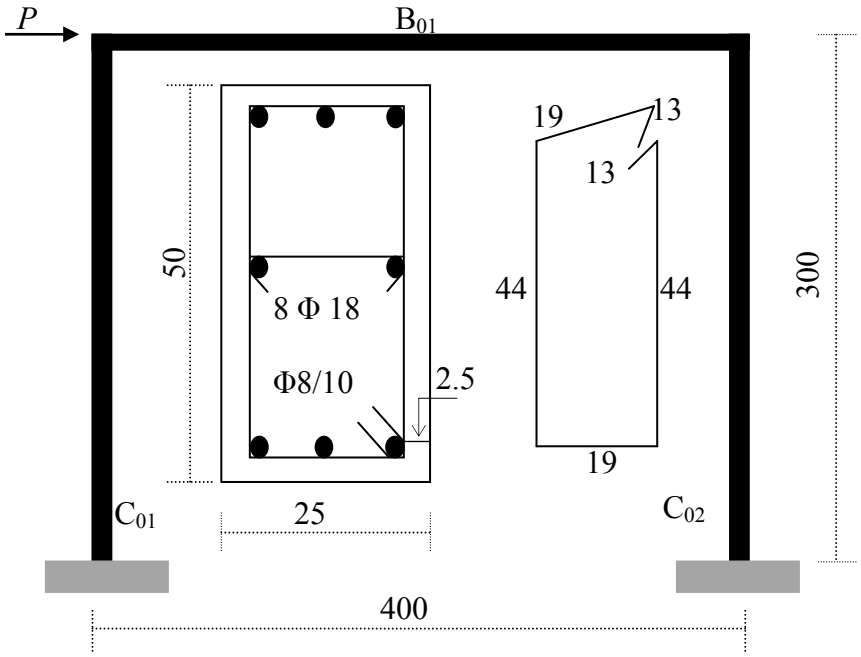

Figure 3.6: Dimensions of assessed reinforced concrete frame.

According to the assumptions in Table 3.1 and by using equation 3.1, calculated corrosion rate of 25, 50, 75 and 100 years were 1.88e-4, 3.75e-4, 5.63e-4, 7.5e-4 g/mm^2 respectively. Once corrosion rate was calculated by using equation 3.1, reduction in concrete strength of each time periods can be obtained as a function of corrosion rate by using equation 3.2.

Table 3. 1: Used values of basic variables.

Symbol	Value	Sources
X_1	32^0C	[current study]
X_2	80 %	[current study]
X_3	20 %	Morinaga (1988)
X_4	3.5%	ACI (2005)
v_c	0.18	Liu and Weyers (1998)
E_{ef}	8517.74 MPa	TS 500 (2000)
f_t	4.2 MPa	TS 500 (2000)
ρ_{rust}	3600 kg/m^3	Liu and Weyers (1998)
ρ_{st}	7850 kg/m^3	Liu and Weyers (1998)
α_{rust}	0.57	Liu and Weyers 1998
d_0	12.5μm	Liu and Weyers 1998

Calculated reduction in concrete strength as a function of corrosion rate was almost 0.5 MPa for each time period that when time reached to 75 years, the calculated reduced concrete strength was equal to 18.4 MPa. The new developed time-dependent corrosion model provides to use obtained values for any required further analyses in order to predict the behaviour of the section of the assessed frame.

3.4.2 Moment-curvature Relationship as a Function of Corrosion Rate

For each time period moment-curvature relations of a rectangular confined column section (C_{01}) was conducted for both developed Kent and Park (1971) and Saatcioglu and Razvi (1992) models by considering both changes in corrosion rate and reduction in concrete strength as a function of time. In order to perform moment-curvature relations a constant 15 tons axial load was assumed for each time period. Figure 3.7 below shows the predicted time-dependent moment-curvature relations by considering corrosion rate and reduced concrete strength for both developed models by Kent and Park (1971), and Saatcioglu and Razvi (1992). There were not much differences between two proposed model by developed Kent and Park (1971), and Saatcioglu and Razvi (1992). Thus, proposed model by Saatcioglu and Razvi (1992) indicates more optimistic result for further steps of case study. Therefore, author of

this thesis used the obtained results of developed Kent and Park (1971) model for moment-curvature relations. It should be noted that even Saatcioglu and Razvi (1992) model would have been used for further analyses; the reduction in performance level would be inevitable in IDA when time-dependent assessed frames are compared with existing frame.

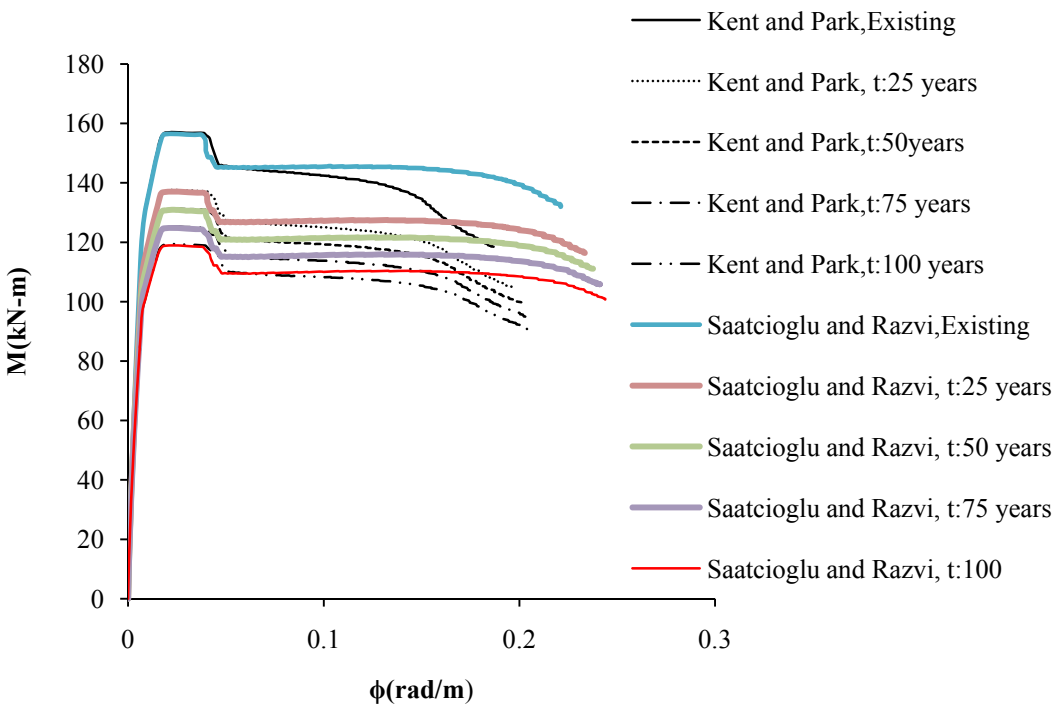

Figure 3. 7: Time-dependent moment-curvature relationship.

In Figure 3.7, time-dependent moment-curvature relationships of assessed reinforced concrete section (C_{01}) basically indicate three segments; the elastic region prior to cracking, the post-cracking branch between the cracking and yield points and the post-yield segment beyond yielding respectively. As shown in Figure 3.7, due to time-dependent corrosion effect, section capacity and energy dissipation reduced with time while rotation increased for less moment value that causes to have more lateral displacement of the assessed frame. The obtained moment-curvature relationships are needed to be idealized as bilinear according to aim of further steps. For doing this, time-dependent moment-curvature relationships of column section

(C_{01}) were bilinear idealized for each time period according to the procedure described by Saatcioglu and Humar 2003. With increasing time and corrosion effects reduction in load carrying capacity of a RC column subjected axial loading can be assessed from moment-load (M-N) interaction diagrams. The results of time-dependent M-N interaction diagrams of all cases of assessed column are plotted and shown in Figure 3.8.

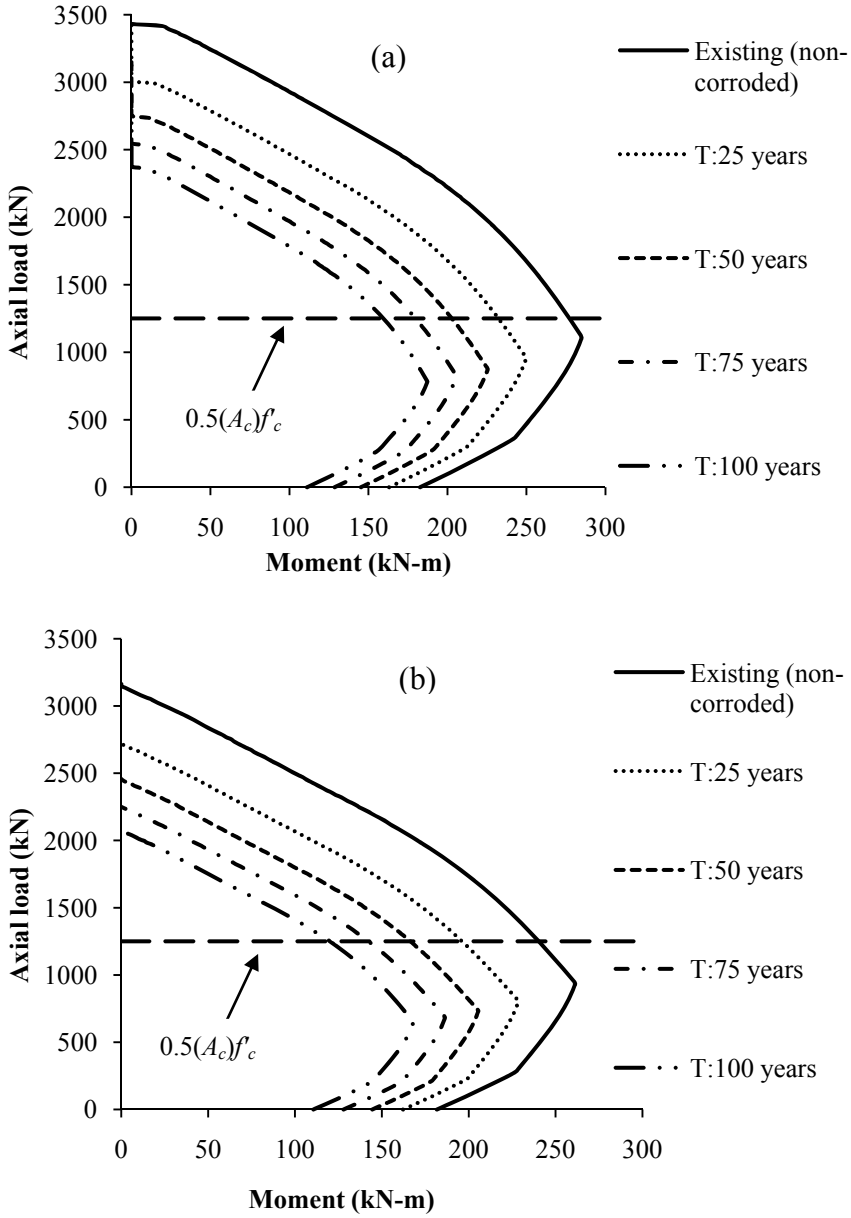

Figure 3.8: Time-dependent M-N diagrams of C01 column: (a) Kent and Park (1971), (b) Saatcioglu and Razvi (1992).

Time-dependent interaction diagrams were used to predict adequately moment capacity of corroded RC section. In Figure 3.8, line of $0.5A_c f'_c$ represents the maximum allowable load that can be carried by a section according to Turkish earthquake code 2007 (TEQ, 2007), where A_c is the cross sectional area of a section. On this line, moment capacity of corroded RC section reduces as a function of time due to corrosion. The moment capacity of C_{01} column of existing structure based on model developed by Kent and Park (1971), was 277 kN-m on this line, but this capacity decreased to 244 kN-m, 220 kN-m, 200 kN-m, 184 kN-m after 25, 50, 75 and 100 years respectively. These results also support the above finding about time-dependent moment-curvature relationships of the corroded column where serious strength degradation occurs due to corrosion.

3.4.3 Time-dependent Load-displacement Relationships

Predicted time-dependent moment-curvature relationships were used to predict lateral displacement (Δ_1) of the frame due to loss of cross sectional area of reinforcement bars and reduce concrete compressive strength. In order to simplify the frame analyses, a rigid beam (B_{01}) was assumed that provides the column curve in double curvature and the point of inflection is at the middle. For each time period of frame analyses, lateral loads were applied incrementally to the frames until the assessed column reach to its ultimate moment capacity. The moments values which were obtained by applying lateral load to the frames, needs to be converted to the displacement of corresponding to the each lateral load by using moment-curvature relationship. For doing this, the moment-area method can be used by integrating the area under the curvature. In Figure 3.9, an example of a cantilever beam is shown to define the general behaviour of the reinforced concrete members.

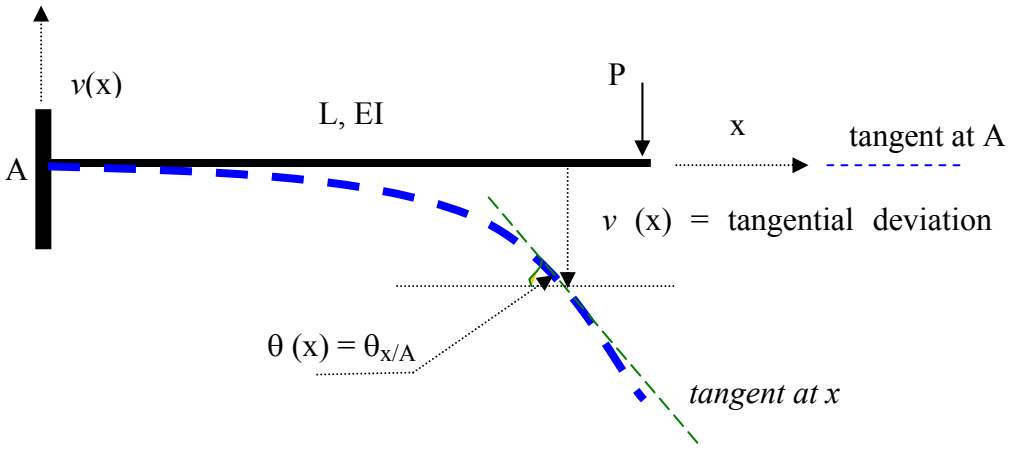

Figure 3.9: An example of a cantilever beam.

The basis of the method starts from the moment curvature equation where the change in slope value θ(x) between two point A and B is termed $\theta_{B/A}$ and is equal to the integral $\int(1/EI)\ M(x)\ dx$. Also the change in displacement value δ(x) between two point A and B is termed $\delta_{B/A}$ and is equal to the integral $\int(1/EI)\ M(x)\ x\ dx$. The values of $\theta_{B/A}$ and $\delta_{B/A}$ are measure between the tangents at the two points. It is noted that while the integral $\int(1/EI)\ M(x)\ dx$ gives the area under M/EI diagram between A and B, the other integral $\int(1/EI)\ M(x)\ x\ dx$ gives the moment of the area under M/EI diagram between A and B and the values of $\theta_{B/A}$ and $\theta_{B/A}$ will be numerically the same (with one positive if counter-clockwise and the other is negative if clockwise). However, the values of $\delta_{B/A}$ and $\delta_{B/A}$ will not be the same as the moment in the first case will be taken about point B and in the second case the moment is about point A. This is a very important consideration when using the moment area method. The use of the first integral to compute $\theta_{/A}$ is called the first moment area theorem, while the use of the second integral to compute $\delta_{B/A}$ is called the second moment area theorem. Once distribution of curvatures of each time period

along the height of the column for a given lateral load and corresponding linear moment diagram was obtained then by integrating area under the curvature diagram rotation along the height of the column can be calculated. It might be useful to notice that in this case study obtained moments values from frame analyses have been recorded for each 1% of the half height of the column (C_{01}) that provides to have more accurate results. Figure 3.10 shows the obtained load-displacement relations by computing the moment of the area relative to the cantilever column to find the top displacement of assessed column (C_{01}) by considering deformation due to reduction in concrete strength and loss of cross sectional area of steel for each time period as a function of corrosion rate.

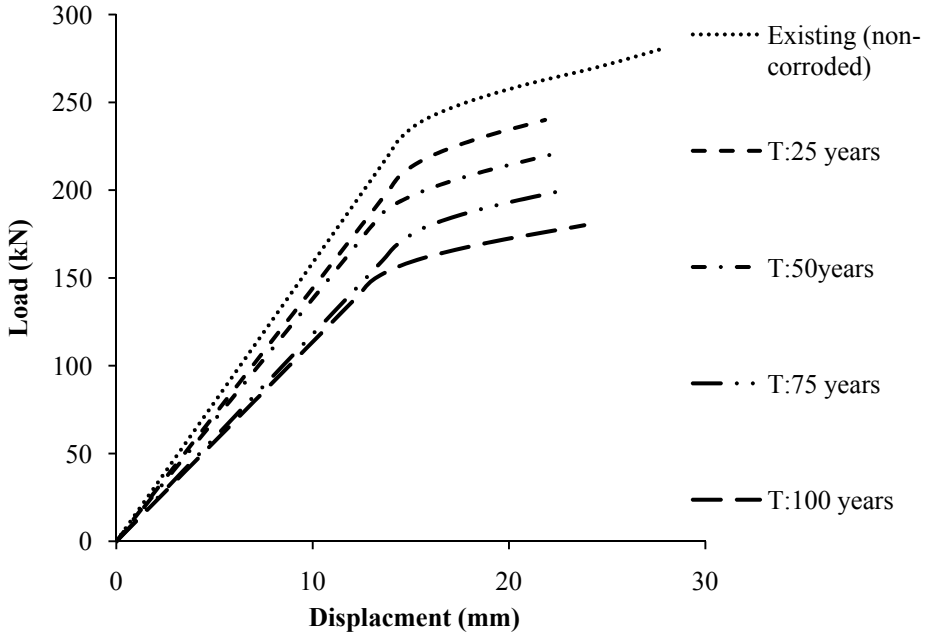

Figure 3.10: Time-dependent load- top displacement relationships.

As shown in Figure 3.10 there is an obvious deterioration in the section capacity due to corrosion resulting decrease in ductility, initial and post yielding stiffness of the existing assessed frame. Due to time-dependent effects of corrosion, reduction in

the initial stiffness of the frame for corresponding time periods of 25, 50, 75 and 100 years are 9%, 14%, 26%, 28% respectively.

3.4.4 Results of Slip Deformation as a Function of Corrosion Rate

In Figure 3.10, time-dependent load-displacement relationships were obtained by considering the two effects of corrosion (time-dependent loss of steel area and reduction in concrete strength) where slip effect was not considered. Therefore, model developed by Sezen and Setzler (2008) was used to define this effect on time-dependent structural behaviour. For each case (existing, 25 years, 50 years, 75 years and 100 years), time-dependent moment-curvature relationships were used to calculate time-dependent effective depth of the neutral axis, strain and stress in reinforcing bar. Time-dependent relationships between calculated maximum moment (M_{max}) of the column base and the corresponding strain (ε_s) in the tensile longitudinal bars are shown in Figure 3.11.

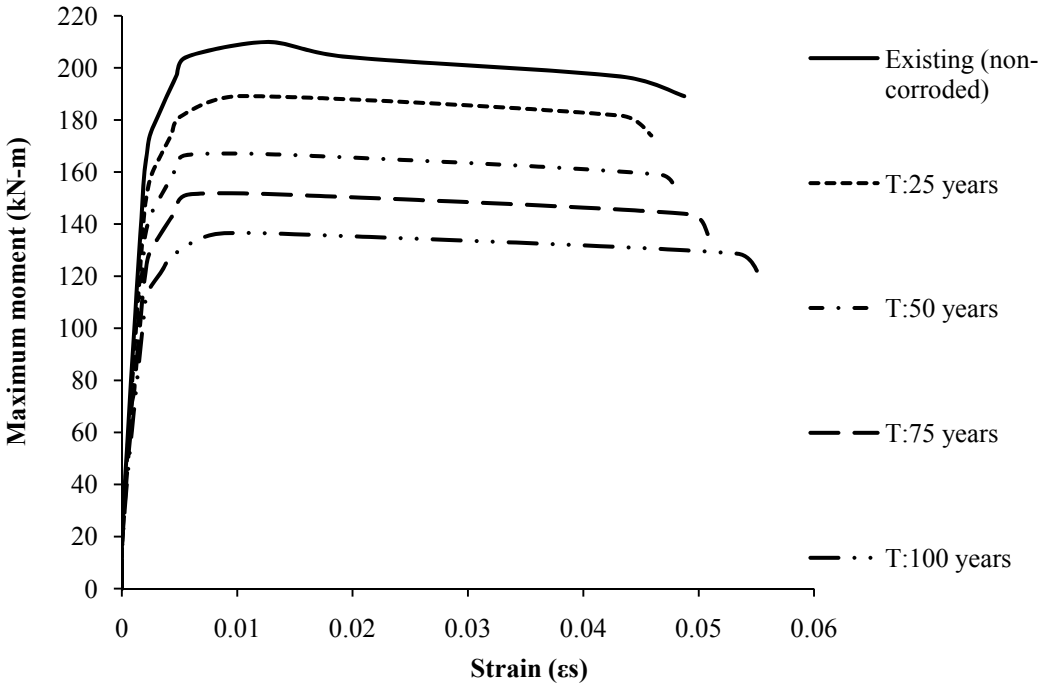

Figure 3.11: Time-dependent moment-strain relationships.

As it is expected, same strain deformation occurs with increasing time with a less amount of moment values. If the force and corresponding time-dependent stress-strain relationships of reinforcement bar embedded in concrete are known, time-dependent slip rotation can be calculated by using equation 2.18 and 2.19. At this point one difficulty happens to predict the slip on the yield plateau region. This problem was also reported in the literature by some authors (e.g., Sezen and Setzler 2008; Alsiwat and Saatcioglu 1992).When the tension steel yields in concrete, the depth of the neutral axis closes to the compression side of the section. In equation 2.19, on the yield plateau region, (d-c) increases and the resulting slip rotation decreases. Thus, no additional slip occurs from yield strain to the start of strain hardening of reinforcement bars. To avoid this problem Sezen and Setzler (2008) recommended using a modest strain hardening on the yield plateau. This recommendation was adopted in this study and a slope of 2% of the elastic modulus of steel is used. Time-dependent lateral force and displacement due to slip as a consequence of corrosion effects are shown in Figure 3.12:

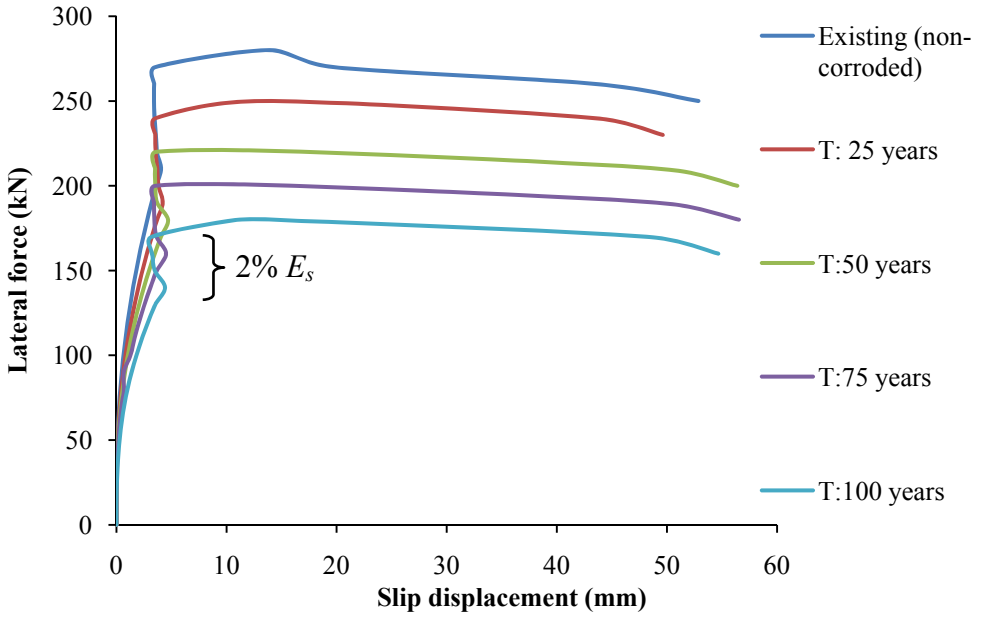

Figure 3.12: Time-dependent slip displacement.

According to slip results, there was a good agreement between obtained time-dependent displacements due to slip and experimentally study done by Sezen and Moehle (2006). Experimental study done by Sezen and Moehle (2006) indicated that slip deformations contributed 25% to 40% of the total lateral displacement. For existing column, calculated additional displacement due to slip was 45%. However, experimental study done by Sezen and Moehle (2006) was not time dependent. Therefore it is inevitable to have more lateral displacement with increasing time by taking into account of corrosion effect. Since each case shows different behaviour at three regions of reinforcing steel, compared load-slip results are summarized in

Table 3. 2: Results of slip displacement at three regions of reinforcement bar.

	Before crushing concrete						**After crushing concrete**	
	$\varepsilon_s<\varepsilon_y$		$\varepsilon_y<\varepsilon_s<\varepsilon_{sh}$		$\varepsilon_s>\varepsilon_{sh}$		$\varepsilon_s>\varepsilon_{sh}$	
Frame	P_{max} (kN)	Δ_s (mm)	P_{max} (kN)	Δ_s (mm)	P_{max} (kN)	Δ_s (mm)	P_{un} (kN)	Δ_s (mm)
Existing	220	4	270	3.5	280	14	250	52
T: 25 years	190	4	240	3.6	250	13	230	50
T: 50 years	180	4.7	220	3.6	Concrete crushed		200	56
T: 75 years	160	4.5	200	3.6	Concrete crushed		180	56
T: 100 years	140	4.5	170	3	Concrete Crushed		160	55

Note: *P*max= maximum load, *P*un=Unloaded column

As shown in Table 3.2, for each plateau of reinforcement bars, more slip displacement occurs with a less amount of lateral force. For instance, at elastic region, calculated slip displacement of existing column was equal to 4 mm when lateral force is 220 kN while same displacement occurred when lateral force was 190 kN after 25 years. Obtained results were more dramatically for 50, 75 and 100 years at strain-hardening region by crushing of concrete. As shown in Table 3.2, for these three cases, concrete crushed before reinforcing bars exceeding strain hardening region due to losing in moment capacities of section. After concrete reaches to maximum compressive strain, almost same amount of slip was recorded with

different amount of lateral force due to corrosion effect. Once the corrosion phases begin, the effect of corrosion resulting in slip will be higher during propagation period which varies from first cracking to loss of load-carrying capacity of section. In order to accurately define the most effected time period of performance level of the assessed frame by additional displacement due to slip as a function of time, obtained results should be supported by IDA. Combined three major effects of corrosion were used to predict time-dependent performance level of the corroded frame in the following section.

3.4.5 Incremental Dynamic Analysis

In this study, the developed time-dependent corrosion model was performed by using IDA. There are several methods to assess the performance level of structures under earthquake ground motions (Villaverde, 2007). Among them IDA is one of the well known. An IDA involves performing a series of nonlinear dynamic analyses in which the intensity of the ground motion selected for the collapse investigation is incrementally increased until the global collapse capacity of the structure is reached (Vamvatsikos and Cornell; 2002, 2004). It also involves plotting an intensity measure (i.e.: peak ground acceleration, spectral acceleration at the fundamental natural period of the structure, S_a) against a damage measure (i.e.: maximum in-story drift or roof drift). In addition, fragility curves can be obtained by IDA. Fragility curves represent expected damage (i.e., IO, LS and CP) as a function of the selected ground motion intensity which was used here as a function of corrosion rate for different time periods. Limit states at each performance level have been defined and summarizing the multi–record IDA curves, 16%, 50% and 84% fragility curves were obtained. At the end, fragility curves of probabilistic structural damage estimation were obtained in terms of PGA for each performance level. In order to perform IDA

NONLIN (Charney 1998) software program was used. By using NONLIN (Charney 1998) software program material nonlinearity can be taken into account by specifying yield strength, initial and post yield stiffness. NONLIN basically uses the equation of motion which was proposed by Chopra, 2001 as given equation below.

$$m\frac{d^2}{dt^2}+c\frac{du}{dt}+ku=-ml\frac{d^2u_g}{dt^2} \tag{3.39}$$

The letter '*m*' denotes the mass matrix of the system which was obtained by lumping the mass according to the degree of freedom, *u* is the displacement vector, *l* is the influence vector, and earthquake ground motion records were defined as $\frac{d^2u}{dt^2}$ which represents the recorded ground acceleration history. For IDA 5% damped first-mode $S_a(T_1, 5\%)$ was selected. The list of used ground motion records presented in Table 3.3, where earthquake moment magnitudes (M) ranging from 4.7 to 7.4, PGA varied from 0.005 to 0.6*g* and peak ground velocity (PGV) was ranged between 2 to 117 cm/sec. In FEMA 273 (1997), the CP for RC frames are defined as when the roof drift reaches 1.5% of the building height. However, according to FEMA 356 (2000) for RC wall buildings a roof drift equal to 1% and 2% of the building height are considered as LS and CP respectively. The performance limits, IO, LS and CP based on the inter-story drift are identified 1%, 2% and 4% in FEMA 356 (2000). A study was done by Yakut and Yılmaz (2008) to correlate the deformation demands with ground motion intensity. In that study 16 reinforced concrete buildings which were designed based on the Turkish earthquake code were analysed under 80 different ground motions. However that study showed a strong correlation between maximum inter-story drift ratio (MIDR) and roof drift ratios (AIDR), there is still a remarkable dispersion in AIDR at a given maximum inter-story drift ratio. The study

performed by Yakut and Yılmaz (2008), and a lower bound of AIDR with probability of exceeding of 90% at specific MIDRs equal to 1% (IO) and 2% (LS) were calculated to find associated performance levels of IO and LS based on the roof drift ratio. In this case, the associated roof drift ratios corresponding to performance levels, IO and LS were 0.48% and 1.34% respectively, were used for the first case study.

Table 3. 3: List of earthquake ground motions (PEER 2009)

No	Event	Station	Angle(^{0})	M	Soil Type	Epicentral Distance (km)	PGA (*g*)	PGV (cm/sec)
1	Oroville1975	Oroville Airport	180	4.79	Soft soil	14	0.036	2.15
2	Oroville1975	Broadbeck Residence	270	4.7	Soft soil	7	0.168	3.35
3	Coalinga 1983	Coalinga	90	4.89	Soft soil	9	0.2	6.4
4	Dinar 1995	Burdur	180	6.4	Soft soil	39	0.3	33.17
5	Duzce 1999	Cekmece	180	7.2	Soft soil	200	0.0153	2.1
6	Duzce1999	Center	270	7.2	Soft soil	1	0.535	70.77
7	Duzce 1999	Sakarya	180	7.2	Soft soil	20	0.45	55.65
8	Erzincan 1992	Center	90	6.69	Soft soil	9	0.515	72.95
9	Kocaeli 1999	Gebze	90	7.4	Soft soil	8	0.244	38.3
10	Imperial Valley 1940	El Centro Array #9	180	6.5	Alluvium	13	0.37	31.74
11	Kobe, Japan 1995	Takatori	90	6.9	Stiff soil	13	0.611	117.14
12	Kocaeli 1999	Aydin	180	7.4	Soft soil	373	0.0054	2.79
13	Kocaeli 1999	Tosya	90	7.4	Soft soil	342	0.0091	5.55
14	Kocaeli 1999	Usak	270	7.4	Soft soil	237	0.014	4.59
15	Loma Prieta 1989	Saratoga - Aloha Ave	90	6.9	Alluvium	27	0.376	48.52
16	Victoria, Mexico 1980	Cerro Prieto	180	6.3	Stiff soil	34	0.5722	27.06
17	Kobe, Japan 1995	Nishi-Akashi	90	6.9	Stiff soil	9	0.4862	35.73
18	Kobe, Japan 1995	Shin-Osaka	270	6.9	Stiff soil	46	0.243	32.82
19	San fernando 1971	Castaic - Old Ridge Route	90	6.6	Alluvium	25	0.255	29.8
20	Kocaeli 1999	Yarimca	180	7.4	Soft soil	19	0.3055	60.51

3.4. 6 Results of Discussion for the Ground Motion Records

By performing IDA, results obtained from assessed frame was compared as a function of time-dependent damage in the reduction of performance levels. Thus, IDA was also used here to see applicability of developed time-dependent corrosion model as a function of time. Figure 3.13 (a-e) shows the selected three IDA curves of S_a versus roof drift ratio of assessed frames as a function of time.

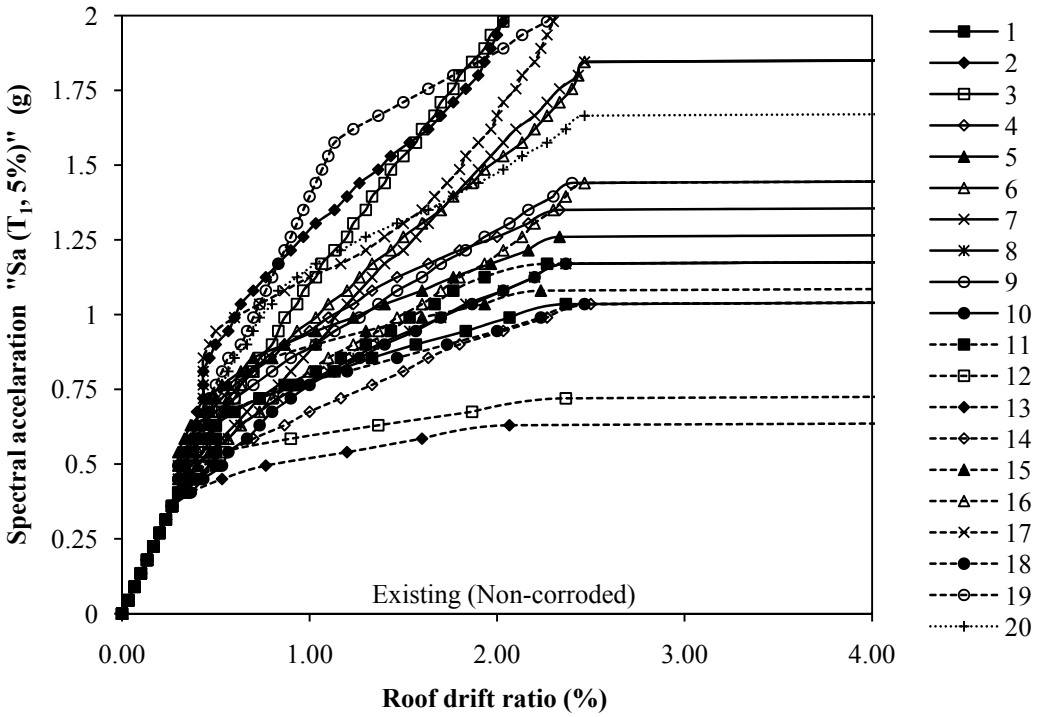

(a)

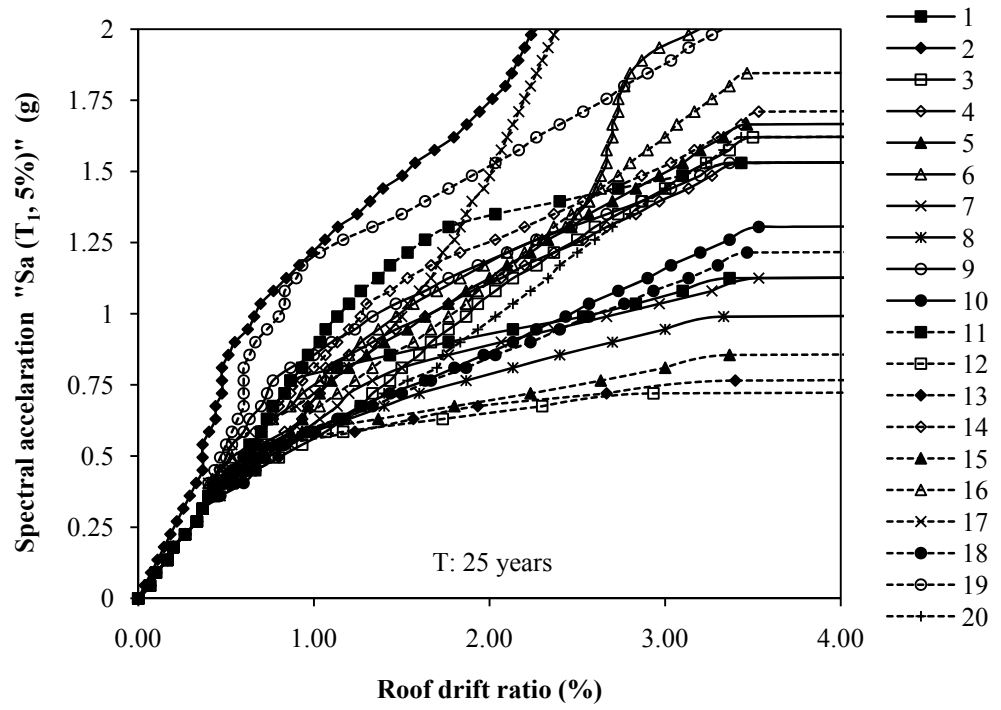
Spectral accelaration "Sa (T1, 5%)" (g)
Roof drift ratio (%)
T: 25 years
0
0.25
0.5
0.75
1
1.25
1.5
1.75
2
0.00
1.00
2.00
3.00
4.00
1
2
3
4
5
6
7
8
9
10
11
12
13
14
15
16
17
18
19
20

(b)

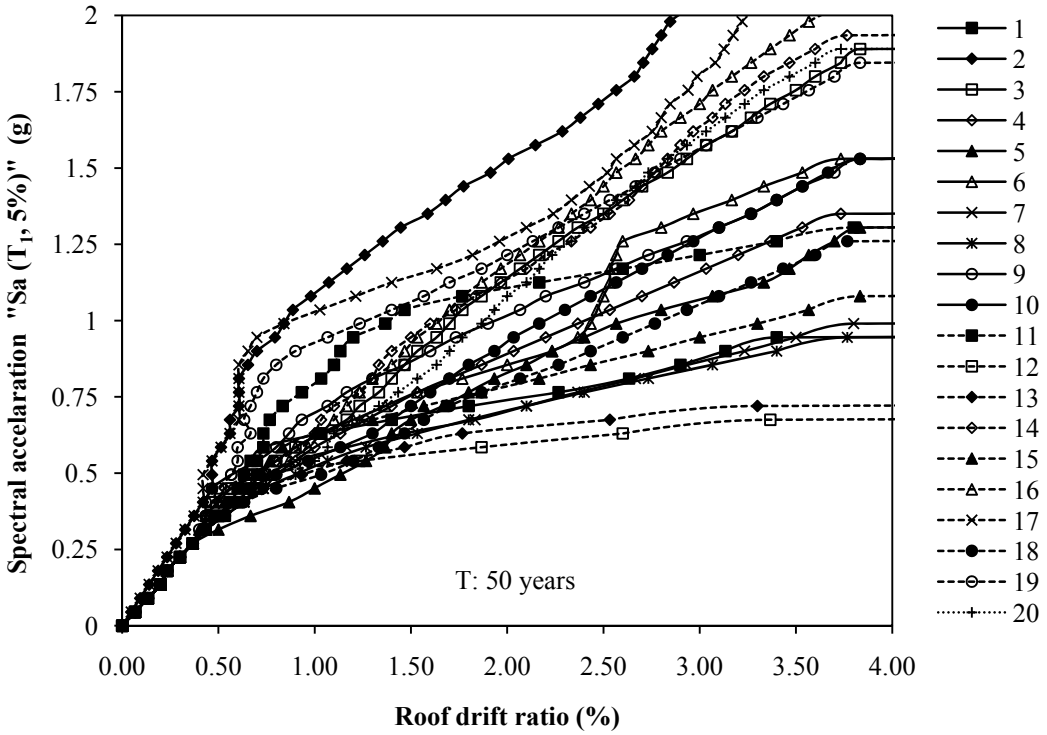
Spectral accelaration "Sa (T1, 5%)" (g)
Roof drift ratio (%)
T: 50 years
0
0.25
0.5
0.75
1
1.25
1.5
1.75
2
0.00
0.50
1.00
1.50
2.00
2.50
3.00
3.50
4.00
1
2
3
4
5
6
7
8
9
10
11
12
13
14
15
16
17
18
19
20

(c)

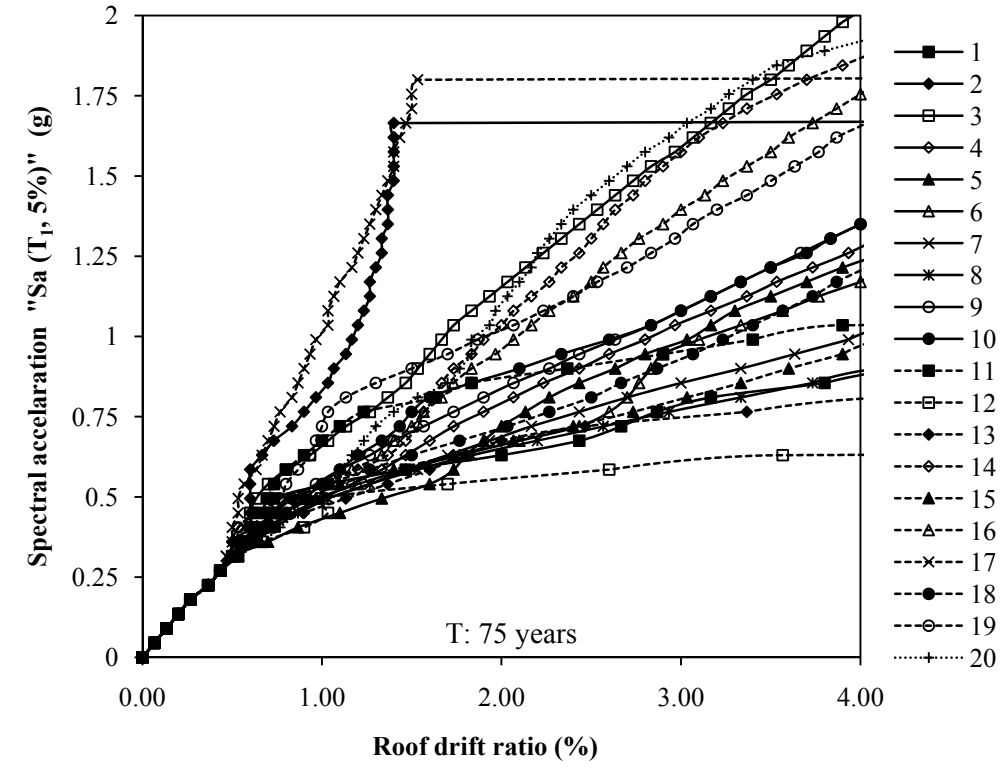

(d)

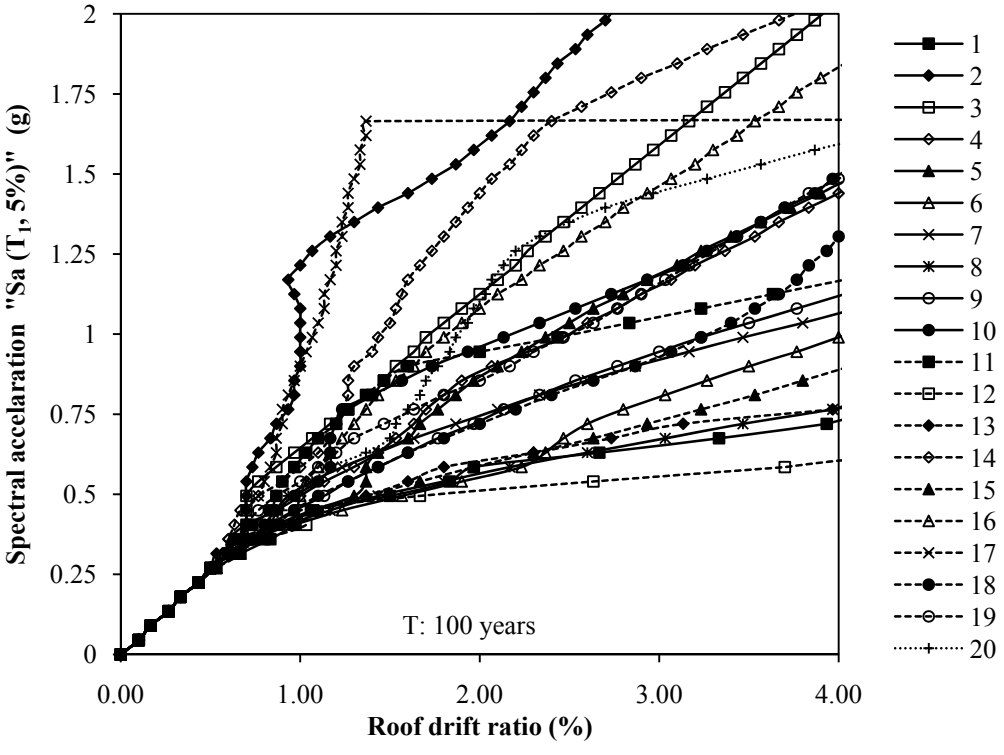

(e)

Figure 3.13: IDA curves: (a) existing, (b) *t*: 25 years, (c) *t*: 50 years, (d) *t*: 75 years, (e) *t*: 100 years.

As shown in Figure 3.13 roof drift ratio increased for the same amount of S_a with increasing time. In order to better understand the changes in roof drift ratio, cumulative distribution function (CDF) of roof drift ratio is needed to be constructed for each time period. Figure 3.14 indicates the CDF of roof drift ratios of each time period according to design base earthquake hazard level (DBE).

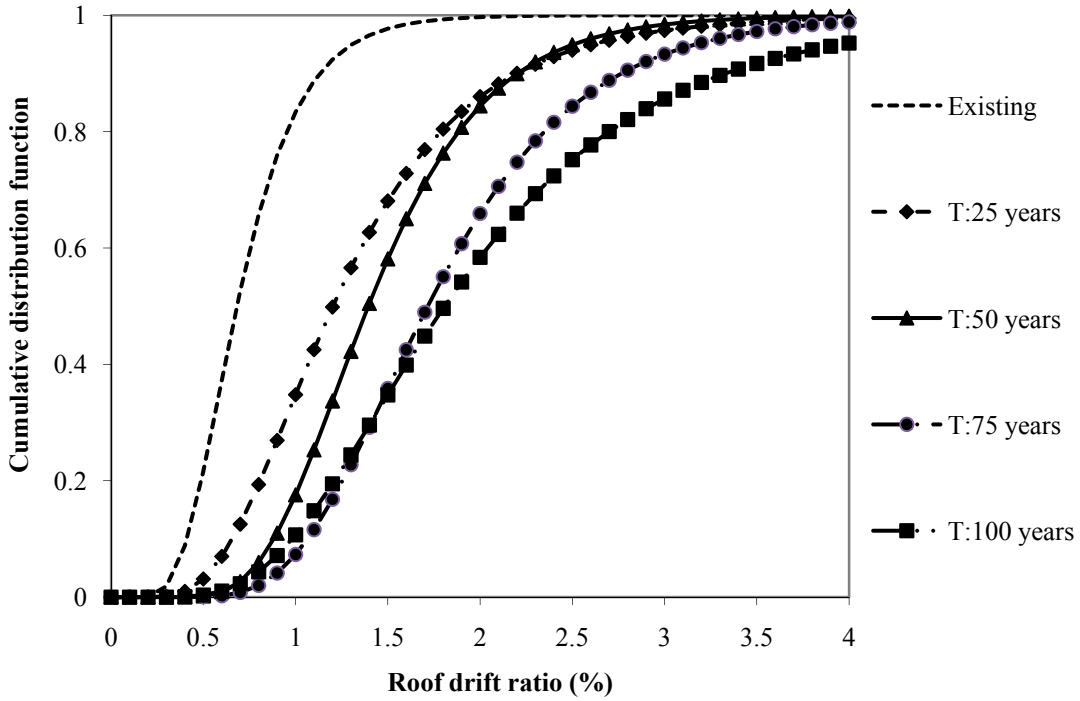

Figure 3.14: Cumulative distribution function of roof drift ratio

The obtained lognormal CDF indicates that there is a serious increasing in roof drift ratios with increasing time due to time-dependent effect of corrosion. For instance, in Figure 3.14, the probabilities of exceeding 2% of roof drift ratio (corresponded to CP limit state) of existing frame was only 0.3% while probabilities of exceeding 2% of roof drift ratio of 25, 50, 75 and 100 years were 14%, 16%, 34%, and 42%, respectively. Figure 3.14 clearly shows that after corrosion induced structure, probabilities of exceeding of roof drift ratio increased as a function of time and caused to decrease the performance level of assessed frame. These probabilities of exceeding of roof drift ratio will be also higher if they are compared with

maximum considered earthquake (MCE) hazard levels. It might be useful to notice that different studies and codes define different thresholds of associated roof drift ratios corresponding to performance levels (IO, LS, CP). Such as FEMA 273 defined the CP of RC frames as roof drift reaches 1.5% of the building height. Even different thresholds of drift ratio were used; the probabilities of exceeding of roof drift ratio would increase due to corrosion when it was compared with existing frame. Limit states at each performance level have been defined and by summarizing the multi–record IDA curves, 16%, 50% and 84% fragility curves were obtained for each time period as a consequence of corrosion damage. Figure 3.15 (a-e) represent multi–record IDA curves (16%, 50% and 84% fragility curves) of each time period.

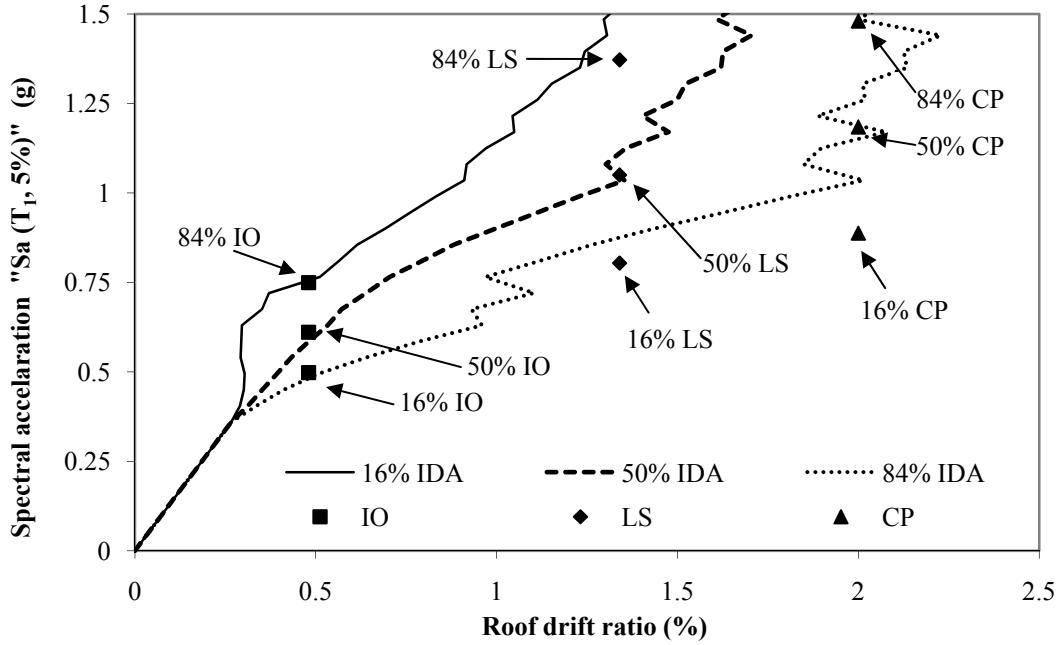

(a)

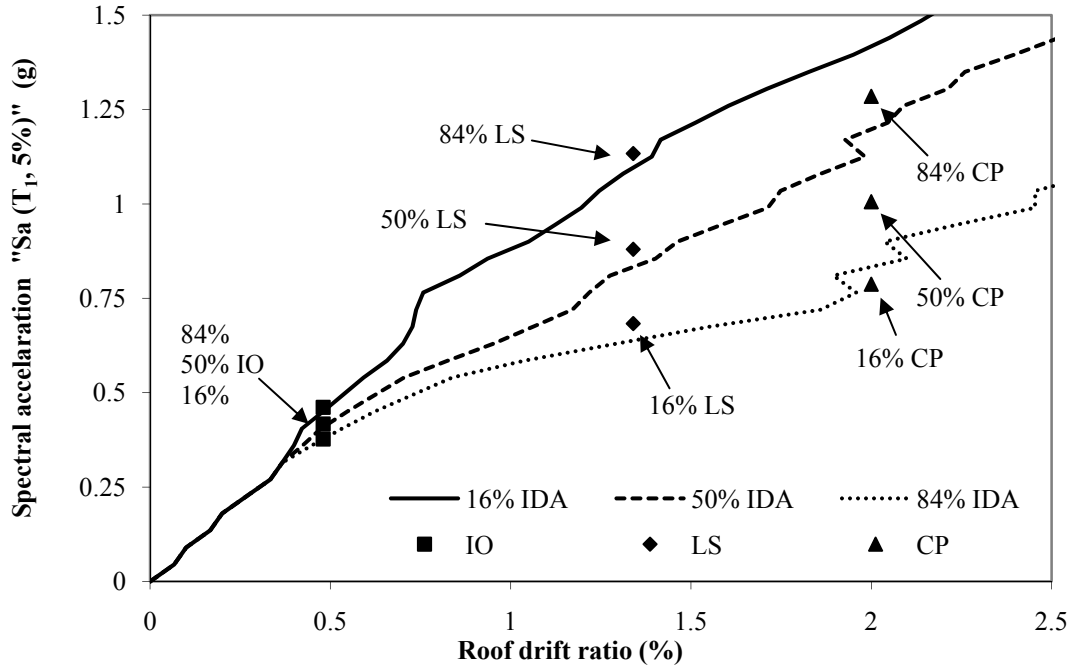
Spectral accelaration "Sa (T1, 5%)" (g)
Roof drift ratio (%)
84% LS
50% LS
84% CP
50% CP
16% CP
84%
50% IO
16%
16% LS
16% IDA
50% IDA
84% IDA
IO
LS
CP

(b)

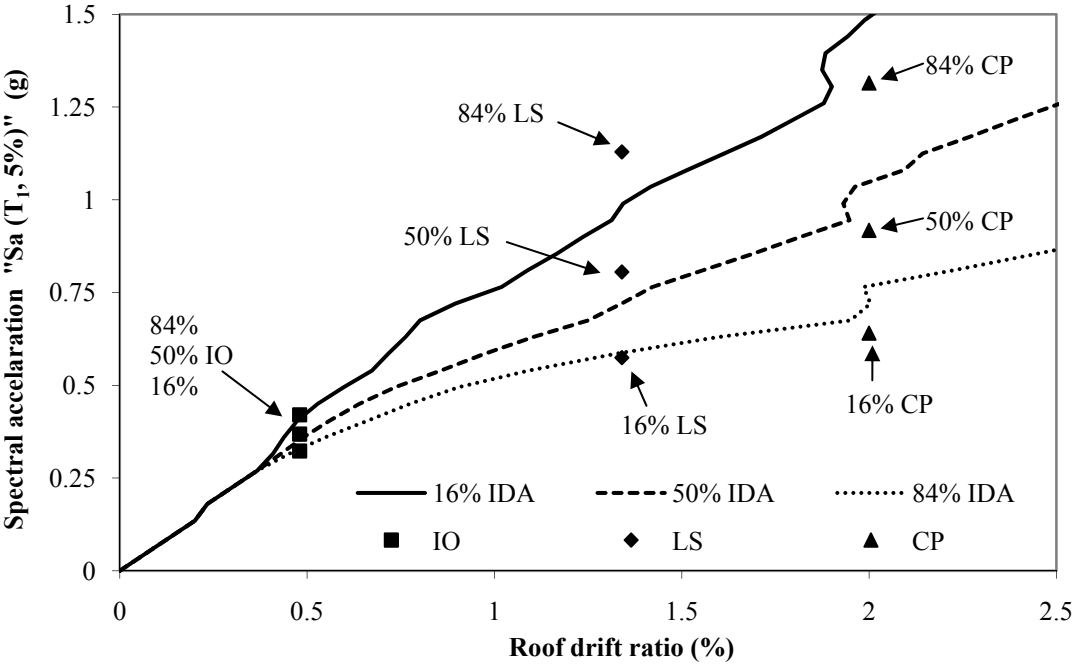
Spectral accelaration "Sa (T1, 5%)" (g)
Roof drift ratio (%)
84% CP
84% LS
50% CP
50% LS
84%
50% IO
16%
16% CP
16% LS
16% IDA
50% IDA
84% IDA
IO
LS
CP

(c)

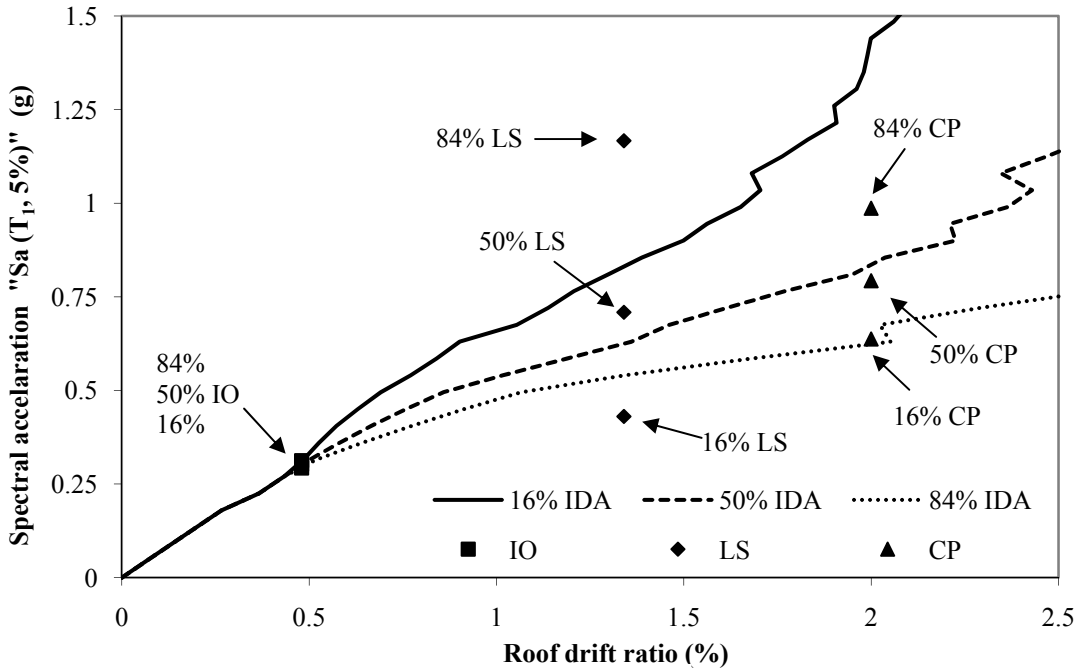

(d)

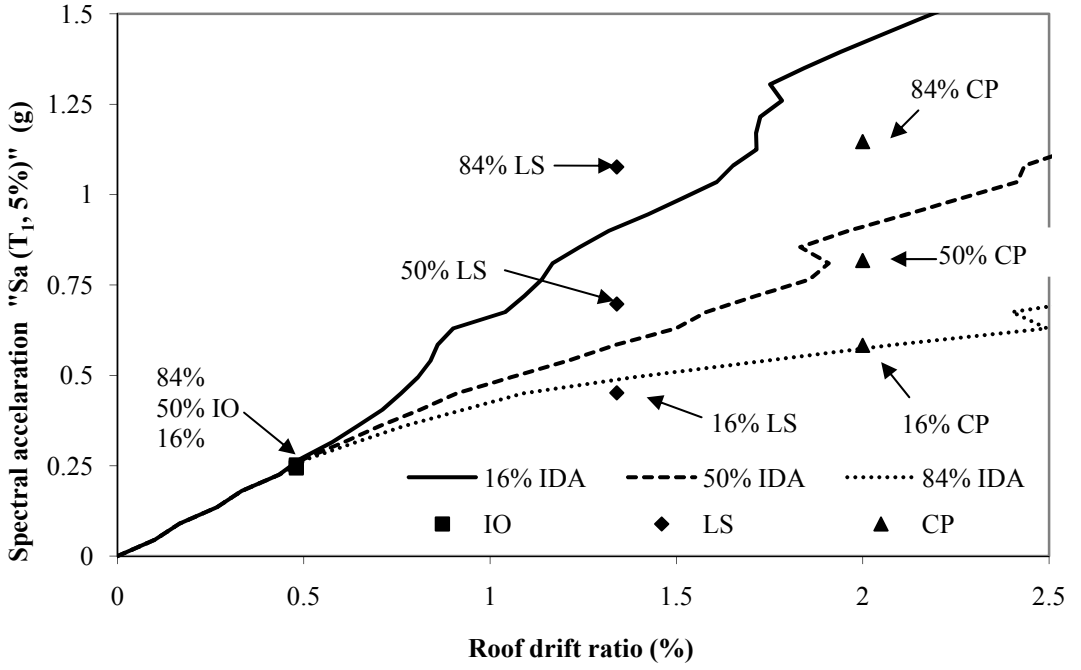

(e)

Figure 3.15: IDA curves and corresponding performance level into their 16%, 50% and 84% fragility :(a) existing frame, (b) *t*: 25 years, (c) *t*: 50 years, (d) *t*: 75 years, (e) *t*: 100 years.

According to the obtained results in Figure 3.15, for the same S_a, roof drift ratio of the frame increased with increasing time. For instance, existing frame (Figure 3.15 (a)) with S_a is equal to 0.75*g*, 84% of earthquake records caused a roof drift ratio

greater than 0.46% while 16% of earthquake records caused a roof drift ratio greater than 1.01%. However, when time period was equal to 25 years at the same S_a, 84% of earthquake records caused a roof drift ratio greater than 0.75% while 16% of earthquake records caused a roof drift ratio greater than 1.93%. Thus, 25 years after construction, due to time-dependent effect of corrosion, 84% of earthquake records caused to reduce performance level from IO to LS whilst 16% of earthquake records caused to reduce performance level from LS to CP. With increasing time at the same S_a of 50 years, 84% of earthquake records caused a roof drift ratio greater than 0.98% while 16% of earthquake records caused a roof drift ratio greater than 1.99%. Thus, for a time period of 50 years, 84% of earthquake records again reduced performance level from IO to LS with a higher percentage of roof drift ratios whilst 16% of earthquake records reduced performance level almost to collapse level based on assumed associated roof drift ratios corresponding to performance levels. Recorded roof drift ratios for both 75 and 100 years at the same S_a, 84% of earthquake records caused a roof drift ratio greater than 1.18%, 1.2% while 16% of earthquake records caused a roof drift ratio greater than 2.49%, 2.67% respectively. Obtained results clearly indicated that behaviour of RC frame damaged by the effect of corrosion as a function of time. By summing up time-dependent reduction in cross sectional area of reinforcement bars, reduction in concrete strength and slip, all these phenomena provides more accurate prediction of performance level of RC structures subject to corrosion as a function of time. This phenomenon plays an important role in evaluation of time to strengthening of structures under the expected seismic motions to prevent serious damage to structures. In order to define the time-dependent performance level of the assessed frame, time-dependent fragility curves of probabilistic structural damage estimation of each time period were obtained in terms

of PGA for each limit state. Figure 3.16 (a-c) show fragility curves in terms of PGA as a function of time. Table 3.4 summarizes the results of fragility curves based on probability of exceeding of limit states as IO, LS and CP of assessed frame as a function of corrosion rate for different time periods at different seismic zones (through Z_1 to Z_4) according to recommended A_0 by Turkish earthquake code (2007).

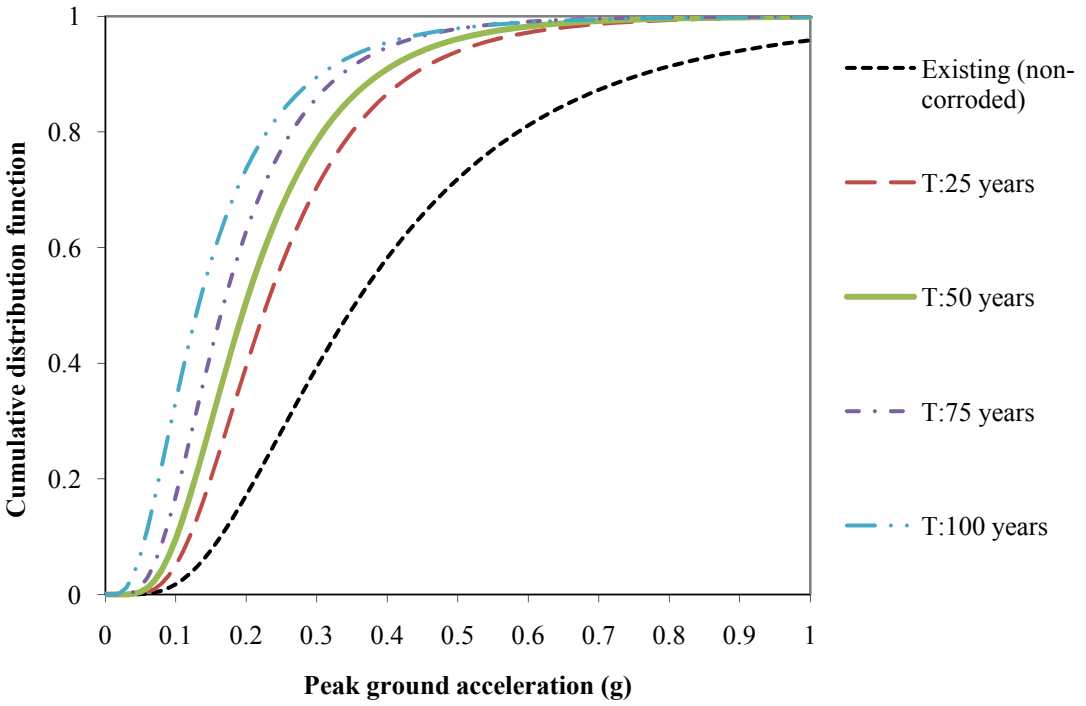

(a)

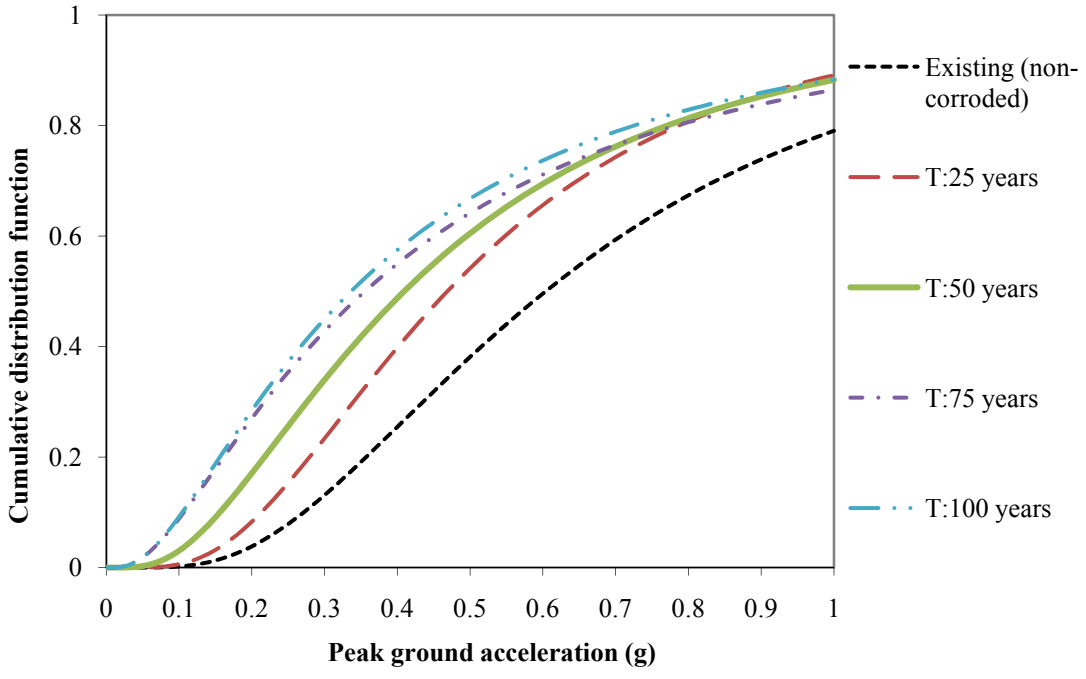

(b)

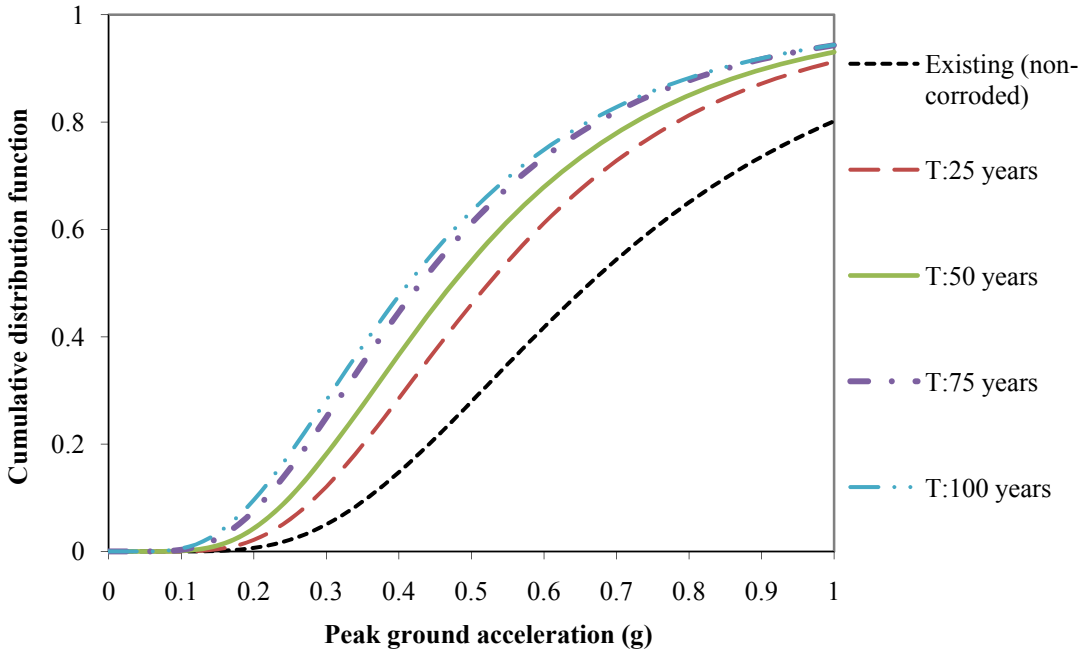

(c)

Figure 3.16: Fragility curves of limit states: (a) immediate occupancy, (b) life safety, (c) collapse prevention.

Table 3. 4: Probability of exceeding of limit states of IO, LS and CP at different seismic zones.

		PGA(*g*)-Seismic Zone			
		A_0: 0.4	**A_0: 0.3**	**A_0: 0.2**	**A_0: 0.1**
Frame	**Limit state**	Z_1	Z_2	Z_3	Z_4
Existing	IO	58	39	17	1.7
	LS	25	13	4	0.19
	CP	15	5	0.65	0.0046
T: 25 years	IO	86	70	39	5
	LS	40	23	8	0.6
	CP	29	12	2	0.02
T: 50 years	IO	91	78	50	10
	LS	49	33	17	3
	CP	37	18	4	0.09
T: 75 years	IO	94	86	63	17
	LS	55	43	27	9
	CP	45	25	8	0.3
T: 100 years	IO	95	89	74	33
	LS	58	45	28	9
	CP	48	28	10	0.5

As shown in Figure 3.16 and Table 3.4, there is a high seismic risk for both first seismic zone (Z_1) and second seismic zone (Z_2) due to time-dependent effects of

corrosion. At first seismic zone, probability of exceeding the limit state corresponding to IO was 58% for existing frame while this probability was 86% after 25 years. This probability of exceeding limit state increased to 91% after 50 years. For CP limit states of first seismic zone, probability of exceeding limit state increased from 15% to 29%, 37% after 25 and 50 years respectively. At second seismic zone, probability of exceeding of limit state corresponding to IO was 39% for existing frame while this probability increased to 70% after 25 years. For the same seismic zone (Z_2), probability of exceeding limit state corresponding to CP was 5% while this probability was 12% after 25 years. Beside these, there were strong relationships between obtained results of slip displacements and fragility curves (Figure 3.13 and 3.17(a-c)). According to Figure 3.12 and results in Table 3.2, during propagation of corrosion phases, additional displacement due to slip has a serious effect to reduce the performance level of the existing frame. According to Table 3.4, probabilities of exceeding of limit states corresponding to the performance levels were rising sharply between the time periods of existing and 25 years. However, for the next time periods, these probabilities of exceeding was increasing slightly, reaching their maximum values as a function of time. Same results were also obtained in Figure 3.14 where probabilities of exceeding 2% of roof drift ratio increased rapidly for the same time periods of ranges, then continued to increase slightly for the next time periods. The following section 3.5 demonstrates another case study of MDOF system.

3.5 A Case Study of Time-dependent Nonlinear Seismic Performance Assessment of a Corroded 50-year-old Reinforced Concrete Building

In this case study, different than previous one, a MDOF system was performed. Particularly, different than previous case study, plastic hinge properties were taken into account by modified moment-curvature relationships due to different effects of corrosion.

In this case study a corroded 50 years age of a high school building was analysed as a function of time. Obtained experimental data at the construction were used to predict the performance level of the structure for different time periods by combining two major effects of corrosion. Deformation due to bond-slip relationships and loss in cross sectional area of reinforcement bars were examined as a function of corrosion rate for different five time periods (i.e., non-corroded, 25,50 (existing) ,75 and 100 years). Time-dependent plastic hinges properties were defined as a consequence of corrosion effects and they were used to perform nonlinear push-over analyses. Then nonlinear IDA was performed under individual 20 earthquake ground motion records to predict the time-dependent performance levels of the structure as a function of corrosion rate. Results showed that corrosion has a serious effect to define time-dependent performance levels of the structures by loosing bond strength.

3.5.1 Description of the Analyzed Structure

Analysed high school building was one of the selected buildings of a project directed by Eren and Sensoy (2010). Eren and Sensoy (2010) in that study developed the strength-age-permeability-corrosion potential relations for the concrete by assessing eight different existing RC building in Famagusta with different distances from sea and different age of the structures. Figure 3.17 shows the analysed existing

high school building for present study. The performed building has three storeys with a total height of 14 m. Distance of building to sea is 840 m which has 90 % probability of corrosion potential based on half cell test.

Figure 3.17: Analysed high school building.

Building consists of three main different blocks. For present study a frame of main entrance block was investigated. Storey heights of the selected frame were identical and equal to 4.7 m. The slabs thickness of the frame is 17 cm, where calculated additional dead and live loads of the slap were 500 kg/m^2. Soil class was classified as soft clay (group D), building importance factor was taken as 1.4 and effective ground acceleration coefficient (A_0) is taken 0.3*g* (seismic zone 2) according to Turkish earthquake code (2007). Comprehensive information was collected for the assessed high school building study done by Eren and Sensoy (2010). With this scope, 20% of the beams and columns were opened to identify amount and dimensional properties of reinforcement bars. Figures 3.18, 3.19 and 3.20 show an opened interior beam, outer and interior columns from the selected frame respectively.

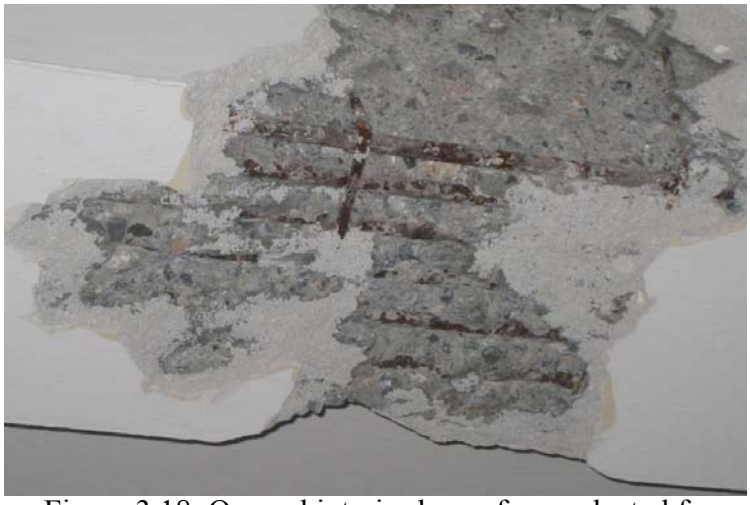

Figure 3.18: Opened interior beam from selected frame.

Figure 3.19: Outface of S_3 column.

Figure 3.20: Inside face of S_3 column.

For present study, a number of reinforcement bars were taken from the outer faces and inside faces of the structural element to calculate the corrosion rate. According to the described standard ASTM G1-03 (2003), mechanical cleaning was done to calculate the corrosion rate by removing the corrosion product from the surface of reinforcement bars. Calculated corrosion rates of outer face and inside face of structural members were 5.37 $\mu A/cm^2$ and 0.64 $\mu A/cm^2$, respectively. In order to indentify the concrete compressive strength, core test was done by taking core samples from 10% of the total number of the columns. Calculated average concrete compressive strength of 50 years after construction was 31 MPa for the corroded RC columns. Based on experimental study, measured concrete cover for columns and beams were 2.5 cm, spacing of reinforcement bars were almost adjacent to each other for many assessed columns. Detail reinforcement bars of columns and beams are shown in Figure 3.21. In Figure 3.21 before corrosion occurred, the lateral reinforcement bars of columns and beams were ϕ10/150 and ϕ10/250 respectively.

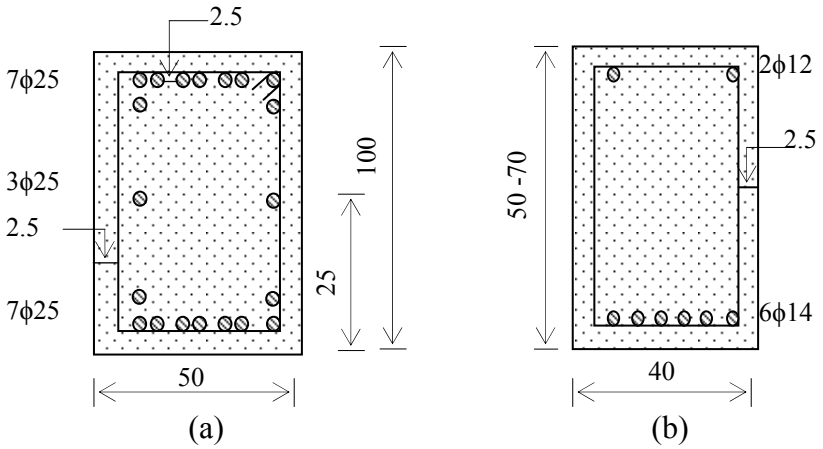

Figure 3.21: Details of reinforcement bars before corrosion induced (dimensions in cm): (a) columns, (b) beams.

Vertical distributed loads that are used in the analyses are depicted in Figure 3.22. Dimensions of all columns are identical and equal to 50 by 100 cm with same detail of reinforcement bars.

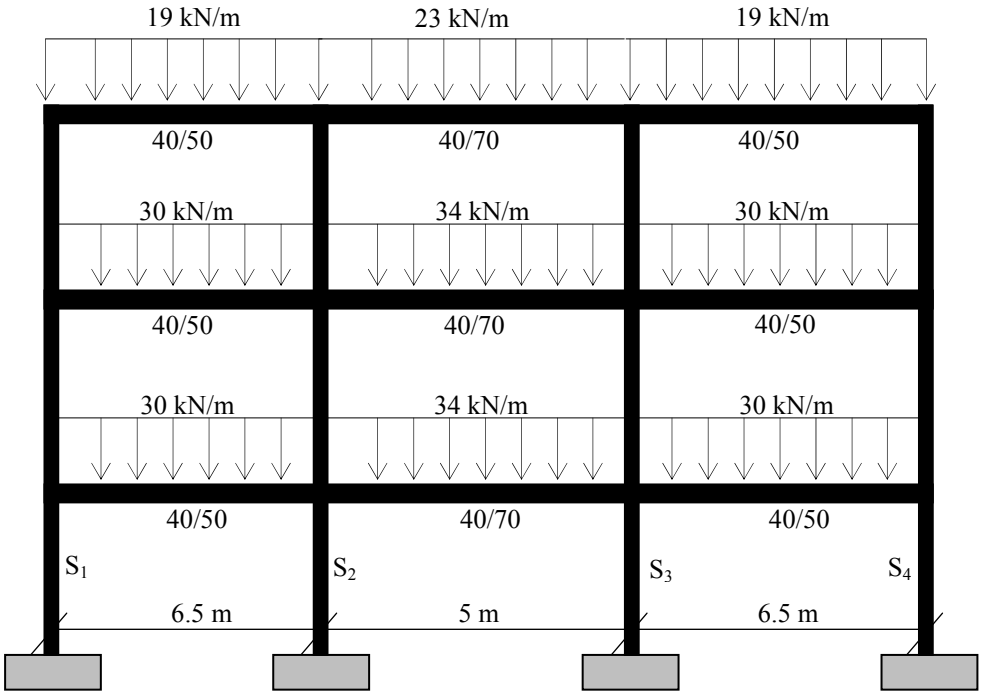

Figure 3.22: Vertical loads used in the analyses.

3.5.2 Time-dependent Behaviour of RC Sections

Once the time-dependent loss in cross sectional area of the reinforcement bars is known, the time-dependent slip deformation can be obtained by using time-dependent moment–curvature relationships as a consequence of corrosion effects. Therefore, the present study goes one step further by considering the bond–slip relationships of the MDOF frame as a consequence of corrosion effects. In this study a novel bond-slip model developed by Sezen and Setzler (2008) was used to predict the slip displacement. The model developed by Sezen and Setzler (2008) has not been performed to predict the performance level of corroded RC members as a function of time. Therefore, uniform bond stress was assumed by Sezen and Setzler (2008). For the present study, in order to predict the slip rotation as a consequence of

corrosion effects, the bond stress was adopted from the study done by Stanish et al. (1999) to calculate the bond stress as a function of corrosion level instead of the uniform bond stress assumed by Sezen and Setzler (2008). With the model developed by Stanish et al. (1999), the 95% confidence level is expressed by equation 3.40:

$$\frac{u_b}{\sqrt{f'_c}} = 0.63 - 0.041x \tag{3.40}$$

where x is the percent of mass loss of the steel bar. The model developed by Stanish et al. (1999) was obtained based on the results of tests of RC slabs without stirrups. It is well known that transverse reinforcement has a major effect on the bond strength between concrete and corroded longitudinal reinforcement. Therefore, in order to ensure the effect of transverse reinforcement, a modification was done for the model develop by Stanish et al. (1999) by using the general development length expression in ACI 318 (2005) which includes the effect of transverse reinforcement. According to ACI 318 (2005), development length can be calculated by given equation. 3.41:

$$l_d = \frac{0.9\psi_s\psi_t\psi_e\lambda}{c_b + K_{tr}} d_b{}^2 \frac{f_y}{\sqrt{f'c}} \tag{3.41}$$

where, ψ_s is the reinforcement size factor, ψ_t is the traditional reinforcement location factor to reflect the adverse effects of the top reinforcement casting position, ψ_e is a coating factor reflecting the effects of epoxy coating, c_b represents the confinement provided by the encasing concrete to resist a bond splitting failure, K_{tr} is the confinement attributed to transverse reinforcement, c_b is a factor that represents the smallest of the side cover. From basic mechanics, the required development length as a function of bond stress can be calculated by given equation 3.42:

$$l_d = \frac{f_y d_b}{4u_b} \tag{3.42}$$

Thus, assuming uniform bond stress, $\frac{u_b}{\sqrt{f'_c}}$ can be written as given equation 3.43:

$$\frac{u_b}{\sqrt{f'_c}} = \frac{f_y d_b}{4l_d}\frac{1}{\sqrt{f'_c}} \tag{3.43}$$

By substituting for l_d from equation 3.41 into equation 3.43, the bond strength of the uncorroded reinforcement bars according to ACI 318 code (2005) can be written as given equation 3.44:

$$\frac{u_b}{\sqrt{f'_c}} = \frac{c_b + K_{tr}}{3.6(\psi_s \psi_t \psi_e \lambda d_b)} \tag{3.44}$$

The ratio of bond strength of corroded to non-corroded reinforcement bars (x=0%) based on the model developed by Stanish et al. (1999) yield as;

$$\frac{\left(\frac{u_b}{\sqrt{f'_c}}\right)^{corroded}}{\left(\frac{u_b}{\sqrt{f'_c}}\right)^{uncorroded}} = 1 - 0.065x$$

Thus, according to ACI 318 (2005), the bond strength with effect of transverse reinforcement and as a function of corrosion rate can be written as given equation 3.45:

$$\frac{u_b}{\sqrt{f'_c}} = (1 - 0.065x)\frac{c_b + K_{tr}}{3.6(\psi_s \psi_t \psi_e \lambda d_b)} \tag{3.45}$$

The proposed equations 3.44 and 3.45 include effect of all parameters on bond strength. If the reinforcement bars are corroded, these derivations assume that effect of corrosion and transverse bars are a reduction in their confinement effect. Given equations 3.44 and 3.45 were adopted in the model developed by Sezen and Setzler (2008) for the prediction of slip rotations as a function of corrosion rate. Experimentally obtained corrosion rates were used to predict loss in cross sectional area of reinforcement bars. As it is expected, due to chloride diffusion which ions or molecules move from an area of higher concentrations to lower concentrations, different corrosion rates occurs for the same structural members. As it is shown in Figures 3.19 and 3.20, outface of the column have more corrosion rate then inside face of the same column. Therefore, in order to predict more accurate time-dependent behaviour of RC sections, different corrosion rates were taken into account in nonlinear analyses based on inside and outface of columns. Based on experimental works, the loss of cross sectional area in the reinforcement bars of the outer faces of columns after 25, 50, 75 and 100 years were 12.45%, 24.89%, 37.34%, and 49.79%, and the loss of cross sectional area of the reinforcement bars in the inside faces of the columns and beams were 1.47%, 2.95%, 4.24%, and 5.89%, respectively. The predicted loss of cross sectional area in the reinforcement bars were used to predict time-dependent moment-curvature relationships. For each story of columns for five different time periods, a total of 60 time-dependent moment-curvature relationships were obtained as a function of corrosion rate for two different models, one developed by Kent and Park (1971) and the other by Saatcioglu and Razvi (1992). A newly developed software program SEMAp (Inet et al., 2009) was used. SEMAp (Inet et al., 2009) lets the user define the exact location and spacing of the reinforcement bars with their mechanical properties. Moreover, the stress-strain

relationships of steel and concrete can be modelled by the user. Predicted time-dependent moment-curvature relationships of ground, first, and second floors of S_1 and S_3 columns are shown in Figures 3.23 and 3.24 respectively.

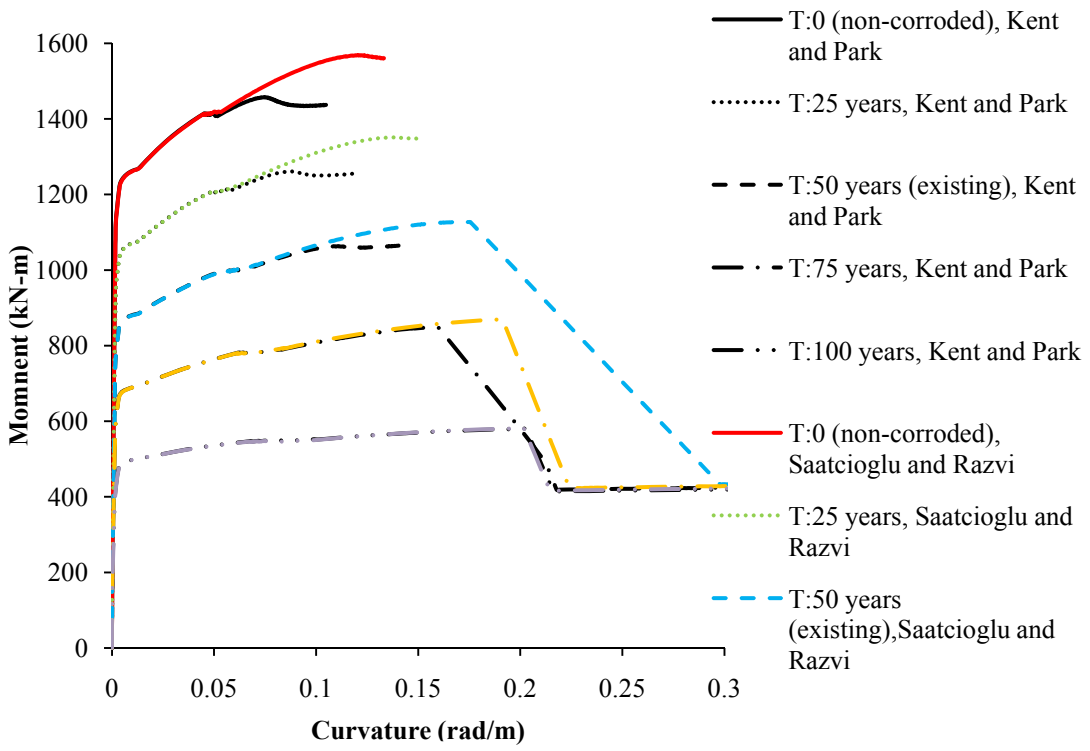

(a)

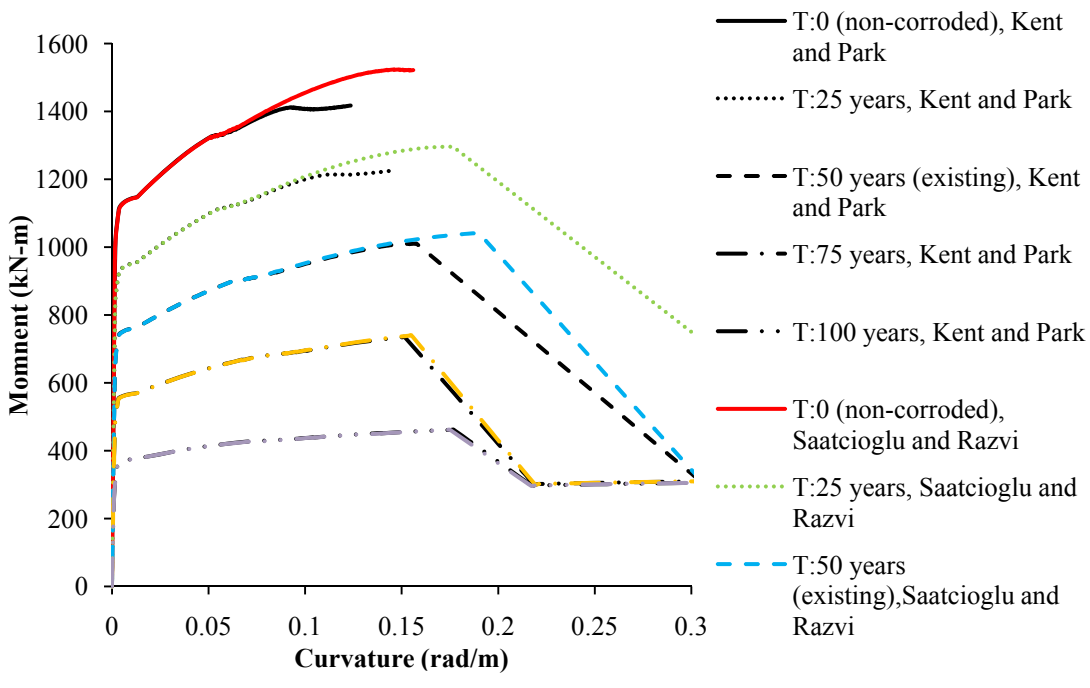

(b)

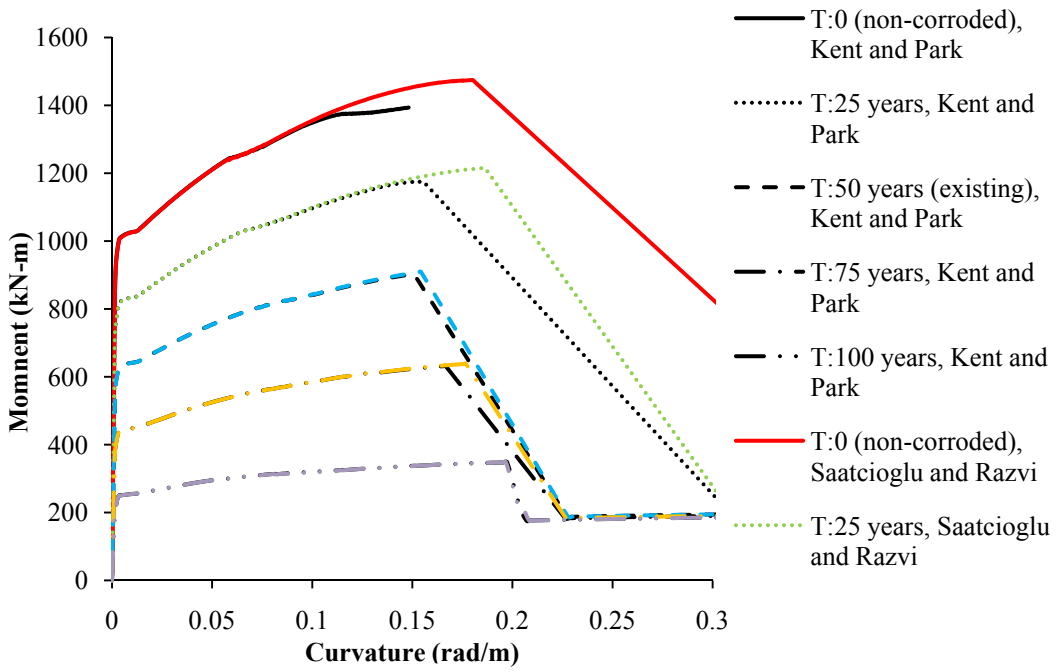

(c)

Figure 3.23: Time-dependent moment-curvature relationships of S_1 column: (a) ground floor, (b) first floor, (c) second floor

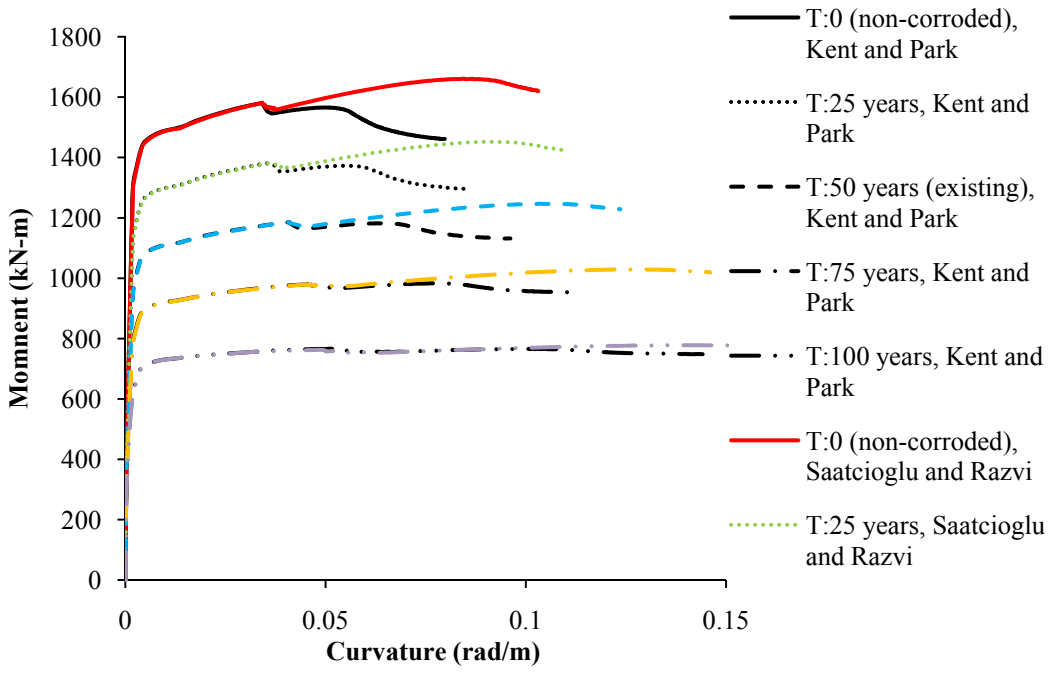

(a)

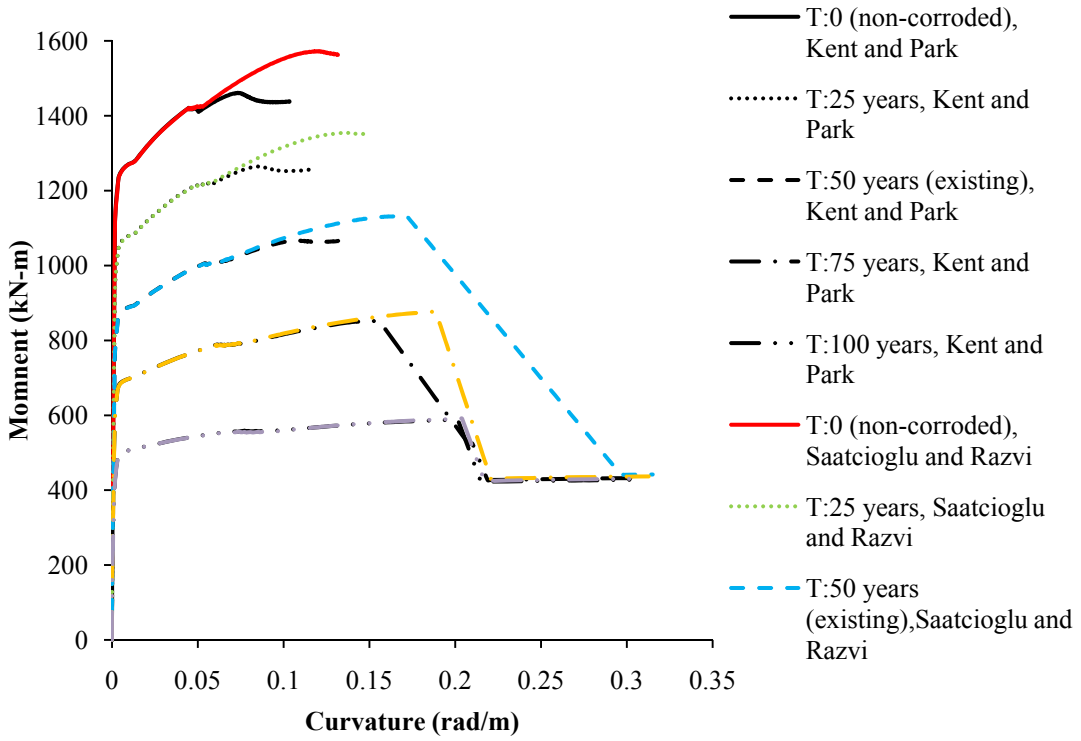

(b)

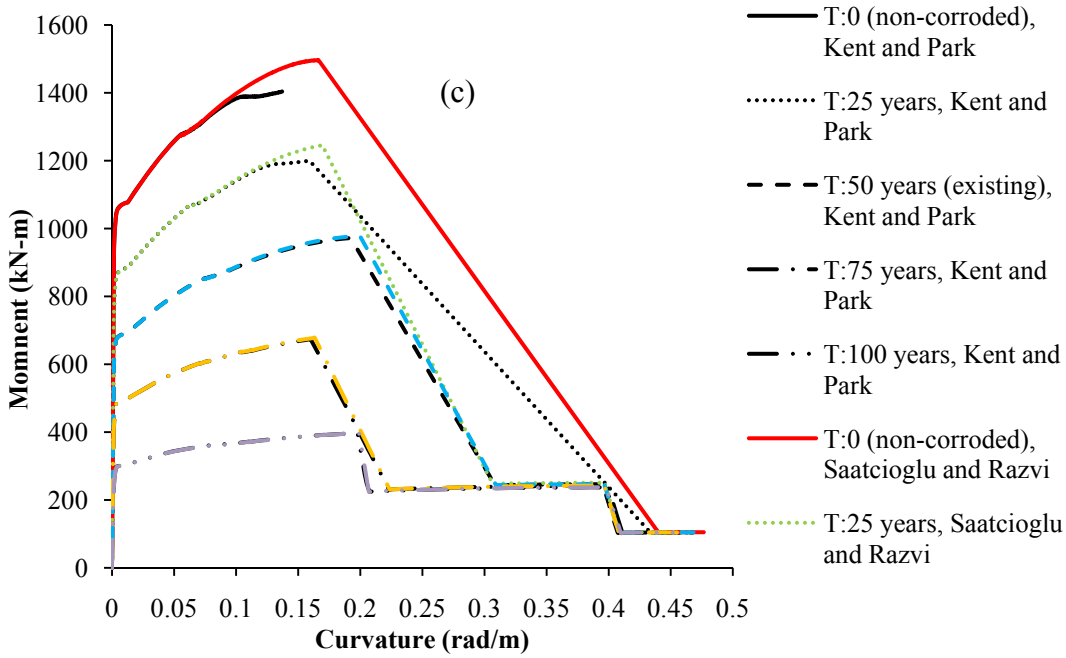

Figure 3.24: Time-dependent moment-curvature relationships of S_3 column: (a) ground floor, (b) first floor, (c) second floor.

As it is known, occurred energy due to friction between composite materials and movement of structures need to be absorbed during earthquakes. Therefore, in order

to prevent heavy damage of RC structures, these energy absorptions can be proven by small damages on structures, that is why it is a general expectation by engineers to have small damages during earthquakes. In Figures 3.23 and 3.24, the area under the curvature represents the stored or dissipated energy by RC columns. As shown in Figures 3.23 and 3.24, due to time-dependent corrosion effect, section capacity and energy dissipation reduced as a function of time whilst rotation increased for fewer amounts of moment values which cause to increase lateral displacement. Stiffness degradation occurs due to premature yielding of reinforcement bars as shown in Figures 3.23 and 3.24. For instance, premature yielding moment of ground floor of S_1 column, corresponding time periods of 25, 50 (existing structure), 75 and 100 years were 15%, 29%, 47%, and 61%, respectively. For the same floor of premature yielding moment of S_3 column, corresponding time periods of 25, 50 (existing structure), 75 and 100 years were 13%, 25%, 38%, and 52%, respectively. Loss in area of tensile steel bars due to corrosion, the depth of the neutral axis also reduces, and curvature increases with a less value of yielding moments. Thus, at crack segment, stiffness of the section reduces as a function of time as a consequence of corrosion effect. Time-dependent changes in the depth of the neutral axis along the corroded RC members of S_1 and S_3 columns are shown in Figures 3.25 and 3.26 respectively. In Figures 3.25 and 3.26, reductions in the depth of the neutral axis were calculated when maximum compressive strain in concrete was equal to 0.003.

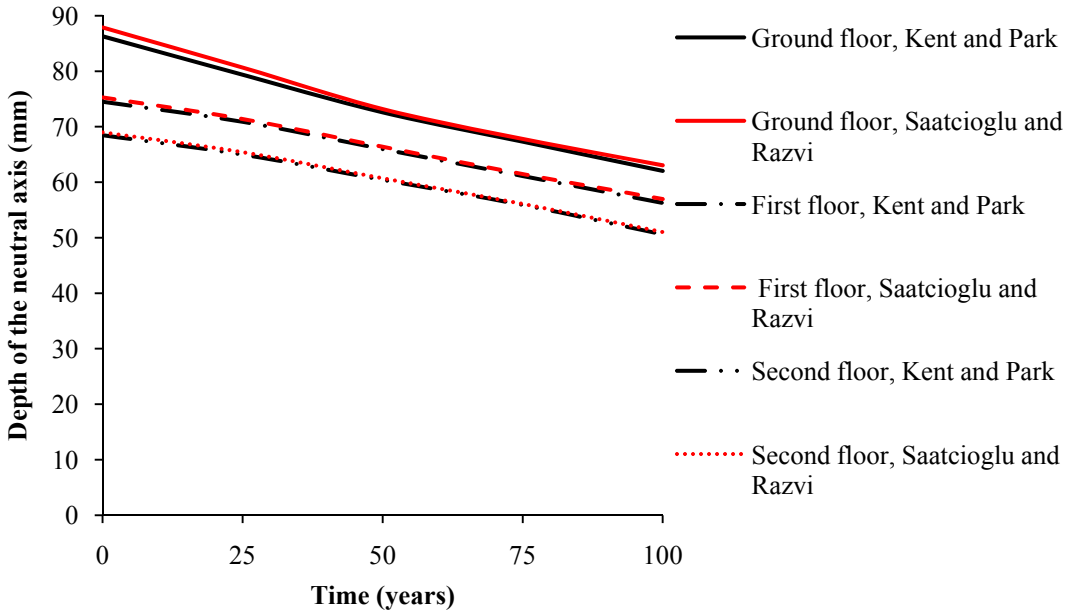

Figure 3.25: Time-dependent changes of the neutral axis of S_1

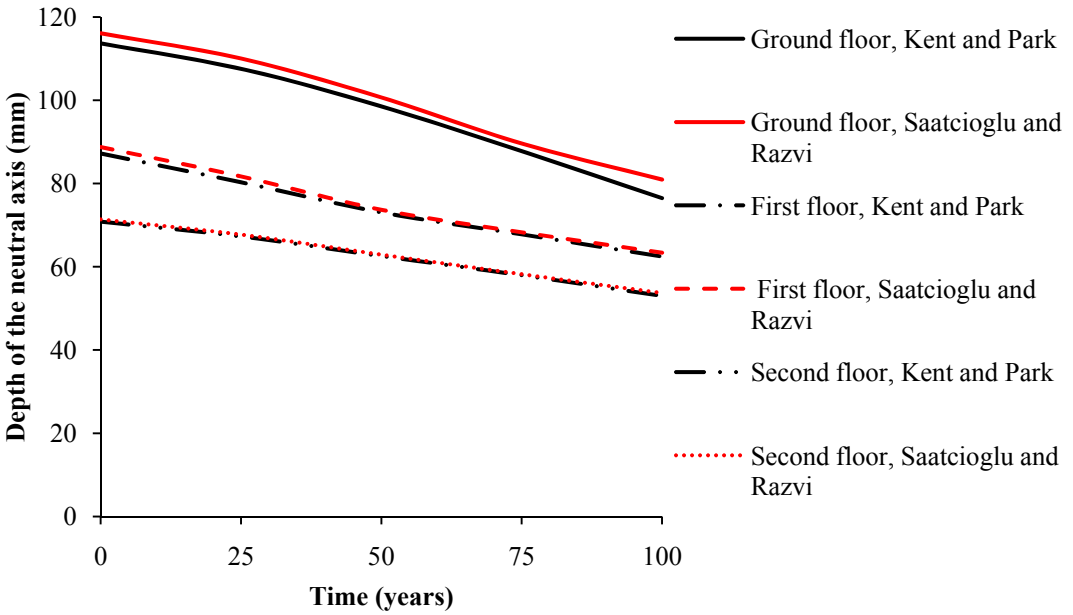

Figure 3.26: Time-dependent changes of the neutral axis of S_3.

Due to time-dependent effects of corrosion, reduction in load carrying capacity of a RC column subjected axial loading can be evaluated from a moment-load (M-N) interaction diagram. The results of time-dependent M-N interaction diagrams of ground floor of S_1 column are plotted in Figure 3.27 as a function corrosion rate by

considering two different models developed by Kent and Park (1971), and Saatcioglu and Razvi (1992).

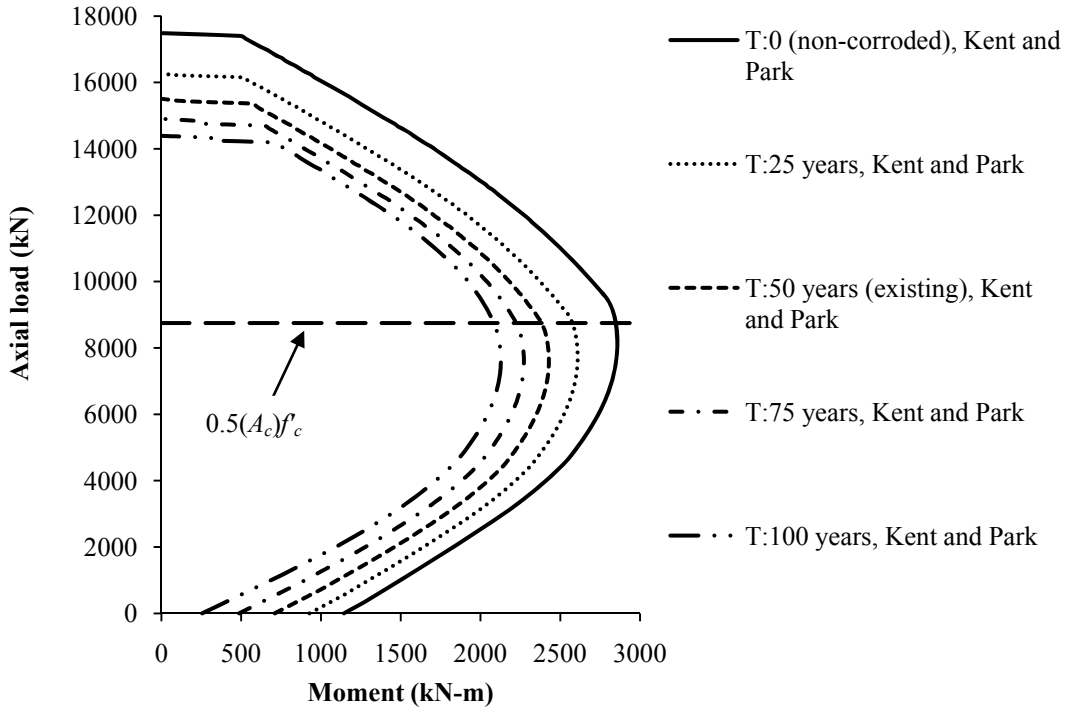

(a)

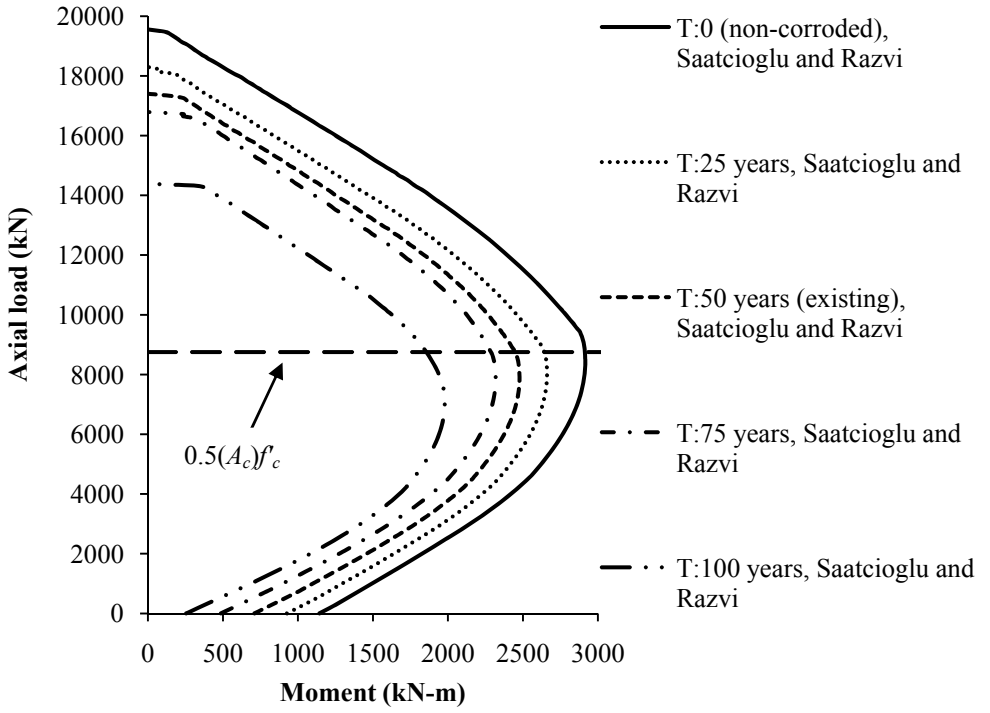

(b)

Figure 3.27: Time-dependent M-N diagrams of S_1 column: (a) Kent and Park (1971), (b) Saatcioglu and Razvi (1992).

Time-dependent interaction diagrams provide prediction of moment capacity of sections. In Figure 3.27, line of $0.5A_c f_c'$ represent the maximum allowable load that can be carried by a section according to Turkish earthquake code (2007), where A_c is the gross sectional area of a section. On this line, moment capacity of a corroded RC section reduced as a function of time due to corrosion. When time was equal to zero (non-corroded), the moment capacity of S_1 column (see Figure 3.27 (a)) based on Kent and Park model (1971) was 2857 kN-m on this line, but this capacity decreased to 2598 kN-m, 2411 kN-m, 2255 kN-m, 2112 kN-m after 25, 50 (existing structure), 75 and 100 years respectively. These results also support the above finding about time-dependent changes of the depth of the neutral axis of the corroded RC sections. Results indicate that reduction in depth of the neutral axis and moment capacity decreases with increased corrosion rate. Based on result of time-dependent moment-curvature relationships, changes in depth of neutral axis and M-N interaction diagrams, there was not much difference between models developed by Kent and Park (1971), and Saatcioglu and Razvi (1992). Therefore, author of this study used results of model developed by Kent and Park (1971) for time-dependent moment-curvature relationships. It should be noted that even model developed by Saatcioglu and Razvi (1992) would have been used for further analyses; the reduction in performance level would be inevitable in IDA when time-dependent assessed frames are compared with non-corroded frame.

3.5.3 Time-dependent Nonlinear Frame Analyses

Predicted time-dependent moment-curvature relationships were used in order to perform time-dependent nonlinear push-over analyses. SAP 2000 (CSI, 2000) program was used to analyse the selected frame. In order to ensure the effects of corrosion on the structural behaviour during push-over analyses, user-defined plastic

hinges properties are needed to be modelled for each corresponding time periods. For this reason nonlinear analysis of RC columns based on the moment-curvature relationships was predicted as a function of corrosion rate for different time periods. Force-deformation behaviour is also needed to be plotted to define the behaviour of a plastic hinge properties. Figure 3.28 shows force-deformation relationships to define the behaviour of a plastic hinge by FEMA-356 (2000). On Figure 3.28 labelled A, B, C, D defines force-deformation behaviour which is detail explained by FEMA-356 (2000). The locations of hinges of assessed frame were located according to study done by Inel and Ozmen (2006) as shown in Figure 3.29.

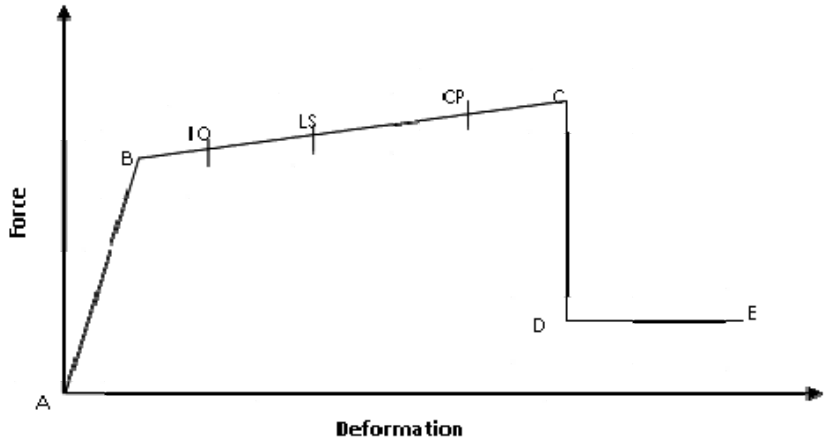

Figure 3. 28: Force-deformation relationship of a plastic hinge.

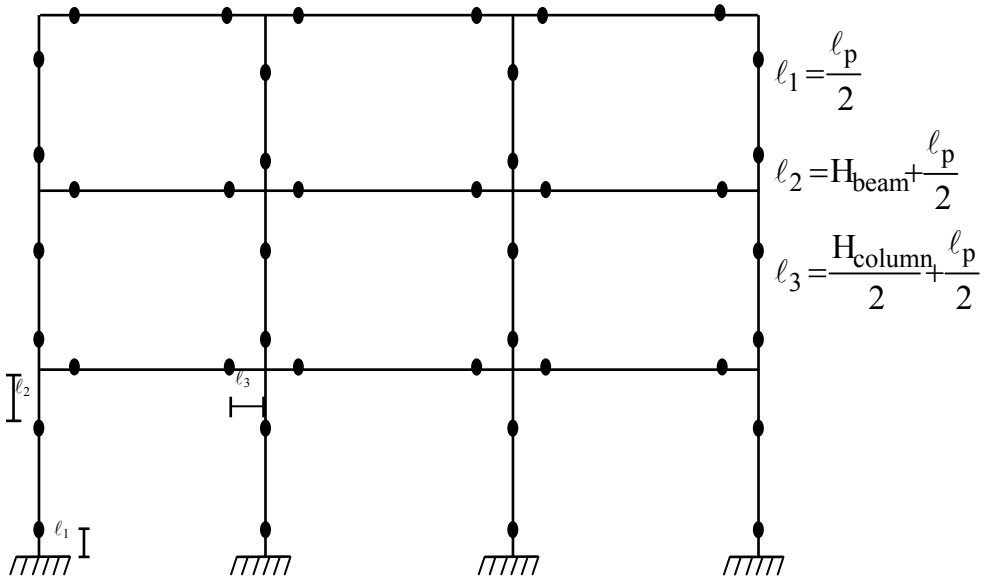

Figure 3.29: Hinge locations at columns and beams.

By using moment-rotation relationships instead of moment-curvature, length of the plastic hinges can be taken into account directly in nonlinear analyses. Therefore, predicted time-dependent moment-curvature relationships as a consequence of corrosion effects are used to calculate rotation of plastic hinges of each case of structural members. The rotation of plastic hinges can be easily calculated by interaction between length of plastic hinge and curvature at a point by given equation 3.46 (Varghese; 2006). Figure 3.30 shows calculated moment-rotation for two different time periods of ground floor of S_1 column.

The rotation of plastic hinge: $\int \varphi ds : \varphi L_p : \theta$ (3.46)

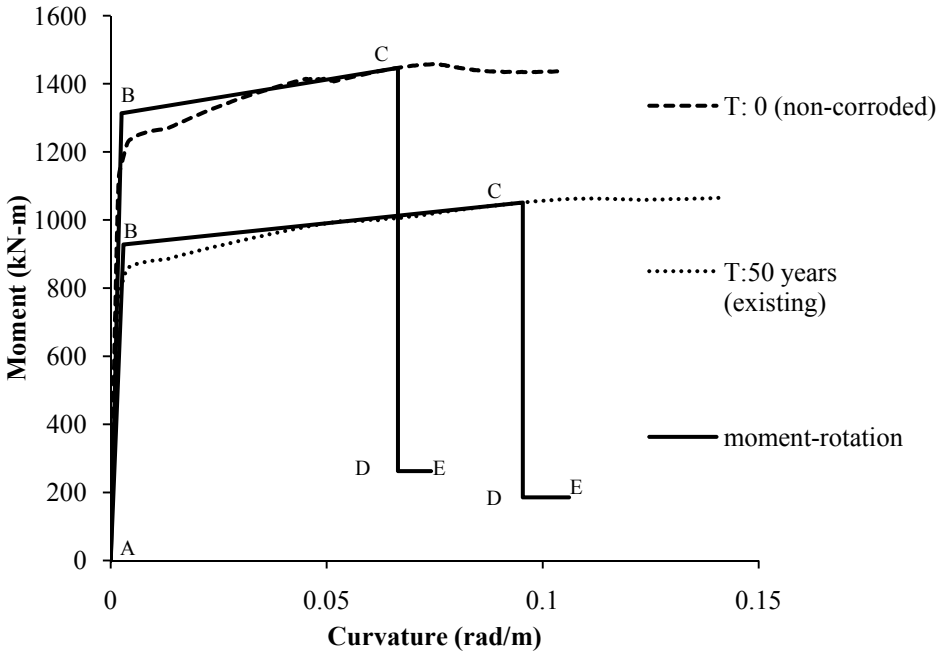

Figure 3.30: Moment-rotation from predicted moment-curvature relationships.

In equation 3.46, L_p is the plastic hinge length, ϕ is the curvature at a point. The lengths of the plastic hinges are calculated according to Park and Paulay (1975) by given equation:

$$L_p = 0.5H \tag{3.47}$$

where H is the related section depth of element.

Predicted time-dependent moment-curvature relationships of columns and beams were used to calculate time-dependent moment-rotation relationships and then plastic hinge properties. For five different time periods, calculated different plastic hinge properties were assigned to each floor at both ends of beams and columns of assessed frame according to corresponding time periods. Thus, assessed frame was analysed according to its own deformation capacity under the time-dependent effect of corrosion. In order to perform nonlinear push-over analyses triangular lateral load pattern was applied to the frame. Of course different load patterns will result in different displacement, but this is not the case to investigate the time-dependent effect of corrosion in nonlinear push-over analyses for present study. Figure 3.31 shows the time-dependent push-over analyses of the selected frame as a function of corrosion rate by taking into account the two major effects of corrosion (loss in cross sectional area of reinforcement bars and reduction in concrete compressive strength).

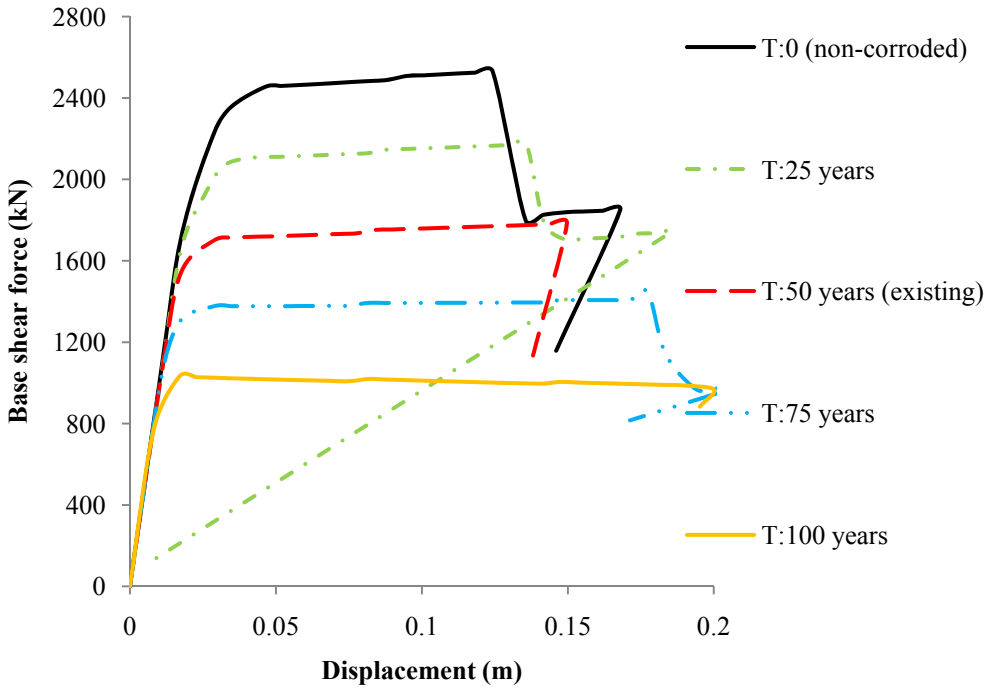

Figure 3.31: Time-dependent load- top displacement relationships.

In Figure 3.31 time-dependent results of push-over analyses indicate that there is an obvious deterioration in the section capacity due to corrosion resulting decrease in ductility, initial and post yielding stiffness of the structure. Predicted first push-over analyses was used to predict time-dependent slip rotation of reinforcement bars of each column of floors by recording time-dependent effective depth of the neutral axis, strain and stress in reinforcing bar from predicted time-dependent moment-curvature relationships (see Figures 3.23 and 3.24). If the force and corresponding maximum moment (M_{max}) of the column base are known, time-dependent slip rotation can be calculated by using equations 2.18 and 2.19. As it was expected more slip rotation occurs for the columns of ground floor due to maximum moment of the column base. Time-dependent relationships between calculated maximum moments and corresponding slip rotations of reinforcement bar embedded in ground floor of S_1 column are shown in Figure 3.32.

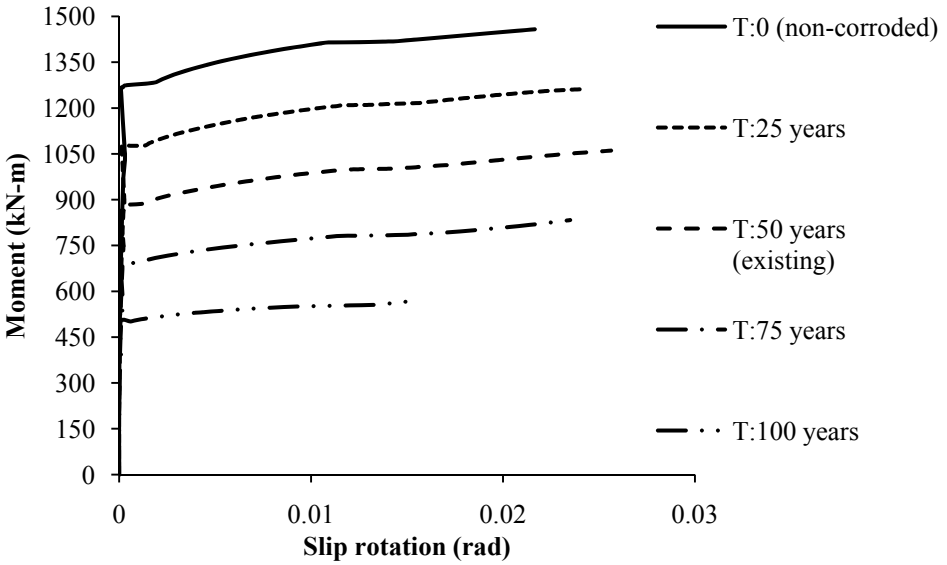

Figure 3.32: Time-dependent slip rotation of S_1 column.

According to results of slip rotation, for each plateau of reinforcement bars, more slip displacement occurs with a less amount of lateral force due to corrosion. Once

the corrosion phases begin, the effect of corrosion resulting in slip will be higher during propagation period which varies from first cracking to loss of load-carrying capacity of sections. In order to ensure the effect of time-dependent slip rotation on the global structural behaviour, target post-yield stiffness of each structural members are modified according to the procedure described by Lepage et al. (2008) as a function of time. For each time period, corrected yield and ultimate points by including the bond-slip relationships provide new coordinates on the time-dependent moment-rotation relationships in order to redefine the load-deformation behaviour of each column. In another words, time-dependent plastic hinge properties were redefined by taking into account the effect of bond-slip relationships for five time periods of each floor of structural members to perform non-linear push over analyses. By using triangular load pattern, predicted relationships between base shear force against control displacement as a function of time is shown in Figure 3.33. Thus, Figure 3.33 represents the results of two combined major effects of corrosion as a function of time.

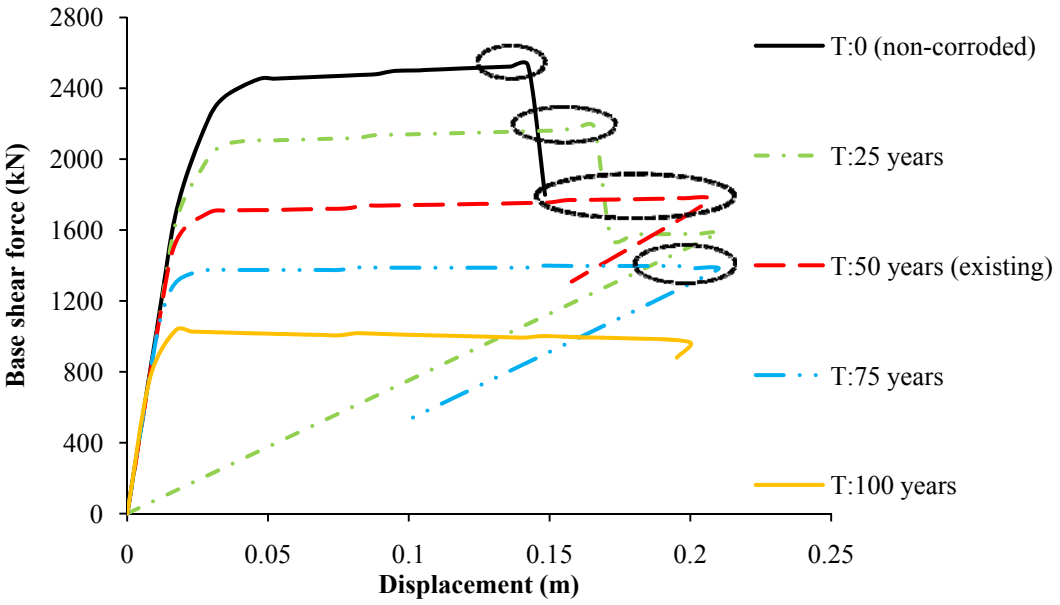

Figure 3.33: Time-dependent load- top displacement relationships due to slip in reinforcement bars.

In Figure 3.33, additional displacements caused by slip are 15%, 22% for non-corroded and 25 years after construction respectively. Recorded additional displacement of existing structure (t: 50 years) by considering slip is 38%. As it is shown in Figure 3.32, by increasing time, same amount of slip occurs for the fewer amounts of moment values due to corrosion. However, effect of slip after 50 years was not effective as much as time period between non-corroded and 50 years after construction. For instance, when time is equal to 75 years, recorded additional displacement due to slip was 18% while no additional displacement was recorded due to slip for the time period of 100 years after performing push-over analyses. This can be explained by the reduction in the moment capacity of the sections. After 50 years, concrete crushes before reinforcing bars exceeding strain hardening region due to losing in moment capacities of section and reaching their ultimate performance level. This is why the procedure described by Lepage et al. (2008) was applied in the present study by modifying the target post-yield stiffness to perform the push-over analyses instead of adding additional displacement due slip to the obtained first time-dependent load-displacement relationships (see Figure 3.33). Combined two major effects of corrosion were used to predict time-dependent performance level of the corroded frame by the following section.

3.5.4 Incremental Dynamic Analysis

Suggested corrosion methodology was performed by using IDA under individual of 20 ground motion earthquake records. Limit states at each performance level have been defined and summarizing the multi–record IDA curves, 16%, 50% and 84% fragility curves were obtained. At the end, fragility curves of probabilistic structural damage estimation were obtained in terms of peak ground acceleration (PGA) for each performance level. For current study, associated roof drift ratios corresponding

to performance levels; immediate occupancy (IO), life safety (LS) and collapse prevention (CP) were adopted from study done by Ramamoorthy et al. (2006) and reduced drift values of 0.5, 1, and 2% were used for IO, LS, and CP respectively. In order to perform IDA NONLIN (1998) software program was used. For IDA 5% damped first-mode spectral acceleration (S_a (T_1, 5%)) was selected. The list of used ground motion records presented in Table 3.5 where earthquake moment magnitudes (M) ranging from 4.7 to 7.51, PGA varied from 0.016 to 0.875*g* and peak ground velocity (PGV) is ranged between 1.65 to 117 cm/sec.

Table 3. 5: List of earthquake ground motions (PEER; 2009)

No	Event	Station	Angle(°)	M	Soil Type	Epicentral Distance (km)	PGA (g)	PGV (cm/sec)
1	Oroville, 1975	Broad beck Residence	270	4.7	Soft soil	7	0.168	3.35
2	Coalinga, 1983	Coalinga	90	4.89	Soft soil	9	0.2	6.4
3	Dinar,Turkey 1995	Burdur	180	6.40	Soft soil	39.57	0.0411	4.65
4	Dinar,Turkey 1995	Center	90	6.40	Soft soil	0.44	0.352	33.17
5	Duzce,Turkey 1999	Bolu	90	7.14	Soft soil	41.27	0.822	59.68
6	Duzce,Turkey 1999	Center	270	7.14	Soft soil	1.61	0.535	70.77
7	Erzican,Turkey 1992	Erzincan	90	6.69	Soft soil	8.97	0.515	72.95
8	Greece,1981	Corinth	90	6.60	Soft soil	19.92	0.24	25.45
9	Izmir, Turkey 1977	Izmir	90	5.30	Soft soil	2.29	0.41	9.23
10	Kobe, Japan 1995	Takatori	90	6.90	Soft soil	13.12	0.616	117.14
11	Kocaeli, Turkey 1999	Balikesir	180	7.51	Soft soil	218.64	0.017	4.88
12	Kocaeli, Turkey 1999	Usak	90	7.51	Soft soil	237	0.016	4.59
13	Kozani, Greece 1995	Karpero	180	5.10	Soft soil	11.85	0.276	13.25
14	New Zealand,1992	Edgecumbe Substation	130	5.70	Alluvium	45.76	0.042	10.19
15	Norcia, Italy 1979	Bevagna	270	5.90	Soft soil	35.97	0.04	1.65
16	Northridge, 1994	Beverly Hills	90	6.69	Soft soil	16.27	0.617	32.82
17	Oroville,1975	Oroville Seismograph	37	5.89	Alluvium	12.58	0.092	3.14
18	San Salvador,1986	Geotech Investig Center	90	5.80	Soft soil	7.93	0.875	47.36
19	Victoria, Mexico 1980	Cerro Prieto	90	6.33	Soft soil	33.73	0.621	27.06
20	Duzce, Turkey 1999	Yarimca	60	7.14	Soft soil	115.89	0.022	5.98

3.5.5 Discussion on results Ground Motion Records

By performing IDA, results obtained from assessed frame were compared as a function of time to investigate the reduction in the performance levels due to corrosion. It should be noted that in this case study, MDOF system turned in through the use of an equivalent SDOF system with properties defined based on the results from pushover analysis. Figs. 3.34(a-b) show IDA curves of non-corroded and existing (*t*: 50 years) frames. In Figs. 3.34(a-b), average inter story drift ratios (AIDRs) were obtained by dividing the maximum roof displacement by the building height (14.1 m).

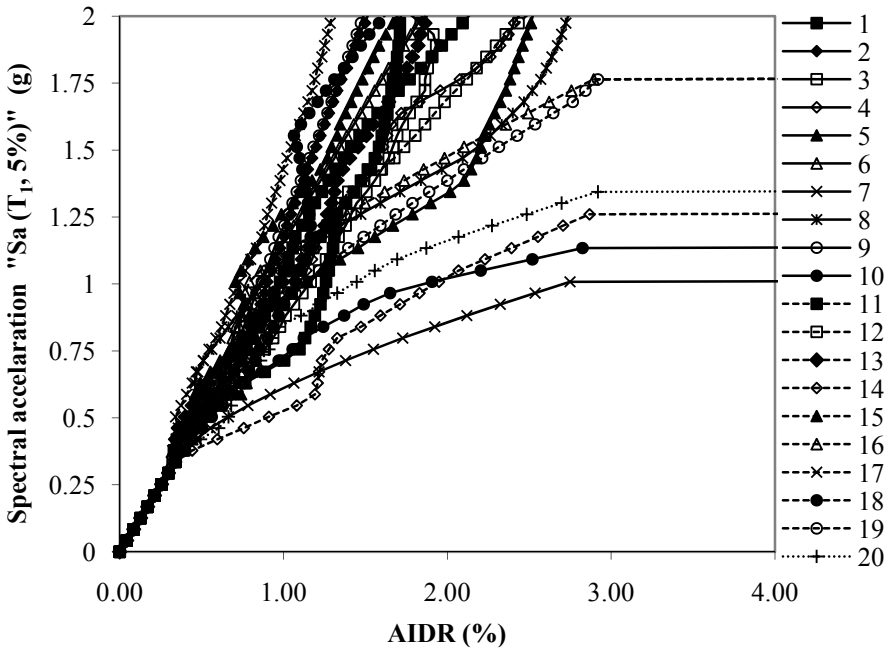

(a)

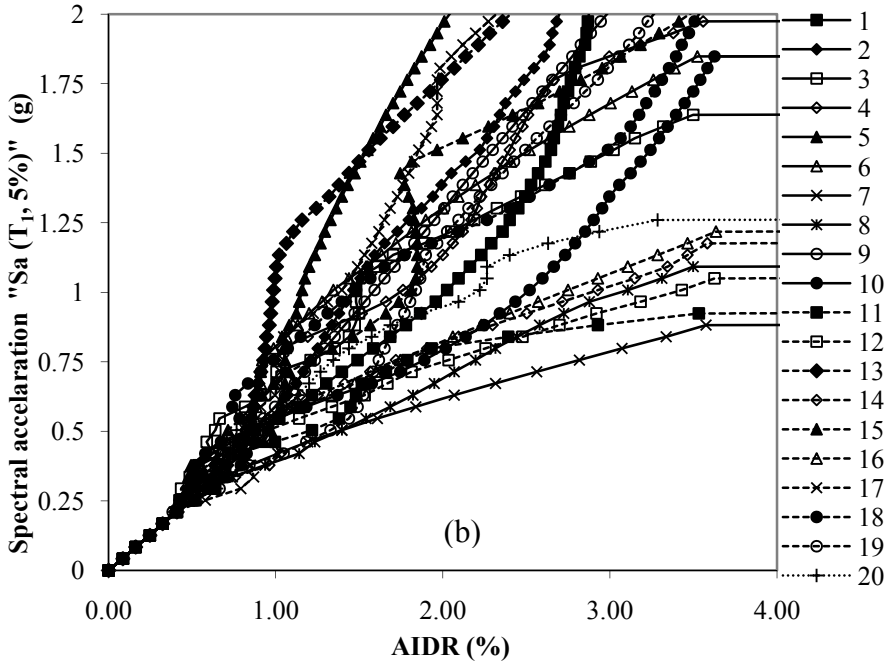

Figure 3.34: IDA curves: (a) T: 0 (non-corroded), (b) T: 50 years (existing).

By increasing the S_a, the building shows a nonlinear response; and based on the property of each record the response of structure was effected by time due to corrosion for different S_a. In order to better understand the changes in roof drift ratio, cumulative distribution function (CDF) of roof drift ratio is needed to be constructed for each time period. Figure 3.35 shows the CDF of roof drift ratios of each time period according to design base earthquake hazard level (DBE).

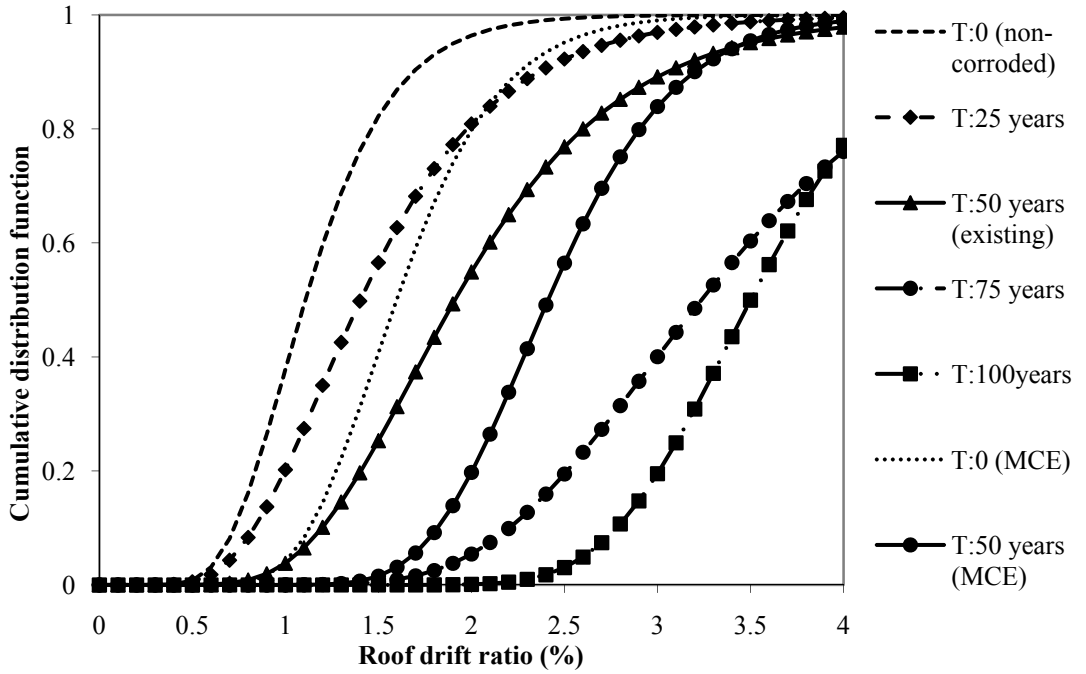

Figure 3.35: Cumulative distribution function of roof drift ratio.

The obtained lognormal CDF indicates that there is a serious increasing of roof drift ratios with increasing time due to time-dependent effect of corrosion. For instance, in Figure 3.35, the probabilities of exceeding 2% of roof drift ratio (corresponded to CP limit state based on DBE) of non-corroded frame was only 3.6% while probabilities of exceeding 2% of roof drift ratios of 25, 50, 75 and 100 years were 19%, 45%, 95%, and 99%, respectively. Figure 3.35 clearly shows that after corrosion induced structure, probabilities of exceeding of roof drift ratio increased as a function of time and caused to decrease the performance level of assessed frame. These probabilities of exceeding of roof drift ratio will be also higher if they are compared with maximum considered earthquake (MCE) hazard levels. In Figure 3.35 selected two time periods (*t*: 0 and *t*: 50 years) of roof drift ratio for non-corroded and existing buildings are also shown at MCE hazard level. According to Figure 3.35, non-corroded building at MCE hazard level has approximately same probability (20%) of exceeding 2% of roof drift ratio as 25 years after construction at

DBE hazard level. This probability for existing building was (t: 50 years MCE) 80% at MCE hazard level. Thus, it is not difficult to indicate that corrosion has a serious damage during earthquake as a function of time. As mentioned earlier, limit states at each performance level have been defined and by summarizing the multi–record IDA curves, 16%, 50% and 84% fragility curves were obtained for each time period as a consequence of corrosion damage. Figure 3.36 (a-d) represent multi–record IDA curves of four time periods.

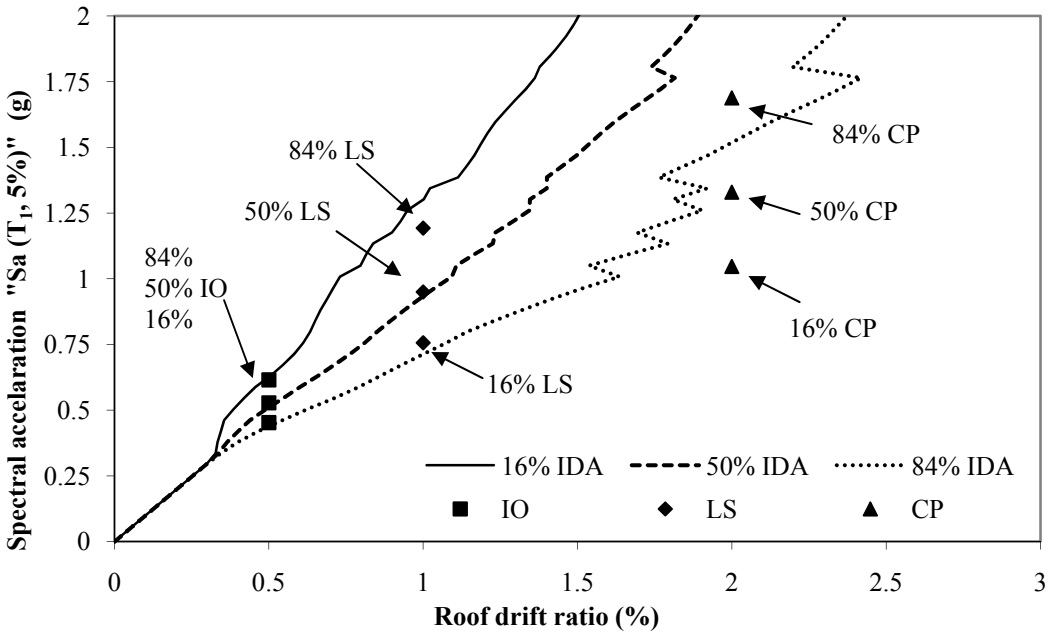

(a)

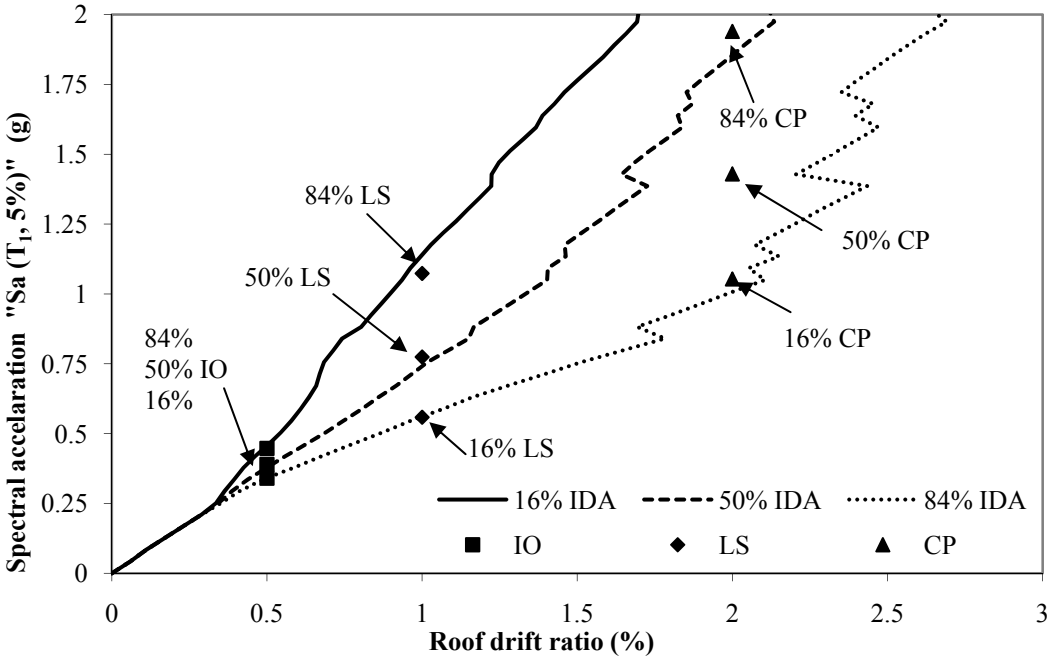
Spectral accelaration "Sa (T1, 5%)" (g)
Roof drift ratio (%)
84% CP
50% CP
16% CP
84% LS
50% LS
16% LS
84%
50% IO
16%
16% IDA
50% IDA
84% IDA
IO
LS
CP

(b)

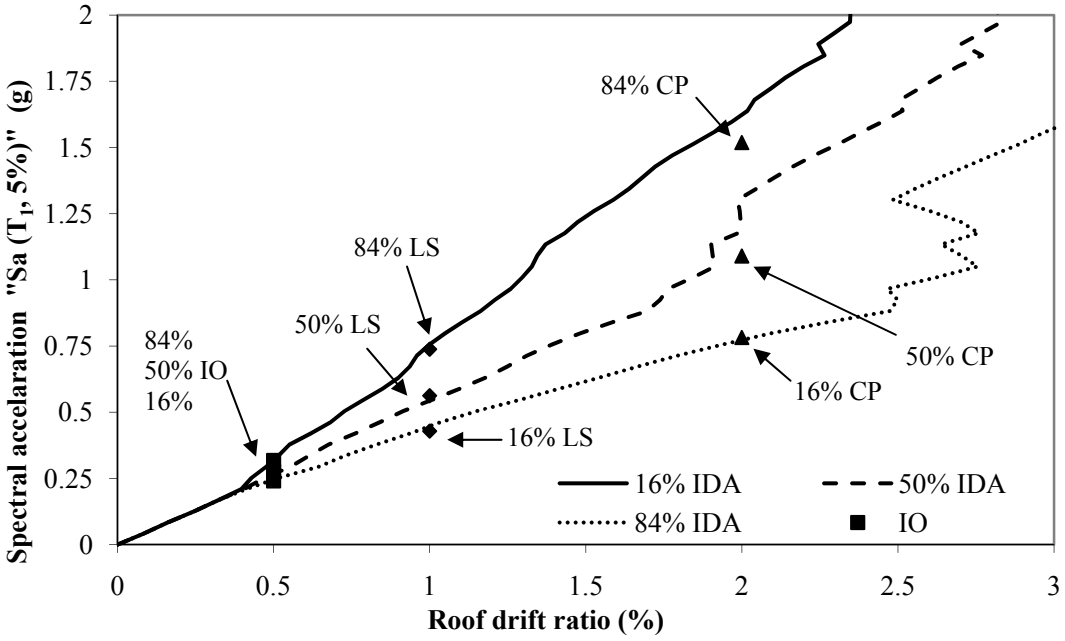
Spectral accelaration "Sa (T1, 5%)" (g)
Roof drift ratio (%)
84% CP
50% CP
16% CP
84% LS
50% LS
16% LS
84%
50% IO
16%
16% IDA
50% IDA
84% IDA
IO

(c)

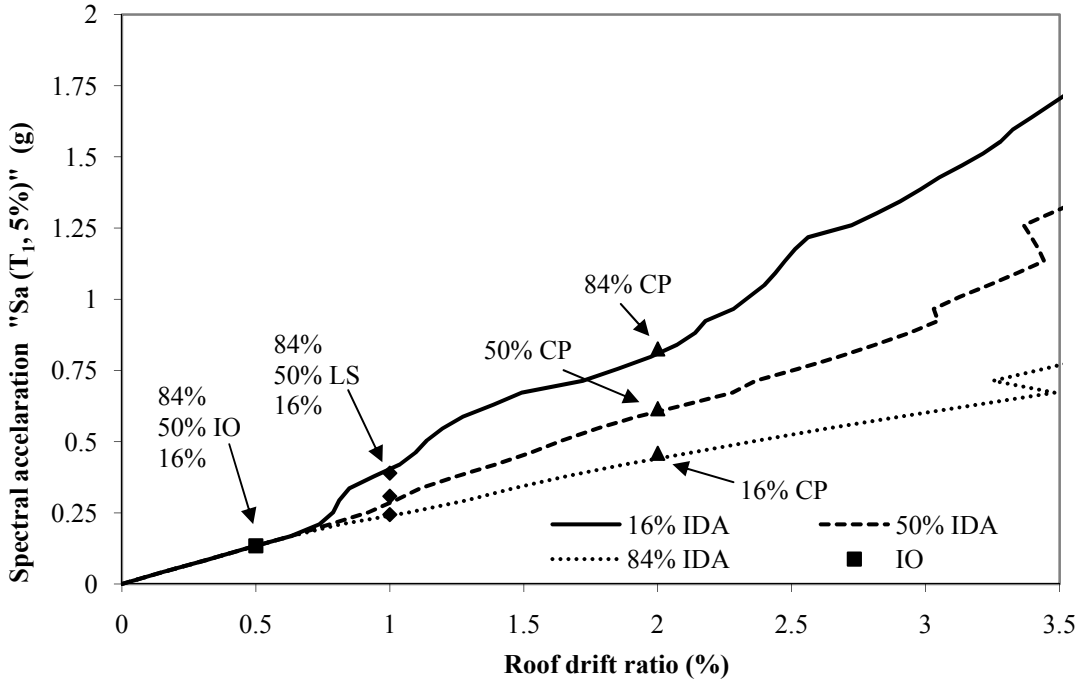

(d)

Figure 3.36: IDA curves and corresponding performance level into their 16%, 50% and 84% fragility: (a) *t*: 0 (non-corroded), (b) *t*: 25 years, (c) *t*: 50 years (existing), (d) *t*: 75 years.

The main goal of IDA curves here was to define the reduction in performance levels of assessed frames according to the considered thresholds of roof drift ratios values of 0.5% (IO), 1% (LS), and 2% (CP). In Figure 3.36 (a), non-corroded frame with S_a is equal to 0.5*g*, 84% of earthquake records caused a roof drift ratio greater than 0.39% while 16% of earthquake records caused a roof drift ratio greater than 0.63%. When time period was equal to 25 years at the same S_a, 84% of earthquake records caused a roof drift ratio greater than 0.54% while 16% of earthquake records caused a roof drift ratio greater than 0.87%. Thus, 25 years after construction, due to time-dependent effect of corrosion, 84% of earthquake records caused to reduce performance level from IO to LS whilst 16% of earthquake records kept the performance level as LS by increasing the roof drift ratio. By increasing time at the same S_a of 50 years (existing structure), 84% of earthquake records caused a roof

drift ratio greater than 0.73% while 16% of earthquake records caused a roof drift ratio greater than 1.15%. Thus, 50 years after construction, 84% of earthquake records caused to reduce performance level from IO to LS whilst 16% of earthquake records caused to reduce performance level from LS to CP. According to the Turkish earthquake code (2007), the expected performance level is IO after an earthquake which building has an important factor of 1.4. Therefore, it can be concluded that the performance level of the existing building seriously affected by corrosion. These reductions in performance levels reaches to collapse level after 75 years for the same S_a where 84% of earthquake records caused a roof drift ratio greater than 1.14% (CP) while 16% of earthquake records caused a roof drift ratio greater than 2.37% (collapse). Of course, by increasing S_a these comparisons will be more dramatically due to corrosion as shown in Figure 3.36 (a-d). In Figure 3.37 (a-c), fragility curves at three performance levels were also predicted in terms of peak ground acceleration as a function of time.

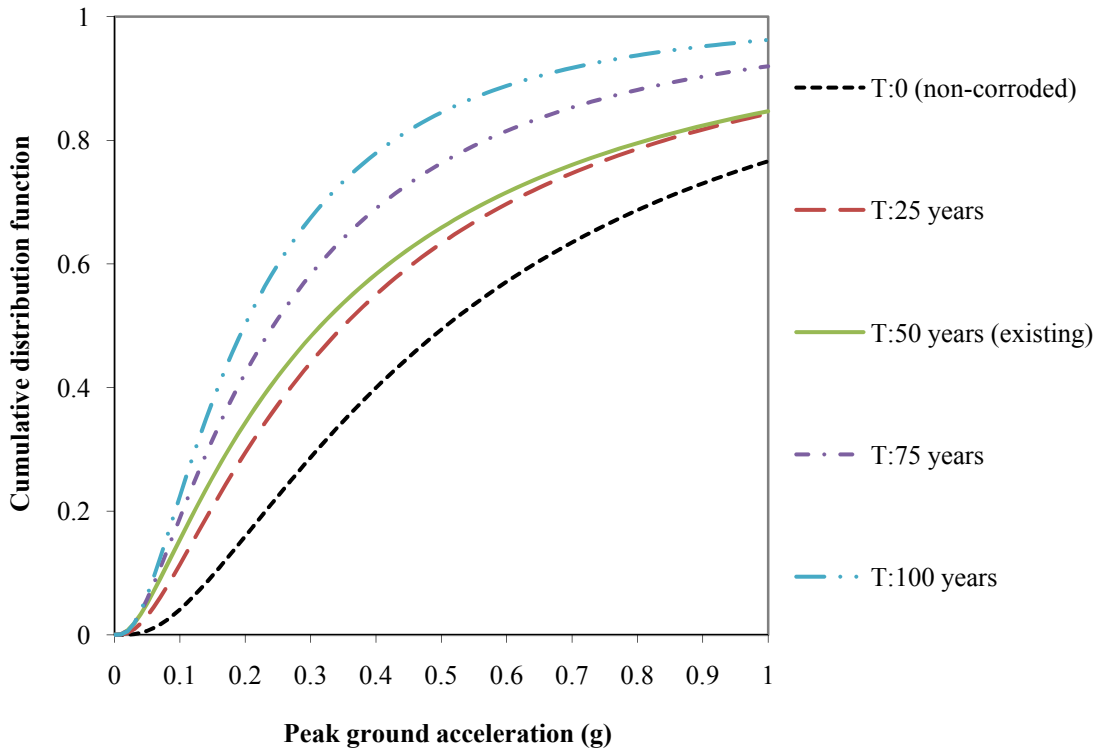

(a)

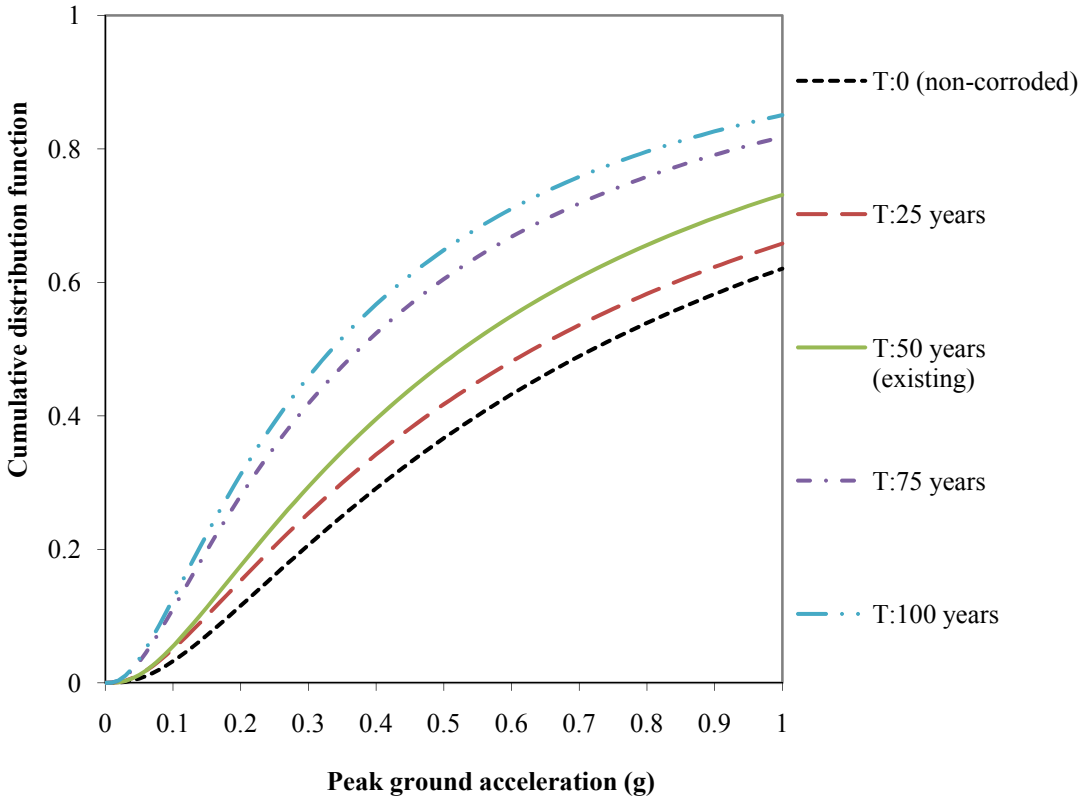

(b)

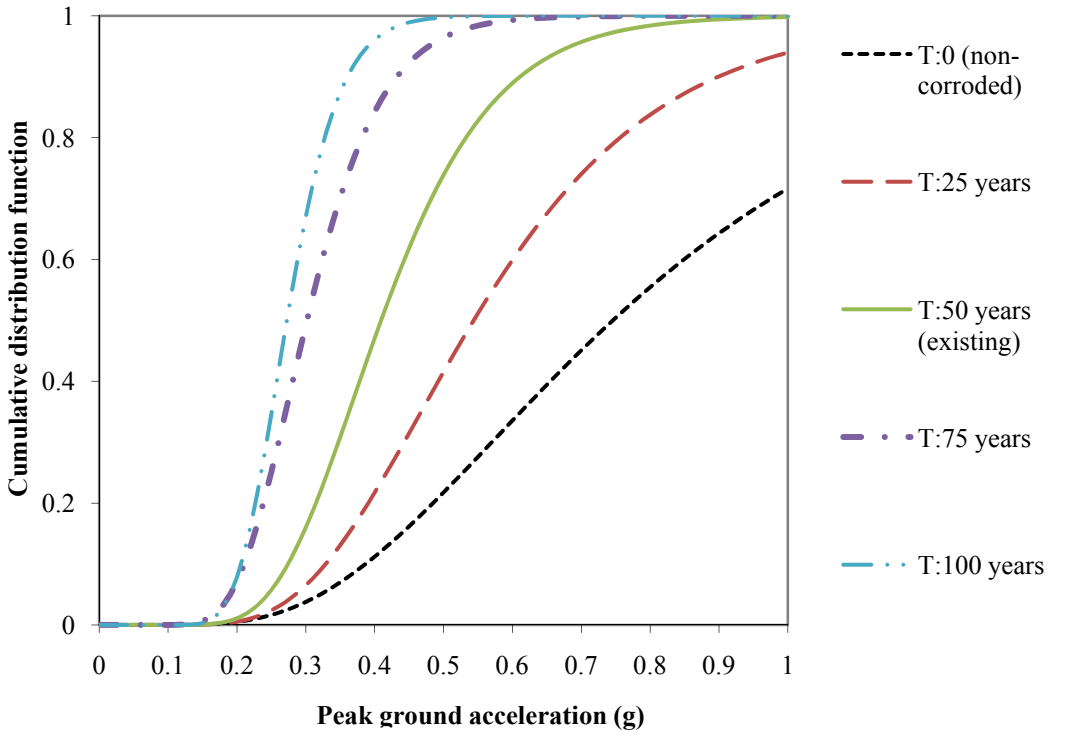

(c)

Figure 3.37: Fragility curves of limit states: (a) immediate occupancy, (b) life safety, (c) collapse prevention.

Table 3.6 summarizes the results of these fragility curves based on probability of exceeding of limit states as IO, LS and CP of assessed frame as a function of corrosion rate for different time periods at different seismic zones (through Z_1 to Z_4) according to recommended A_0 by Turkish earthquake code (2007).

Table 3. 6: Probability of exceeding of limit states of IO, LS and CP at different seismic zones.

Frame	**Limit state**	**Seismic Zone-PGA(g)**			
		A_0:0.4	A_0:0.3	A_0:0.2	A_0:0.1
		Z_1 (%)	Z_2 (%)	Z_3 (%)	Z_4 (%)
T: 0 (non-corroded)	IO	39	29	16	4
	LS	29	20	11.5	3.2
	CP	11	3.8	0.5	4.4E-05
T: 25 years	IO	55	44	29	11.4
	LS	34.2	25.4	15.3	5.06
	CP	22	6.5	0.54	5.5E-04
T: 50 years (existing)	IO	58.3	48.2	34.3	15.4
	LS	39.5	29.4	17.5	5.5
	CP	47	16	1.09	5.2E-03
T: 75 years	IO	69	58	42	19
	LS	52	42	28	11
	CP	84	49	7	0.04
T: 100 years	IO	78	67	50	22
	LS	57	46	31	12.5
	CP	96	67	7.8	0.06

As shown in Figure 3.37 (a-c) and summarised results in Table 3.6; exceptions of seismic zone four (Z_4), there is a high seismic risk for other seismic zones due to time-dependent effects of corrosion. At first seismic zone (Z_1) of non-corroded frame, probability of exceeding the limit state corresponding to IO was 39% while this probability was 55% after 25 years. This probability of exceeding limit state increased to 58%, 69% after 50 and 75 years respectively. For CP limit states of first seismic zone, probability of exceeding limit state increased from 11% to 22%, 47% , 84% after 25, 50 and 75 years respectively. At second seismic zone of non-corroded frame, calculated probability of exceeding of limit state corresponding to IO was

29% while this probability increased to 48% for existing frame. For the same seismic zone (Z_2) of non-corroded frame, probability of exceeding limit state corresponding to CP was 3.8% while this probability was 16% for existing frame. Results clearly showed that performance levels of the structure are affected due to corrosion by increasing time. By taken into account the time-dependent loss in cross sectional area of reinforcement bars, and slip, all these phenomena provides more accurate prediction of performance level of RC structures subject to corrosion as a function of time. This phenomenon plays an important role in evaluation of time to strengthening of structures under the expected seismic motions to prevent serious damage of structures.

3.6 Third case study: Effect of Corrosion Damage on the Performance Level of a 25-year-old Reinforced Concrete Building in North Cyprus

In this case study, different than previous case studies, a three dimensional system was performed. Particularly, different than first case study and like second case study, plastic hinge properties were taken into account by modified moment-curvature relationships due to different effects of corrosion.

A corroded, 25-year-old high school building which has been demolished at an earlier time was analyzed as a function of corrosion rate. Bond-slip relationships were taken into account in nonlinear analyses as a function of corrosion rate for different time periods (i.e; non-corroded (*t*: 0), existing (*t*: 25) and 50 years after construction); and they were used to ensure the effect of time-dependent slip rotation on the global structural behaviour by modifying the target post-yield stiffness of each structural member. Nonlinear push-over analyses were performed by defining the

time-dependent plastic hinge properties as a consequence of corrosion effects. In order to define the performance levels of three different time periods, nonlinear IDA were performed for 20 earthquake ground motion records as a function of corrosion rate. Results showed that bond-slip relationship between concrete and steel is very important in evaluating the non-linear behaviour of corroded RC structures.

3.6.1 Description of the Analyzed Building

Figures 3.38 and 3.39 show the general view and plan of analyzed high school building with dimensions of beams (dimensions in cm), respectively.

Figure 3.38: Analyzed high school building.

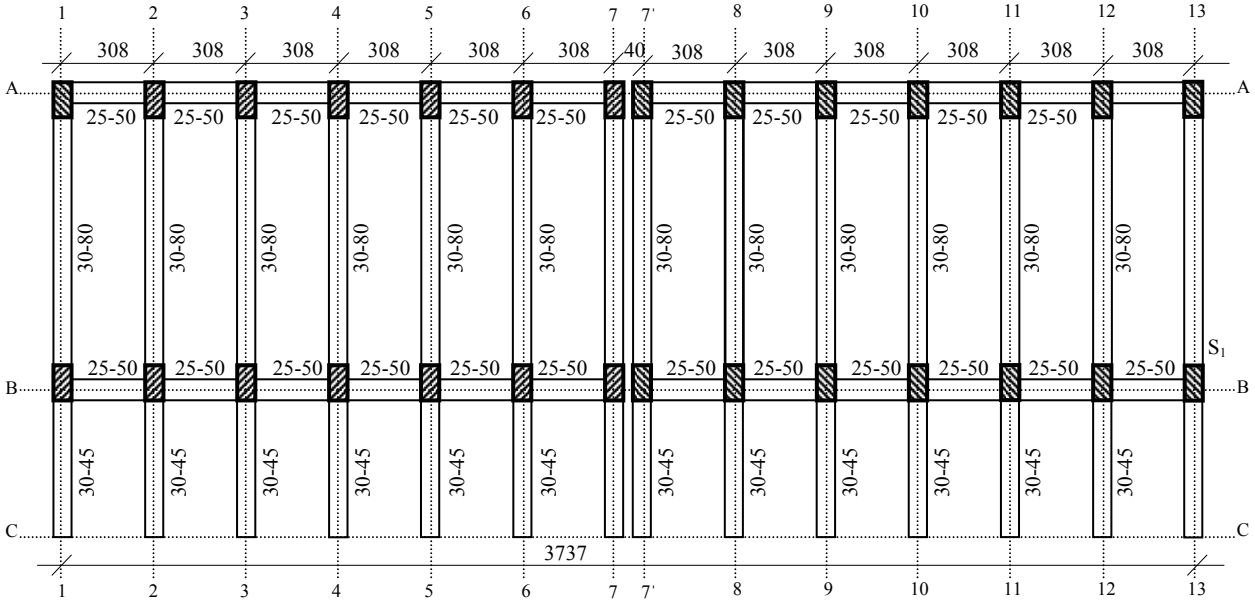

Figure 3.39: Plan of building.

In Figure 3.39, all columns had 30× 45 cm cross section. The plan of the building was symmetrical about in X direction having a total length and width of 37.37 m and 8.87 m, respectively. The building has one story, with a total height of 4.10 m. The distance from the building to the sea was 2380 m, which gave an 85% probability of corrosion potential based on half-cell tests. The slab thickness of the building was 15 cm, and the calculated additional dead and live loads of the slab were 1.5 kN/m^2. The calculated total weight of the structure was 400 kN. The soil class was classified as soft clay (group D), the building importance factor was taken as 1.4, and the effective ground acceleration coefficient (A_0) was taken as 0.3 *g* (seismic zone 2) according to Turkish earthquake code 2007 (TEQ, 2007). The field evaluations were done in order to model and assess the RC structure by series of destructive and non-destructive tests. Because of safety issues where spalling of concrete was exited due to corrosion, the building was rounded by barrier tape for safety consideration after the primarily structural condition survey of the building. In order to identify the amount and dimensional properties of the reinforcement bars, selected columns faces were opened from the different point of the building. For the beams and the remaining columns, non-destructive (ferro scanning) method was used to define the amount of reinforcement bars. Figure 3.40 shows an opened outer column from the building. Most of the reinforcement details of beams were visible due to the volume expansion of the corrosion rust which caused spalling of concrete cover as shown in Figure 3.41. Based on the experimental study, the measured concrete covers for the columns and beams were 3.5 cm where the details of the reinforcement bars are also shown in Figures 3.40 and 3.41, respectively.

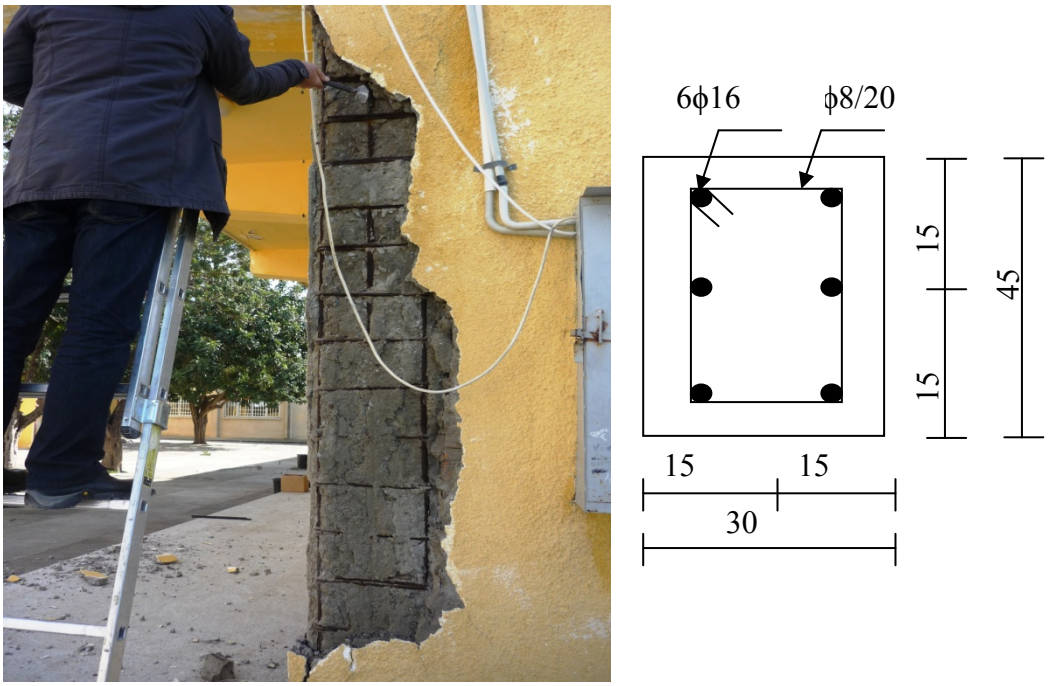

Figure 3.40: Outface of S_1 column.

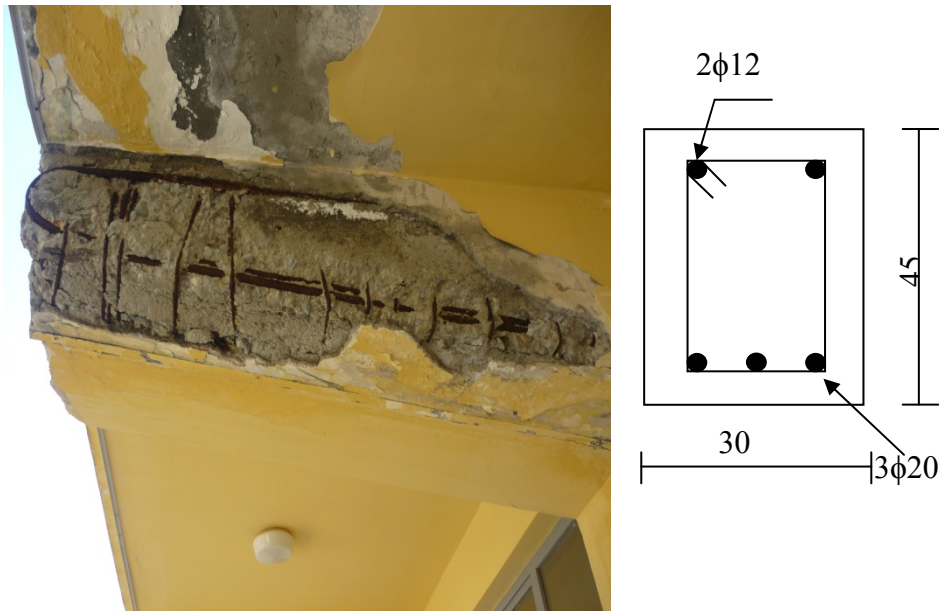

Figure 3.41: Volume expansion of corrosion rust.

3.6.2 Corrosion Rate and Non-linear Material Modelling

A number of corroded and non-corroded reinforcement bars were taken from the building to investigate the mechanical properties and the corrosion rate of

reinforcement bars. The mechanical properties of the non-corroded reinforcement bars where the yield strength (f_{sy}) was 303 MPa, the rupture strength (f_{su}) was equal to 433 MPa, the yield strain (ε_{sy}) was equal to 0.0015, the strain hardening (ε_{sh}) was equal to 0.011, the rupture extension (ε_{su}) was equal to 16%, and the elastic modulus of strain hardening region (E_{sh}) was equal to 1745 MPa. The elastic modulus of concrete ($E_C = 3250\sqrt{f'_C} + 14000$ MPa) was calculated according to Turkish standard 500 (TS 500, 2000). In order to calculate the corrosion rate of reinforcement bars of columns and beams, chemical cleaning was done by using hydrochloric acid (12% by weight of water) to remove the corrosion product from the surface of reinforcement bars according to the described standard ASTM G1-03 (ASTM G1-03, 2003). Calculated corrosion rate 25 years after construction was 2.43 μA/cm^2. Thus, the calculated mass losses (Δ_w) of longitudinal reinforcement bars of columns were 16.84% and 33.7% after 25 and 50 years, respectively (Δ_{w25}: 16.84%, Δ_{w50}: 32.13%). Because of corrosion, the mechanical properties of a reinforcement bar change as a function of mass loss. Therefore, a well known empirical model developed by Lee and Cho (2009) was used to predict the mechanical properties of corroded reinforcement bars. The model developed by Lee and Cho (2009) calculates the yield point, the minimum rupture strength and the elastic modulus of corroded reinforcement bars by using equations 3.48 to 3.51.

$$f_{cy} = (1 - 1.24(\Delta_W / 100)) f_{sy} \tag{3.48}$$

$$f_{csu} = (1 - 1.07(\Delta_W / 100)) f_{su} \tag{3.49}$$

$$E_{cs} = (1 - 0.75(\Delta_W / 100)) E_S \tag{3.50}$$

$$\varepsilon_{csu} = (1 - 1.95(\Delta_W / 100)) \varepsilon_{su} \tag{3.51}$$

where f_{cy} is the yield strength, E_{cs} is the elastic modulus, f_{csu} is the the rupture strength, and ε_{csu} is the rupture extension of corroded reinforcement bars. It might be useful to indicate that, there was a reasonable good agreement between obtained mechanical properties of corroded reinforcement bars in 25 years and developed empirical model by Lee and Cho (2009). In order to model the stress-strain relationships of confined columns, three models developed by Kent and Park (1971), Saatcioglu and Razvi (1992) and Mander et al. (1988) were used. For each case (non-corroded (t: 0), 25 (existing), and 50 years), the models that gave higher demands (lower elastic and inelastic stiffness and lower yield strength) were selected to be used in nonlinear analyses. In order to model the stress-strain relationship of steel, the developed model by Mander (1984) was used.

3.6.3 Time-dependent Behaviour of Reinforced Concrete Sections

Experimentally obtained corrosion rate was used to predict the loss in cross sectional area of reinforcement bars, and the reduction in concrete strength as a function of time. Based on the experimental works and obtained corrosion rate, the loss in cross sectional area of reinforcement bars of columns after 25 and 50 years were 8.81% and 17.62%, respectively. Once the corrosion rate is known as a function of time, the reduction in concrete strength can be predicted as a function of time based on a model developed by Vecchio and Collins (1986). In this case study, in order to predict the time-dependent crack width as a function of corrosion rate, the attack penetration was predicted according to the well know Faraday's law and adopted into the model developed by Molina et al. (1993). The attack penetration by Faraday's law is given in equation 3.52.

$$X = 0.0116.I_{corr}.t \tag{3.52}$$

where I_{corr} is the corrosion intensity ($\mu A/cm^2$), t is the time in years, and 0.0116 is a conversion factor of $\mu A/cm^2$ into mm/year for steel. As shown in equation 3.52, the attack penetration is a function of corrosion rate. Thus, predicted time-dependent attack penetration gives the time-dependent crack width as a function of corrosion rate (see equation (3.5)). The calculation of the time-dependent crack width provides a time-dependent reduction in concrete strength by using the model developed by Vecchio and Collins (1986). The ratio of the volumetric expansion of the oxides with respect to the virgin material was assumed to be same for all reinforcement bars and taken as 2 according to experimental works. As a consequence of increases in tensile strain in concrete due to corrosion, the calculated reduced concrete strength after 25 and 50 years was 20.25 MPa and 17 MPa, respectively. The predicted loss of cross sectional area in the reinforcement bars and the reduction in concrete compressive strength were used to predict the time-dependent moment-curvature relationships. For each column and beam of three different time periods (t: 0, t: 25 and t: 50 years), a total of 63 time-dependent moment-curvature relationships were predicted as a function of corrosion rate for three different models, one developed by Kent and Park (1971) and the others by Saatcioglu and Razvi (1992) and Mander et al. (1988). The predicted time-dependent moment-curvature relationships of S_1 column is shown in Figure 3.42.

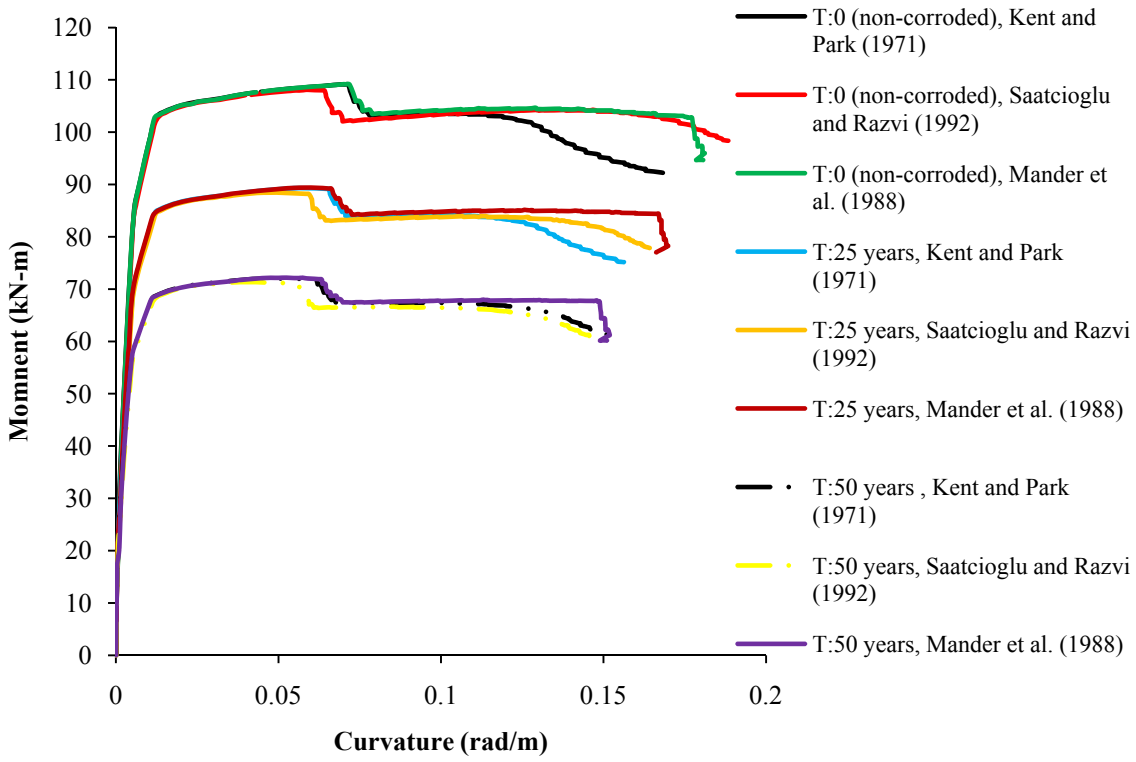

Figure 3.42: Time-dependent moment-curvature relationships of S_1 column.

As shown in Figure 3.42, due to time-dependent corrosion effects, dissipated energy by a RC column decreases as a function of time while the rotation increases for lower moment values, which increases the lateral displacement. The reduction in load carrying capacity of a RC column subjected to axial loading can be evaluated from a moment-load (M-N) interaction diagram. The results of the time-dependent M-N interaction diagrams of the S_1 column is plotted in Figure 3.43 as a function of corrosion rate by considering two different models developed by Kent and Park (1971) and Saatcioglu and Razvi (1992). The results of the model developed by Mander et al. (1988) was very close to the developed model by Kent and Park (1971). In Figure 3.43, the line of $0.5A_c f_c'$ represents the maximum allowable load that can be carried by a section according to TEC 2007 (2007). On this line, the moment capacity of a corroded RC section decreases as a function of time due to corrosion. For instance, when time is equal to zero (non-corroded), the moment

capacity of the S_1 column based on the Kent and Park model (1971) was 219 kN-m on this line, but this capacity decreased to 167 kN-m, and 118 kN-m after 25 (existing structure), and 50 years, respectively. Based on results of the time-dependent moment-curvature relationships, there was not much difference between the models developed by Kent and Park (1971), Saatcioglu and Razvi (1992) and Mander et al. (1988). Therefore, the authors of this article used the results of the model developed by Kent and Park (1971) for time-dependent moment-curvature relationships.

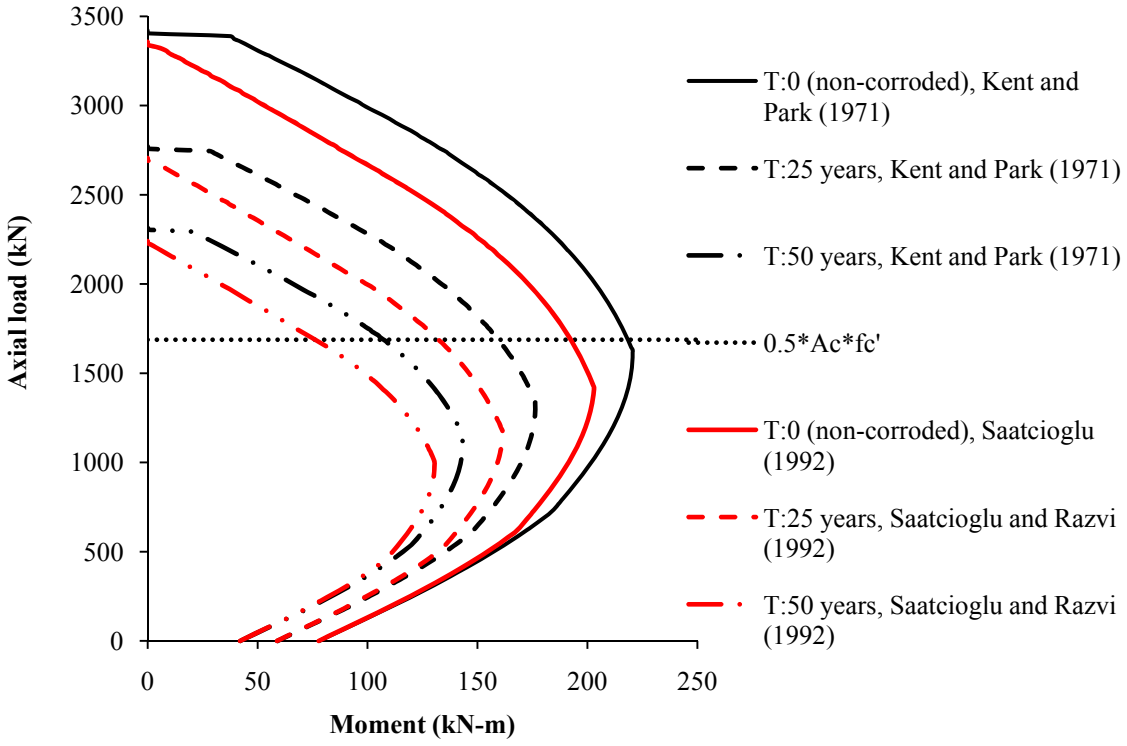

Figure 3.43: Time-dependent M-N diagrams.

3.6.4 Capacity Curve of the Building as a Function of Corrosion Rate

Non-linear static push-over analyses were performed for each time period (*t*: 0, *t*: 25 and *t*: 50 years) as a consequence of two corrosion effects (the loss in cross sectional area of reinforcement bars and the reduction in concrete strength). The

SAP 2000 (CSI, 2000) program was used to analyze the structure. The vertical distributed and earthquake loads that were used in the analyses are depicted in Figure 3.44.

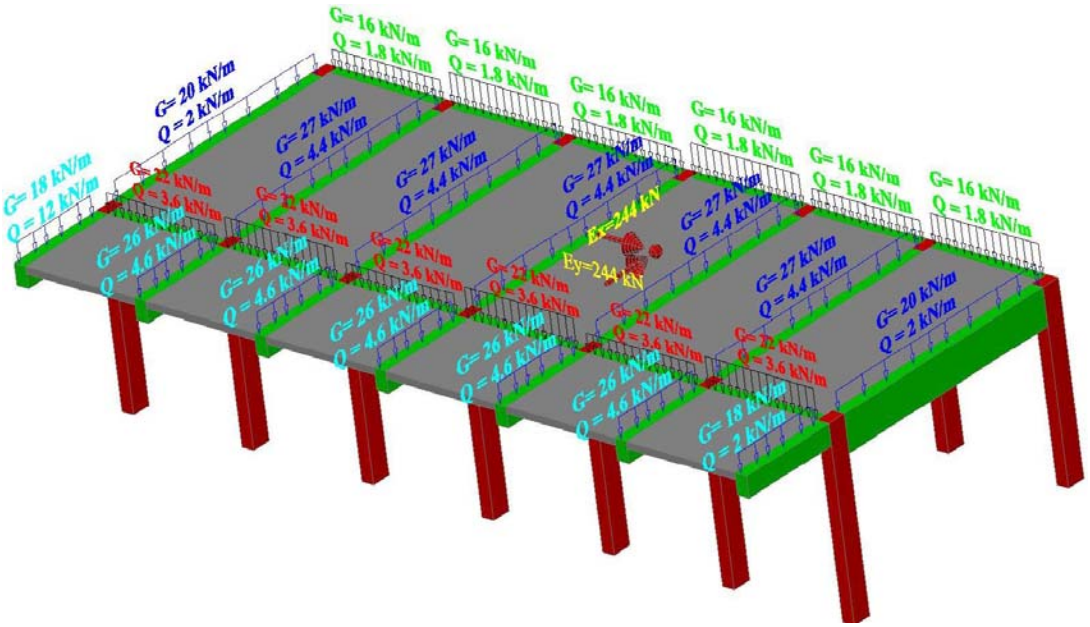

Figure 3.44: Used vertical and earthquake loads in the analyses.

In Figure 3.44 additional eccentricity effects ±5% E_x and E_y were also considered in the analyses. In order to ensure the effects of corrosion on the structural behaviour during push-over analyses, for each time period of structural members, user-defined plastic hinge properties were calculated from the predicted time-dependent moment-curvature relationships (see Figure 3.42). The length of the plastic hinges was taken into account by using moment-rotation relationships instead of moment-curvature relationships. Therefore, predicted time-dependent moment-curvature relationships were used to calculate time-dependent moment-rotation relationships where the rotation of the plastic hinges is the interaction between the length of the plastic hinges and curvature at a point. For each time period, the calculated plastic hinge properties were assigned to each both ends of the beams and the columns of the assessed building according to the corresponding time periods. Thus, the assessed

building was analyzed according to its own deformation capacity under the time-dependent effects of corrosion. The locations of the plastic hinges of the structural members were located according to the study done by Inel and Ozmen (2008). Figure 3.45 shows the comparison between the capacity curves plotting the base shear force against the control displacement for the structure in non-corroded and for other two different time periods as a function of corrosion rate.

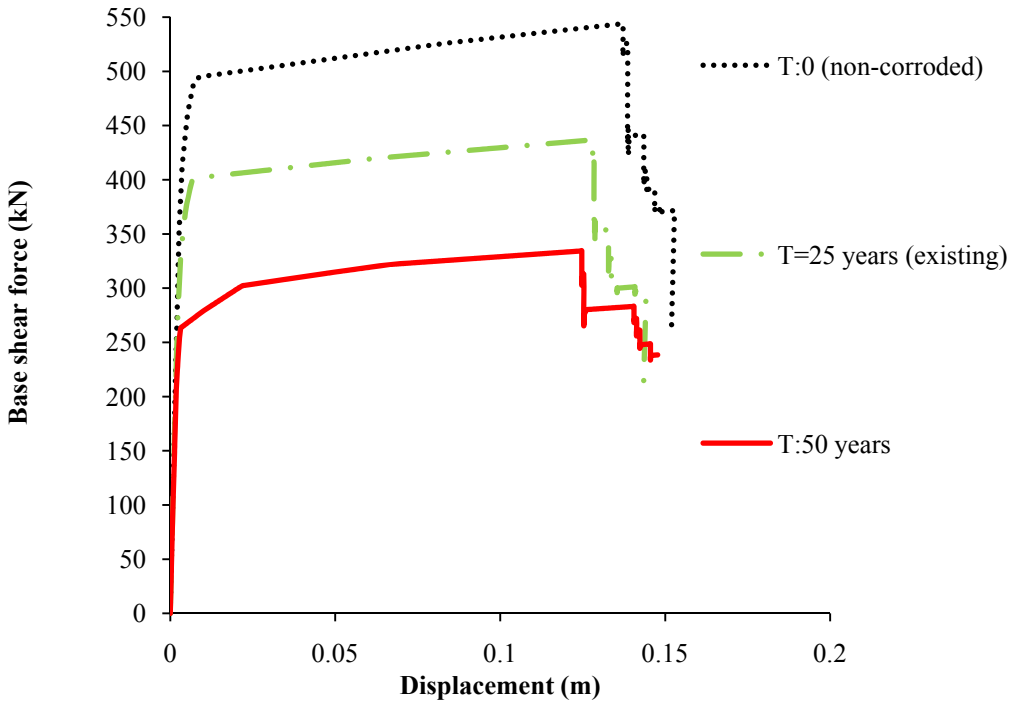

Figure 3.45: Time-dependent capacity curves for non-corroded and corroded building.

As shown in Figure 3.45, there is a serious reduction of the load bearing capacity for the corroded structure with respect to non-corroded structure. The results significantly indicated that for the same amount of base shear force displacement increases as a function of time due to corrosion. Moreover, it can be observed that the mechanism of plastic hinges was affected by corrosion. For instance, the collapse mechanism of non-corroded structure which started at a top displacement of 0.137 m when the base shear force was 544 kN. However, for the time periods of 25

(existing) and 50 years, collapse mechanism started at a top displacement of 0.128 m and 0.124 m when the base shear force was 437 kN and 334 kN, respectively.

3.6.5 Capacity Curve of the Building by Modified Plastic Hinge Properties due to Slippage of Reinforcement Bars

Because of corrosion, the bond strength in RC members decreases which cause to increase the displacement of the global structure by slippage of reinforcement bars. Previously predicted base shear force against the control displacement (see figure 3.45) was performed without considering the bond-slip relationships. Proposed model by Sezen and Setzler (2008) was used to calculate slip rotation (θ_s) by using equations 2.18 and 2.19. In this case study, in order to predict the slip rotation as a function of mass loss due to corrosion, the bond stress was adopted from the study done by Lee et al. (2002) instead of the uniform bond stress assumed by Sezen and Setzler (2008). Since, mechanical properties of reinforcement bars change as a function of mass loss, slip rotation can be calculated as a function of time. The results of force and corresponding maximum moment from the predicted first pushover analyses (see Figure 3.45) were used to predict the time-dependent slip rotation by using equations 2.18 and 2.19. In order to obtain time-dependent slip rotation due to corrosion, time-dependent moment-curvature relationships were used to calculate the strain and stress in the reinforcing bar as a consequence of corrosion effects. The time-dependent relationships between calculated maximum moments and corresponding slip rotations and displacements of the reinforcement bars embedded in S_1 column are shown in Figures 3.46 and 3.47, respectively.

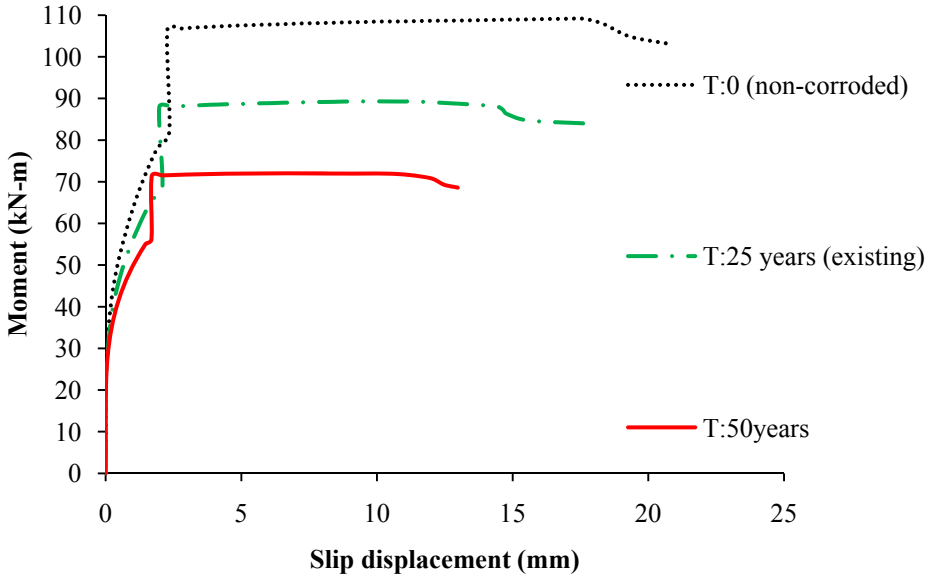

Figure 3.46: Time-dependent slip rotation.

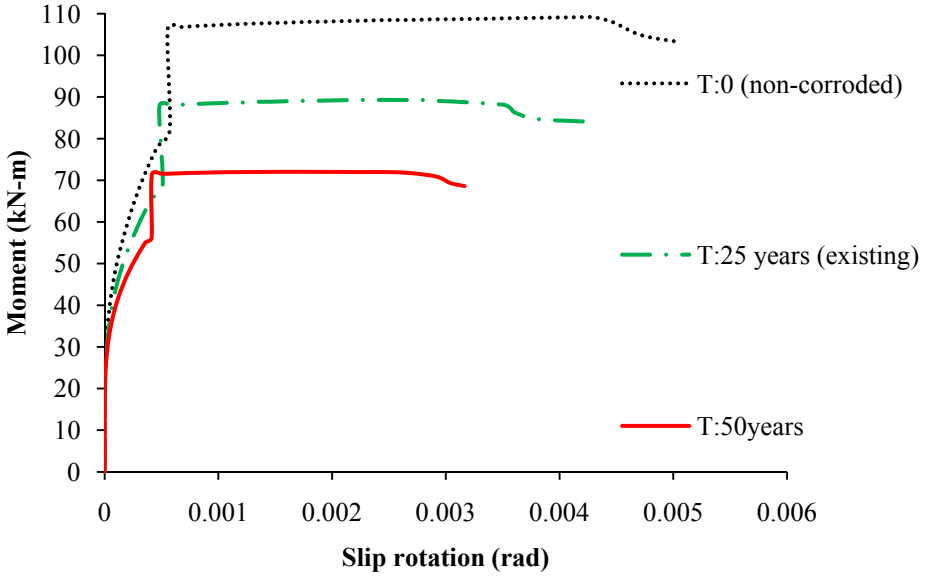

Figure 3.47: Time-dependent slip displacement.

In order to ensure the effect of time-dependent bond-slip relationships due to corrosion on the structural behaviour, the previously defined plastic hinge properties need to be modified. Therefore, predicted time-dependent slip rotations (see figure 3.46) were used to modify the time-dependent moment-curvature relationships (see figure 3.42). For each time period of structural member, plastic hinge properties were redefined by taking into account the effect of bond-slip relationships. Second push-over analyses by considering the effect of bond-slip relationship were performed.

The predicted time-dependent capacity curve due to slippage is shown in Figure 3.48.

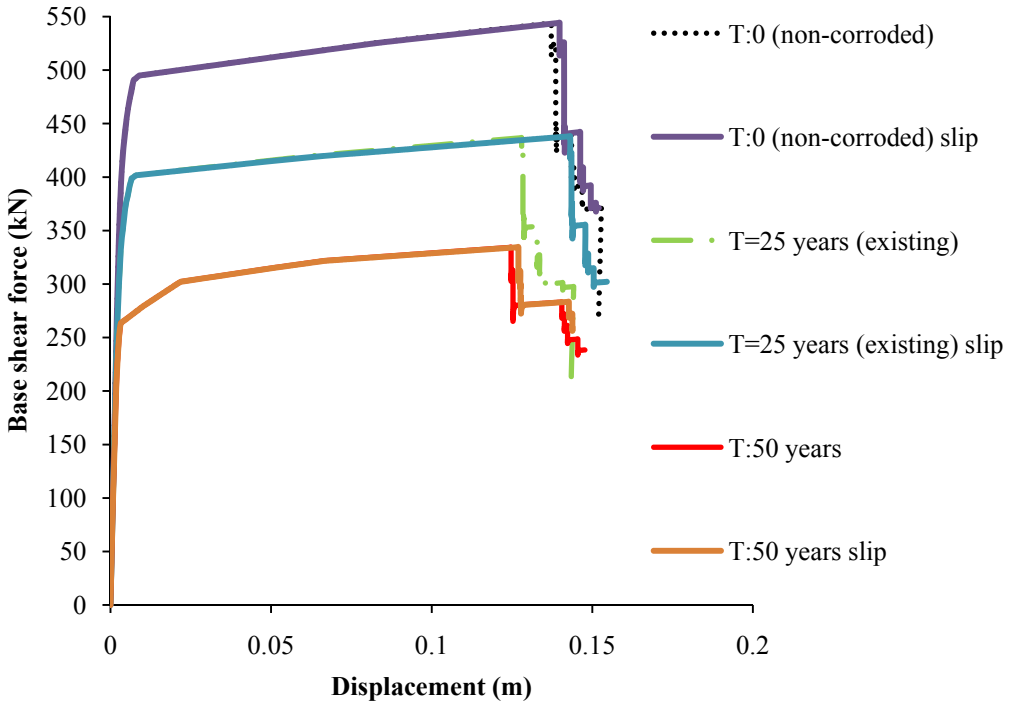

Figure 3.48: Time-dependent capacity curves by bond-slip relationships.

3.6.6 Seismic Performance Analyses

IDA was performed to predict the performance level of the assessed building as a function of corrosion rate. For IDA, the 5% damped first-mode spectral acceleration (S_a (T_1, 5%)) was selected. Twenty ground motion records were used to predict the performance levels of the building as a function of time, where the selected 12 motions records of pseudo velocity versus to period in seconds are shown in Figure 3.49. Figure 3.50(a-b) shows the IDA curves of non-corroded and existing (t: 25 years) building. As it is shown in Figure 3.50, due to effects of corrosion premature dynamic instability occurs at the flat lines, where the roof drift ratio of corroded structure was greater than non-corroded structure. There are still contradictions exist in the available literature about defining the limit states of performance levels. Results of time-history analyses of non-corroded building showed that flat line at S_a

(T_1, 5%) occurred around 1.5% of roof drift ratio. Therefore, associated roof drift ratio corresponding to performance level of collapse prevention (CP) was selected as 1.5% while 0.5% and 1% were selected for immediate occupancy (IO) and life safety (LS), respectively. A probabilistic analysis is required to predict the performance level of the building as a function of time.

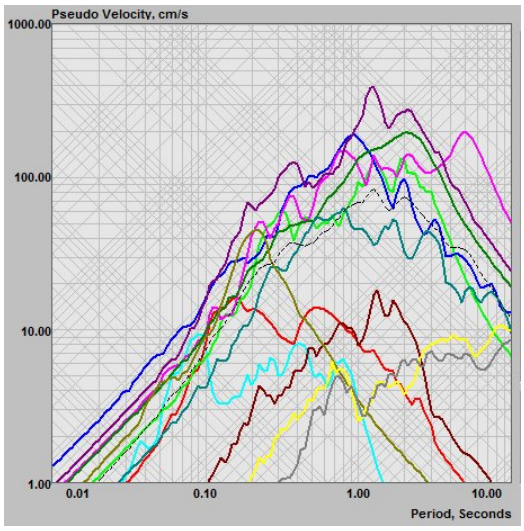

Figure 3.49: Pseudo velocity spectrum for used ground motion records.

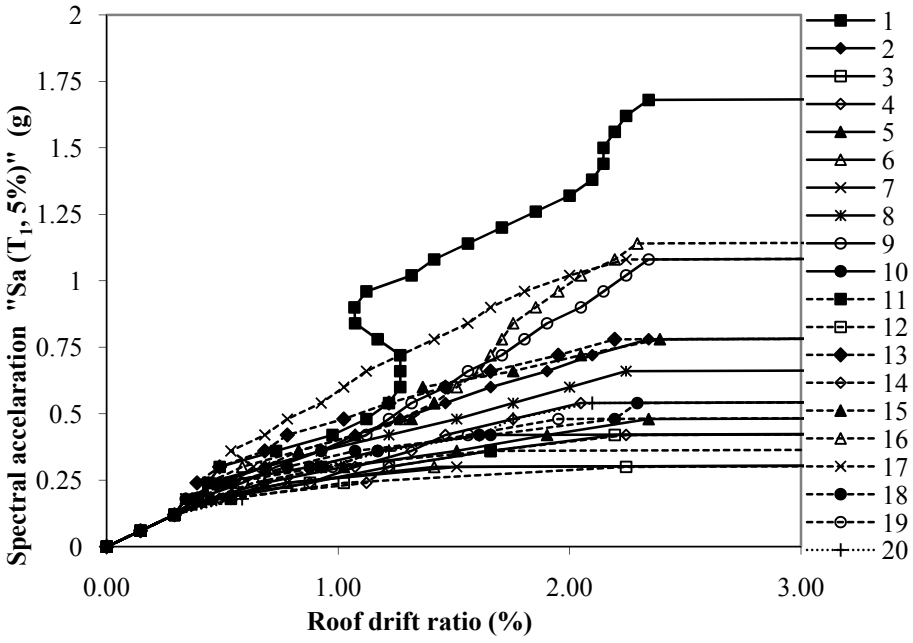

(a)

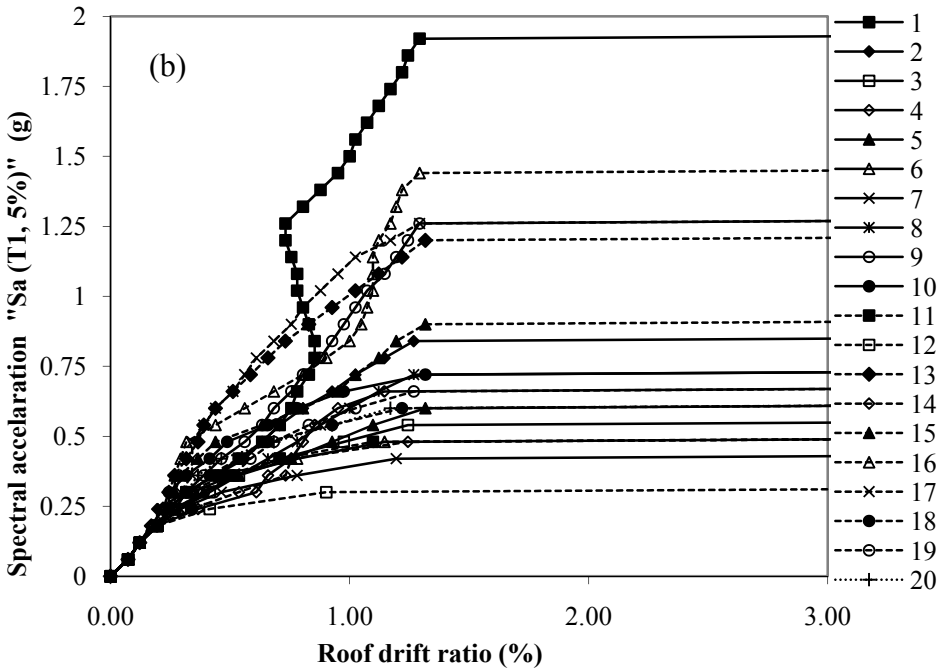

Figure 3.50: IDA curves: (a) T: 0 (non-corroded), (b) T: 25 years (existing).

The predicted lognormal fragility curves in terms of peak ground acceleration (PGA) at the performance level of collapse prevention (CP) are shown in Figure 3.51.

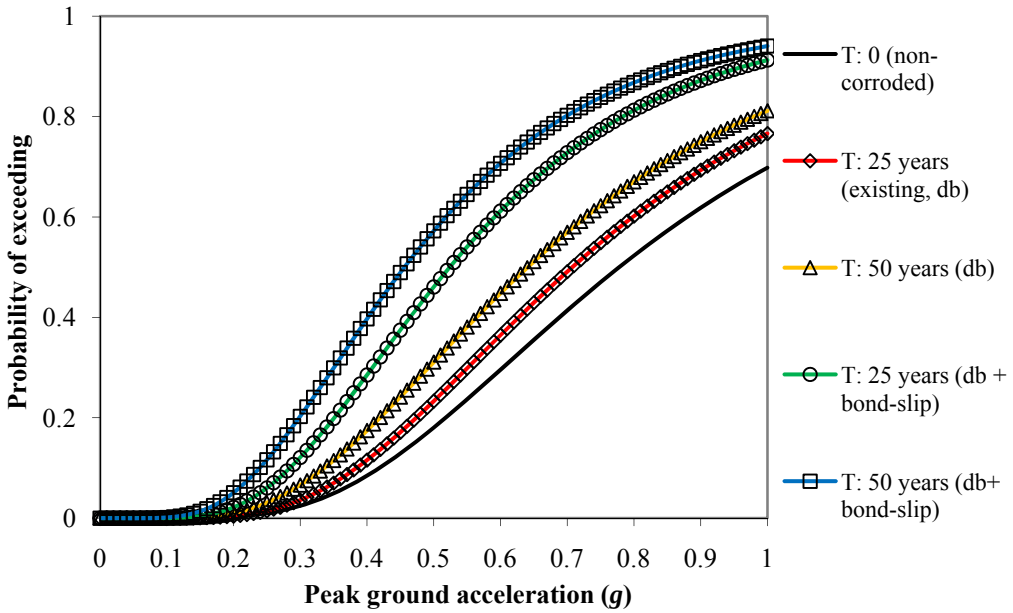

Figure 3.51: Time-dependent fragility curves for the collapse prevention limit state.

In Figure 3.51, for the non-corroded building, the probability of exceeding the limit state corresponding to CP was 46% when the PGA was equal to 0.75*g*. As

shown in Figure 3.51, this probability of exceeding increased as a function of time and showed different results according to the considered effects of corrosion. Therefore, the comparisons of the effects of corrosion by only loss of cross sectional area (d_b) of reinforcement bar, and the combined three effects of corrosion due to bond-slip relationships and reduction in concrete strength are also shown in Figure 3.51. As shown in Figure 3.51, the reduction in the performance level of the building does not only depend on losing cross sectional area (d_b) of reinforcement bars where the reduction in the bond strength and thus slippage of reinforcement bars due to corrosion needs to be considered for seismic analysis. For instance, in Figure 3.51, 25 years after construction (T: 25 years, d_b), if only the loss of cross sectional area of reinforcement bars was considered; the probability of exceeding the limit state corresponding to CP was 55% when PGA was equal to 0.75*g*. However, this probability of exceeding increased to 77% for the same PGA when the three effects of corrosion were taken into account (T: 25 years, d_b + bond-slip). For the same PGA of 50 years after construction (T: 50 years, d_b + bond-slip); the probability of exceeding the limit state was 84% while this probability was 62% if only d_b was considered. The time-dependent results clearly show that the probabilities of exceeding of limit state increase as a function of corrosion rate which causes to reduce the performance level of the structure.

Chapter 4

EXPERIMENTAL STUDY ON THE BOND STRENGTH BETWEEN REINFORCEMENT BARS AND CONCRETE AS A FUNCTION OF CONCRETE COVER, STRENGTH, CRACK WIDTH AND CORROSION LEVEL

4.1 Introduction

In this chapter novel models to predict the ultimate bond strength of uncorroded and corroded specimens were developed by series of experiments. The effects of permeability of concrete by designing two different water/cement ratios (*w/c*) and three concrete cover depths (*c*) on corrosion rate were investigated by accelerated corrosion method. A correction coefficient was suggested to correlate between design mass loss according to Faraday's law and actual mass loss as a result of accelerated corrosion method. By performing pull-out test, bond strengths were investigated for different concrete compressive strengths, cover depths, crack widths and corrosion rates in this chapter. At the end novel models were developed to predict the ultimate bond strength as a function of corrosion rate, concrete compressive strength, concrete cover depths and crack widths. Developed new bond strength models were compared with different previously developed models as described in Chapter 2.3.

In this study, single size bar was used and effect of cover-to-bar-diameter ratio (*c*/*D* ratio) on corrosion and bond strength were considered. The developed bond

strength models in this study varied for concrete compressive strength between 23 MPa and 51 MPa for three different concrete cover depths; and do not directly represent the bond behaviour of reinforced concrete beams. However, it is expected that the relationships obtained in this study will allow bond-slip modelling of reinforced concrete buildings to carry out seismic performance assessment and enhance previously developed models by using the same methodology.

4.2 Frame Work of Experimental Study

A total of 90 specimens were tested in the current study. The experimental program consisted of two phases. In the first phase, different corrosion levels were investigated by considering the permeability of the concrete matrix and concrete covers. For doing this, test specimens were divided into two main groups based on two types of concrete mixtures with a *w/c* ratio of 0.75 and another concrete mixture with a *w/c* ratio of 0.4. Each main group was subdivided into three smaller groups corresponding to the three different concrete covers: c = 15 mm, c = 30 mm and c = 45 mm. The samples in each subgroup were then subjected to corrosion for different time periods using an accelerated corrosion method (4 days to 12 days). The contact resistivity was recorded for each specimen at 1 minute interval to monitor the amount of corrosion level by using Faraday's law. The crack width (W_{cr}) of the specimens was visually observed and measured with an EL35-2505 crack detection microscope.

In the second phase, pull-out test was applied for each specimen to predict the ultimate bond strength and bond-slip relationships for different corrosion levels and considering the effects of different concrete covers and concrete strength levels. Frame work of experimental study is shown in Figure 4.1.

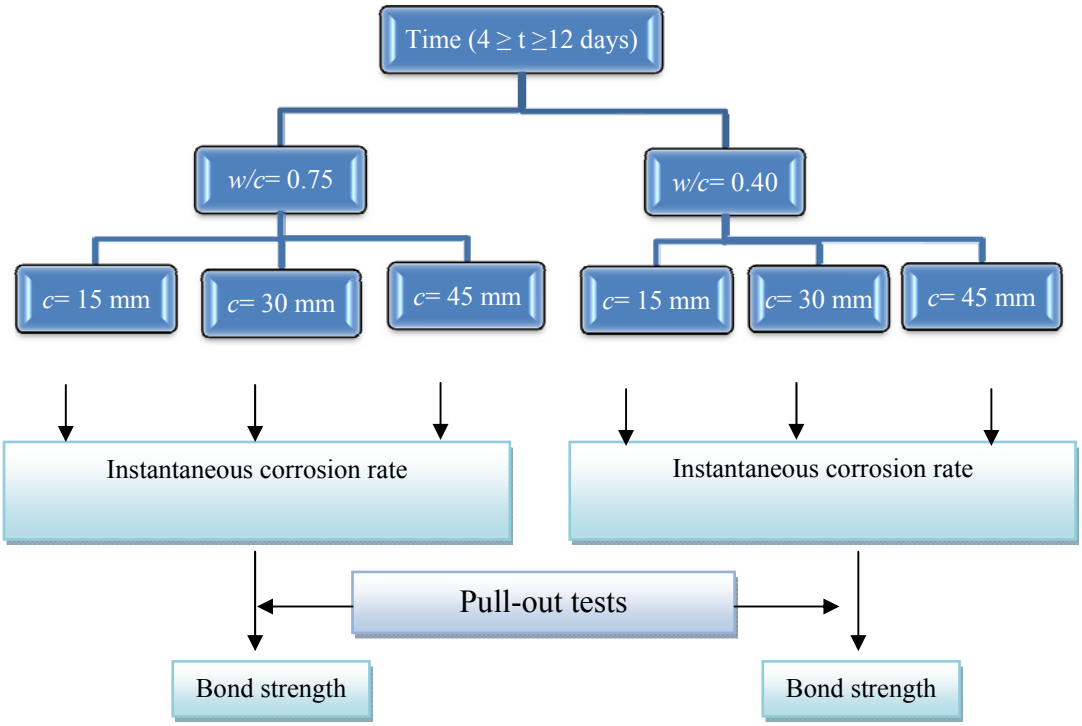

Figure 4.1: Frame work of experimental study.

4.3 Materials

4.3.1 The Reinforcement Bars

According to the purpose of this experimental study, non-corroded reinforcement bars were needed to be used. However, there were no non-corroded reinforcement bars in the market of Famagusta which also represent the current condition of construction industry in North Cyprus. Therefore, reinforcement bars were provided from harbour of Famagusta. Figure 4.2 shows the general conditions of reinforcement bars in the market of Famagusta and Figure 4.3 shows the used non-corroded reinforcement bars for the present study.

Figure 4.2: General condition of reinforcement bars in the market of Famagusta.

Figure 4.3: Used non-corroded reinforcement bars.

Each reinforcement bars were prepared by having same length before carrying them to the material lab at EMU as shown in Figure 4.4.

Figure 4.4: Cutting of reinforcement bars.

Deformed steel bars, 14 mm in diameter and 250 mm in length were used for each specimen. Tensile tests were performed on six randomly selected reinforcement bars to calculate the actual mechanical properties of reinforcement bars. Recorded mechanical properties of the reinforcement bars were determined as follows: the yield strength (f_{sy}) was equal to 458 MPa, the rupture strength (f_{su}) was equal to 606 MPa, the yield strain (ε_{sy}) was equal to 0.075, and the strain hardening (ε_{sh}) was equal to 0.103. Figure 4.5 shows the stress-strain curve of the reinforcement bars used for present study.

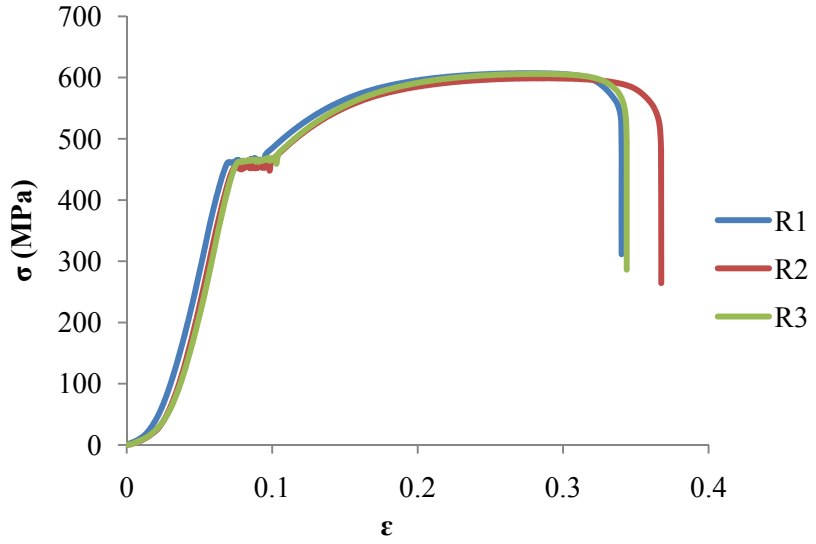

Figure 4.5: Stress-strain curve of used reinforcement bars.

4.3.2 The Concrete

Two types of concrete mixtures with a *w/c* ratio of 0.75 (f_c'= 23 Mpa) and another concrete mixture with a *w/c* ratio of 0.4 (f_c '= 51 MPa) was designed by using BRE method of mix design (BRE, 1975) as upper and lower bound. Several trial castings were done in order to achieve the expected concrete compressive strength at 28 days (see Figures 4.6 and 4.7). A mould-releasing chemical was applied to the inside

surface of specimen moulds. First, coarse and fine aggregates were loaded into the mixer for 3 minutes, and a further 3 minutes after water was added.

Figure 4.6: Trial mix design with a water/cement ratio of 0.75.

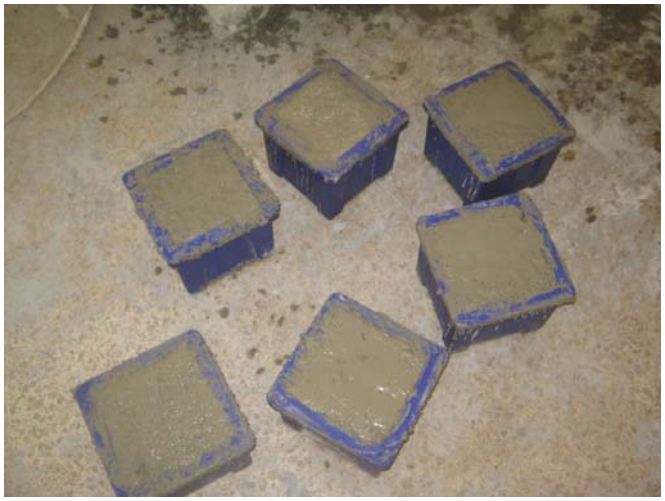
Figure 4.7: Trial mix design with a water/cement ratio of 0.40.

During each trial, slump of fresh mix was measured, thus it provided to control the amount of water and cement for further casting.


Figure 4.8: Slump test of designed concrete specimens.

Compaction was carried out by a table vibrator. After placing and compacting concrete, the specimen surface was smoothed with a steel trowel. Figures 4.9 and 4.10 show the compaction and surface smoothing of concrete specimens.

Figure 4.9: Compaction of specimens by table vibrator.

Figure 4.10: Smoothing the surface of specimens.

The concrete specimens were kept in a curing room maintained at 22 °C and 90% relative humidity for 24 hours. Then, specimens were cured in a water thank at 22 °C for 28 days. The first trial results of concrete compressive strength of concrete mixture with a *w/c* ratio of 0.4 are shown in Figure 4.11.

(a) (b) (c)

Figure 4.11: Trial results of concrete compressive strength of concrete mixture with a water/cement ratio of 0.40: (a) First specimen; (b) Second specimen; (c) Third specimen.

After several trials, expected results of concrete compressive strength were achieved according to the given amount of cement, water and aggregates as given in Tables 4.1 and 4.2. For further casting, design tables (Tables 4.1 and 4.2) were used for the main concrete specimens.

Table 4. 1: Concrete mix design with a *w/c* ratio of 0.75.

Concrete mix design form — Job title: W/C=0.75

Stage	Item		Reference or calculation	Values
1	1.1	Characteristic strength	Specified	20 N/mm² at 28 days
				Proportion defective ..... %
	1.2	Standard deviation	Fig 3	..... N/mm² or no data ..... N/mm²
	1.3	Margin	C1 or Specified	(k = ...) ..... × ..... = ... N/mm²
				..... N/mm²
	1.4	Target mean strength	C2	..... + ... = 25 N/mm²
	1.5	Cement strength class	Specified	42.5/52.5
	1.6	Aggregate type: coarse Aggregate type: fine		Crushed/uncrushed Crushed/uncrushed
	1.7	Free-water/cement ratio	Table 2, Fig 4	0.75 — Use the lower value: 0.75
	1.8	Maximum free-water/cement ratio	Specified	.....
2	2.1	Slump or Vebe time	Specified	Slump 100 mm mm or Vebe time ..... s
	2.2	Maximum aggregate size	Specified	20 mm
	2.3	Free-water content	Table 3	225 — 225 kg/m³
3	3.1	Cement content	C3	225 + 0.75 = 300 kg/m³
	3.2	Maximum cement content	Specified	..... kg/m³
	3.3	Minimum cement content	Specified	..... kg/m³
				use 3.1 if ≤ 3.2 use 3.3 if > 3.1 — 300 kg/m³
	3.4	Modified free-water/cement ratio		.....
4	4.1	Relative density of aggregate (SSD)		2.65 known/assumed
	4.2	Concrete density	Fig 5	2380 kg/m³
	4.3	Total aggregate content	C4	2380 − 300 − 225 = 1855 kg/m³
5	5.1	Grading of fine aggregate	Percentage passing 600 µm sieve	35 (0.35) %
	5.2	Proportion of fine aggregate	Fig 6	52 (0.52) %
	5.3	Fine aggregate content	C5	1855 × 0.52 = 965 kg/m³
	5.4	Coarse aggregate content	C5	1855 − 965 = 890 kg/m³

Quantities	Cement (kg)	Water (kg or litres)	Fine aggregate (kg)	Coarse aggregate (kg) 10 mm T3=1	20 mm T2=1.5	40 mm T2=3
per m³ (to nearest 5 kg)	300	225	965	162	243	485
per trial mix of ..... m³	4.5	3.38	14.48	2.43	3.65	7.28

Table 4. 2: Concrete mix design with a *w/c* ratio of 0.40.

Concrete mix design form — Job title: W/C=0.4

Stage	Item		Reference or calculation	Values
1	1.1	Characteristic strength	Specified	40 N/mm² at 28 days
				Proportion defective ..... %
	1.2	Standard deviation	Fig 3	..... N/mm² or no data ..... N/mm²
	1.3	Margin	C1 or Specified	(k = ...) ..... × ..... = ... N/mm² ..... N/mm²
	1.4	Target mean strength	C2	..... + ... = 45 N/mm²
	1.5	Cement strength class	Specified	42.5/52.5
	1.6	Aggregate type: coarse Aggregate type: fine		Crushed/uncrushed Crushed/uncrushed
	1.7	Free-water/cement ratio	Table 2, Fig 4	0.4
	1.8	Maximum free-water/cement ratio	Specified	Use the lower value: 0.4
2	2.1	Slump or Vebe time	Specified	Slump 100 mm mm or Vebe time ..... s
	2.2	Maximum aggregate size	Specified	20 mm
	2.3	Free-water content	Table 3	225 → 225 kg/m³
3	3.1	Cement content	C3	225 ÷ 0.4 = 563 kg/m³
	3.2	Maximum cement content	Specified	..... kg/m³
	3.3	Minimum cement content	Specified	..... kg/m³
				use 3.1 if ≤ 3.2 use 3.3 if > 3.1 → 563 kg/m³
	3.4	Modified free-water/cement ratio		.....
4	4.1	Relative density of aggregate (SSD)		2.65 known/assumed
	4.2	Concrete density	Fig 5	2380 kg/m³
	4.3	Total aggregate content	C4	2380 − 563 − 225 = 1592 kg/m³
5	5.1	Grading of fine aggregate	Percentage passing 600 µm sieve	35 (0.35) %
	5.2	Proportion of fine aggregate	Fig 6	47 (0.47) %
	5.3	Fine aggregate content	C5	1592 × 0.47 = 716 kg/m³
	5.4	Coarse aggregate content	C5	1592 − 778 = 876 kg/m³

Quantities	Cement (kg)	Water (kg or litres)	Fine aggregate (kg)	Coarse aggregate (kg) 10 mm T3=1	20 mm T2=1.5	40 mm T2=3
per m³ (to nearest 5 kg)	563	225	716	160	240	477
per trial mix of ..... m³						

4.4 Methods

In this study two types of methods were used. First one was a method which is called electro-chemical method to corrode the reinforcement bars. Second method was pull-out test to investigate the ultimate bond strength of non-corroded and corroded reinforcement bars. The methodology performed for these two tests were explained by the following sub-sections.

4.4.1 Accelerated Corrosion Method

In present study, an electrochemical method was used to corrode reinforcement bars. Before mixing the concrete, the reinforcement bars were cleaned to make sure about the exact mass of each reinforcement bar by removing dust and small iron particles that can be broken easily during pullout. Figure 4.12 shows the general cleaning procedure of a reinforcement bar. After cleaning the reinforcement bars, the mass of the each reinforcement bar was recorded and they were aligned and fastened to the moulds.

Figure 4.12: Cleaning surface of reinforcement bars.

Specimens were removed from curing tank after 28 days and fully immersed in a 3.5% sodium chloride by weight of water for 4 days before subjecting to accelerated

corrosion method. Before and during accelerated corrosion method, the temperature of the water of each specimen was tried to be kept constant at 20 °C (±2 °C). The shape and the geometry of the specimens of three concrete covers are shown in Figure 4.13.

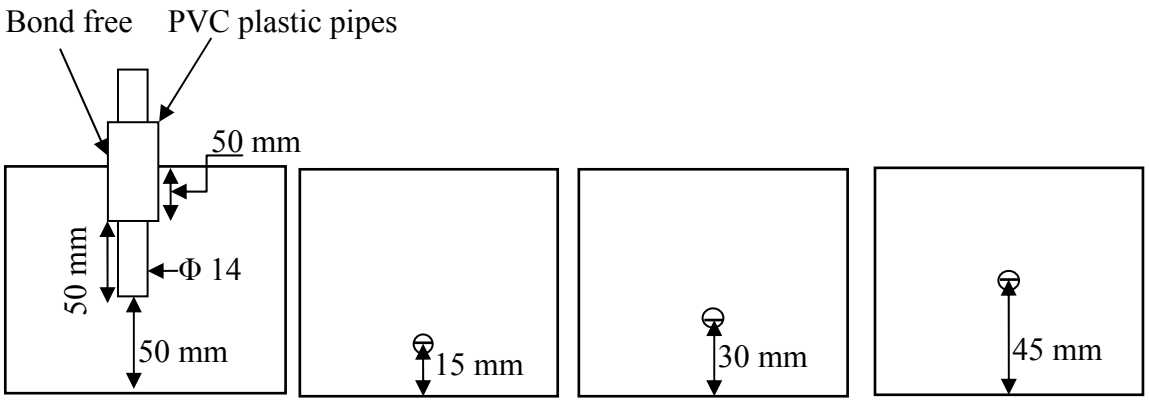

Figure 4.13: Shape and geometry of specimens.

In Figure 4.13, deformed reinforcement bars 14 mm in diameter were placed in the cubes with different concrete covers. The embedded length was set at 50 mm to ensure bond failure. To prevent contact between the concrete and the reinforcement bars while maintaining the required concrete cover on the surface of the concrete specimen, 50 mm lengths of the reinforcement bars were placed inside PVC pipes. The direct current was impressed on the main steel bar embedded in the concrete. The direction of the electric current which was connected to the samples with the reinforcement bars as the anode and copper plate as the cathode. The current was passed from the reinforcement bars to the copper plate placed inside of 5% salt solution (NaCl). Pure water was used and 5% salt solution by the weight of water was dissolved for each specimen as shown in Figure 4.14. The setup for the accelerated corrosion process is shown in Figure 4.15.

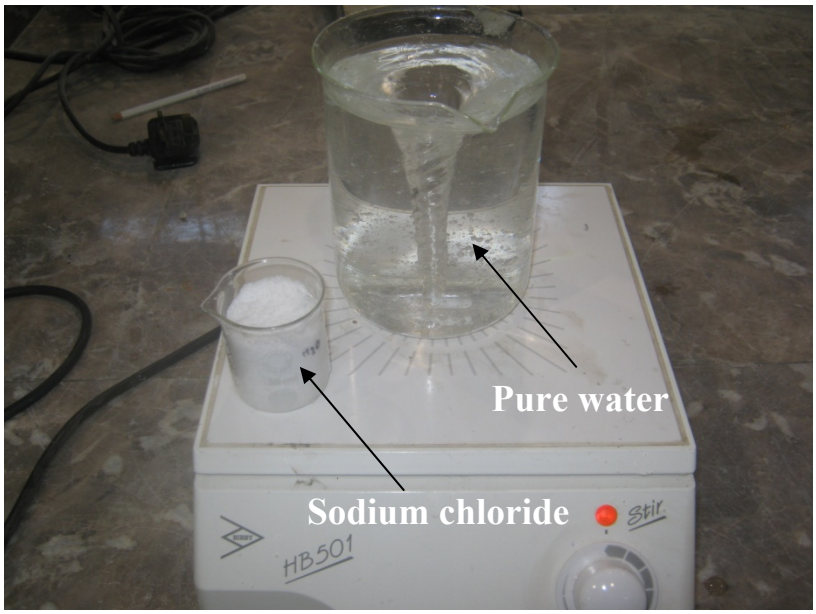

Figure 4.14: Dissolved NaCl in pure water.

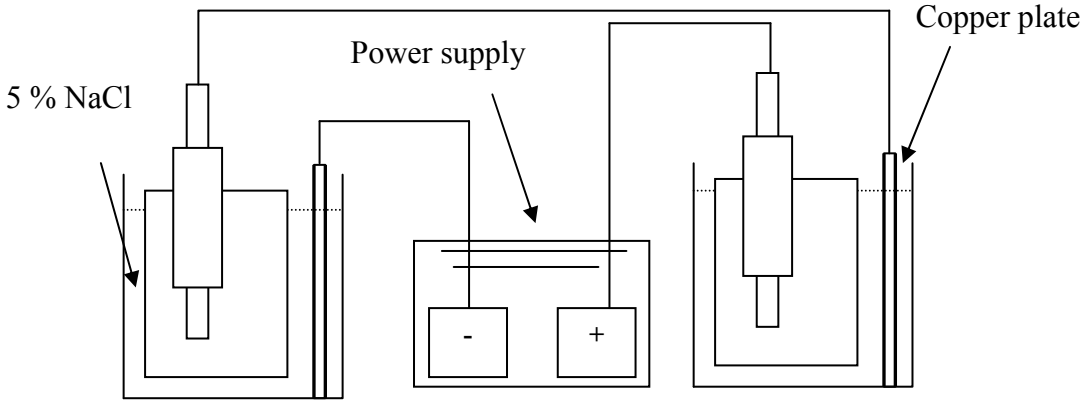

(a)

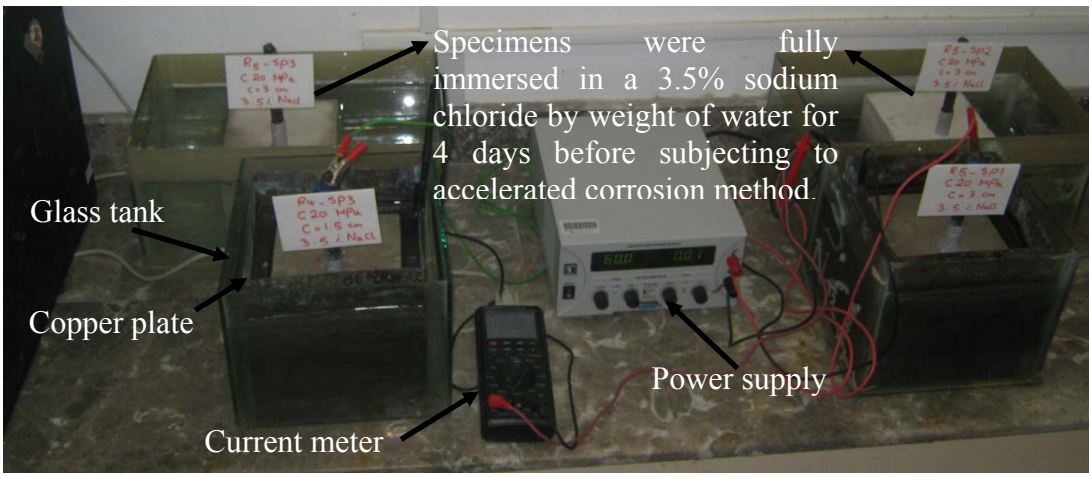

(b)

Figure 4.15: Set-up of electro-chemical method: (a) Electrical circuit of system; (b) general view of set-up.

As shown in Figure 4.15, a current meter was also used to record the average current of each specimen to calculate the resistivity of concrete specimens for different conditions. The designed (theoretical) mass loss of the reinforcement bars due to corrosion was calculated according to Faraday's law using equation 4.1:

$$\text{mass loss} = \frac{t(s) \times I(A) \times 55.847}{2 \times 96{,}487} \tag{4.1}$$

where t is the time and I is the current. Equation 4.1 is based on Faraday's Law, which states: (1) The mass of substance formed or consumed in electrolysis is proportional to the amount of charge passing through it; (2) The mass of a substance formed or consumed in electrolysis is also proportional to its molar mass; (3) The mass of a substance formed or consumed in electrolysis is inversely proportional to number of electrons per mole needed to cause the indicated change in the oxidation state. The quantity of applied charge of any electrolysis is given by the product of applied current and the duration of exposure. For the corrosion process, for each mole of iron oxidized, 2 mols of electrons are given out, consuming a charge of 2×96487 coulombs (C). The mass loss is then calculated by multiplying the applied charge by the molar mass (55.847 g/mol for iron) and dividing by charge needed per mole (Fang et al., 2006). However developed model by Faraday was performed for the reinforcement bars which were directly immersed to glass tank. In another word, the developed model was not for the reinforcement bars which were immersed into concrete specimens. Amount of time and energy is needed to initiate the corrosion when the reinforcement bars immerse in concrete. Therefore, it is possible to obtain different corrosion levels rather than designed amount of corrosion level. Thus, in this study, the actual corrosion level or percentage mass loss of each specimen was

calculated by equation 4.2 and corrosion level was controlled by depending on Faraday's Law.

$$C_L = \frac{G_0 - G_1}{G_0} \times 100\% \tag{4.2}$$

In Equation 4.2, where G_0 is the initial weight of the reinforcement bars before corrosion and G_1 is the weight of the reinforcement bars after the removal of the corrosion products.

4.4.2 Pullout Test

The pullout tests were carried out for both corroded and non-corroded specimens. The bond tests were carried out by Instron 3385H universal testing machine with a capacity of 250 kN. The applied loads were controlled via computer, using displacement control at a rate of 10 mm/minute. Setup of the pull-out testing machine is shown in Figure 4.16. As shown in Figure 4.16, an apparatus was especially designed and adapted to avoid any changes in bond strength during the pullout test.

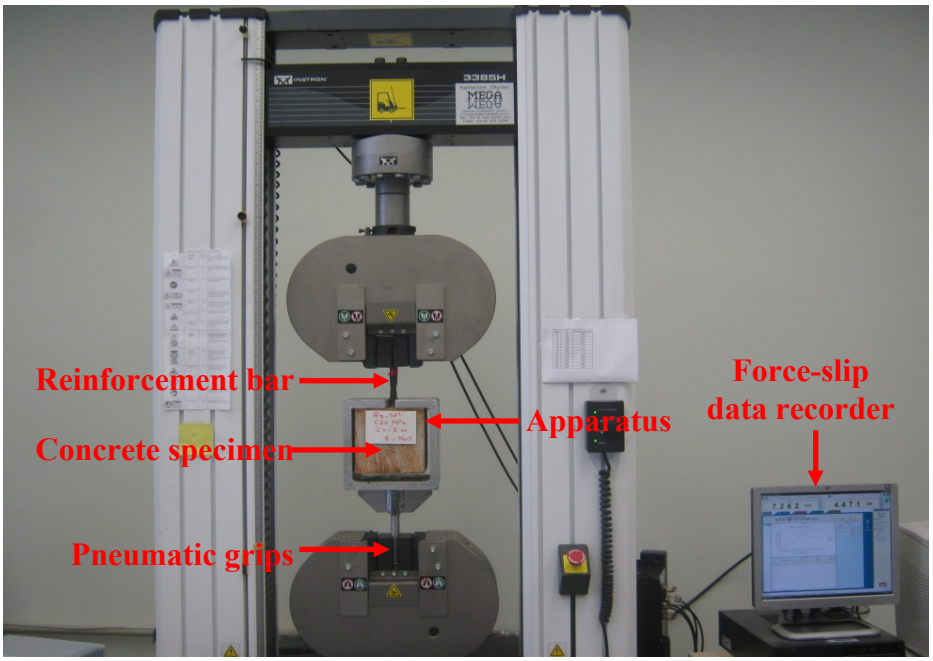

Figure 4. 16: Setup of the pullout testing machine

Figure 4.17: Designed apparatus for pullout test

The stress and displacement values of designed apparatus for different vertical loads are also shown in following Figures.

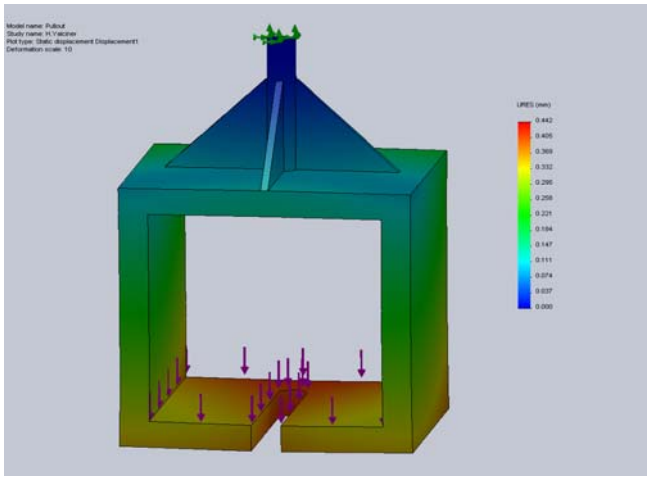

Figure 4.18: Displacement values of designed pullout apparatus under 25 kN vertical loads.

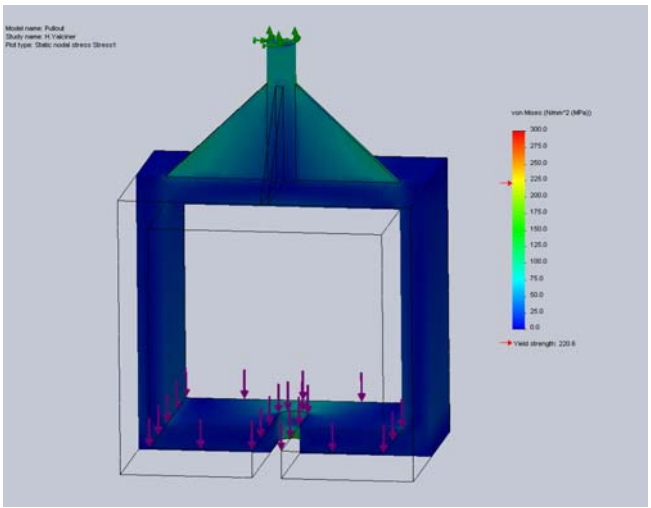

Figure 4.19: Stress values of designed pullout apparatus under 25 kN vertical loads

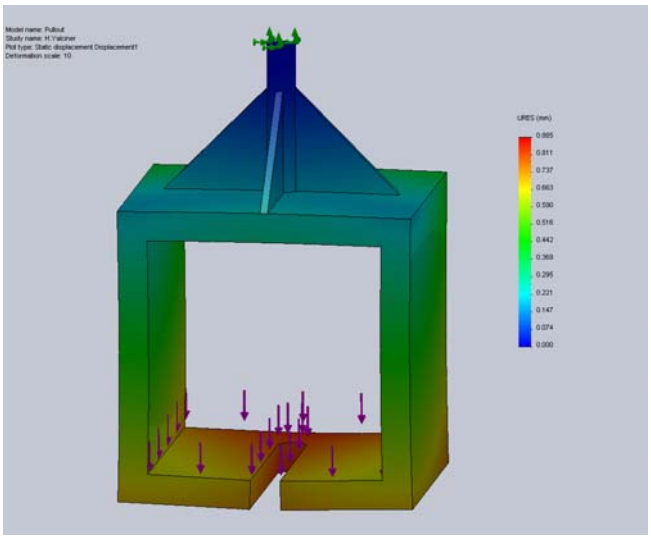

Figure 4.20: Displacement values of designed pullout apparatus under 50 kN vertical loads.

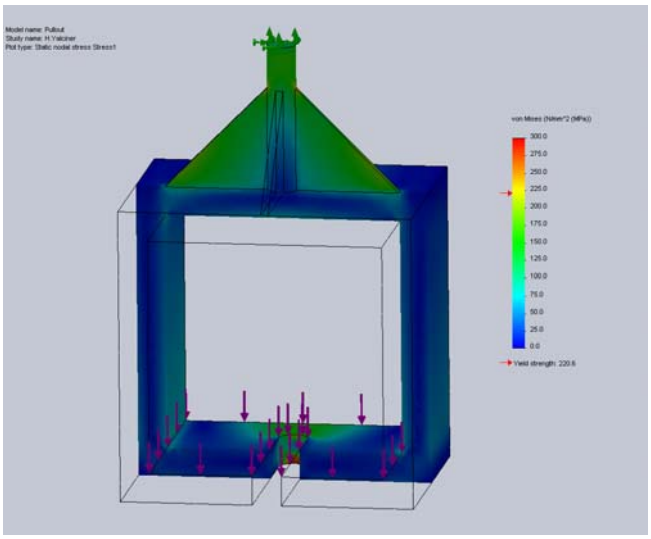

Figure 4.21: Stress values of designed pullout apparatus under 50 kN vertical loads.

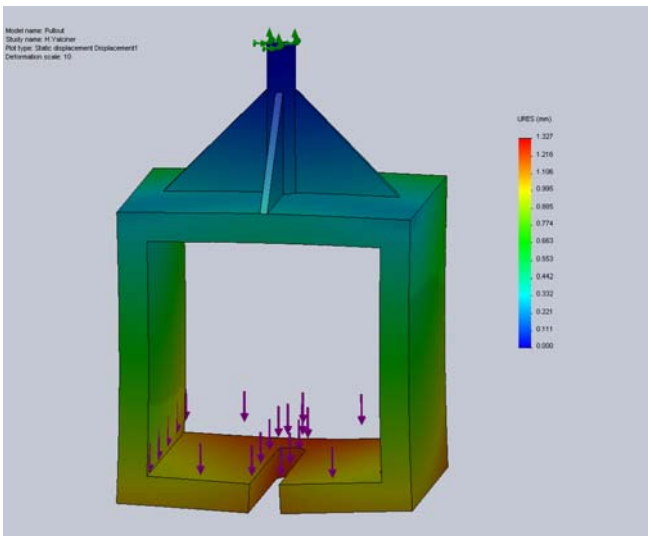

Figure 4.22: Displacement values of designed pullout apparatus under 75 kN vertical loads.

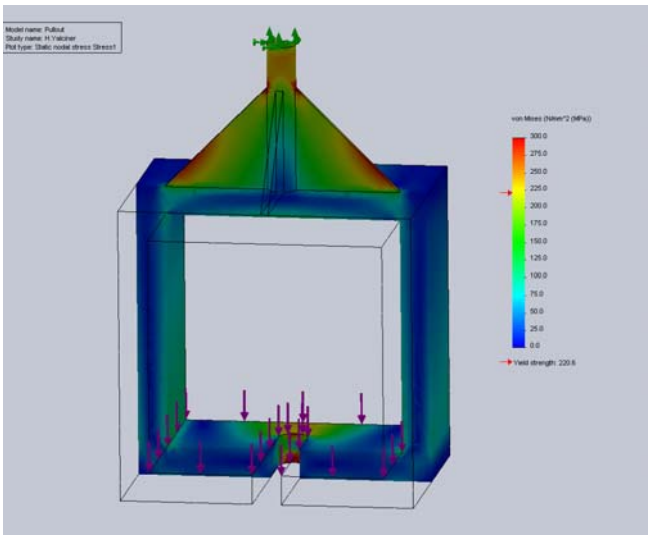

Figure 4.23: Stress values of designed pullout apparatus under 75 kN vertical loads.

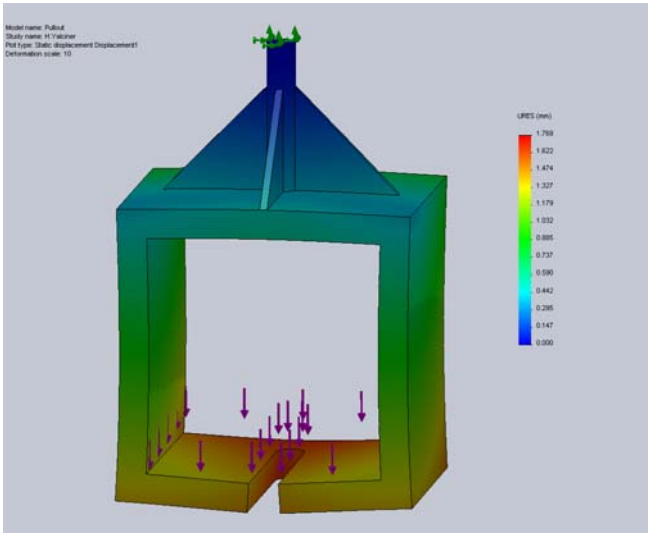

Figure 4.24: Displacement values of designed pullout apparatus under 100 kN vertical loads.

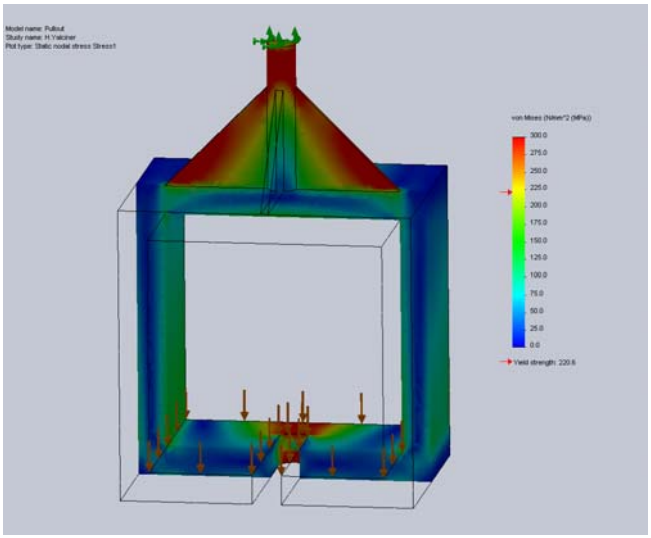

Figure 4.25: Stress values of designed pullout apparatus under 100 kN vertical loads.

As shown in Figures through Figure 4.18 to 4.25, displacement and stress values of the designed apparatus was negligible under applied over loads at different points. During pullout tests, maximum pullout forces were recorded to calculate the ultimate bond strength (τ_{bu}) according to equation 4.3:

$$\tau_{bu} = \frac{P_{\max}}{\pi DL} \text{ (MPa)} \tag{4.3}$$

Where; $P_{\max}$ is the ultimate pullout load and D and L are the diameter and bond length of the reinforcement bars, respectively.

4.5 First Trial of Accelerated Corrosion Method

4.5.1 Designed Formworks, Casting and Curing of Concrete Specimens for First Trial

Several trials were done to perform the electro-chemical method correctly. First trial showed that it was not possible to align and fasten the reinforcement bars by hand or manually for the correct concrete cover depths and embedment length of reinforcement bars. Therefore, in order to make sure about the correct concrete cover depths and embedment length of reinforcement bars, special formworks were designed for different concrete cover depths. Figures 4.26 and 4.27 show the designed special formworks and alignment of the reinforcement bars for different concrete cover depths, respectively.

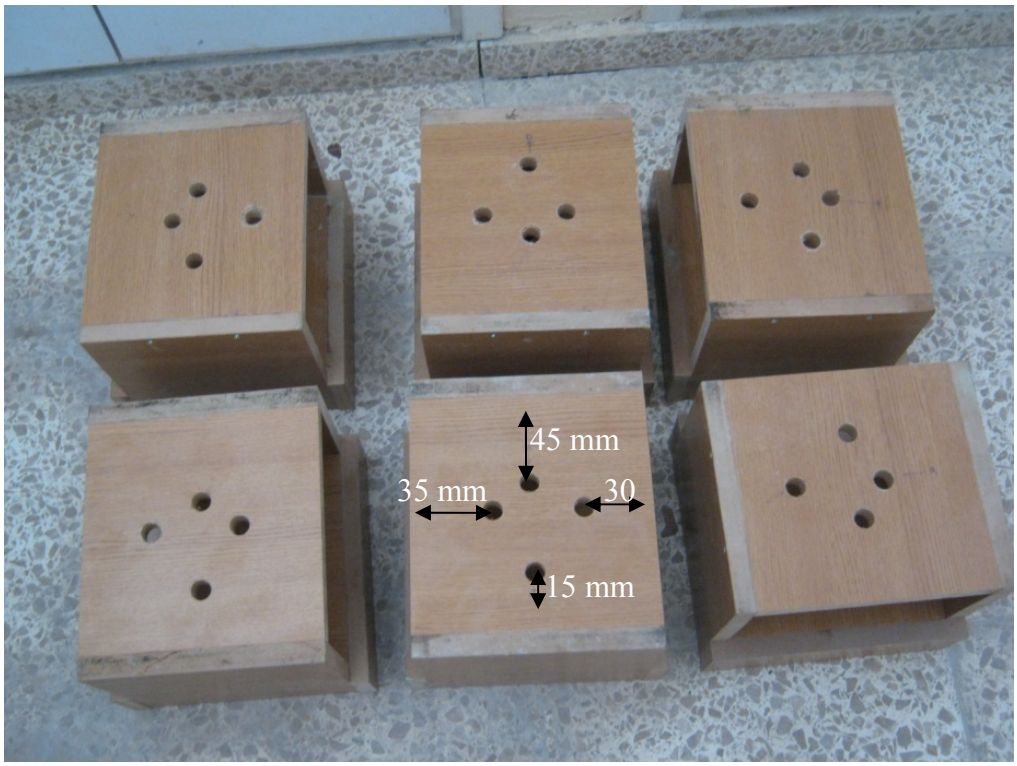

Figure 4.26: Designed special formworks to align the reinforcement bars.


Figure 4.27: Alignment of the reinforcement bars for different concrete cover depths.

As shown in Figure 4.27, designed formworks provided to set the exact concrete covers. Secondly, another problem was to set the correct embedment length of the reinforcement bars. In order to solve this problem, fixers were used for the first trial as shown in Figure 4.28.

Figure 4.28: Fixers used for the embedment length of the reinforcement bars.

As shown in Figure 4.29, because of the shape of the designed formworks, embedment length of the reinforcement bars thus bond strength could be changed during the demoulding of the formworks.

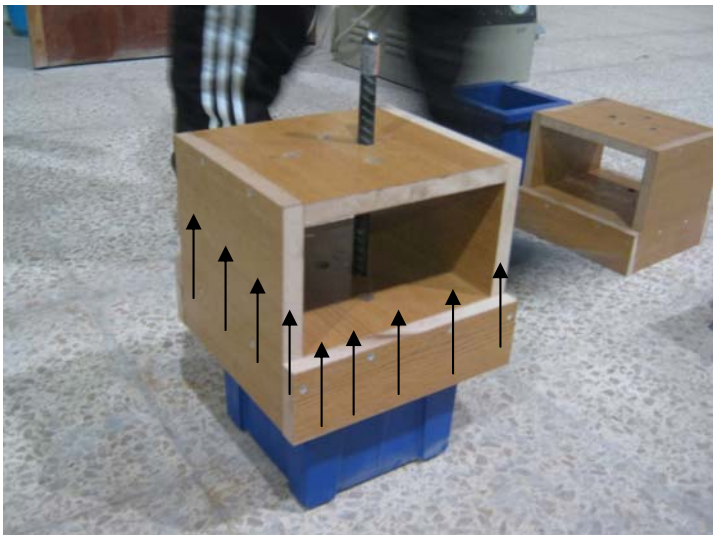

Figure 4.29: Direction of demoulding of formworks.

In order to prevent any changes in embedment length of the reinforcement bars and especially in the bond strength during demoulding, the edge of each reinforcement bars were smoothened as shown in Figure 4.30.

Figure 4.30: Smoothing the edge of reinforcement bars.

Before aligning and fastening the reinforcement bars, each reinforcement bars and holes of formworks were checked to see that formworks easily comes upward without vibrating the reinforcement bars.

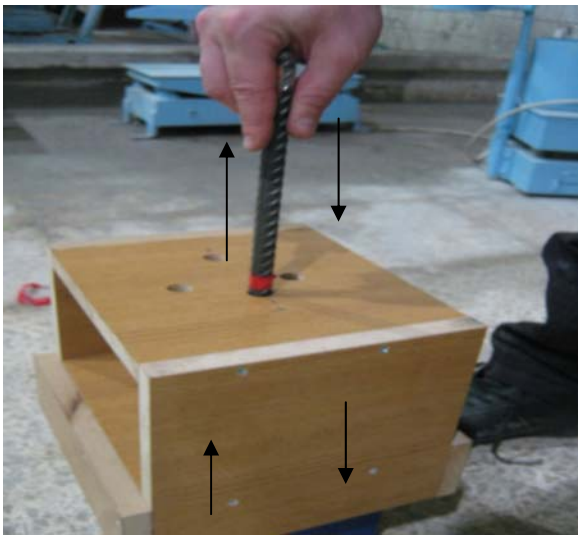

Figure 4.31: Checking holes of formworks before pouring concrete.

After recording the total mass and embedment length of each reinforcement bar, moulds were ready for pouring concrete. Figure 4.32(a-b) shows the general setup for the concrete specimens before pouring the concrete with 15 mm, 35 and 45 mm concrete cover depths.

(a)

(b)

Figure 4.32: Setup of the concrete specimens before pouring concrete: (a) 15 mm and 35 mm concrete covers; (b) 45 mm concrete cover.

Concrete mix proportions given in Table 4.1 were used for the first trial of accelerated corrosion method. After pouring concrete, specimens were carried into the curing room for one day. Figure 4.33 shows the curing room of first trial concrete specimens maintained at 22°C (± 2°C) and 90% relative humidity for 24 hours.

(a)

(b)

Figure 4.33: Curing of concrete specimens for 24 hours: (a) 15 mm and 35 mm concrete covers; (b) 45 mm concrete cover.

Demoulding and transporting of concrete specimens were done with great care to avoid any disturbance of the reinforcement bars. Figure 4.34 shows the general view of demoulded concrete specimens kept 24 hours in room curing.

(a)

(b)

Figure 4.34: General view of demoulded concrete specimens kept 24 hours room in the curing: (a) 15 mm and 35 mm concrete covers; (b) 45 mm concrete cover.

After demoulding the formworks, specimens were cured in water tank at a temperature of 22°C for 28 days before accelerated corrosion method as shown in Figure 4.35.

Figure 4.35: 28 days water curing of first trial concrete specimens.

4.5.2 Results of First Trial of Accelerated Corrosion Method and Failure in Trial due to Occurred Local Corrosion

When considering the structural effects of corrosion, it is necessary to distinguish differences between general and local corrosion:

- General corrosion leads to a more uniform loss of reinforcement section, and is generally associated with carbonation and some chloride-induced corrosion. It results in longitudinal cracks along the length of the reinforcement due to rust growth.
- Local corrosion leads to a pitting form of corrosion, and the loss in cross-section can be around four to eight times that of general corrosion. It can occur when the oxygen supply is limited. Less rust product will be generated, and surface cracking may not result unless general corrosion is also present (Webster; 2000).

In this study, uniform corrosion was the interest to reach the objective of the study. However, results of the first trials were not parallel to the scope of the study

due to occurred local corrosion. As it is shown in Figure 4.36 local corrosion occurred for each concrete specimen at the end of applied electro-chemical method.

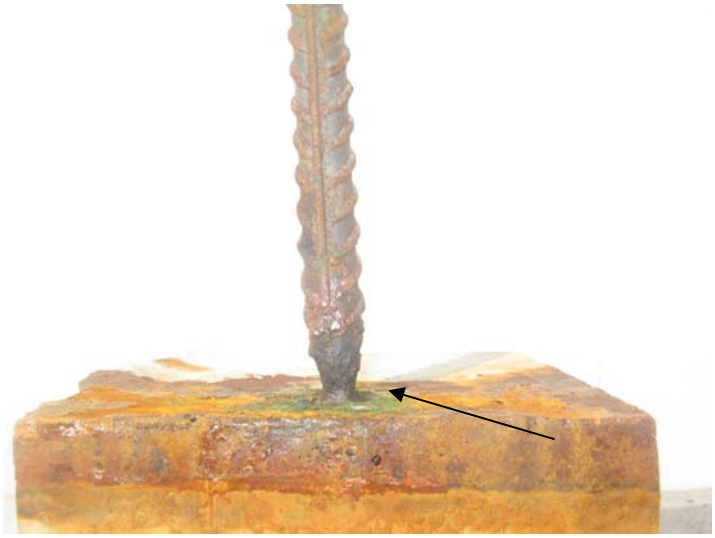

(a)

(b)

Figure 4.36: Local corrosion: (a) concrete cover: 15 mm; (b) concrete cover: 30 mm.

Each concrete specimen was broken in order to investigate the local corrosion better. It was observed that most of the reinforcement bars would already rupture due to local corrosion occurred. Figure 4.37 shows one of the condition of the reinforcement bar due to local corrosion.

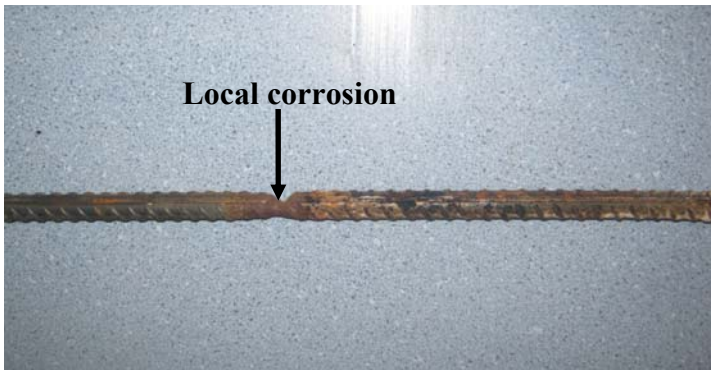

Figure 4.37: Condition of a reinforcement bar after breaking the concrete sample.

4.5.3 Solutions to Prevent Local Corrosion

4.5.3.1 Painting the Contact Area of the Reinforcement Bars

In order to prevent local corrosion at the surface of the concrete and reinforcement bars, different trials were performed. The first idea was to paint part of the reinforcement bars connected to the surface of the concrete. Figure 4.38 shows the painted contact area of reinforcement bar in order to prevent local corrosion.


Figure 4.38: Painted reinforcement bar to prevent local corrosion.

This method showed that painting was not adequate enough to prevent the local corrosion. It was observed that, 2 hours after starting the accelerated corrosion method, paint was removing out from the reinforcement bars.

4.5.3.2 Polyvinyl Chloride (PVC) Pipe to Prevent the Contact between Concrete and Reinforcement Bar

PVC pipes were used for the second trial to prevent the contact between concrete and reinforcement bar. Figure 4.39 shows the second trial of accelerated corrosion method by using PVC pipes in order to prevent the local corrosion.

Figure 4.39: Prevention of local corrosion by PVC pipes.

Before using PVC pipes, it was observed that bleeding of water was only at the surface of concrete specimens. On the other hand, it was observed that after using PVC pipes, bleeding of the water occurred at both surface of concrete and the closer side of the concrete cover (longitudinal). This observation is shown in Figure 4.40. This observation was important to understand the direction and the path of the electric current in the system.

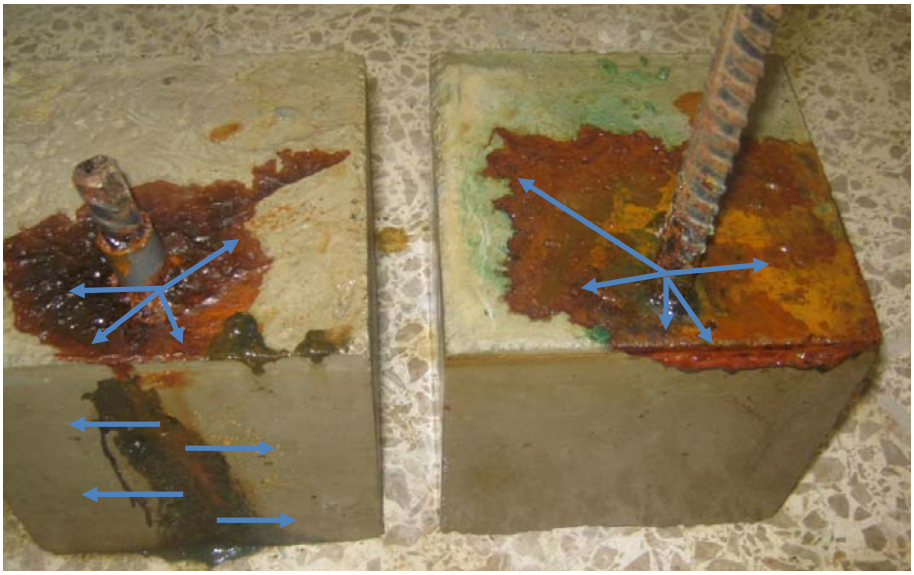

Figure 4.40: The direction of water bleeding with and without PVC pipes.

Another observation that can be investigated during electro chemical method is cracking of concrete due to volumetric expansion by corrosion rust. Corrosion is an electrochemical process during which metallic iron is converted to rust, creating volumetric expansion of the steel bars and also causing extremely high tensile forces within the concrete cover. By using PVC pipes, due to volumetric expansions cracks were observed for different concrete specimens. Figure 4.41 shows the occurred cracks at the top surface of concrete specimen after using PVC pipes.

Figure 4.41: Volumetric expansion of a corroded reinforcement bar.

After accelerated corrosion method, the concrete specimens were broken to check the condition of reinforcement bars. Figure 4.42 shows the one of the broken concrete specimen after accelerated corrosion method. As shown in Figures 4.42 and 4.43, uniform corrosion was obtained by using PVC pipes where local corrosion did not occur.

Figure 4.42: Broken concrete specimen after using PVC pipes.

Figure 4.43: Obtained uniform corrosion along the length of a reinforcement bar.

4.6 Designed New Formworks with PVC Pipes

Decision of using PVC pipes to prevent local corrosion required to design new formworks to align and fasten the reinforcement bars. Therefore, according to the aim of the experimental study in this thesis, new formworks were designed for each different concrete cover depths. New formworks were made of plywood. Figure 4.44 shows the 150 mm square plywood plates before building up cubic forms. Required concrete cover depths were designed carefully for each specimen as shown in Figure 4.45.

Figure 4.44: Pieces of plywoods.

Figure 4.45: Opening concrete covers on one side of plywoods.

After opening the required concrete covers on plywoods, they were ready to form cubic form. Figure 4.46 shows the completed formworks by using PVC pipes and plywood.

(a)

(b)

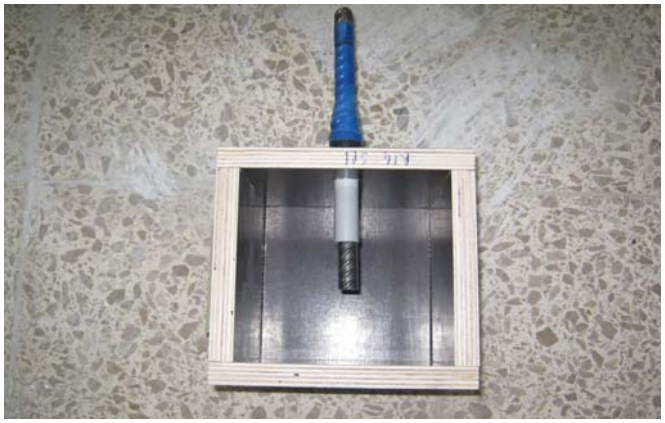

(c)

Figure 4.46: (a) Preparing of PVC pipes, (b) PVC pipes for main specimens, (c) General view of setup for prepared formwork.

4.7 Main Concrete Specimens for Tests

4.7.1 Mixing, Casting and Curing of Concrete Specimens with a Water/Cement Ratio of 0.75

As it was mentioned in the introduction of Chapter 4, test specimens were divided into two main groups based on the *w/c* ratios of 0.75 or 0.40. First casting was done for the concrete mixture with a *w/c* ratio of 0.75 for three different concrete covers: *c* = 15 mm, *c* = 30 mm and *c* = 45 mm. Figure 4.47 shows the set up of concrete specimens with a *w/c* ratio of 0.75 before casting concrete.

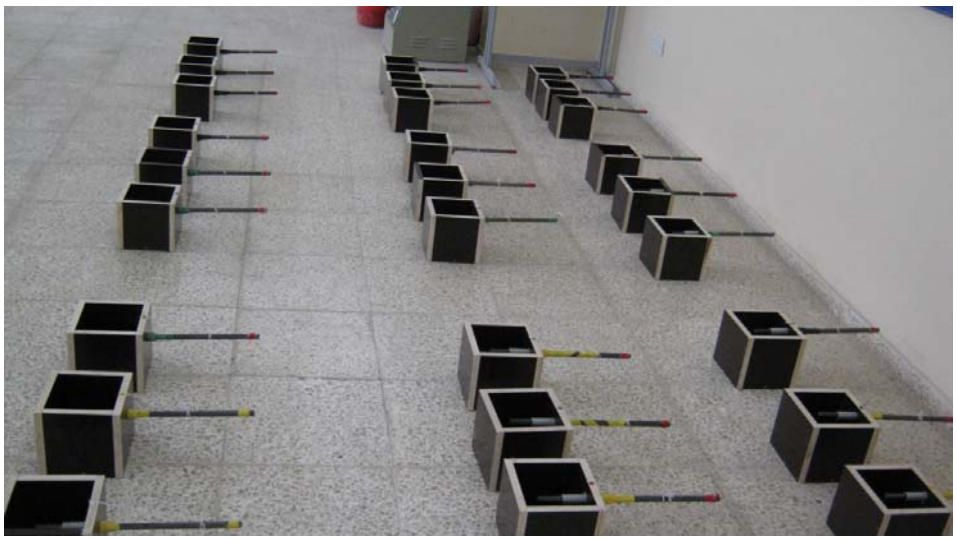

Figure 4.47: Set up of first group (*w/c*= 0.40) of 27 specimens before casting concrete.

The procedure of casting concrete was described in section 4.3.2. Previously given mix design in Table 4.1 was used for concrete specimens with *w/c* ratios of 0.75. Figure 4.48 shows the concrete specimens after pouring and compacting concrete.

Figure 4.48: First group of concrete specimens (*w/c*= 0.75) after compacting.

After compacting the concrete, concrete specimens were kept in the curing room for 24 hours. Figure 4.49 shows the room curing of first concrete specimens (*w/c*= 0.75).

Figure 4.49: Curing of concrete specimens with a water/cement ratio of 0.75

After one day of curing, specimens were carried to water tank at 22°C (± 2 °C) for 28 days. Figures 4.50 and 4.51 show during and 28 days after water curing of concrete specimens with *w/c* ratios of 0.75.

Figure 4.50: 28 days water curing of concrete specimens with a water/cement ratio of 0.75.

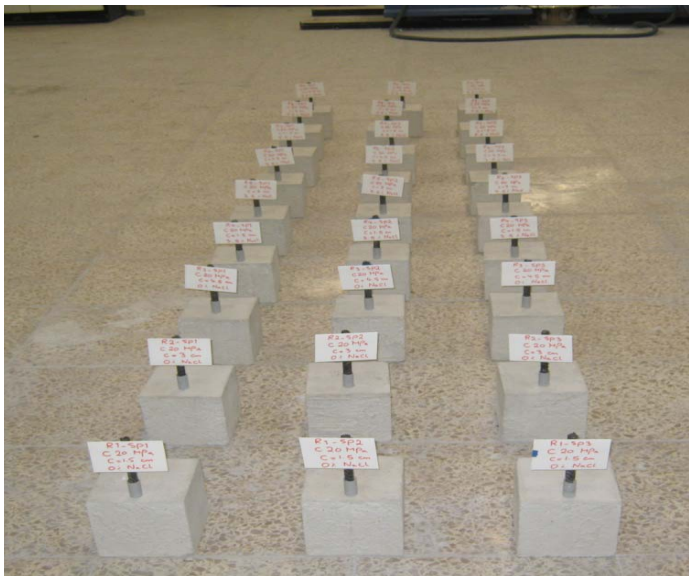

Figure 4.51: 28 days after water curing of concrete specimens with a water/cement ratio of 0.75.

4.7.2 Mixing, Casting and Curing of Concrete Specimens with a Water/Cement Ratio of 0.40.

Procedure described in section 4.7.1 was repeated for other concrete specimens with a *w/c* ratio of 0.40. Figures 4.52, 4.53, 4.54, 4.55 show set up of concrete specimens (*w/c*= 0.40) before casting concrete, after casting concrete, moist room curing for 24 hours, and water curing for 28 days, respectively. Figure 4.56 shows the prepared concrete specimens before accelerated corrosion method.

Figure 4.52: Set up of concrete specimens (*w/c*= 0.40) before casting concrete.

Figure 4.53: Second group of concrete specimens (*w/c*= 0.40) after casting concrete.

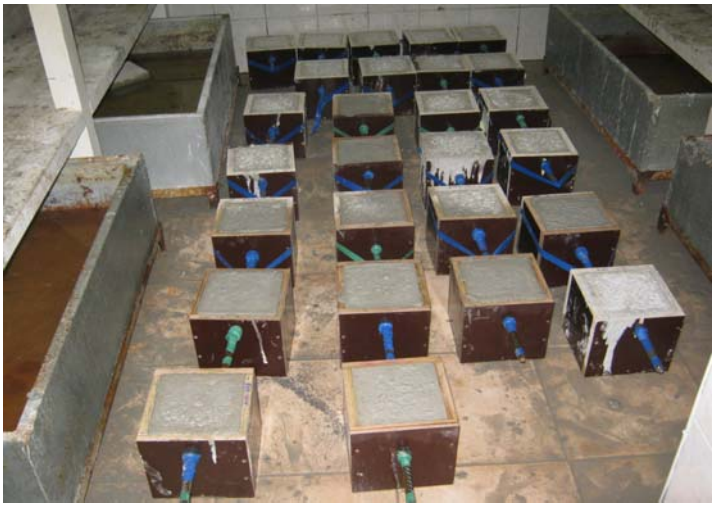

Figure 4.54: Moist room curing of concrete specimens with a water/cement ratio of 0.40.

Figure 4.55: 28 days water curing of concrete specimens with a water/cement ratio of 0.40.

Figure 4.56: 28 days after water curing of concrete specimens with water/cement ratios of 0.75 and 0.40.

Chapter 5

RESULTS AND DISCUSSIONS

5.1 Introduction

The experimental study was performed according to the methodologies described in Chapter 4.4. The detailed results and analysis of all experimental and analytical studies will be presented in this chapter. The test results will be presented into two sections. The first section provides the results of accelerated corrosion method. In the first section, the effects of three concrete cover depths and strength levels of concrete on the mass loss and resistivity of concrete were discussed. The second section provides the results of pull-out tests. In the second section, the effects of three concrete cover depths and strength levels of concrete on the bond strength of uncorroded and corroded specimens were discussed. Bond-slip relationships for the different corrosion levels were compared in two different concrete mixes and three concrete cover depths. The new developed models to predict the ultimate bond strength of corroded and uncorroded reinforcement bars were also presented in this chapter.

5.2 Results of Accelerated Corrosion Method

Described procedure in section 4.4.1 was performed for accelerated corrosion method and the test results were analysed for the following parameters:

- Achieved corrosion levels,
- Effects of concrete covers and strengths on corrosion levels,

- A comparison between theoretical and calculated actual corrosion mass losses,
- Concrete resistivity.

5.2.1 Achieved Corrosion Levels

After pull-out tests, to calculate the mass losses of each reinforcement bars, chemical cleaning was applied by using hydrochloric acid to remove the corrosion products from the surface of the reinforcement bars according to described standard ASTM G1-03 (ASTM G1-03, 2003). Figure 5.1 and 5.2 show selected corroded reinforcement bars before and after cleaning the corrosion products from the surface of the reinforcement bars.

Figure 5.1: Before cleaning of reinforcement bars.

Figure 5.2: Final statement of reinforcement bars.

The actual corrosion level or percentage mass loss of each specimen was calculated by using equation 4.2. Table 5.1 and Table 5.2 show the gravimetric test results and comparisons between the theoretical (estimation of mass loss by Faraday's law) and calculated actual mass losses of specimens with *w*/*c* ratios of 0.75, and 0.40 respectively. The specimens were designated R_1SP_1 to R_9SP_3 for the concrete specimens having *w*/*c* ratios of 0.75 (see Table 5.1), $R_{10}SP_1$ to $R_{18}SP_3$ for the concrete specimens having a *w*/*c* ratio of 0.40 (see Table 5. 2).

Table 5.1: Gravimetric test results of concrete mixtures with a *w/c* ratio of 0.75.

Specimen	*c* (mm)	Faraday's mass loss (gr)	Actual mass loss (gr)	Corrosion level C_L (%)	Applied corrosion time (hr)
R_1SP_1	15	Non-corroded	Non-corroded	-	-
R_1SP_2	15	Non-corroded	Non-corroded	-	-
R_1SP_3	15	Non-corroded	Non-corroded	-	-
R_2SP_1	30	Non-corroded	Non-corroded	-	-
R_2SP_2	30	Non-corroded	Non-corroded	-	-
R_2SP_3	30	Non-corroded	Non-corroded	-	-
R_3SP_1	45	Non-corroded	Non-corroded	-	-
R_3SP_2	45	Non-corroded	Non-corroded	-	-
R_3SP_3	45	Non-corroded	Non-corroded	-	-
R_4SP_1	15	38.28	26.00	8.90	97.00
R_4SP_2	15	10.45	12.00	4.10	72.00
R_4SP_3	15	9.67	7.20	2.47	108.05
R_4SP_4	15	9.52	7.97	2.72	95.00
R_4SP_5	15	13.92	12.66	4.32	72.00
R_4SP_6	15	14.27	12.69	4.33	72.00
R_4SP_7	15	13.46	11.98	4.09	72.00
R_4SP_8	15	21.58	19.07	6.51	85.00
R_4SP_9	15	67.54	42.54	14.52	120.00
R_5SP_1	30	3.98	4.00	1.37	97.00
R_5SP_2	30	10.08	10.00	3.45	169.00
R_5SP_3	30	19.21	16.00	5.56	202.00
R_5SP_4	30	4.38	4.10	1.40	97.00
R_5SP_5	30	5.40	4.95	1.69	97.00
R_5SP_6	30	5.07	4.69	1.60	97.00
R_5SP_7	30	11.26	10.46	3.57	169.00
R_5SP_8	30	16.90	15.70	5.36	202.00
R_5SP_9	30	68.58	48.78	16.65	216.00
R_6SP_1	45	3.20	2.00	0.69	97.00
R_6SP_2	45	6.11	5.00	1.69	210.53
R_6SP_3	45	10.74	7.60	2.66	330.48
R_6SP_4	45	2.34	1.99	0.68	216.00
R_6SP_5	45	2.26	1.93	0.66	216.00
R_6SP_6	45	2.82	2.47	0.84	266.00
R_6SP_7	45	2.92	2.58	0.88	266.00
R_6SP_8	45	5.06	4.68	1.60	270.00
R_6SP_9	45	11.47	11.15	3.81	200.00
R_7SP_1	15	301.40	57.00	18.75	289.15
R_7SP_2	15	49.39	26.60	8.90	216.00
R_7SP_3	15	84.69	42.80	14.66	120.00
R_8SP_1	30	30.51	20.40	6.87	288.98
R_8SP_2	30	74.81	52.00	17.33	216.00
R_8SP_3	30	25.02	27.00	6.40	190.27
R_9SP_1	45	24.92	19.00	6.27	289.18
R_9SP_2	45	2.36	2.00	0.68	216.00
R_9SP_3	45	10.68	11.40	3.81	200.50

Table 5.2: Gravimetric test results of concrete mixtures with a *w/c* ratio of 0.40.

Specimen	*c* (mm)	Faraday's mass loss (gr)	Actual mass loss (gr)	Corrosion level C_L (%)	Applied corrosion time (hr)
$R_{10}SP_1$	15	Non-corroded	Non-corroded	-	-
$R_{10}SP_2$	15	Non-corroded	Non-corroded	-	-
$R_{10}SP_3$	15	Non-corroded	Non-corroded	-	-
$R_{11}SP_1$	30	Non-corroded	Non-corroded	-	-
$R_{11}SP_2$	30	Non-corroded	Non-corroded	-	-
$R_{11}SP_3$	30	Non-corroded	Non-corroded	-	-
$R_{12}SP_1$	45	Non-corroded	Non-corroded	-	-
$R_{12}SP_2$	45	Non-corroded	Non-corroded	-	-
$R_{12}SP_3$	45	Non-corroded	Non-corroded	-	-
$R_{13}SP_1$	15	3.43	4.00	1.33	97.00
$R_{13}SP_2$	15	41.59	22.00	7.48	144.83
$R_{13}SP_3$	15	19.61	13.00	4.47	90.92
$R_{13}SP_4$	15	4.25	2.25	0.77	72.00
$R_{13}SP_5$	15	4.14	2.34	0.80	72.00
$R_{13}SP_6$	15	4.48	2.65	0.90	80.00
$R_{13}SP_7$	15	4.06	2.74	0.94	80.00
$R_{13}SP_8$	15	26.18	22.16	7.56	144.83
$R_{13}SP_9$	15	10.48	9.66	3.30	94.00
$R_{14}SP_1$	30	1.38	0.00	0.00	97.00
$R_{14}SP_2$	30	17.45	15.00	5.14	295.78
$R_{14}SP_3$	30	22.44	16.00	5.46	256.23
$R_{14}SP_4$	30	3.88	1.89	0.65	192.00
$R_{14}SP_5$	30	3.79	1.99	0.68	192.00
$R_{14}SP_6$	30	4.03	2.25	0.77	210.00
$R_{14}SP_7$	30	4.02	2.26	0.77	210.00
$R_{14}SP_8$	30	6.08	4.98	1.70	240.00
$R_{14}SP_9$	30	21.04	13.04	4.45	255.00
$R_{15}SP_1$	45	1.64	0.00	0.00	97.00
$R_{15}SP_2$	45	10.44	8.00	2.69	528.00
$R_{15}SP_3$	45	Not recorded	1.00	0.34	576.00
$R_{15}SP_4$	45	1.70	0.90	0.31	576.00
$R_{15}SP_5$	45	2.96	1.16	0.40	576.00
$R_{15}SP_6$	45	2.61	1.21	0.41	576.00
$R_{15}SP_7$	45	16.48	13.87	4.73	816.00
$R_{15}SP_8$	45	15.38	12.83	4.38	816.00
$R_{15}SP_9$	45	14.62	12.20	4.17	816.00
$R_{16}SP_1$	15	43.80	26.40	8.95	288.57
$R_{16}SP_2$	15	24.21	20.00	6.90	216.00
$R_{16}SP_3$	15	12.93	10.00	3.41	94.00
$R_{17}SP_1$	30	37.46	29.00	9.90	289.03
$R_{17}SP_2$	30	23.34	14.00	4.86	216.00
$R_{17}SP_3$	30	5.29	5.00	1.72	242.00
$R_{18}SP_1$	45	3.38	1.00	0.34	289.03
$R_{18}SP_2$	45	Not recorded	1.00	0.34	576.00
$R_{18}SP_3$	45	14.13	9.00	3.08	816.00

In order to obtain different corrosion levels, different corrosion times were applied for concrete specimen that was varied from 4 days to 34 days. Figure 5.3 shows some selected concrete specimens with w/c ratios of 0.75 and 0.40 for different applied corrosion time at three different concrete cover depths.

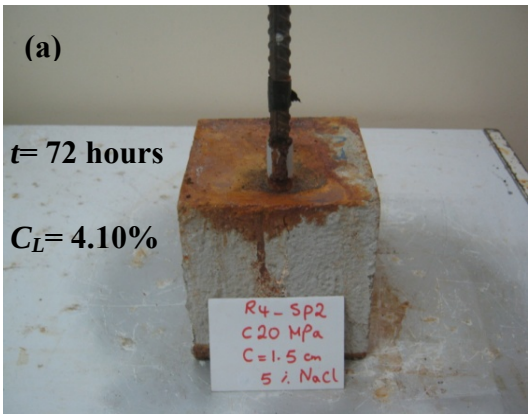

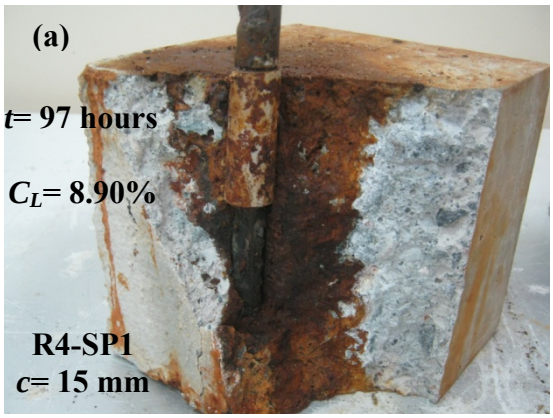

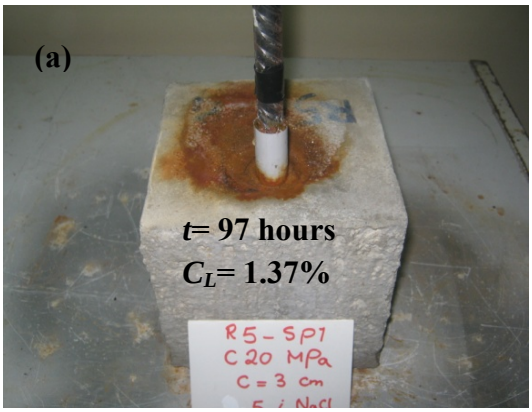

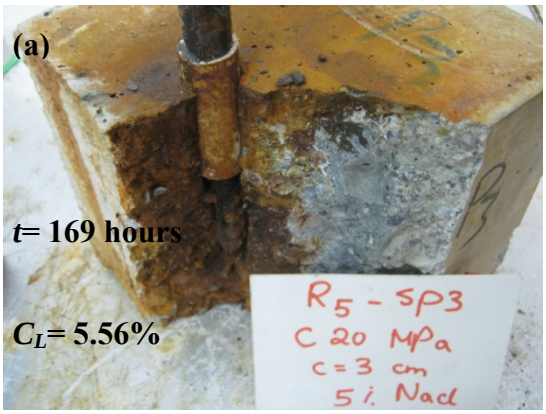

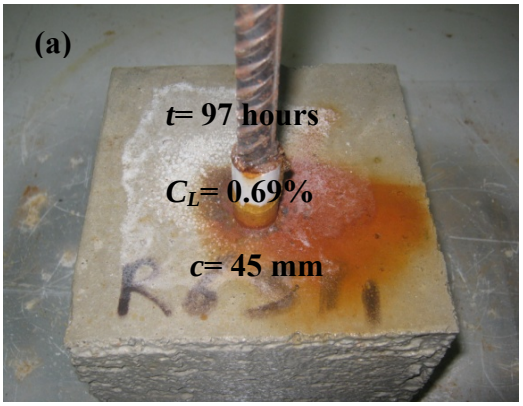

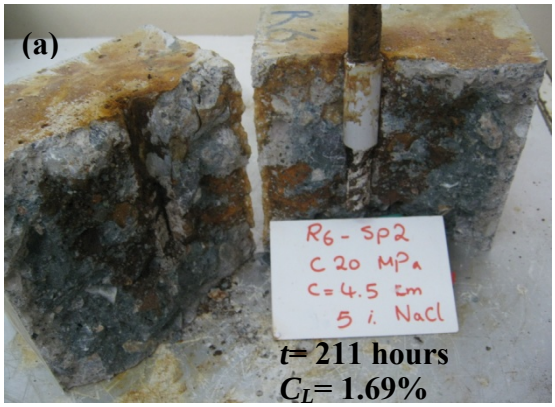

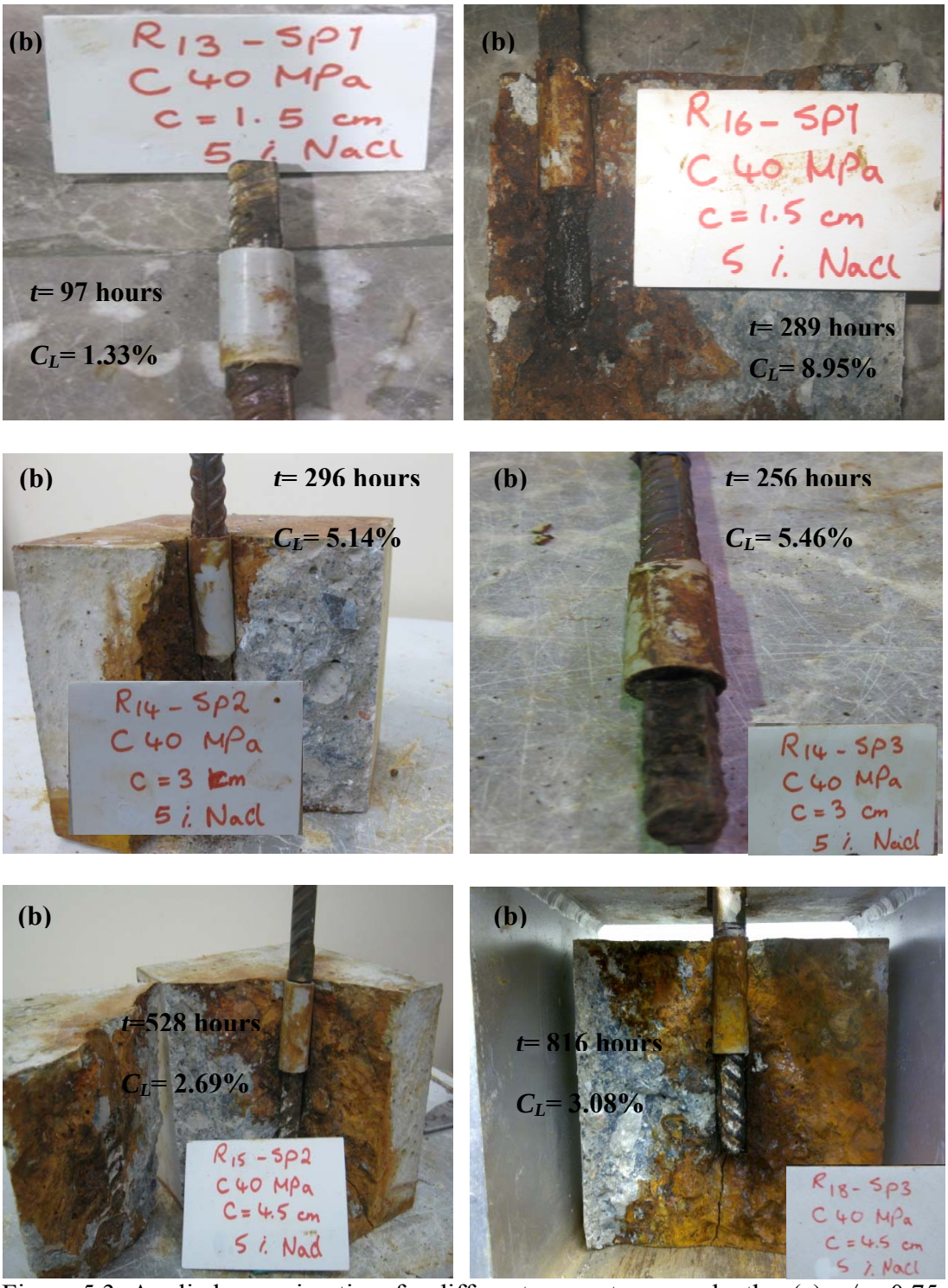

Figure 5.3: Applied corrosion time for different concrete cover depths: (a) *w/c*= 0.75, (b) *w/c*= 0.40.

As it was expected, at the same concrete cover depths and same concrete strength levels, corrosion levels increased with increased corrosion time. Figure 5.4 shows the

graphical results of different applied corrosion time for concrete specimens with a *w/c* ratio of 0.75.

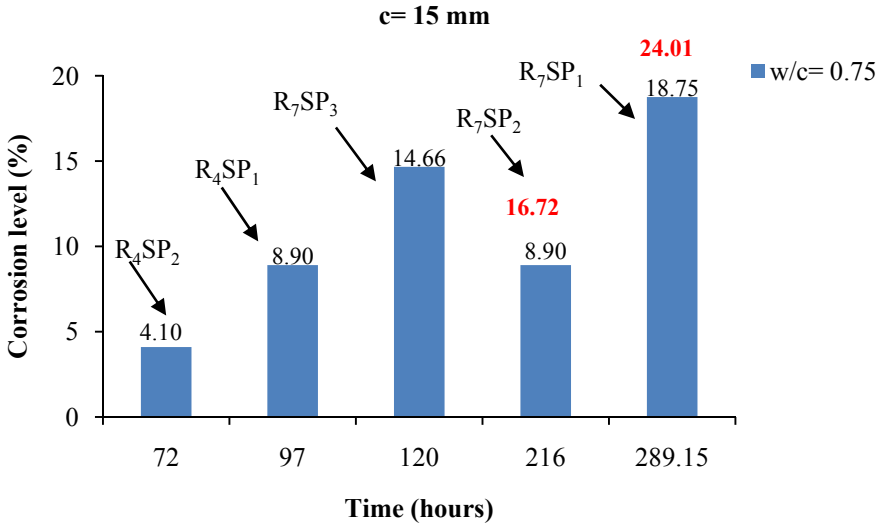

Figure 5.4: Applied corrosion time at the same concrete cover depth of 15 mm.

As it is shown in Figure 5.4, corrosion levels increased with increased applied corrosion time. In this study the highest amount of corrosion level was obtained for the concrete specimen named as R_7SP_1. Spalling of concrete was occurred for this concrete specimen at the end of the applied electro chemical method as shown in Figure 5.5.

Figure 5.5: Spalling of concrete with highest amount of corrosion level.

As shown in Figures 5.4 and 5.9, although specimens cured under the same environmental conditions, it is possible to obtain more or less corrosion levels at early stages of corrosion process due to occurred premature cracking of concrete or occurred local corrosion (see Figure 5.6).

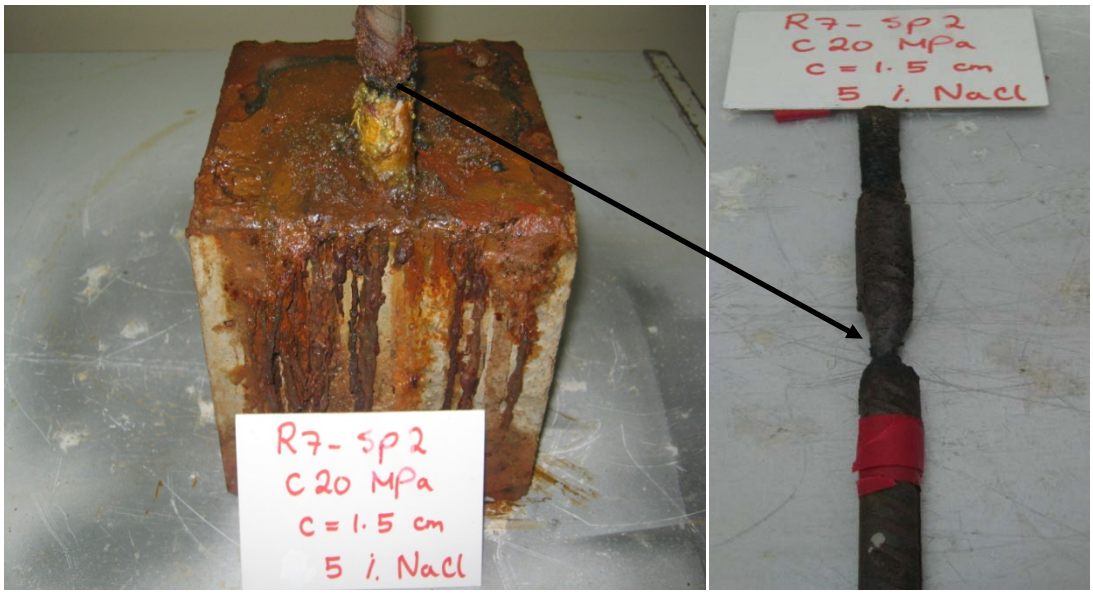

Figure 5.6: Local corrosion.

As shown in Figure 5.4, even the applied corrosion time of R_7SP_2 was more than that applied corrosion time of R_7SP_3, the calculated corrosion level of R_7SP_2 was less then R_7SP_3 due to occurred local corrosion at R_7SP_2. Archimedes's principle (see Figure 5.7) was used in the case of occurred local corrosion to determine the actual corrosion level in the embedded lengths of the reinforcement bars rather than direct weighting.

Figure 5.7: Application of Archimedes's principle due to occurred local corrosion.

Figure 5.4 shows that the corrosion levels for R_7SP_1, and R_7SP_2 were measured to be 24.01% and 16.72%, respectively, by direct weighting; using Archimedes's principle, the values were obtained to be 18.75%, and 8.90%, respectively. The recorded maximum crack width was 0.94 mm for the concrete specimens having the *w/c* ratio of 0.75 with the lowest *c/D* ratio (*c*= 15mm) as shown in Figure 5.8.

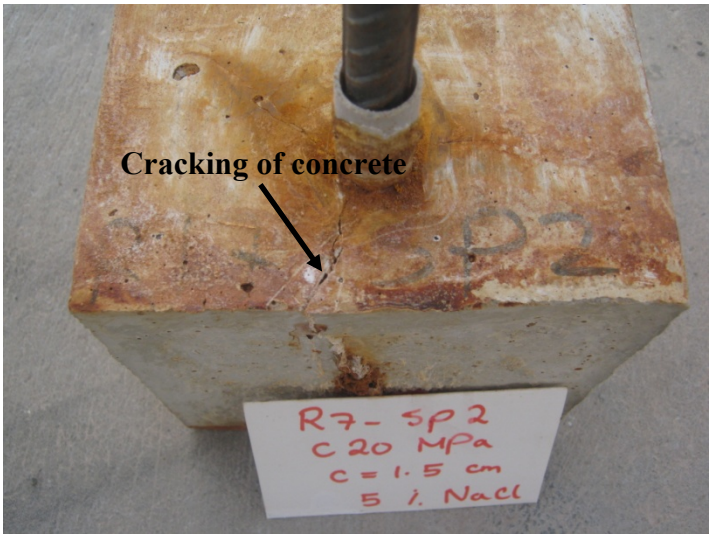

Figure 5.8: Recorded maximum crack width with a *w/c* ratio of 0.75 for the lowest *c/D* ratio.

Figure 5.9 shows the applied corrosion time for the same concrete cover depth of 30 mm having a *w/c* ratio of 0.75.

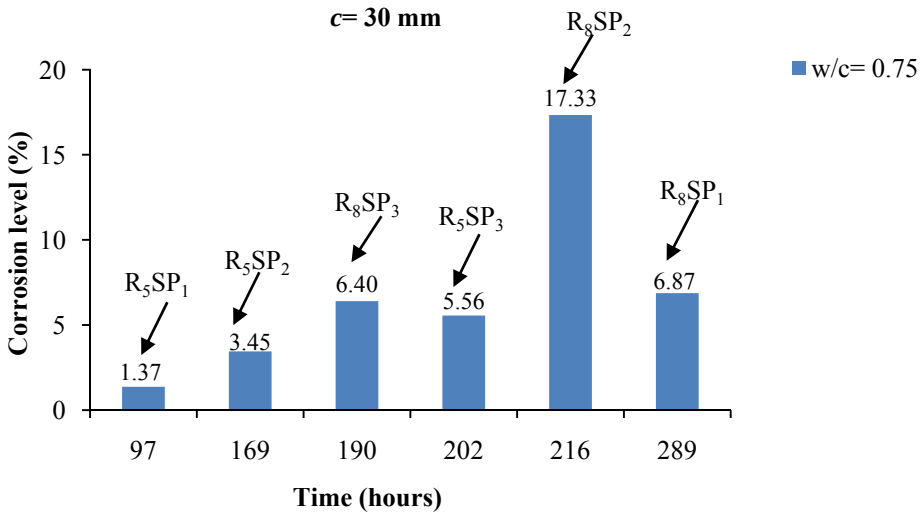

Figure 5.9: Applied corrosion time for the same concrete cover depth of 30 mm.

As shown in Figure 5.9, at the same concrete cover depth of 30 mm, as it was expected, the actual corrosion levels increased with increased corrosion time. In Figure 5.9, during accelerated corrosion method, cracking of concrete occurred for two concrete specimens named as R_5SP_2, and R_8SP_3. Figure 5.10 shows the recorded crack width for these two concrete specimens.

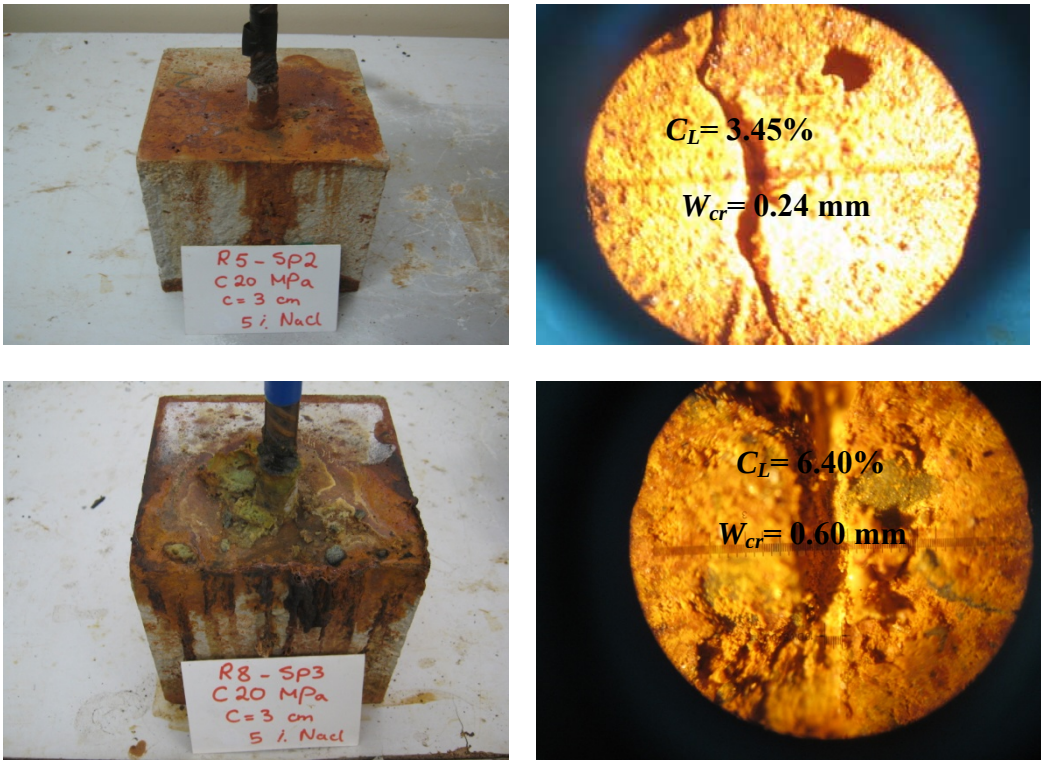

Figure 5. 10: Recorded crack width of concrete specimens with the concrete cover of 30 mm.

In this thesis, the recorded crack widths were important for developing the bond strength models. Therefore, during accelerated corrosion method, occurred crack on concrete specimens were carefully recorded. The given results in Figure 5.4 and 5.9 represent the general results of other concrete classes for different concrete cover depths where corrosion level increased with increased corrosion time. The next subsection compares obtained corrosion levels for two different concrete strength levels by considering the effects of concrete cover depths.

5.2.2 Effects of Concrete Cover Depths and Strength Levels on Corrosion Levels

In this study two different concrete strength levels (i.e., f_c'= 23 MPa and f_c '= 51 MPa) and three concrete cover depths (i.e., c = 15 mm, 30 mm and 45 mm) provided comparison of the results of corrosion levels under the impact of cover depths and strength levels. Figure 5.11 (a-b) shows the effect of concrete cover depths on obtained corrosion levels for the concrete samples with the same w/c ratios under the applied same corrosion time. As shown here, the effect of concrete cover depths on the corrosion levels were significant; increasing concrete cover depth decreased the corrosion level.

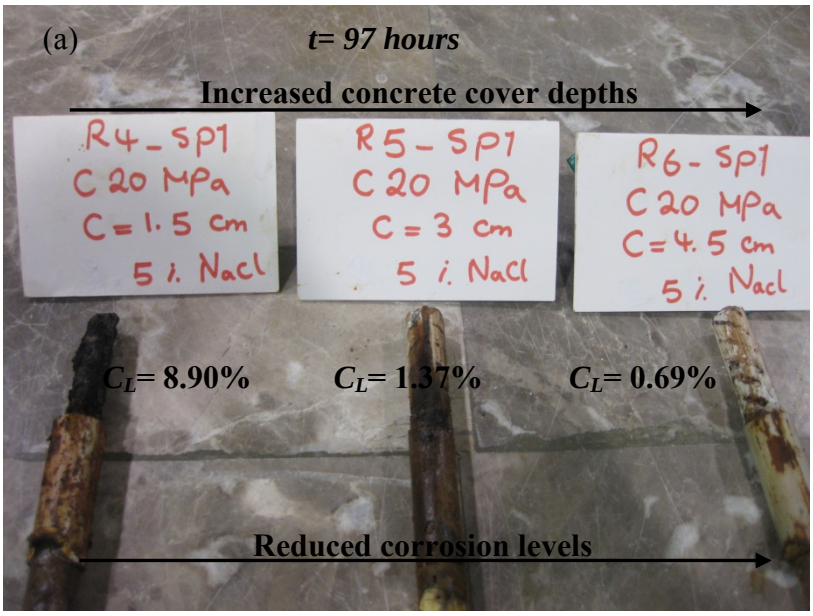
(a)
t= 97 hours
Increased concrete cover depths
R4-SP1
C 20 MPa
C=1.5 cm
5 i. NaCl
R5-SP1
C 20 MPa
C=3 cm
5 i. NaCl
R6-SP1
C 20 MPa
C=4.5 cm
5 i. Nacl
CL= 8.90%
CL= 1.37%
CL= 0.69%
Reduced corrosion levels

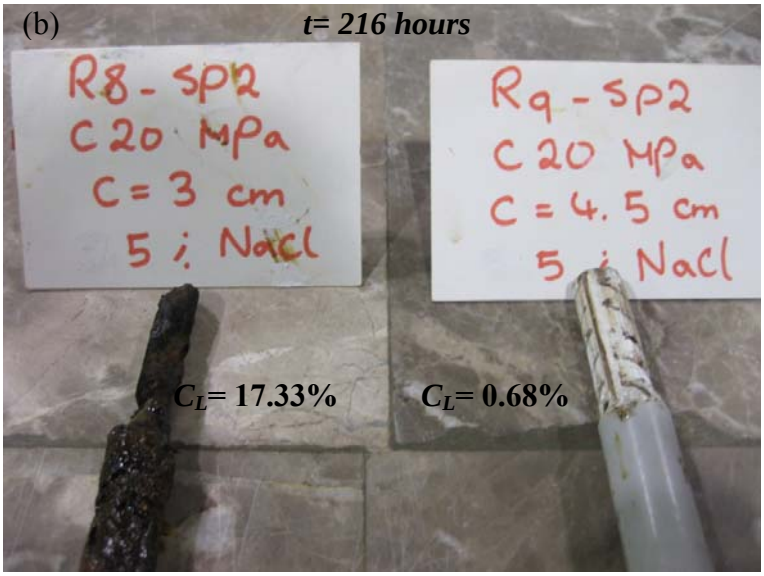
(b)
t= 216 hours
R8-SP2
C 20 MPa
C=3 cm
5 i. NaCl
R9-SP2
C 20 MPa
C=4.5 cm
5 i. NaCl
CL= 17.33%
CL= 0.68%

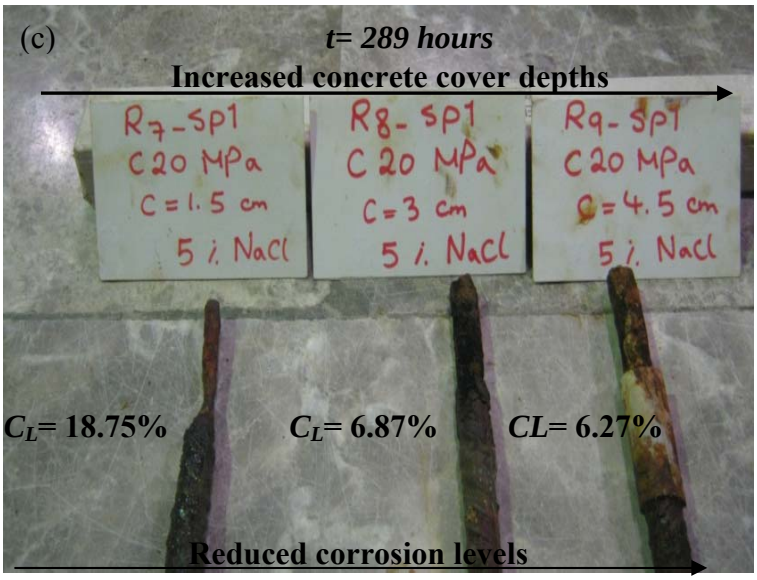
(c)
t= 289 hours
Increased concrete cover depths
R7-SP1
C20 MPa
C=1.5 cm
5 i. NaCl
R8-SP1
C20 MPa
C=3 cm
5 i. NaCl
R9-SP1
C20 MPa
C=4.5 cm
5 i. NaCl
CL= 18.75%
CL= 6.87%
CL= 6.27%
Reduced corrosion levels

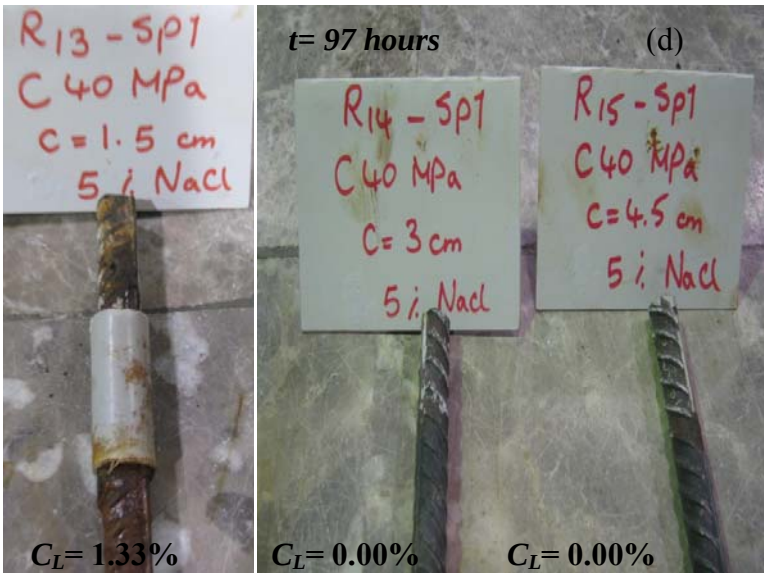
R13-SP1
C40 MPa
C=1.5 cm
5 i. NaCl
t= 97 hours
(d)
R14-SP1
C40 MPa
C=3 cm
5 i. NaCl
R15-SP1
C40 MPa
C=4.5 cm
5 i. NaCl
CL= 1.33%
CL= 0.00%
CL= 0.00%

Figure 5.11: Effect of concrete cover depths on corrosion levels: (a) *w/c*=0.75 (*t*= 97 h), (b) *w/c*=0.75 (*t*= 216 h), (c) *w/c*=0.75 (*t*= 289 h), (d) *w/c*= 0.40 (*t*= 97 h), (e) *w/c*= 0.40 (*t*= 216 h), (f) *w/c*= 0.40 (*t*= 289 h).

In Figure 5.11, the results indicated that for the same applied corrosion time, the corrosion levels decreased with increasing concrete cover depths. For instance in Figure 5.11(a) (*t*= 97 h), the corrosion level of R_4SP_1 (C_L= 8.90%) reduced to 1.37% and 0.69% by increasing cover depth from 15 mm to 30 mm and 45 mm, respectively. For another applied corrosion time of 216 h (see Figure 5.11(b)), the corrosion level of R_8SP_2 (C_L= 17.33%) reduced to 0.68% by increasing cover depth

from 30 mm to 45 mm at the same concrete strength level. Same results can be also observed for the highest concrete strength level. In Figure 5.11(f) with increased concrete cover depth from 15 mm to 30 and 45 mm, the calculated corrosion levels reduced from 11.53% to 9.90% and 0.34%. It should be noted that, as it is shown in Figure 5.11(f), the actual corrosion level of $R_{16}SP_1$ was 8.95% by applied Archimedes's principle due to occurred local corrosion.

The concrete cover depths were not a single parameter, but also concrete compressive strengths had a significant effect on obtained corrosion levels. The reduced permeability of the concrete with 0.40 *w/c* ratio likely reduced corrosion of the reinforcement bars. Because increasing the *w/c* ratio increases capillary porosity (Cabrera, 1993). The differences in the corrosion levels obtained at a fixed corrosion time showed that more energy was needed to initiate corrosion in the concrete mixture with a *w/c* ratio of 0.40 than that with *w/c* ratio of 0.75. The comparisons between two concrete strength levels at the same concrete covers are shown in Figure 5.12 for higher applied corrosion time of reduced *w/c* ratio of 0.40.

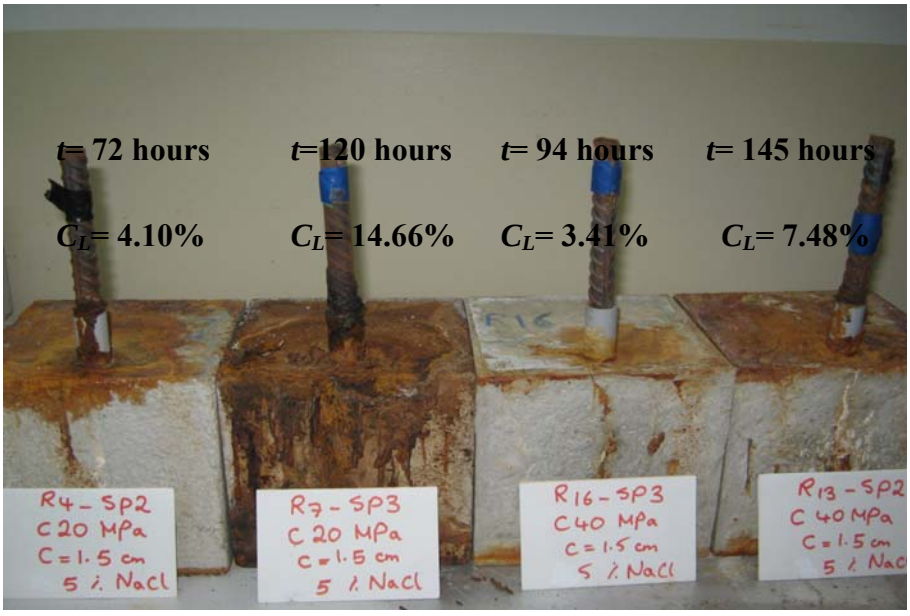

Figure 5.12: Effect of concrete compressive strength on corrosion levels for higher applied corrosion time of reduced *w/c* ratio of 0.40.

As shown in Figure 5.12, the concrete compressive strength has a significant effect on calculated corrosion levels. In Figure 5.12, even the applied corrosion time of $R_{16}SP_3$ was more than that of R_4SP_2, obtained corrosion level was less for $R_{16}SP_3$ due to reduced *w/c* ratio. In Figure 5.12 same results can be observed between R_7SP_3 and $R_{13}SP_2$. With a more applied corrosion time of 145 hours, the calculated corrosion level of $R_{13}SP_2$ was less (C_L= 7.48%) which corrosion level was more for R_7SP_3 (C_L= 14.66%) with a less applied corrosion time of 120 hours due to increased *w/c* ratio. Previous comparisons were done for the higher applied corrosion time of high strength level of concrete (*w/c*= 0.40). If the corrosion levels of two concrete strength levels were compared for the fixed applied corrosion time at the same concrete cover depths, the effect of *w/c* ratios or concrete strength levels on corrosion levels were more significant and results were more dramatic for the concrete specimens with *w/c* ratios of 0.75. Figure 5.13 shows the effect of concrete compressive strength on corrosion levels for different fixed corrosion times:

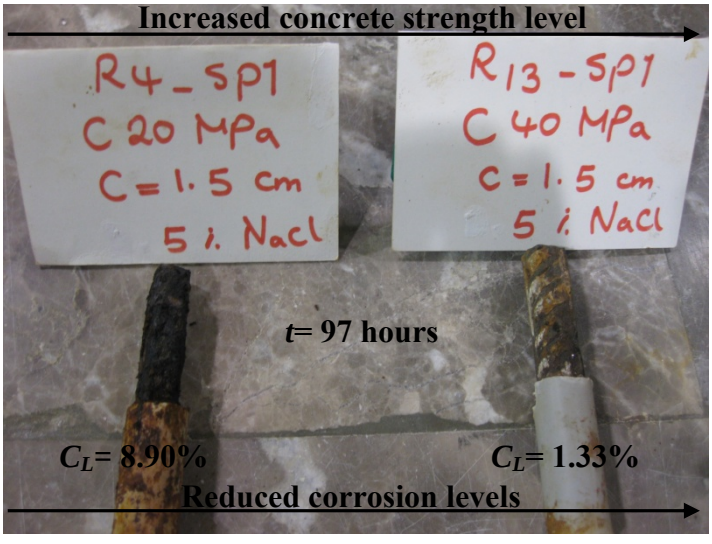

(a)

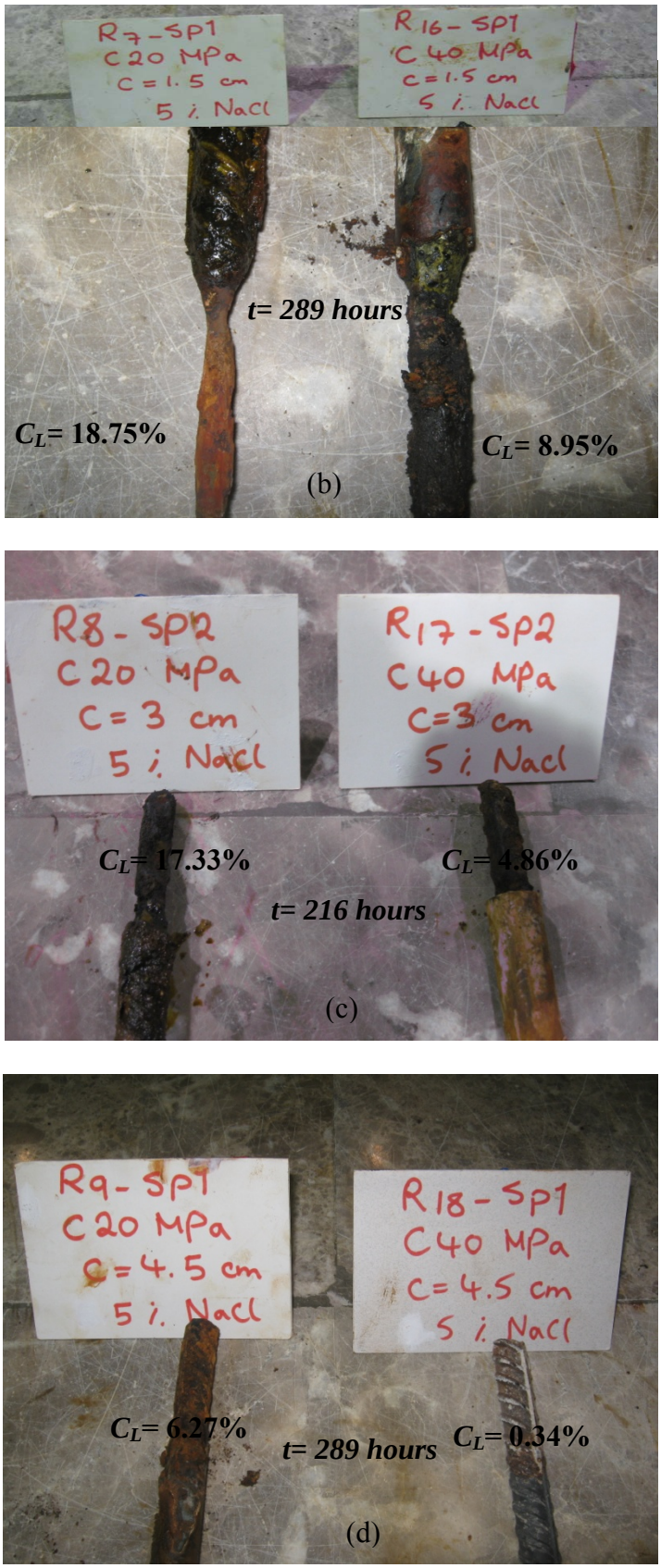

Figure 5.13: Effect of concrete compressive strength on corrosion level for a fix corrosion time: (a) concrete cover depth of 15 mm, t= 97 h; (b) concrete cover depth of 15 mm, t= 289 h; (c) concrete cover depth of 30 mm, t= 216 h (d) concrete cover depth of 45 mm, t= 289 h.

As shown in Figure 5.13, at the same concrete cover depths and for the same fixed corrosion time, the corrosion level reduced with reduced *w/c* ratio. For instance in Figure 5.13(a), the calculated corrosion level of R_4SP_1 reduced from 8.90% to 1.33% by reducing *w/c* ratio form 0.75 to 0.40. In Figure 5.13, the results clearly show that reduced *w/c* ratio from 0.75 to 0.40 reduced the calculated corrosion levels at least 50% where 94% reduction in corrosion level occurred for the concrete cover depth of 45 mm (see Figure 5.13(d)). Figure 5.14 (a-c) illustrates the effects of both concrete cover depths and *w/c* ratios on the corrosion levels for different applied corrosion times for selected specimens. In Figure 5.14(a-c), the red coloured values indicate the total corrosion level (not actual corrosion level in the embedment length) before applied Archimedes's principle due to occurred local corrosion.

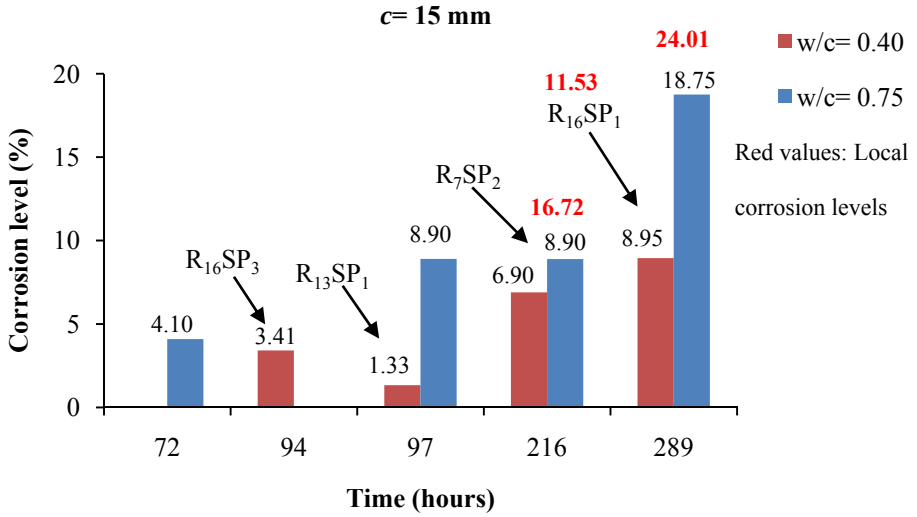

(a)

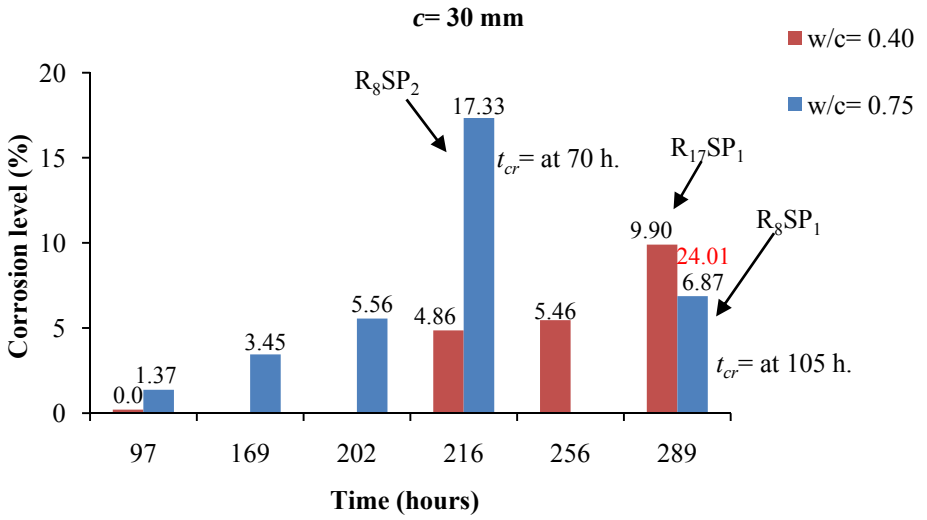

(b)

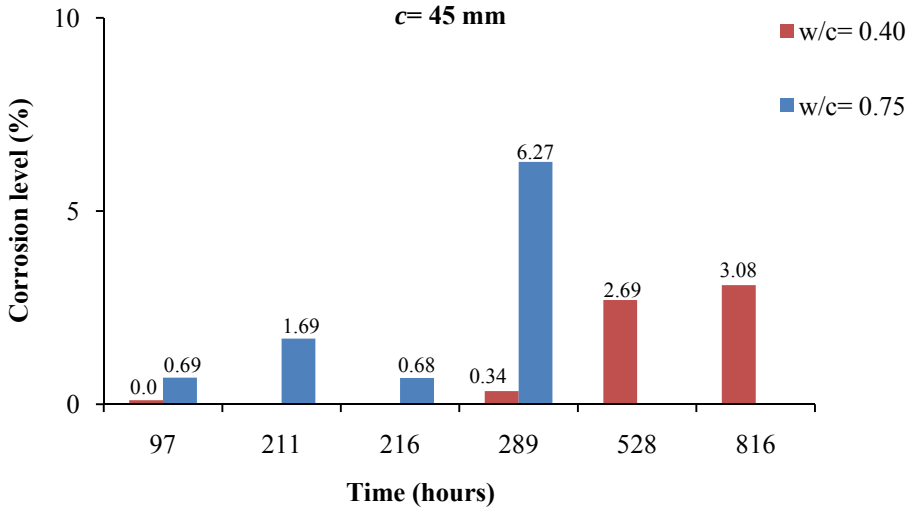

(c)

Figure 5.14: Effect of concrete cover depth and *w/c* ratio on corrosion level: (a) *c* = 15 mm; (b) *c* = 30 mm; (c) *c* = 45 mm.

As shown in Figure 5.14(a-c), at the same concrete cover depth with same corrosion time, the effect strength level on corrosion level was significant where reduced *w/c* ratio significantly reduced corrosion levels. As it was mentioned earlier, premature cracking and occurred local corrosion might be a reason to have more and less corrosion levels at earlier stages of applied corrosion time. As shown in Figure 5.14 (a-b), due to the premature cracking of $R_{16}SP_3$ and R_8SP_2 compared with $R_{13}SP_1$

and R_8SP_1, respectively, more corrosion was observed at an earlier stage due to the increased permeability of the concrete in the former. In Figure 5.14(a), premature cracking of $R_{16}SP_3$ caused to have more corrosion level rather than $R_{13}SP_1$ at an earlier applied corrosion time of 94 h. This was due to occurred cracking of $R_{16}SP_3$. Figure 5.15 shows the cracking of concrete specimen $R_{16}SP_3$. The maximum recorded crack width on the surfaces of $R_{16}SP_3$ was 0.60 mm where no cracks were recorded for $R_{13}SP_1$. The calculated resistivity values can be also used to describe this issue better. Therefore, the recorded concrete resistivity values were also used to estimate the time required for the growth of fine cracks (t_{cr}). In Figure 5.14(b), the resistivity of R_8SP_2 began to decrease at 70 hours, whereas it decreased at 105 hours for R_8SP_1. In Figure 5.14(b), with a corrosion time of 289 h, the actual calculated corrosion level of high strength concrete level looked like that it was more than the calculated corrosion level of R_8SP_1 (low strength level of concrete). The total corrosion level of R_8SP_1 was 24.01% which corrosion level was than modified to 6.87% due to occurred local corrosion. That's why the calculated actual corrosion level with a high *w/c* ratio was lower than low *w/c* ratio. It should be noted that concrete resistivity and premature cracking had no influence on the bond strength. Therefore, the corrosion levels determined from the actual mass losses in the reinforcement bars and the recorded concrete crack widths were used to develop the proposed strength model. If the obtained corrosion levels compared for 45 mm concrete cover depths, the results were more dramatic for the low strength level of concrete. As shown in Figure 5.14(c), 816 h were needed in order to obtain 3.08% corrosion level for high strength concrete level where 6.27% of corrosion level was obtained within 289 h for low strength level of concrete. At the same applied corrosion time of 289 h, the calculated corrosion level of high strength concrete was

only 0.34%. Under the same applied corrosion time (t = 97 hours), corrosion level for the sample with a w/c ratio of 0.40 was 0.00% where it was 0.69% for the sample with a w/c ratio of 0.75. Based on the given results in Figure 5.14(a-c), it can be concluded that that reducing the w/c ratio of the concrete was more effective than increasing the concrete cover depth for improving the resistance of the concrete against thus corrosion levels.

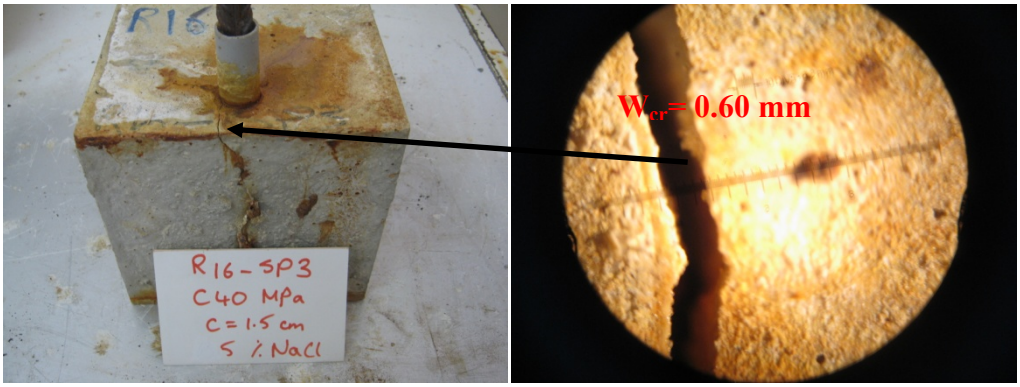

Figure 5.15: Premature cracking of concrete.

5.2.3 Comparison of Theoretical and Actual Corrosion Mass Losses: Developed Model to Correlate the Actual and Theoretically (Faraday's law) Estimated Mass Losses

As described in section 4.4.1, it is possible to obtain differences between the designed corrosion levels based on Faraday's law and actual corrosion levels. Comparing the results given in Tables 5.1 and 5.2, there were differences between the calculated and theoretically estimated corrosion mass losses based on Faraday's law. Such differences have been reported previously in the literature (e.g., Amleh and Ghosh 2006; Chung et al. 2004). However, in this study, different concrete classes and concrete cover depths were evaluated; thus, upper and lower bounds for the correlation between the actual and theoretically estimated mass losses were obtained. By considering the typical environmental conditions used in our

experiments, equation 5.1 and Figure 5.16 can be used to correlate the actual and theoretically estimated mass losses in future studies.

Actual mass loss = 0.703 × theoretical mass loss – 0.15 (gr) (5.1)

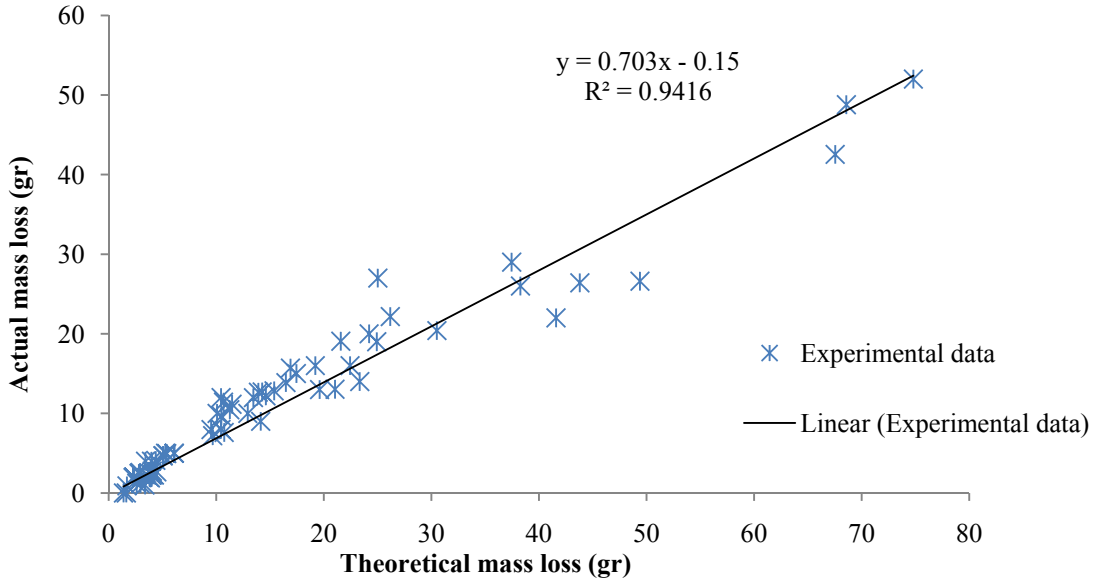

Figure 5.16: Correlation between actual and theoretically estimated mass loss.

5.2.4 Results of Resistivity of Concrete

If the steel is actively corroding, resistivity measurements may give additional information: it may show the location of strongest steel corrosion in the structure. In general, within one structure, relative corrosion rates can be predicted. Resistivity measurements can be used at any time during the service life of a concrete structure and under any circumstances, provided the temperature is higher than 0^0 (Guliker et al. 2000). Hence, the electrical resistance of the concrete plays an important role in determining the magnitude of corrosion at any specific location (Berkely and Pathmanaban 1990). This factor is measured in terms of electrolytic resistivity of concrete and is usually expressed in ohm-meters. Although the concrete resistivity was not the main interest of this study, it was used to monitor the corrosion level. Under the same environmental conditions, the relationships between concrete

resistivity and corrosion time for both the low and high strength concrete levels were determined, as shown in Figure 5.17.

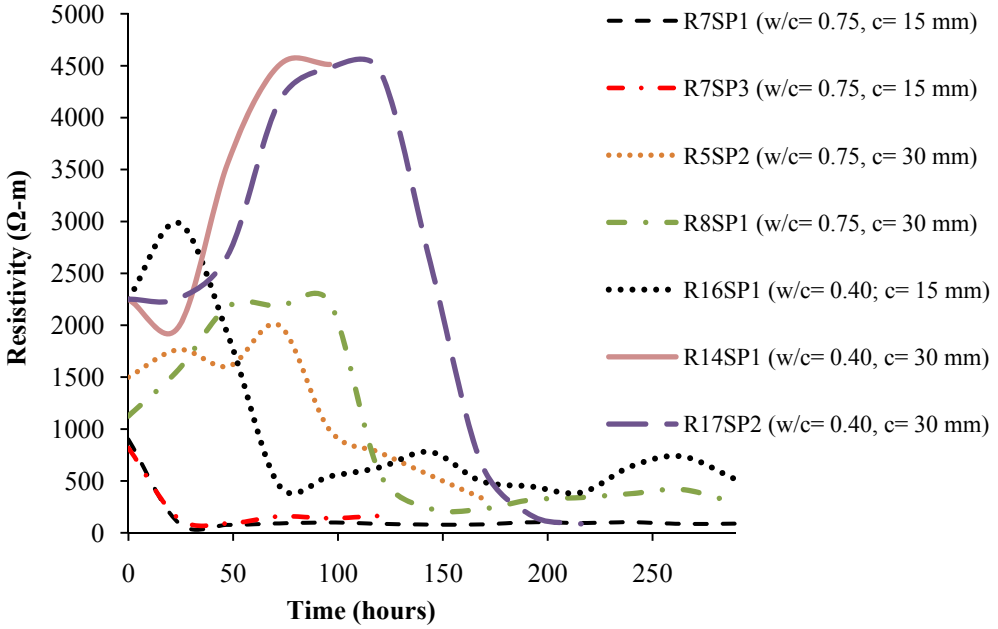

Figure 5.17: Relationship between resistivity of concrete and time with concrete cover depths of 15 and 30 mm.

The resistivity results obtained by calculating the average current over 24 h from the current recorded at one minute intervals are presented in Figure 5.17. The results clearly show that reducing the w/c ratio of the concrete was more effective than increasing the concrete cover depth for improving the resistance of the concrete against chloride attack. Figure 5.17 shows the resistivity of specimens R_5SP_2 and R8SP1 (*w/c* = 0.75 and *c* = 30 mm); although they had 30 mm concrete covers, the resistance of these concrete against chloride attack was less than that of the concrete specimens with the lower *w/c* ratio having a 15 mm concrete cover depth (e.g., $R_{16}SP_1$). Thus, a 50% reduction in concrete cover depth with the higher concrete strength level provided 34% more resistance than the lower concrete strength level. It was observed that the resistivity increased quickly during the initial period of the corrosion process; this continued for a long time, and then the resistivity dropped down quickly beginning with the initiation of visible surface cracks. Increasing in

resistivity of concrete due to corrosion can be explained by isolated surface due to corrosion around the reinforcement bars. The contact resistivity is a quantity that increases monotonically with an increasing amount of interfacial phase (rust), because the interfacial phase has a higher volume electrical resistivity than steel and even likely a higher resistivity than concrete as well (Fang et al. 2004). In Figure 5.17, the concrete specimens R_7SP_1 and R_7SP_3, the resistivity started to drop drown at the beginning of corrosion process, likely due to the closer contact surface of the reinforcement bars. The comparison of the results of resistivity between low and high strength concrete levels with 45 mm concrete cover depths are shown in Figure 5.18.

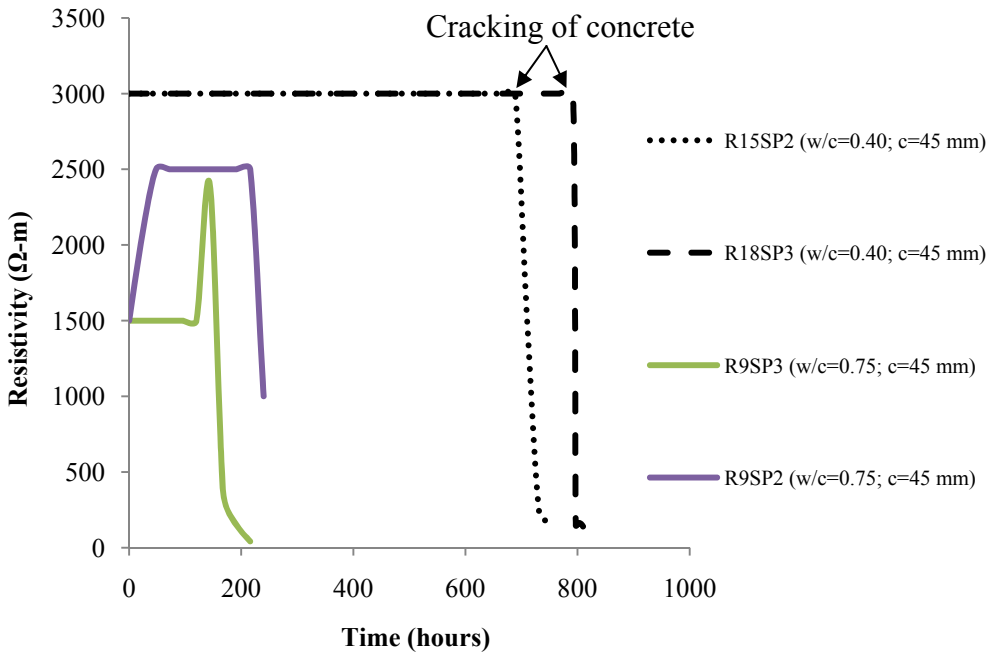

Figure 5.18: Relationship between resistivity of concrete and time with cover depth of 45 mm.

As shown in Figure 5.18, with increased concrete depth of 45 mm, the initial resistance values of high strength concrete were two times higher than that of low strength concrete levels. As it was mentioned earlier, electrical resistivity increases at the interfacial phase of corrosion. As shown in Figure 5.18, for a certain period of

time, resistance of low strength level of concrete increased while the current of high strength concrete was constant from the beginning until the time of cracking of concrete. Since the corrosion rates of low strength concrete levels were more at the interfacial period of corrosion, occurred corrosion rust caused increased the resistivity results for low strength level of concrete. Although resistance of low strength level of concrete increased at interfacial phase, the resistivity values could not be able to reach to the value of high strength concrete levels. As shown in Figure 5.18, between two strength levels of concrete, there were almost 600 h differences that created cracks on concrete. Although the concrete specimens were cured under the same conditions, due to the complex concrete matrix, including many unknown variables, non-uniform corrosion behaviour was observed during the accelerated corrosion procedure. In this study, only two concrete specimens displayed this nonuniform behaviour, as shown in Figure 5.19.

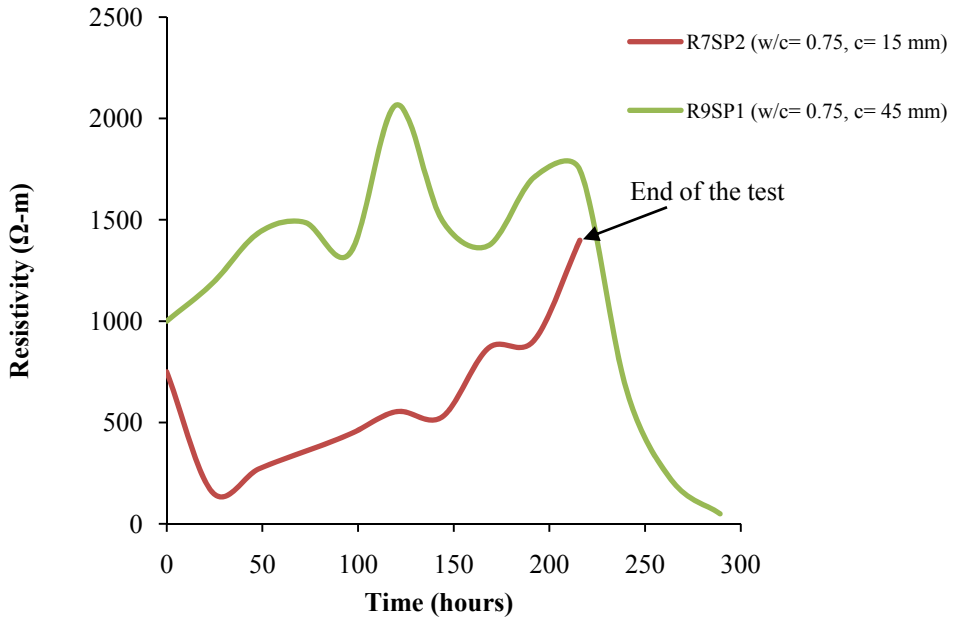

Figure 5.19: Non-uniform corrosion behaviour.

5.4 Results of Pullout Tests

The pullout tests were carried out for both corroded and non-corroded specimens according to the procedure described in section 4.4.2. Recorded maximum pullout forces thus calculated ultimate bond strength (τ_{bu}) values of concrete mixture with *w/c* ratios 0.75 and 0.40 for three different concrete cover depths are given in Tables 5.3 and 5.4, respectively.

Table 5.3: Calculated ultimate bond strength (τ_{bu}) values of concrete mixtures with *w/c* ratios 0.75.

Specimen	*c* (mm)	Corrosion level C_L (%)	Maximum bond strength τ_{bu} (MPa)
R_1SP_1	15	-	9.1
R_1SP_2	15	-	9.4
R_1SP_3	15	-	9.2
R_2SP_1	30	-	14.0
R_2SP_2	30	-	12.3
R_2SP_3	30	-	13.5
R_3SP_1	45	-	12.1
R_3SP_2	45	-	17.3
R_3SP_3	45	-	15.0
R_4SP_1	15	8.90	3.7
R_4SP_2	15	4.10	13.0
R_4SP_3	15	2.47	11.2
R_4SP_4	15	2.72	11.7
R_4SP_5	15	4.32	12.2
R_4SP_6	15	4.33	12.2
R_4SP_7	15	4.09	13.0
R_4SP_8	15	6.51	3.2
R_4SP_9	15	14.52	2.1
R_5SP_1	30	1.37	18.0
R_5SP_2	30	3.45	9.6
R_5SP_3	30	5.56	3.3
R_5SP_4	30	1.40	17.9
R_5SP_5	30	1.69	16.9
R_5SP_6	30	1.60	17.0
R_5SP_7	30	3.57	8.9
R_5SP_8	30	5.36	3.7
R_5SP_9	30	16.65	2.1
R_6SP_1	45	0.69	19.1
R_6SP_2	45	1.69	13.4
R_6SP_3	45	2.66	12.4
R_6SP_4	45	0.68	17.9
R_6SP_5	45	0.66	18.9
R_6SP_6	45	0.84	18.3
R_6SP_7	45	0.88	18.2
R_6SP_8	45	1.60	13.7
R_6SP_9	45	3.81	1.3
R_7SP_1	15	18.75	4.3
R_7SP_2	15	8.90	3.0
R_7SP_3	15	14.66	2.0
R_8SP_1	30	6.87	6.5
R_8SP_2	30	17.33	1.8
R_8SP_3	30	6.40	5.5
R_9SP_1	45	6.27	3.2
R_9SP_2	45	0.68	18.0
R_9SP_3	45	3.81	1.3

Table 5.4: Calculated ultimate bond strength (τ_{bu}) values of concrete mixtures with *w/c* ratios 0.40.

Specimen	*c* (mm)	Corrosion level C_L (%)	Maximum bond strength τ_{bu} (MPa)
$R_{10}SP_1$	15	-	19.6
$R_{10}SP_2$	15	-	14.3
$R_{10}SP_3$	15	-	20.0
$R_{11}SP_1$	30	-	20.9
$R_{11}SP_2$	30	-	21.7
$R_{11}SP_3$	30	-	21.0
$R_{12}SP_1$	45	-	21.2
$R_{12}SP_2$	45	-	27.4
$R_{12}SP_3$	45	-	27.8
$R_{13}SP_1$	15	1.33	18.5
$R_{13}SP_2$	15	7.48	3.5
$R_{13}SP_3$	15	4.47	6.3
$R_{13}SP_4$	15	0.77	22.3
$R_{13}SP_5$	15	0.80	22.4
$R_{13}SP_6$	15	0.90	21.7
$R_{13}SP_7$	15	0.94	21.5
$R_{13}SP_8$	15	7.56	3.5
$R_{13}SP_9$	15	3.30	7.5
$R_{14}SP_1$	30	0.00	20.4
$R_{14}SP_2$	30	5.14	6.2
$R_{14}SP_3$	30	5.46	2.4
$R_{14}SP_4$	30	0.65	23.8
$R_{14}SP_5$	30	0.68	23.9
$R_{14}SP_6$	30	0.77	23.5
$R_{14}SP_7$	30	0.77	23.4
$R_{14}SP_8$	30	1.70	14.0
$R_{14}SP_9$	30	4.45	4.2
$R_{15}SP_1$	45	0.00	28.3
$R_{15}SP_2$	45	2.69	7.6
$R_{15}SP_3$	45	0.34	26.2
$R_{15}SP_4$	45	0.31	31.6
$R_{15}SP_5$	45	0.40	31.0
$R_{15}SP_6$	45	0.41	30.8
$R_{15}SP_7$	45	4.73	3.0
$R_{15}SP_8$	45	4.38	3.4
$R_{15}SP_9$	45	4.17	3.9
$R_{16}SP_1$	15	8.95	3.0
$R_{16}SP_2$	15	6.90	8.0
$R_{16}SP_3$	15	3.41	6.8
$R_{17}SP_1$	30	9.90	5.9
$R_{17}SP_2$	30	4.86	1.7
$R_{17}SP_3$	30	1.72	13.8
$R_{18}SP_1$	45	0.34	26.9
$R_{18}SP_2$	45	0.34	31.7
$R_{18}SP_3$	45	3.08	6.1

5.4.1 Newly Developed Bond Strength Models for Uncorroded Specimens

The ultimate bond strengths of corroded and uncorroded specimens were calculated by using the initial cross-sectional dimensions of the reinforcement bars. Figure 5.20 shows the relationship between concrete compressive strength and the maximum bond strength for different concrete covers in the case of uncorroded specimens.

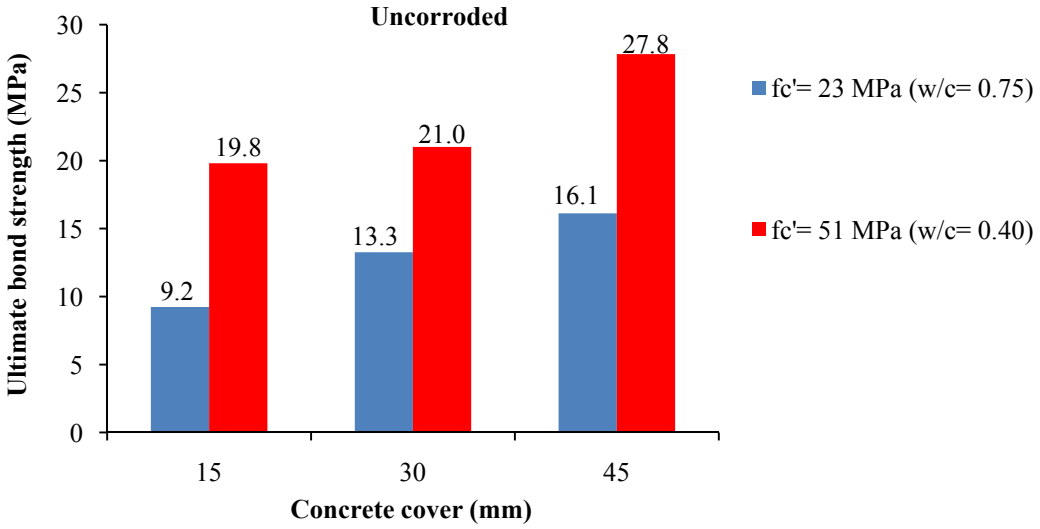

Figure 5.20: Ultimate bond strengths of uncorroded specimens.

The values given in Figure 5.20 are the average bond strengths of 18 concrete specimens for each concrete strength level. As shown here, the bond strength depends on both concrete compressive strength and the concrete cover depths. The results showed that up to a cover-to-bar-diameter (c/D) ratio of 3.2, the bond strength increased with increasing concrete tensile strength, and no significant increase was recorded for the c/D ratios above 3.2. As shown in Figure 5.20, the effect of concrete cover depth on bond strength was more significant for the concrete specimens having lower tensile strength. For example, when the concrete cover depth was increased from 15 mm to 30 mm, the bond strength of the concrete with a w/c ratio of 0.75 was increased by 43.7%, whereas it increased 6% for the concrete specimens having a

w/*c* ratio of 0.40. With further increases in concrete cover depth, differences in bond strength increases between the two concrete strengths were moderate. For example, when the concrete cover depth was increased from 15 mm to 45 mm, the bond strengths of concrete specimens with *w*/*c* ratios of 0.40 and 0.75 increased by 41% and 52%, respectively. As expected, for concrete covers of the same depth, bond strength increased as the *w*/*c* ratio was reduced. On reducing the *w*/*c* ratio from 0.75 to 0.40, bond strengths increased by 58% and 73% with concrete covers 30 mm and 45 mm thick, respectively. In the case of the uncorroded specimens, increasing the concrete compressive strength with a given concrete cover depth yielded a higher bond strength than increasing the concrete cover depth for a given concrete strength. The following equation was developed to predict the ultimate bond strength of uncorroded specimens using linear regression analysis, where the coefficient of correlation (R^2) was 0.96.

$$\tau_{bu} = -2.7143 + 0.3621 f_c' + 2.3296\left(\frac{c}{D}\right) \text{ (MPa)} \qquad (5.2)$$

In contrast to previous models, the model developed in equation 5.2 provides a way to predict the ultimate bond strength not only as a function of concrete strength but also as a function of the *c*/*D* ratio.

5.4.2 Newly Developed Bond Strength Models for Corroded Specimens

Figures 5.21 (a-b) show the bond strengths of corroded reinforcement bars with ratios of *w*/*c* = 0.75 and *w*/*c* = 0.40, respectively.

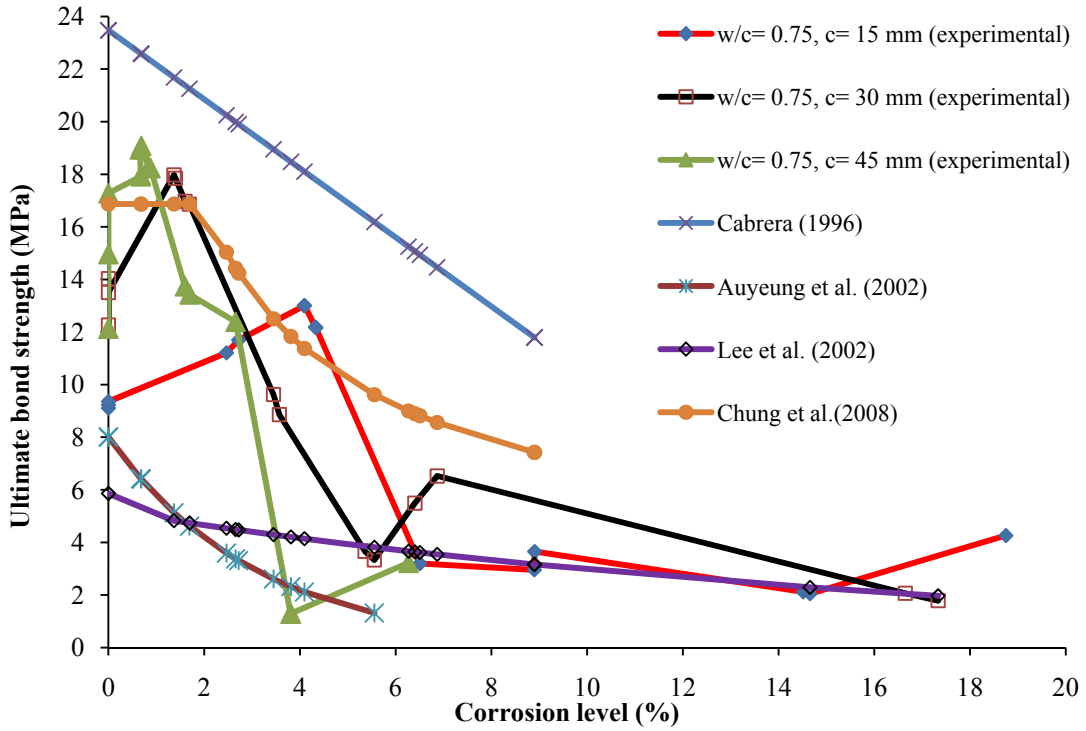

(a)

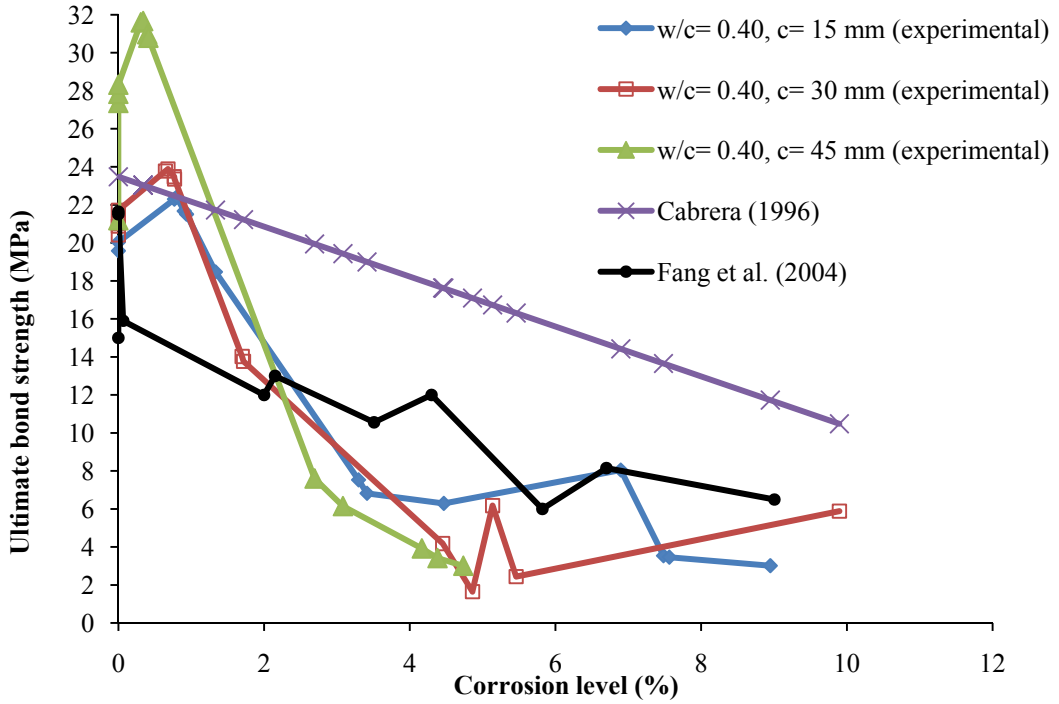

(b)

Figure 5.21: Bond strength of corroded specimens: (a) *w/c*= 0.75, (b) *w/c*= 0.40.

In the studies by Auyeung et al. (2000) and Chung et al. (2008), the bond strength relationships for corroded reinforcement bars were defined by two segments with a limiting corrosion level. However, there is disagreement on this corrosion level limit.

Auyeung et al. (2000) reported that bond strength decreases rapidly when the corrosion mass loss exceeds 1%, whereas it was reported by Chung et al. (2008) that increasing in bond strength was negligible up to a corrosion level of 2%. The previous studies performed by Auyeung et al. (2000) and Chung et al. (2008) were considered one type of concrete strength level and concrete cover depth. Therefore, previous studies were not adequate to define the bond strength of corroded reinforcement bars for different strength levels of concrete at different concrete cover depths.

As shown in Figure 5.21, the results of the present study showed that bond strengths in corroded specimens depend on the c/D ratio, the concrete compressive strength and the crack width. An interesting result was obtained for the lower-strength concrete at the lowest c/D ratio (w/c = 0.75 and c = 15 mm). As shown in Figure 5.21(a), up to a corrosion level of 4%, bond strength increased and then decreased for a given corrosion level. However, increases in bond strength occurred at lower levels of corrosion with higher c/D ratios. For the low levels of corrosion, the average bond strength likely increased due to the increased roughness of the steel bar caused by the confined corrosion products (Amleh 2006). Our results showed that this phenomenon was more obvious when greater confinement of the bar in the concrete is encountered during pullout testing. For example, in Figure 5.21(a), the bond strength at the lowest c/D ratio increased by approximately 41% at a corrosion level of 4%. For a higher c/D ratio (c/D = 2.143 or c = 30 mm), bond strength was increased by 51% at the lower corrosion level of 1.4% and then decreased nonlinearly beyond 1.4%. For the highest c/D ratio (c/D = 3.214 or c = 45 mm), bond strength was increased by approximately 33% at the lowest corrosion level of 0.68% and then decreased nonlinearly beyond 0.68%. This can be explained by the

frictional properties of the interface between the reinforcement bars and the concrete and by the crack width. The lugs of the reinforcement bars at the lowest *c*/*D* ratio disappeared or were severely damaged due to corrosion, which decreased the transfer of stress from the reinforcement bars to the surrounding concrete. As shown in Figure 5.22, the lugs of the reinforcement bars at the lowest *c*/*D* ratio disappeared which turned in the reinforcement bars to act like a smooth reinforcement bars.

Figure 5.22: Damaged lugs of the reinforcement bars.

With respect to these results, it should be noted that the cracking of concrete increased with concrete depth. Figure 5.23 shows the effect of various *c*/*D* ratios on concrete cracking after the pullout tests.

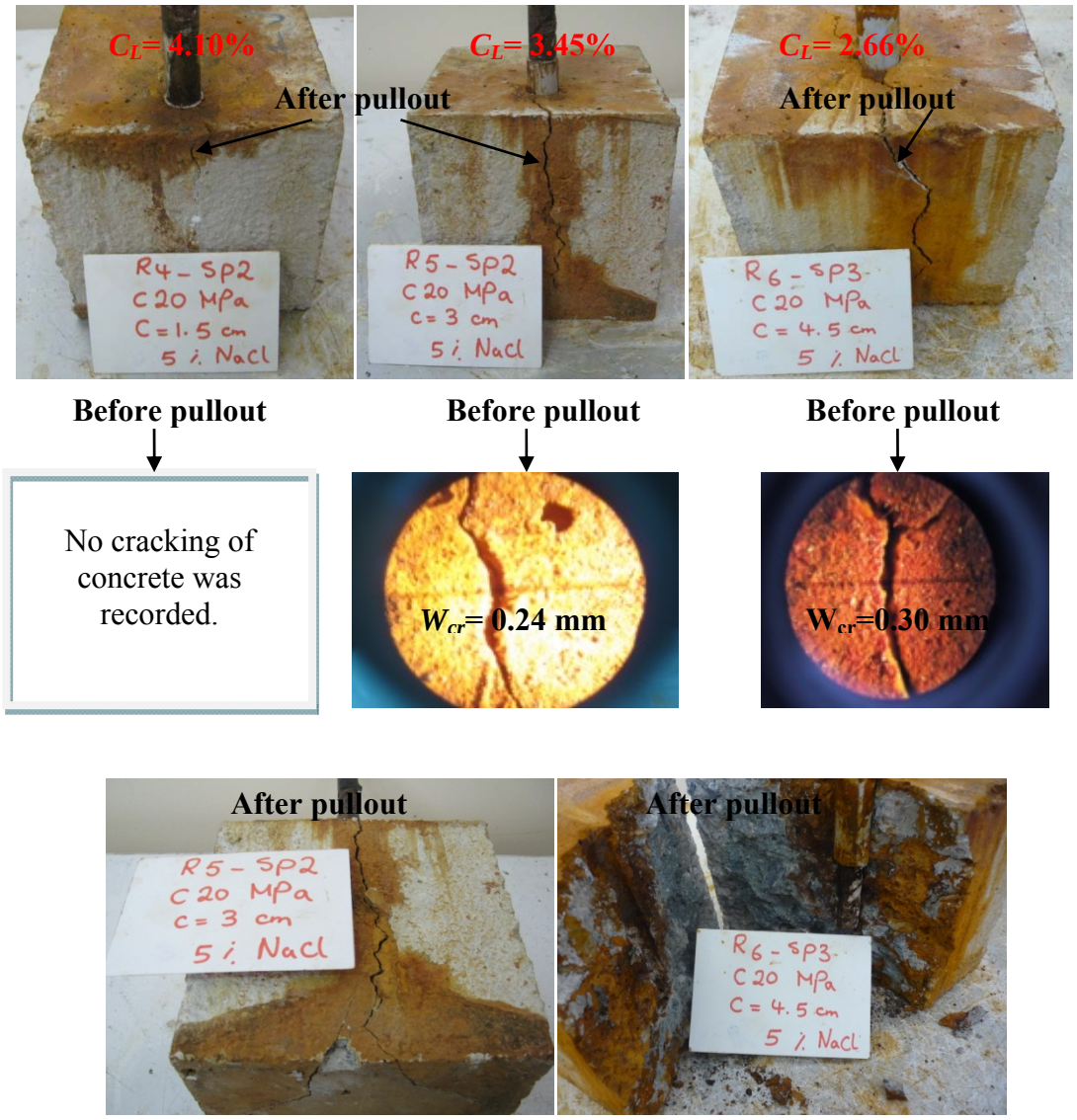

Figure 5.23: Effect of *c*/*D* ratio on cracking of concrete.

As shown in Figure 5.23, crack width increased with increasing *c*/*D* ratio at the lower corrosion levels when compared with lower *c*/*D* ratios at higher corrosion levels. For example, in Figure 5.23, even though the corrosion level of R_4SP_2 was 54% more than that of R_6SP_3, the observed crack width was wider for R_6SP_3 after the pullout test. Same results can be observed between R_5SP_2 and R_6SP_3. Even though the corrosion level of R_5SP_2 was more than that of R_6SP_3, the observed crack width was wider for R_6SP_3 after the pullout test. As shown in Figure 5.21(a), for the same *w*/*c* ratio, an increase in the *c*/*D* ratio yielded a different behaviour than at the lower *c*/*D* ratio. The likely reason for this is that the cracks observed in the specimens with

the higher *c*/*D* ratio caused a reduction in bond strengths at lower corrosion levels. After the accelerated corrosion process, the maximum recorded crack widths on the surfaces of concrete specimens supported these results. As shown in Figure 5.23, the maximum recorded crack widths on the surfaces of concrete specimens R_5SP_2 and R_6SP_3 were 0.24 mm and 0.30 mm, respectively, whereas no cracks were observed on R_4SP_2.

Another important result of this study was the observation showing that with increasing concrete tensile strength, the degradation of bond strength at higher concrete strengths was more than that with lower-strength concrete (see Figure 5.21(b)). The results showed that the higher-strength concrete became more brittle than in the uncorroded condition. Chang (2002) reported that bond degradation is more significant for concrete with a higher *w*/*c* ratio. However, the data reported by Lee et al. (2008) and in the present study disagrees with results given by Chang (2002). Figure 5.24 shows the reductions in bond strengths for two concrete strength levels having almost the same corrosion levels.

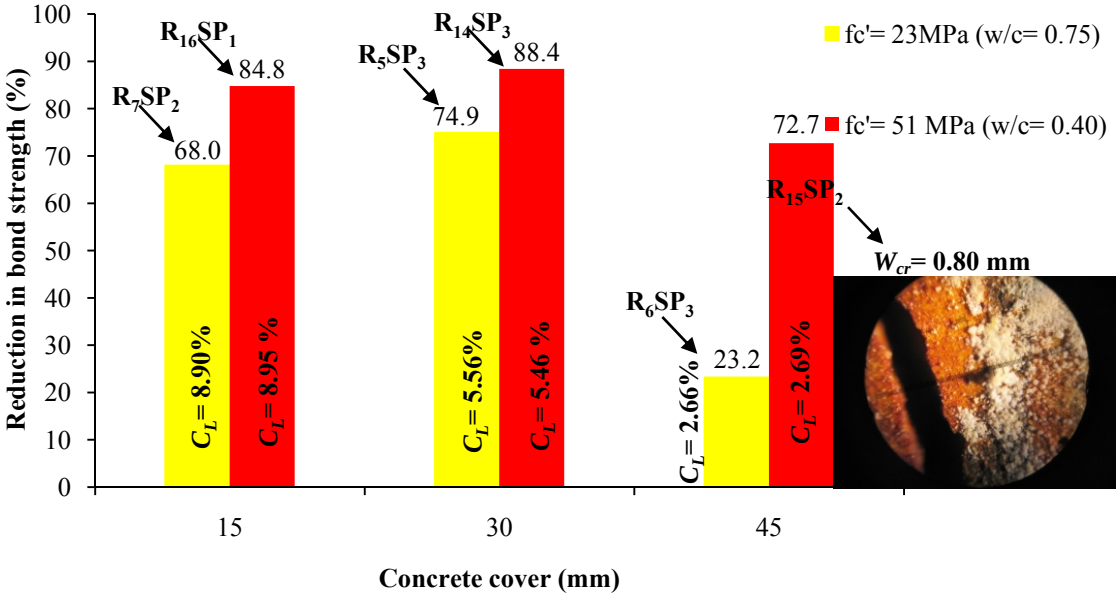

Figure 5.24: Reduction in bond strength.

Based on the results shown in Figure 5.24 and the bond-slip relationships given in the next section, it was clear that the effect of corrosion was more dramatic for concrete with a higher strength level. The measured maximum crack widths on the surface of the concrete samples clearly support this interpretation. At the same corrosion levels, the maximum crack width of the high-strength concrete was greater than that of the low-strength concrete during the accelerated corrosion process. As shown in Figure 5.24, the crack width of $R_{15}SP_2$ was 0.80 mm, whereas the crack width of R_6SP_3 was 0.30 mm (see Figure 5.24) at the same corrosion level. Same results can be also observed during pullout test of concrete specimens. In Figure 5.25 splitting of concrete specimens are shown for higher and lower strength levels of concrete.

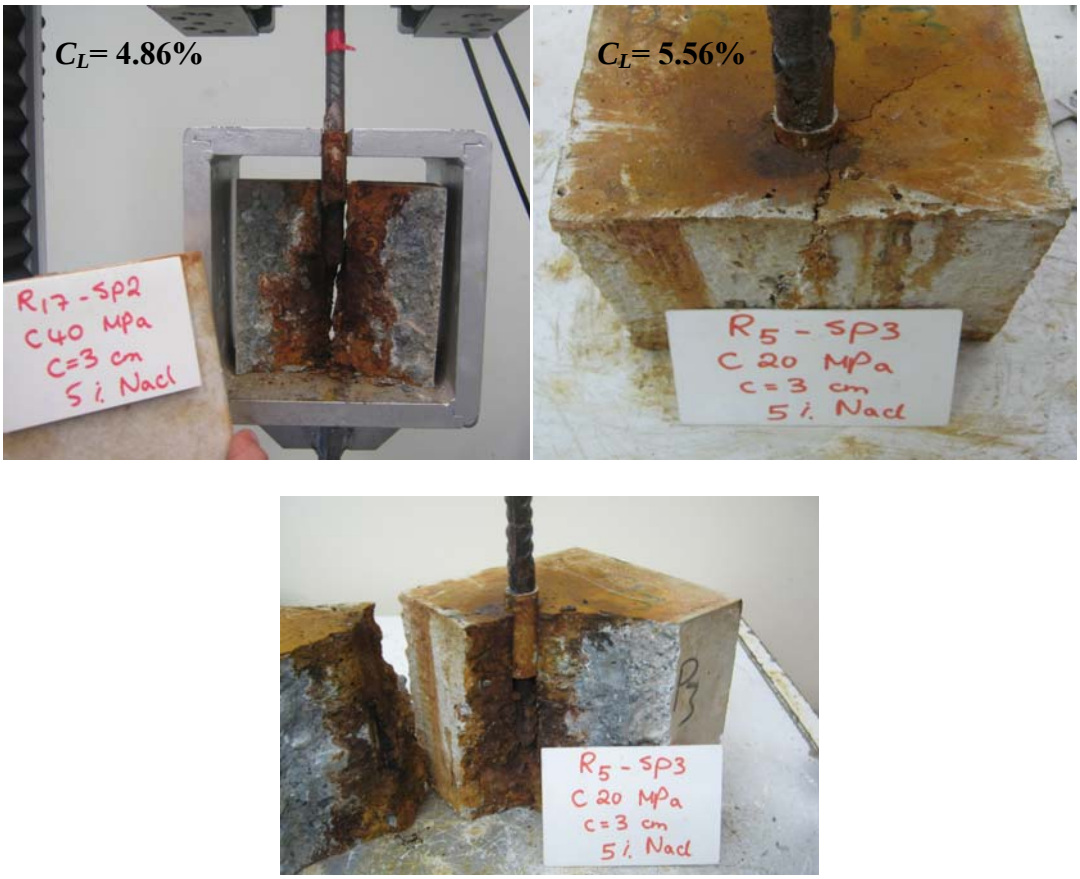

Figure 5.25: Splitting of concrete due to corrosion.

As shown in Figure 5.25, even if the corrosion level of high strength concrete was more than that of low strength level of concrete (R_5SP_3), the splitting of high strength level of concrete was more dramatic at a lower corrosion level when it was compared with low strength level of concrete at a higher corrosion level. In order to better reflect the degradation of bond strength at higher concrete strengths levels, the comparisons between two concrete strength levels at the same concrete cover depths are shown in Figure 5.26.

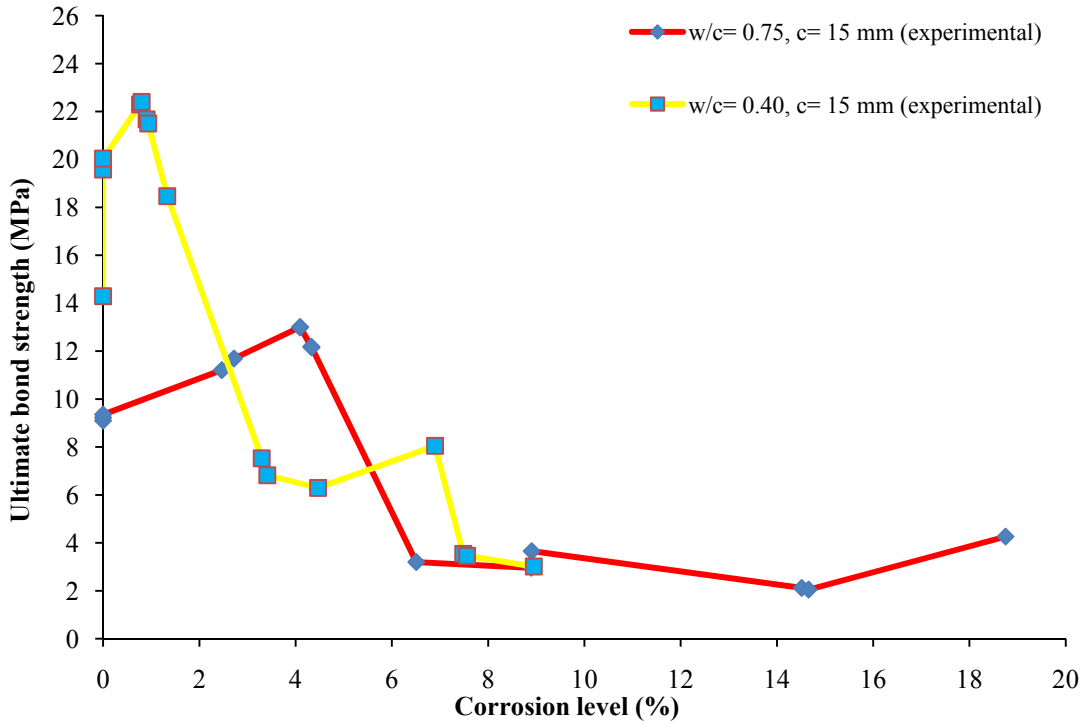

(a)

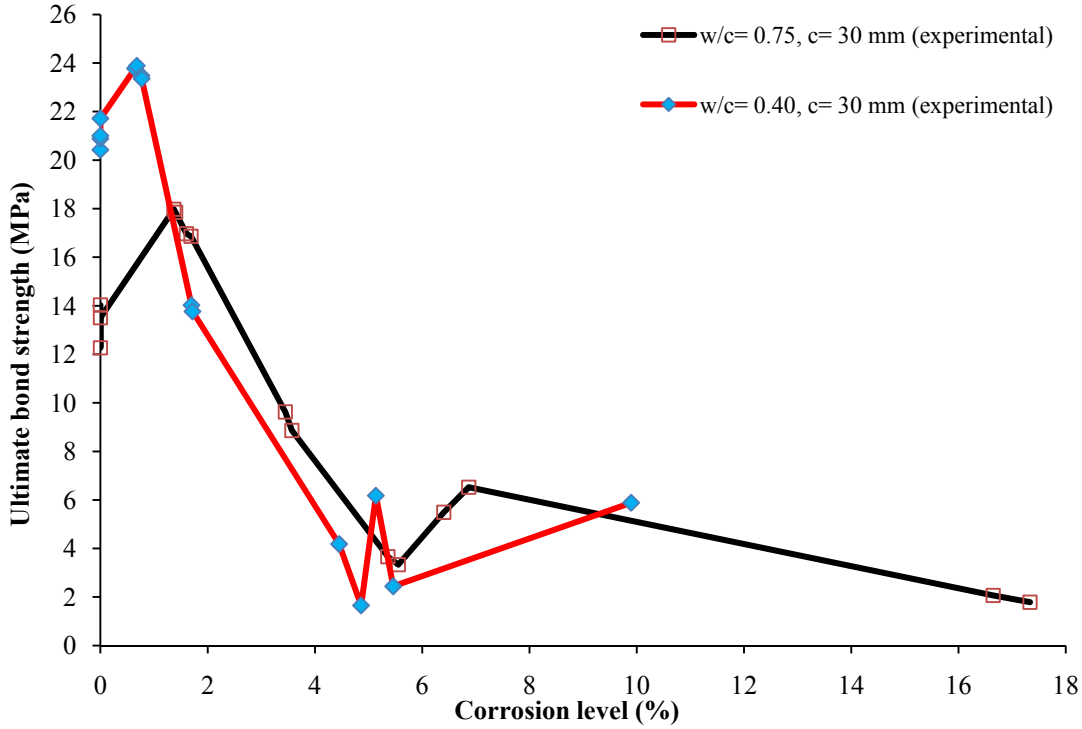

(b)

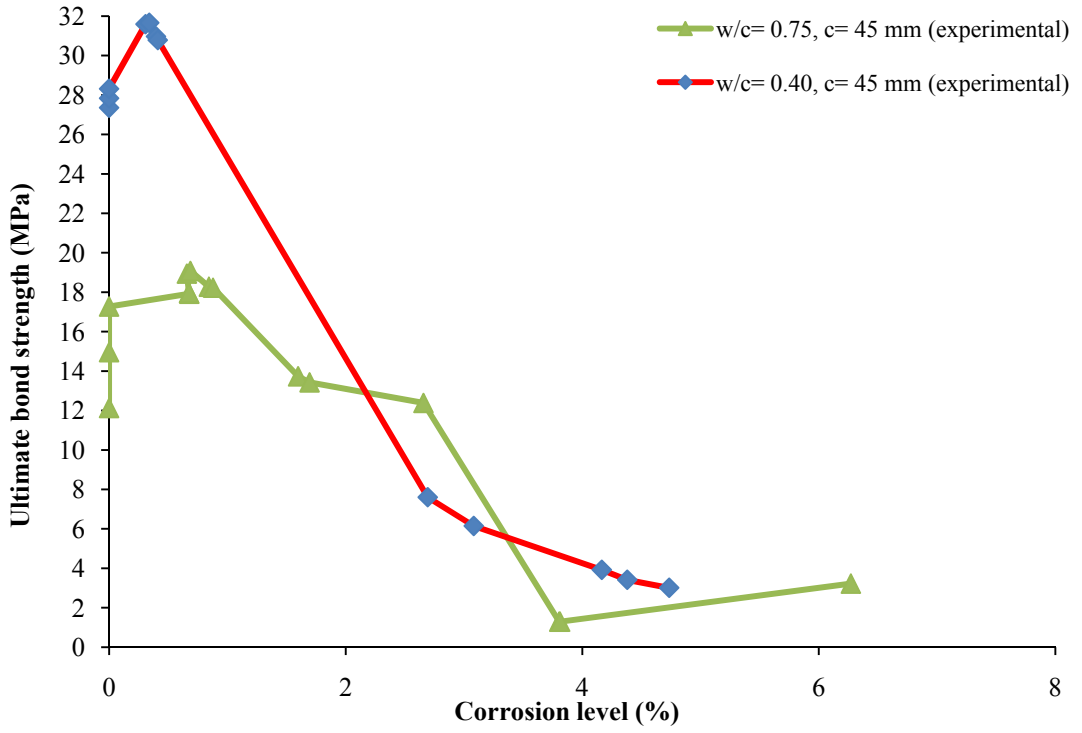

(c)

Figure 5.26: Comparisons of bond strengths of two concrete strength levels at the same concrete cover depths.

As shown in Figure 5.26(a-c), the bond strength of high strength concrete level began to reduce for lower corrosion levels when they were compared with low strength level of concrete. For instance, in Figure 5.26(a), the bond strength of lower strength level of concrete started to decrease after reaching the 4% of corrosion level where it was 0.8% of corrosion level for higher strength level of concrete. With increasing concrete cover depths as shown in Figures 5.26(a-b), the decreasing in bond strengths began to reduce with lower corrosion levels. For instance, in Figure 5.26(b), the bond strength of lower strength level of concrete started to decrease after reaching the 1.37% of corrosion level where it had 0.68% corrosion level for higher strength level of concrete.

In Figure 5.21(a-b), the experimental results of this study were compared with the previously developed models found in the literature. As shown in Figure 5.21(b), Fang et al. (2004) did not provide an equation to predict the ultimate bond strength. Therefore, the available experimental data from the pullout tests done by Fang et al. (2004) were directly plotted in Figure 5.21(b); the concrete strength in that study was 52.1 MPa. This comparison shows that the previous empirical bond strength equations underestimate or overestimate bond strengths for different conditions. Among them, the latest study by Chung et al. (2008) gave better results. It should be noted that in the study of Chung et al. (2008) the reinforcement bars were corroded before and after casting concrete, and a single concrete strength and a single concrete cover depth were evaluated.

As shown in Figure 5.21(a), the previous empirical models developed (e.g., (Cabrera 1996; Auyeung et al. 2002; Lee et al. 2002) predict that the bond strength should decrease with increasing corrosion level, but these models do not represent the actual corrosion behaviour, especially when different c/D ratios and concrete

strengths are taken into account. As a result of combining different *c*/*D* ratios and concrete strengths to predict the bond strength, the following equations were obtained using linear and nonlinear regression analyses. To accurately predict the ultimate bond strength, the developed models were separated into two parts. Considering the scatter in the experimental data, two equations were derived for the ascending branch (see Eqs. (5.3) and (5.4)) based on the *c*/*D* ratios and the given limits of the corrosion levels.

$$\text{if } c/D < 2 \quad \text{and} \quad \begin{matrix} 0 \le C_L \le 4 & \text{for} & f_c' = 23\,\text{MPa} \\ 0 \le C_L \le 0.8 & \text{for} & f_c' = 51\,\text{MPa} \end{matrix}$$

$$\tau_{bu} = 0.40551 f_c' - 0.25306 \left(\frac{c}{D}\right) + 0.97926\, C_L \text{ (MPa)} \qquad (R^2 = 0.98) \quad (5.3)$$

$$\text{if } c/D \ge 2 \quad \text{and} \quad \begin{matrix} 0 \le C_L \le 1.4 & \text{for} & f_c' = 23\,\text{MPa} \\ 0 \le C_L \le 0.68 & \text{for} & f_c' = 51\,\text{MPa} \end{matrix}$$

$$\tau_{bu} = e^{(0.01572 f_c' + 0.22957 \left(\frac{c}{D}\right) + 0.13946 C_L + 1.75913)} \text{ (MPa)} \quad (R^2 = 0.94) \quad (5.4)$$

For the descending branch of the bond strength curve in Figure 5.21(a-b), the relation is given by equation 5.5. If the corrosion levels are above the limits given by equations 5.3 and 5.4, the proposed equation 5.5 can be used to calculate the bond strength for the descending branch. In other words, if $1 \le c/D \le 3.2$, then

$$\tau_{bu} = e^{(0.01667\, f_c\text{'}-1.06499\, W_{cr} + 0.20658\, \frac{c}{D} - 0.12928\, C_L + 1.80139)} \text{ (MPa)}$$

$(R^2 = 0.96)$ (5.5)

can be used conveniently. The experimentally obtained results were compared with those obtained with the proposed analytical models, as shown in Figure 5.27.

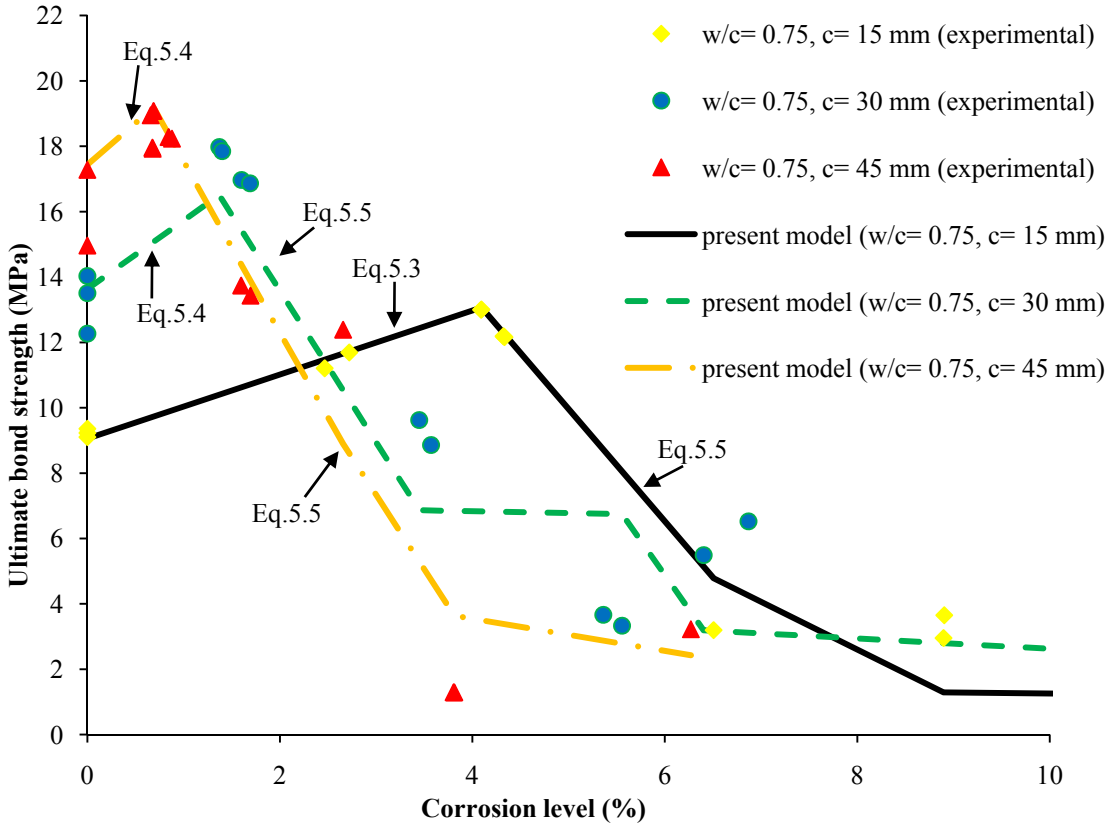

(a)

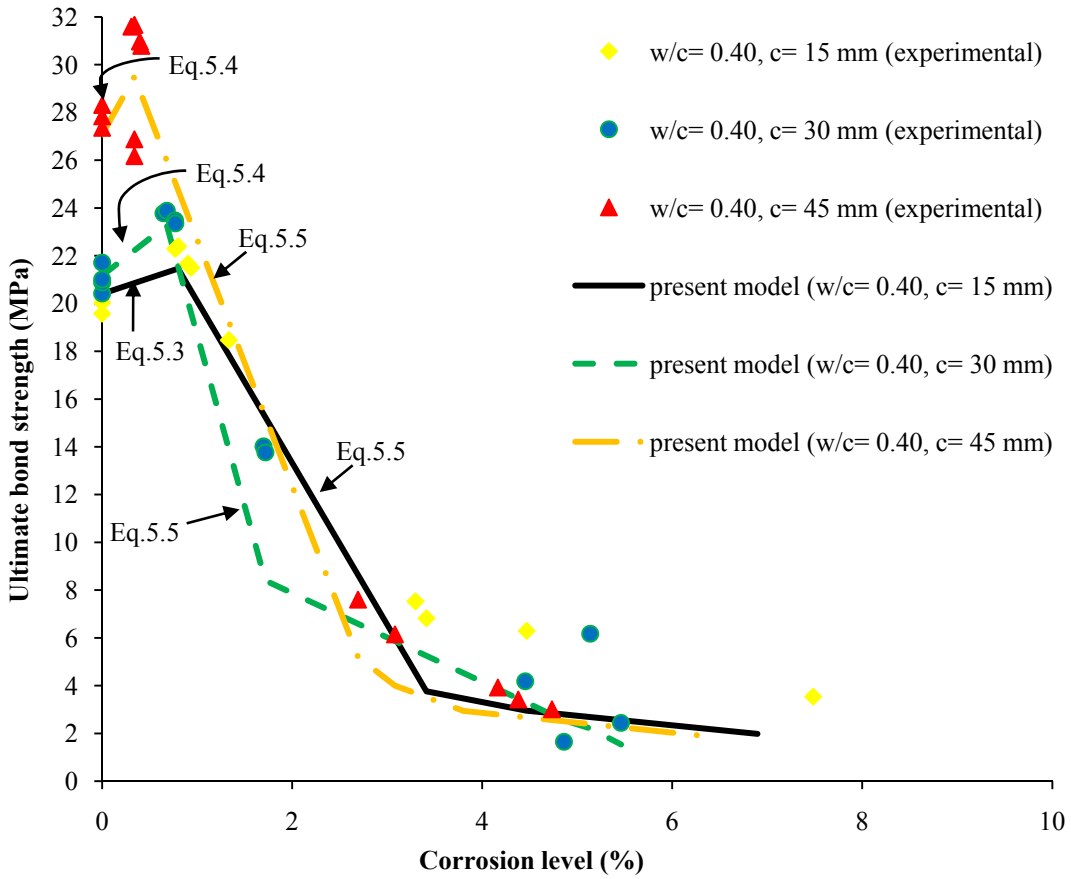

(b)

Figure 5.27: Validation of proposed models: (a) *w/c*= 0.75; (b) *w/c*= 0.40.

As shown in Figure 5.27, the proposed equations correctly predict the bond strengths. It is thus possible to predict the bond strength as a function of crack width and corrosion levels for different *c*/*D* ratios and concrete strengths. As shown in Figure 5.21(a), whereas previous models show a decrease in bond strength with increasing corrosion level, the newly proposed model shows a more realistic behaviour reflecting the actual bond strength. It is possible to monitor bond strength behaviour at both low and high corrosion levels with cracked or uncracked concrete conditions for different *c*/*D* ratios and concrete strengths by using relations given in Eqs. (5.3-5.4).

5.4.3 Bond-slip Relationships

The bond-slip relationships for selected uncorroded specimens are shown in Figure 5.28. This relation showed that, the slippage of the reinforcement bars decreases with increasing *c*/*D* ratio and concrete strength. The results presented in Figure 5.28 were in agreement with the relationships obtained for bond strength. It can be seen in Figure 5.28 that the peak of the curve of the high-strength concrete is relatively sharp, but the curve has a flat top for the low-strength concrete. The results show that at the same applied load, slip displacement was less for the higher-strength concrete than for the lower-strength concrete. Moreover, the *c*/*D* ratio has a significant effect on the slip displacement, which tends to decrease with an increasing *c*/*D* ratio. For example, in Figure 5.28, the slip displacement at the maximum bond strength of R_1SP_1 was reduced by 35% due to the increased *c*/*D* ratio of R_3SP_2. For the same concrete cover depth (c = 30 mm), the recorded slip displacement at the maximum bond strength of R_2SP_2 was reduced by 20% with a 32% increase in concrete tensile strength for $R_{11}SP_2$. Similarly, comparing the two concrete strength levels at a 45 mm cover depth, the slip displacement at maximum bond strength of R_3SP_2 was reduced by 19% from that of the higher-strength $R_{12}SP_2$. Thus, it can be said that percentage reduction in slip displacement due to the higher-strength concrete is almost the same for further increases in cover depth for the uncorroded specimens.

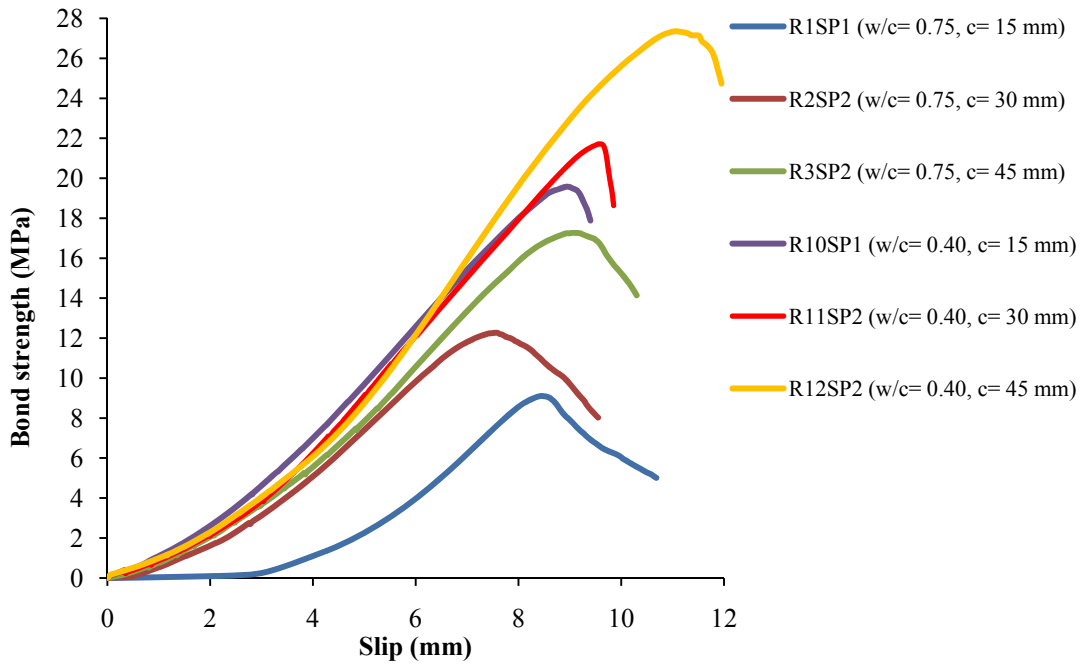

Figure 5.28: Bond-slip relationships of uncorroded specimens.

The bond-slip relationships for corroded specimens are as given in Figure 5.29(a-b). These relationships were important in verifying our findings regarding the bond strength degradation of higher-strength concrete due to corrosion.

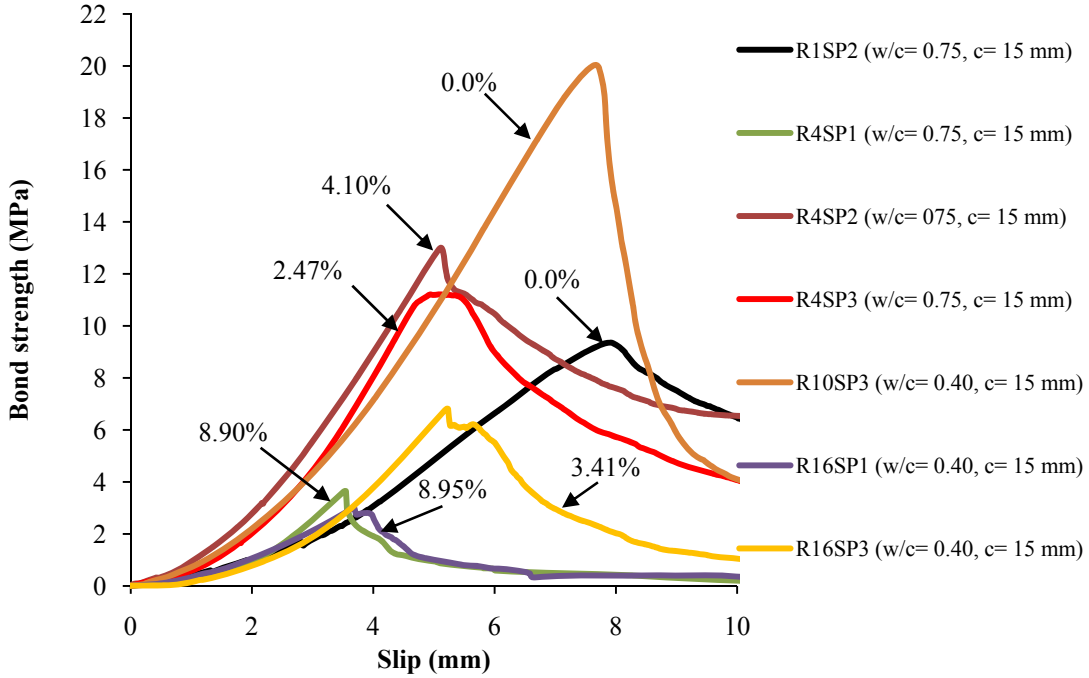

(a)

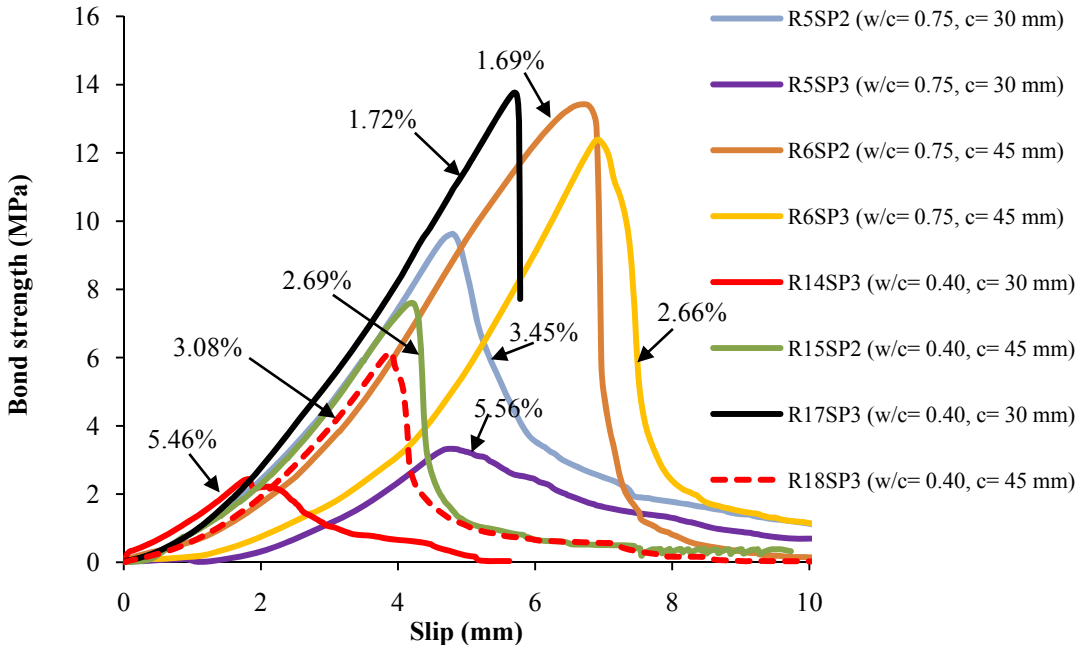

(b)

Figure 5.29: Bond-slip relationships of corroded specimens: (a) c = 15 mm; (b) c = 30 mm and 45 mm.

As shown in Figure 5.29(a), when the c/D ratio was less than two (c = 15 mm), more slip displacement occurred at lower corrosion levels for higher-strength concrete due to the opening of longitudinal cracks during the pullout tests. As mentioned earlier, the occurrence of cracks during accelerated corrosion played an important role in the case of the corroded specimens. In Figure 5.29(a), the measured maximum crack width on the surface of $R_{16}SP_3$ was 0.60 mm, whereas no cracks were observed on R_4SP_3 and R_4SP_2. It was suggested that the results obtained in this study are adequate to define the general behaviour of corrosion effects on bond strength. In Figure 5.29(a), the slip displacement of R_1SP_2 at the maximum bond strength was reduced by 48% due to the increased corrosion level of R_4SP_2 (4%). However, at the maximum bond strength of the higher-strength concrete ($R_{16}SP_3$), the slip displacement increased by 34% at the lower corrosion level of 3.4%. In Figure 5.29(a), it can be seen that when the corrosion level was relatively a large

value (e.g., R_4SP_1 and $R_{16}SP_1$), the effect of corrosion on slip displacement was almost the same for the different concrete strength levels due to more localised and extensive cracking of the concrete surface during the pullout test. As illustrated in Figure 5.29(b), the bond-slip relationship showed different behaviours with increasing *c*/*D* ratio for the two different concrete strength levels. As shown in Figure 5.29(b), the bond strength with the higher *w*/*c* ratio was greater than that with the lower *w*/*c* ratio at almost the same corrosion level (see R_6SP_3 and $R_{15}SP_2$). However, the results were different for slip displacement. When the slip displacements for the two concrete strength levels are compared for the same concrete cover depth (*c* = 30 mm), e.g., R_5SP_3 and $R_{14}SP_3$, it can be seen that less displacement occurred in the higher-strength concrete at an almost identical corrosion level. Similar results were also observed for several other specimens, such as R_6SP_3 and $R_{15}SP_2$, with a concrete cover of 45 mm. This can be explained by the increased resistance to the slippage of the reinforcement bars set in higher-strength concrete until the time it split. In Figure 5.30(a-b), splitting of the concrete specimens along the corrosion cracks is shown. As shown in Figure 5.30, at the same corrosion levels, wider cracks occurred for higher-strength concrete, which caused a loss of bond strength. Up to a given value of applied load, the higher-strength concrete provided less displacement, but for further increases in load it exhibited more brittle behaviour, with a sharp decrease occurring at the peak of the curve, as displayed by specimen $R_{17}SP_3$. A good relationship was obtained when the results were compared for different concrete cover depths. Figure 5.29(b) shows that with a concrete cover depth of 30 mm and *w*/*c*= 0.75 (R_5SP_2), the value of slip displacement was almost the same at the maximum bond strength of $R_{15}SP_2$ (*c* = 45 mm and *w*/*c* = 0.4) at a higher corrosion level of 3.45%. Same behaviour was also observed with

R_6SP_2 and $R_{17}SP_3$. In contrast with the previous samples (R_5SP_2, $R_{15}SP_2$), slip displacement was less for the higher-strength concrete ($R_{17}SP_3$) at the almost same corrosion level due to a lower cover depth.

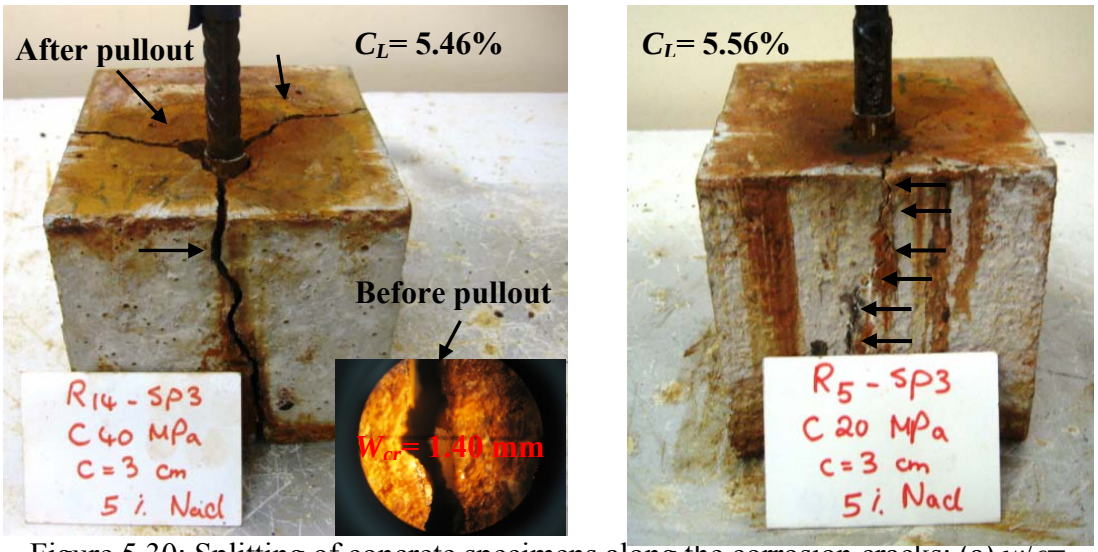

Figure 5.30: Splitting of concrete specimens along the corrosion cracks: (a) *w/c*= 0.40, (b) *w/c*= 0.75.

The wider cracking of higher strength concrete rather than lower strength level of concrete can be explained by exceeded stress level inside of concrete. This was due to higher permeability of concrete specimens with higher *w/c* ratios of 0.75. Accelerated corrosion method showed that with a higher *w/c* ratio, the corrosion products were flowing throughout. While the colour of water in glass tank was changed to red colour for higher *w/c* ratio, it was closer to original colour for lower *w/c* ratio. With lower permeable concrete (*w/c*= 0.40) thus maintained expansive corrosion products caused to increase the internal pressure which resulted in premature cracking of concrete due to volumetric expansion.

Chapter 6

CONCLUSIONS

Based on the investigations and analysis of current study, the following conclusions can be drawn.

In the first part of this thesis, studied and developed corrosion models were combined with structural assessment methods as a function of time to predict the time-dependent performance level of corroded RC buildings as a function of corrosion rate. The results showed that:

a) The effects of the corrosion rate include not only the loss of the cross sectional area of the reinforcement bars but also slippage, and reduction in concrete compressive strength which must be taken into account for structural assessment.

b) As a consequence of corrosion effects, plastic hinge properties were calculated as a function of corrosion rate. Additional displacement due to slippage of reinforcement bars by losing bond strength due to corrosion was considered to predict the time-dependent seismic performance levels of the RC building. The calculated time-dependent properties of the plastic hinges were an important tool for defining the time-dependent performance levels of each case by taking into account the bond-slip relationships. It has been found that in non-linear analyses, the effect of slip gives more accurate results by modifying the post-yield stiffness

of the structural elements rather than summing up the additional displacement due to slippage of reinforcement bars.

c) It might be useful to redefine the thresholds of corrosion rates by taking into account other effects of corrosion, i.e., not only loss of the cross sectional area of the reinforcement bars, but also bond slip relationships need to be taken into account.

d) The present study showed that service life of concrete structures is limited by corrosion of reinforcement where the quality of concrete, mainly the permeability, and the cover thickness and environmental factors affect the remaining service life of structures.

e) Additional studies are also required for more accurate performance assessments of three dimensional MDOF systems by taking into account the torsion effects under the impact of corrosion. Finally, the methodology presented herein can serve as a guide for structural engineers to reduce the economical impact of corrosion due to time and to define potential time-dependent seismic risks for further expected earthquakes.

In the second part of this thesis, series of experimental studies were performed to predict the ultimate bond strength of corroded and uncorroded specimens. Novel models were developed to predict the ultimate bond strength as a function of corrosion rate, concrete compressive strength and crack width. The results showed that:

a) Using the newly developed bond strength equations, based on the limitations specified before, it is possible to predict the bond strength as a function of corrosion levels, concrete strength levels, crack width and c/D ratios.

b) Previously developed bond strength equations yielded significantly underestimated or overestimated results; the bond strength decreases rapidly in these models.

c) In the case of the uncorroded specimens, bond strength increased with increasing concrete strength level and *c*/*D* ratio, where the *c/D* ratio of 3.2 and a *w/c* ratio of 0.40 yielded the highest ultimate bond strength in this study.

d) In the case of the uncorroded specimens, bond strength increased up to a *c/D* ratio of 3.2, and no significant enhancement observed above this ratio.

e) When the *c*/*D* ratio increased in the uncorroded specimens, the percentage increase in ultimate bond strength of the lower-strength concrete was more than that of the higher-strength concrete. Indeed, this is a normal behaviour since the reinforcement bars used were deformed. The radial pressure from the lugs of the reinforcing bars causes high tensile stresses on concrete. The resistance of the specimen to these radial stresses depends on both the compressive strength and *c*/*D* ratio. Thus, as the *c*/*D* ratio increases for lower-strength level of concrete, resistance to these radial pressure will increase.

f) In the case of the uncorroded specimens, increasing the concrete compressive strength for a given concrete cover depth yielded higher bond strength than increasing the concrete cover for a given concrete strength.

g) At the same corrosion level, the measured maximum surface crack width of the higher-strength concrete was more than that of the lower-strength concrete. This was due to higher permeability of concrete specimens with higher *w*/*c* ratios of 0.75. Accelerated corrosion method showed that with a higher *w*/*c* ratio, the corrosion products were flowing throughout the concrete. Meanwhile, the colour of water in glass tank was changed to red. On the other hand, lower permeability

of concrete (w/c= 0.40) maintained expansive corrosion products. These products increased the internal pressure which resulted in premature cracking of concrete due to volumetric expansion.

h) The splitting of the higher-strength concrete was more dramatic than that of the lower-strength concrete at the same corrosion level since initial cracks have been already observed during accelerated corrosion method as explained above.

i) An increase in crack width was observed with increasing c/D ratio at lower corrosion levels when compared with a lower c/D ratio at higher corrosion levels.

j) Pull-out tests on corroded high-strength concrete specimens showed more brittle behaviour (sharp decrease in bond strength-slip curve occurred at the peak bond strength values as shown in Figure 15(b)) compared with its uncorroded condition.

k) The degradation of bond strength in the higher-strength concrete was more pronounced than in the lower-strength concrete. The underlying mechanism of this again was the cause of expansion of the corrosion products as explained above in conclusion number g.

l) In the case of the uncorroded specimens, the slippage of reinforcement bars decreased with increasing c/D ratio and concrete strength.

m) In the case of the corroded specimens, the slip displacement was less for the lower-strength concrete at the lowest c/D ratio.

n) When the c/D ratio was increased in the case of the corroded specimens, the slip displacement was less for the higher-strength concrete at the same corrosion level and c/D ratio.

It is expected that the differences in bond strength and slip behaviour for corroded reinforcements with different concrete classes and c/D ratios highlighted in this study

may provide guidance for the performance evaluation of existing reinforced concrete buildings, especially in the earthquake-prone regions. Although performed experimentally study in this thesis was based on pullout tests with prepared specimens and may therefore not reflect the actual behaviour of reinforced concrete sections under the influence of bending, where both concrete and the reinforcement are in tension, the results and findings of this study are general and may be used directly and as a guide for further studies.

PUBLICATIONS

As a consequence of developed models in this study, a number of publications have been provided in the literature:

1. Hakan Yalciner, Serhan Sensoy, Ozgur Eren. (2012). Time-dependent seismic performance assessment of a single-degree-of-freedom frame subject to corrosion. *Engineering Failure Analysis*. 19,109-122. (SCI Expanded)

2. Hakan Yalciner, Ozgur Eren, Serhan Sensoy. (2011). An experimental study on the bond strength between reinforcement bars and concrete as a function of concrete cover, strength and corrosion level, Cement and Concrete Research,2011, under review. (SCI Index)

3. Hakan Yalciner, Serhan Sensoy, Ozgur Eren. (2011). Effect of corrosion damage on the performance level of a 25-year-old reinforced concrete building. *Journal of Shock and Vibration.* (Accepted, in press).

REFERENCES

ACI Committee 408. (1979). Suggested development, splice, and standard hook provisions for deformed bars in tension (ACI 408.1R-79), American Concrete Institute, Farmington Hills, MI, p. 3.

ACI Committee 201. (1991). Guide to durable concrete. *ACI Materials Journal*. 88(5).

Ahmad, S. (2003). Reinforcement corrosion in concrete structures, its monitoring and service life prediction–a review. *Cement and Concrete Composites*, 25(4-5), 459-471.

Akgül, F., Frangopol, F., & Dan, M. (2004). Lifetime performance analysis of existing prestressed concrete bridge superstructures. *Journal of Structural Engineering*, *ASCE*, 130(12), 1889-1903.

Almusallam, A.A., Al-gahtani, A.S., Aziz, A.R., & Rasheeduzzafar (1996). Effect of reinforcement corrosion on bond strength. *Construction and Building Materials*. 10(2), 123–129.

Al-Saadoun SS, Rasheeduzzafar, & Al-Gahtani A.S. (1992). Mix design considerations for durable concrete in the Arabian Gulf environment. *The Arabian Journal for Science Engineering*. 17(1), 17-33.

Alsiwat, J. M., & Saatcioglu M. (1992). Reinforcement anchorage slip under monotonic loading. *Journal of Structural Engineering*, *ASCE*, 118(9), 2421-2438.

Al-Sulaimani, G.J., Kaleemullah, M., Basunbul, I.A., & Rasheeduzzafar. (1990). Influence of corrosion and cracking on bond behaviour and strength of reinforced concrete members. *ACI Structural Journal*. 87(2), 220–231.

American Concrete Institute (ACI 318-05) (2005). Building code requirements for structural concrete. *American Concrete Institute* (1989). Building Code Requirements for Reinforced Concrete, ACI, Detroit., ACI 318-89.

Amleh, L., & Mirza, S. (1999). Corrosion influence on bond between steel and concrete. *ACI Structural Journal*. 96(3), 415–423.

Andrade, C., Alonso, C., & Molina, F.J. (1993). Cover cracking as a function of rebar corrosion: Part I-experimental test. *Materials and Structures*. 26(8):453-464.

Apostolopoulos, C.A., & Pasialis, V.P. (2010). Effects of corrosion and ribs on low cycle fatigue behavior of reinforcing steel bars S400. *Journal of Materials Engineering and Performance*. 19(3): 385-394.

Auyeung, Y., Balaguru, P., & Chung, L. (2000). Bond behavior of corroded reinforcement bars. *ACI Materials Journal*. 97(2), 214–220.

Bažant, Z.P. (1979). Physical model for steel corrosion in concrete sea structures-application. *ASCE Journal of Structural Division*. 105(6), 1155-1166.

Bentur, A., Diamond, S., & Berke, N.S. (1997). Steel corrosion in concrete: fundamentals and civil engineering practice. 2nd ed. London: E&FN Spon.

Berkely, K.G.C., & Pathmanaban, S.(1990). Cathodic protection of reinforcement steel in concrete. London, Butterworths & Co. Ltd.

Berto, L., Vitaliani, R., Saetta, A., & Simioni, P. (2009). Seismic assessment of existing reinforced concrete structures affected by degradation phenomena. *Structural Safety*. 31(4), 284-297.

Bhargava, K., Ghoshb, A.K., Mori, Y., &Ramanujam, S. (2006). Model for cover cracking due to rebar corrosion in RC structures. *Engineering Structures*. 28, 1093–1109

BRE Centre for Concrete Construction. (2001). Guide to the maintenance, repair and monitoring of reinforced concrete structures. DME Rep. No. 4 Watford, UK.

Cabrera, J.G. (1996). Deterioration of concrete due to reinforcement steel corrosion. *Cement and Concrete Composites*. 18 (1), 47–59.

Canadian Standards Association. (1994). Design of concrete structures, CSA A23.3-94, Rexadle, ON, Canada.

Cape, M. (1999). Residual service-life assessment of existing R/C structures, MS thesis, Chalmers Univ. of Technology, Goteborg (Sweden) and Milan Univ. of Technology (Italy, Erasmus Program), p.133.

Capozucca, R. (1995). Damage to reinforced concrete due to reinforcement corrosion. *Construction and Building Marerials.* 9(5), p295-303.

Chang, J.J. (2002). A study of the bond degradation of rebar due to cathodic protection current. *Cement and Concrete Research*. 32, 657–663.

Charney, F.A. (1998). NONLIN V-7: Nonlinear dynamic time history analysis of single degree of freedom systems, Blacksburg, Virginia, Advanced Structural Concepts, Inc.

Chernin, L., & Val, D.V. (2008) .Prediction of cover cracking in reinforced concrete structures due to corrosion. In: Proceedings of the 1st international conference on construction heritage in coastal and marine environments (MEDACS08), LNEC, Lisbon.

Choea, D. E., Gardonia, P., Rosowskya, D., & Haukaas, T. (2009). Seismic fragility estimates for reinforced concrete bridges subject to corrosion. *Structural Safety*. 31(4), 275-283.

Choe, D.E., Gardoni, P., Rosowsky, D., & Haukaas, T. (2008). Probabilistic capacity models and seismic fragility estimates for RC columns subject to corrosion. *Reliability Engineering and System Safety*, 93(3), 383–393.

Chopra, A.K., & Goel, R.K. (1999). Capacity-demand-diagram methods for estimating seismic deformation of inelastic structures: SDF systems report no

PEER, (Pacific Earthquake Engineering Research Centre University of California Berkeley, 1999).

Chung, L., Cho, S.H., Kim, J.H.J., & Yi, S.T. (2004). Correction factor suggestion for ACI development length provisions based on flexural testing of RC slabs with various levels of corroded reinforcing bars. *Engineering Structures.* 26(8) 1013–1026.

Coronelli, D., & Gambarova, P. (2004). Structural assessment of corroded reinforced concrete beams: Modeling guidelines. *ASCE Journal of Structural Engineering.* 130(8), 1214-1224

Dhir, R.K., Jones, M.R., & McCarthy, M.J. (1994). PFA concrete: chloride-induced reinforcement corrosion. *Magazine of Concrete Research.* 46(169), 269-77.

Dogangun, A., Karaca, Z., Durmus, A., & Sezen, H. (2009). Cause of damage and failures in silo structures. *ASCE, Journal of Performance of Constructed Facilities*. 23(2), 65-71.

Eligehausen, R., Popov, E.P., & Bertero, V.V. (1983). Local bond stress-slip relationships of deformed bars under generalized excitations. Rep. No. UCB/EERC-83/23, Pacific Earthquake Engineering Research Center, University of California, Berkeley, p. 169.

El Maaddawy, T., & Soudki, K. (2007). A model for prediction of time from corrosion initiation to corrosion cracking. *Cement and Concrete Composites*. 29(3), 168-175.

Eren, O., Sensoy, S. (2010). Determination of strength permeability-age of concrete for existing reinforced concrete structures. Rep. No. BAP-A-07-15, Department of Civil Engineering, Faculty of Engineering, Eastern Mediterranean University, Famagusta, p. 1-33.

Fang, C., Lundgren, K., Chen, L., & Zhu, C. (2004). Corrosion influence on bond in reinforced concrete. *Cement and Concrete Research*. 34 (11), 2159–2167.

Fajfar, P. (2000). A nonlinear analysis method for performance-based seismic design. *Earthquake Spectra*. 16(3):573–592.

Fajfar, P. (2002). Structural analysis in earthquake engineering – A breakthrough of simplified non-linear methods. *12th European Conference on Earthquake Engineering*, London, Paper No. 843.

FEMA 273. (1997). Federal Emergency Management Agency-NEHRP Guidelines for the seismic rehabilitations of buildings, Washington D.C., USA.

FEMA 356. (2000). Prestandard and commentary for the seismic rehabilitation of buildings, Prepared by the American Society of Civil Engineers for the Federal Emergency Management Agency, Washington, D.C. Publ. No. 356.

Ferreira, R.M. (2004). Probability based durability analysis of concrete structures in marine environment. University of Minho School of Engineering Department of Civil Engineering, Doctor of Philosophy.

Ghods, P., Isgor, O.B., Pour –Ghaz, M. (2007). A Practical method for calculating the corrosion rate of uniformly depassivated reinforcing bars in concrete. *Materials and Corrosion*. 58(4), 265-272.

Goto, S., & Roy, D.M.(1981). The effect of w/c ratio and curing temperature on the permeability of hardened cement paste. *Cement and Concrete Research*. 11(4), 575-579.

Gulikers, J. (2005). Theoretical considerations on the supposed linear relationships between concrete resistivity and corrosion rate of steel reinforcement. *Materials and Corrosion*. 56(6), 393-403.

Hawkins, N.M., Lin, I., & Ueda, T. (1987). Anchorage of reinforcing bars for seismic forces. *ACI Structural Journal.* 84(5), 407-418.

Ho, D.W.S., & Lewis RK. Carbonation of concrete and its prediction. *Cement and Concrete Research*. 17, 489–504.

Hoar, T.P. (1967). The anodic behavior of metals. *Corrosion Science*.7, 341-355.

Hognestad, E. (1951). A study of combined bending and axial load in reinforced concrete members. *Bulletin 399*. University of Illinois Engineering Experiment Station, Urbana, p.128.

Inel, M., Ozmen, H.B., & Bilgin H. (2009). SEMAp: Modelling and analysing of confined and unconfined concrete sections. *Scientific and Technical Research Council of Turkey*. Project No. 105M024.

Cagatay, I.H.(2005). Experimental evaluation of buildings damaged in recent earthquakes in Turkey. *Engineering Failure Analysis*. 12(3), 440–452.

Isgor, O.B., Razaqpur, A.G.(2004). Finite element modelling of coupled heat transfer, moisture transport and carbonation processes in concrete structures. *Cement and Concrete Composites*. 26(1), 57-73.

Isgor, O.B., & Razaqpur, A.G. (2006). Modelling steel corrosion in concrete structures. *Materials and Structures*. 39(3), 291-302.

Jaegermann, C. (1990). Effect of water–cement ratio and curing on chloride penetration into concrete exposed to Mediterranean sea climate. *ACI Materials Journal*. 87(4), 333–339.

Kapasny, L. & Zembo, S. (1993). The influence of the reinforcement corrosion on the load-bearing capacity of the reinforced concrete structures. *In Proc. Int. Conf RILEM. Bratislava,* p. 124-127

Kato, B., (1979). Mechanical properties of steel under load cycles idealizing seismic action. *CEB Bulletin D'Information*. 131, 7–27.

Kwak, H.G, & Kim, S.P. (2002). Nonlinear analysis of RC beams based on moment–curvature relation. *Computers and Structures*. 80(7-8), 615–628.

Kent, D.C. & Park, R. (1973). Cyclic load behaviour of reinforcing steel. *Strain*. 9(3), 98-103.

Kent, D.C., & Park, R. (1971). Flexural members with confined concrete. *ASCE Journal of the Structural Division*. 97(7), 1969–1990.

Kobayashi, K., & Suttoh, K. (1991). Oxygen diffusivity of various cementitious materials. *Cement and Concrete Research*. 21, 273–84.

Lee, H.S., Noguchi, T., & Tomosawa, F. (2002). Evaluation of the bond properties between concrete and reinforcement as a function of the degree of reinforcement corrosion. *Cement and Concrete Research*. 32(8), 1313–1318.

Lee, H.S., & Cho, Y.S. (2009). Evaluation of the mechanical properties of steel reinforcement embedded in concrete specimen as a function of the degree of reinforcement corrosion", *International Journal of Fracture*, 157(1-2), p. 81-88.

Lehman, D. E., & Moehle, J. P. (2000). Seismic performance of well-confined concrete bridge columns. *Pacific Earthquake Engineering Research Center*. Report No. PEER-1998/01, University of California, Berkeley, p. 316.

Lepage, A., Delgado, S.A., & Dragovich J.J. (2008). Appropriate models for practical nonlinear dynamic anaylyses of reinforced concrete frames. I*n: Proceedings of the 14th world conference on earthquake engineering*.

Li, C.Q.(2003). Life cycle modelling of corrosion affected concrete structures–propagation. *ASCE Journal of Structural Engineering*.129(6), 753-761.

Li, C.Q. (2003). Life cycle modelling of corrosion affected concrete structures–initiation. *ASCE Journal of Materials in Civil Engineering*. 15(6), 594-601.

Li, C.Q., Lawanwisut, W., Zheng, J.J., & Kijawatworawet, W. (2005). Crack width due to corroded bar in reinforced concrete structure. *International Journal of Materials and* Structural *Reliability*. 3(2), 87-94.

Li, C.Q., Lawanwisut, W., & Zheng, J.J. (2005). Time-dependent reliability method to assess the serviceability of corrosion-affected concrete structures. *ASCE Journal of Structural Engineering*. 131(11), 1674-1680.

Li, C.Q. & Melchers, R.E. (2006). Time-dependent serviceability of corrosion affected concrete structures. *Magazine of Concrete Research*. 58(9), 567–574.

Li, C.Q., Melchers R.E., & Zheng, J.J. (2006). Analytical model for corrosion-induced crack width in reinforced concrete structures . *ACI Structural Journal.* 103(4), 479-487.

Li, C.Q., Zheng, J.J., Lawanwisut, W., & Melchers, R.E. (2007). Concrete delamination caused by steel reinforcement corrosion. *Journal of Materials in Civil Engineering.*19(7), 591-600.

Liu, H.K., Tai, N.H., & Lee, W.H. (2002). Effect of seawater on compressive strength of concrete cylinders reinforced by non-adhesive wound hybrid polymer. *Composites Science and Technology*. 62(16), 2131-2141.

Liu, Y., & Weyers, R.E. (1998). Modelling the time-to-corrosion cracking in chloride contaminated reinforced concrete structures. *ACI Materials Journal*. 95(6), 675-681.

Lundgren, K. (2007). Effect of corrosion on the bond between steel and concrete: An overview. *Magazine of Concrete Research*. 59(6), 447-461.

Mangat, P.S., & Elgarf, M.S. (1999). Bond characteristics of corroding reinforcement in concrete beams. *Materials and Structures*. 32(2), 89-97.

Mander, J.B. (1984). Seismic Design of Bridge Piers, PhD Thesis, University of Canterbury, New Zealand.

Mander, J.B., M.J.N Priestley, & R. Park. (1988). Theoretical stress-strain model for confined concrete. *ASCE Journal of Structural Engineering*. 114(8), 1804-1825.

McCarter, W.J., & Vennesland, Ø. (2004). Sensor systems for use in reinforced concrete structures. *Construction and Buildings Materials*. 18(6), 351–358.

Molina, F.J., Alonso, C., & Andrade, C. (1993). Cover cracking as a function of rebar corrosion, part 2: Numerical model. *Materials and Structures*. 26(9), 532-548.

Morinaga, S. (1988). Prediction of service life of reinforced concrete buildings based on rate of corrosion of reinforcing Steel. *Institute of Technology, Shimizu corporation*. Tokyo, Japan, Special Rep. No. 23p. 82.

Mozer, J.D., Bianchini A.C., Kesler, C.E. (1965). Corrosion of reinforcing bars in concrete. *ACI Journal Proceedings*. 62(8), 909-932.

Ohtsu, M., & Yoshimura, S. (1997). Analysis of crack propagation and crack initiation due to corrosion of reinforcement. *Construction and Building Materials*. 11(7–8), 437–442.

Otani, S., & Sozen, M.A. (1972). Behaviour of multi-story reinforced concrete frames during earthquakes. *Structural Research Series*. University of Illinois, Urbana. No. 392, p. 551.

Ouglova, A., Berthaud, Y., Foct, F., Francois, M., Ragueneau, Fr., & Petre-Lazar, I. (2008). The influence of corrosion on bond properties between concrete and reinforcement in concrete structures. *Materials and Structures*. 41(5), 969-980.

Pacific Earthquake Engineering Research Center. (2009). *PEER strong motion database*. University of California, Berkeley, http://peer.berkeley.edu.

Pantazopoulou, S.J., & Papoulia, K.D. (2001). Modelling cover-cracking due to reinforcement corrosion in RC structures. *ASCE Journal of Engineering Mechanics*. 127(4), 342-351.

Park, R., & Paulay, T. (1975). Reinforced concrete structures. New York: John Wiley & Sons; 769 pages.

Park, R., Priestly, M.J.N., & Gill, W.D. (1982). Ductility of square confined concrete columns. *ASCE Journal of the Structural Division*. 108(4), 929–950.

MICHAEL, P. (2000). The assessment of corrosion damaged concrete structures. PhD thesis. University of Birmingham.

Peterson, H., & Popov, E.P. (1977). Constitutive relations for generalized loadings. *ASCE Journal of Engineering Mechanics Division*. 103(EM4), p.611-627

Ramamoorthy, S.K., Gardoni, P., & Bracci, J.M. (2006). Probabilistic demand models and fragility curves for reinforced concrete frames. *ASCE Journal of Structural Engineering*. 132(10), 1563-1572.

Rasheeduzzafar. (1992). Influence of cement composition on concrete durability. *ACI Materials Journal*. 89(6), 574–86.

Rasheeduzzafar, Dakhil, F.H., Al-Gahtani, A.S., Al-Saadoun S.S., & Bader, M.A. (1990). Influence of cement composition on the corrosion of reinforcement and sulfate resistance of concrete. *ACI Materials Journal*. 87(2), 114–22.

Revathy, J., Suguna, K., & Raghunath, P.N. (2009). Effect of corrosion damage on the ductility performance of concrete columns. *American Journal of Engineering and Applied Sciences*. 2(2), 324-327.

Rodriguez, J., Ortega, L.M., Casal, J. & Diez, J.M. (1996). Assessing Structural Conditions of Concrete Structures with Corroded Reinforcement. *Concrete in the Service of Mankind: Concrete Repair,* Rehabilitation and Protection**,** First Ed. E & FN Spon, London, p. 65-78.

Saatcioglu, M., Alsiwat, J.M., & Ozcebe, G. (1992). Hysteretic behaviour of anchorage slip in R/C members. ASCE *Journal of Structural Engineering*. 118(9), 2439-2458.

Saatcioglu, M., & Humar, J. (2003). Dynamic analysis of buildings for earthquake resistant Design. *Canadian Journal of Civil Engineering*. 30, 338–359.

Saatcioglu, M. & Razvi S.R.(1992). Strength and Ductility of Confined Concrete. *ASCE Journal of Structural Engineering.* 118(6), 1590-1607.

Sezen, H. (2002). Seismic behaviour and modelling of reinforced concrete buildings column. Ph.D. thesis. University of California, Berkeley.

Sezen, H, & Moehle J.P.(2006). Seismic test of concrete columns with light transverse reinforcement. *ACI Structural Journal*. 103(6), 824-849.

Sezen, H., & Setzler, E.J. (2008). Reinforcement slip in reinforced concrete columns. *ACI Structural Journal*. 105(3), 280-289.

Shamsad, A. (2003). Reinforcement corrosion in concrete structures, its monitoring and service life prediction—a review. *Cement and Concrete Composites*. 25, 459–471

Shannand, M.J., & Shaia, H.A. (2003). Sulphate resistance of high-performance concrete, *Cement and Concrete Composites*. 25(3), 363– 370.

Shibata, T.(2002). Cost of corrosion in Japan. *Corrosion Science Technology*. 31(2), 97-102.

Song, H.W., & Saraswathy, V. (2007). Corrosion monitoring of reinforced concrete structures-A Review. *International Journal of Electrochemical Science*. 2, 1-28.

Stanish, K., Hooton, R.D., & Pantazopoulou, S.J. (1999). Corrosion effects on bond strength in reinforced concrete. *ACI Structural Journal*. 96(6), 915-921.

Stanton, J.F., & McNiven, H.D. (1979). The development of a mathematical model to predict the flexural response of reinforced concrete beams to cyclic loads, using system identification. *Pacific Earthquake Engineering Research Center*. University of California, Berkeley, Rep. No UCB/EERC-79/021979.

Tapan, M., & Aboutaha, R.S. (2008). Strength evaluation of deteriorated RC bridge columns. *ASCE Journal of Bridge Engineering*. 13(3), 226-236.

Thoft-Christensen, P. (1998). Assessment of the reliability profiles for concrete bridges. *Engineering Structures*. 20(11), 1004-1009.

Thompson, K.J., & Park, R. (1978). Stress-strain model for grade 275 reinforcing steel for cyclic loading. *Bulletin of the New Zealand National Society for Earthquake Engineering*. 11(2), 101-109.

Turkish Ministry of Public Works and Settlement . (2007). Specification for structures to be built in disaster areas. Ankara.

Turkish Standards Institute, TS500. (2000). Requirements for design and construction of reinforced concrete structures. Ankara, Turkey.

Tuutti, K .(1980). Service life of structures with regard to corrosion of embedded steel. Performance of concrete in marine environment, *ACI SP-65*. Detroit, Michigan, p. 223–36.

TUUTTI, K. (1982). Corrosion of steel in concrete, *Swedish Cement and Concrete Research Institute*, Report 4-82, p. 469.

Uhlig, H.H. (1950). The Cost of corrosion to the united states. *Corrosion*. 6, 29-33.

Vandewalle, L., & Mortelmans, F. (1988). The bond stress between a reinforcement bar and concrete: Is it theoretically predictable?. *Materials and Structures*. 21(3), 179-181.

Varghese, P.C. (2006). Advanced reinforced concrete design 2nd edition. India: Prentice-Hall press, p. 399.

Vecchio, F., & Collins, M. P. (1986) The modified compression field theory for reinforced concrete elements subjected to shear. Proc. ACI, 83(2): 219–231.

Vidal, T., Castel, A., & François, R. (2007). Corrosion process and structural performance of a 17 year old reinforced concrete beam stored in chloride. *Cement and Concrete Research*. 37(11), 1551-1561.

Villaverde, R. (2007). Methods to assess the seismic collapse capacity of building structures: State of the art. *ASCE Journal of Structural Engineering*. 133(1), 57-66.

Vu, K.A.T., & Stewart, M.G.(2000). Structural reliability of concrete bridges including improved chloride-induced corrosion models. *Structural Safety*.22(4), 313-333.

Yakut, A., & Yılmaz, H. (2008). Correlation of deformation demands with ground motion intensity. *Journal of Structural Engineering*. 134(12), p.1818-1828.